

UNIVERSITÀ DEGLI STUDI DI NAPOLI
“FEDERICO II”



Department of Agraria

Ph.D.
in
AGROBIOLOGY AND AGROCHEMISTRY
XXVII Cycle

**Phytotoxic metabolites produced by
Botryosphaeriaceae involved in
cultivated and forest plants diseases**

Ph.D. dissertation by
Sara Basso

Tutor: Dott. Andolfi Anna
Co-tutor: Prof. Antonio Evidente

2012-2015

INDEX

1. INTRODUCTION	page 6
1.1. <i>Botryosphaeriaceae</i>	page 6
1.2. Secondary metabolites in plant-microbe interactions	page 7
1.2.1. Phytotoxin insensitivity of plants and disease resistance	page 8
1.2.2. Mechanism of action	page 9
1.3. <i>Botryosphaeriaceae</i> involved in grapevine trunk diseases (GTDs)	page 12
1.4. <i>Botryosphaeriaceae</i> pathogen of forest plants	page 14
2. AIM OF THESIS	page 17
3. MATERIALS AND METHODS	page 18
3.1. Fungi	page 18
3.2. General procedures	page 18
4. EXPERIMENTAL SECTION	page 20
4.1 Production, extraction and purification of phytotoxins by <i>Neofusicoccum austral</i> strain BOT48.	page 20
4.1.1. Cyclobotryoxide	page 21
4.1.2. 3-Methylcatechol	page 21
4.1.3. Tyrosol	page 21
4.1.4. Acetylation of cyclobotryoxide	page 21
4.2. Production, extraction and purification of phytotoxins by <i>Lasiodiplodia mediterranea</i> strain BL101.	page 23
4.2.1. Lasiojasmonate A	page 24
4.2.2. 16-O-Acetylbotryosphaerilactones A and C	page 24
4.2.3. Lasiojasmonates B and C	page 24
4.2.4. (1R,2R)-Jasmonic acid	page 25
4.2.5. (1R,2R)-Methyl jasmonate	page 25
4.2.6. Botryosphaerilactone A	page 25
4.2.7. (3S,4R,5R)-4-Hydroxymethyl-3,5-dimethyldihydro-2-furanone	page 25

4.2.8. (3R,4S)-Botryodiplodin	page 26
4.2.9. Acetylation of Botryosphaerilactone A	page 26
4.2.10. Acetylation of (3R,4S)-Botryodiplodin	page 26
4.2.11. Alkaline hydrolysis of Lasiojasmonates A-C	page 26
4.3. Production, extraction and purification of metabolites by <i>Lasiodiplodia mediterranea</i> strain B6.	page 27
4.3.1. Lasiolactols A and B	page 28
4.3.2. Botryosphaeriodiplodin	page 28
4.3.3. (5R)-5-Hydroxylasiodiplodin	page 28
4.3.4. Methylation of Botryodiplodin	page 29
4.3.5. 7-O-(S)- α -Methoxy- α -trifluoromethyl- α -phenylacetate (MTPA) ester of 13-O-Methylbotryosphaeriodiplodin	page 29
4.3.6. 7-O-(R)- α -Methoxy- α -trifluoromethyl- α -phenylacetate (MPTA) ester of 13-O-Methylbotryosphaeriodiplodin	page 30
4.4. Production, extraction and purification of phytotoxins by <i>N. australe</i> strain BL24	page 30
4.4.1. Botryosphaerone D	page 31
4.4.2. 3,4,8-Trihydroxy-6-methoxy-3,4-dihydro-1(2H)-naphthalenone	page 31
4.5. Production, extraction and purification of phytotoxins by <i>Diplodia quercivora</i> strain BL9	page 31
4.5.1. Diplopimarane	page 32
4.5.2. 6-O-Methyl and 6,7-O,O'-Dimethyldiplopimarane	page 33
4.5.3. 6,7,14-O,O',O''-Triacetyldiplopimarane	page 33
4.5.4. 6-O- <i>p</i> -Bromobenzoyl Ester of Diplopimarane	page 33
4.5.5. 15,16-Dihydrodiplopimarane	page 34
4.5.6. 14-O-(S)- α -Methoxy- α -trifluoromethyl- α -phenylacetate (MTPA) ester of 6,7-O,O'-Dimethyldiplopimarane	page 34
4.5.7. 14-O-(R)- α -Methoxy- α -trifluoromethyl- α -phenylacetate (MTPA) ester of 6,7-O,O'-Dimethyldiplopimarane	page 35

4.5.8. Conversion of Sphaeropsidin A into Diplopimarane	page 35
4.5.9. Sphaeropsidin A and C	page 35
4.5.10. (+)-Epiepoformin	page 36
4.5.11. Crystal Structure Determination of Diplopimarane	page 36
4.6. Production, extraction and purification of Oxysporone	page 37
4.6.1. Preparation of oxysporone derivatives	page 37
4.6.2. 4- <i>O</i> -Acetyloxysporone	page 37
4.6.3. 2,3-Dihydrooxysporone	page 37
4.6.4. 4- <i>O</i> -Dehydrooxysporone	page 38
4.6.5. 4- <i>O</i> - <i>p</i> -Bromobenzoyloxysporone	page 38
4.6.6. 2-(4-Pyronyl)acetic acid	page 39
4.6.7. 4- <i>O</i> -Acetyl-2,3-dihydrooxysporone	page 39
4.6.8. 2-(2,3-Dihydro-4-pyronyl)acetic acid	page 39
4.6.9. Methyl ester of 2-(4-pyronyl)acetic acid	page 40
4.7. Biological assays	page 41
4.7.1. Phytotoxic activity	page 41
4.7.1.1. Leaf puncture assays	page 41
4.7.1.2. Cutting assays	page 41
4.7.2. Zootoxic activity assays	page 42
4.7.3. Antifungal activity	page 42
4.7.4. Analysis of data	page 43
5. RESULTS AND DISCUSSION	page 44
5.1. Chemical and biological characterization of phytotoxins from <i>Neofusicoccum australe</i> strain BOT48	page 44
5.2. Purification and chemical characterization of phytotoxins by <i>Lasiodiplodia mediterranea</i> strain BL101	page 47
5.3. Chemical and biological characterization of phytotoxins by <i>Lasiodiplodia mediterranea</i> strain B6.	page 55

5.4. Purification and chemical characterization of phytotoxins by <i>Neofusicoccum australe</i> strain BL24.	page 58
5.5 Purification and chemical characterization of phytotoxins from <i>Diplodia quercivora</i> strain BL9.	page 60
5.6 Synthesis and chemical characterization of oxysporones derivatives	page 68
6. CONCLUSION	page 72
7. REFERENCES	page 73

1. INTRODUCTION

1.1. *Botryosphaeriaceae*

Species of *Botryosphaeriaceae* occur in most parts of the world under various ecological niches, and are found as endophytes, parasites and saprophytes on a vast number of both annual and perennial plants (Barr, 1972; von Arx, 1987). Several species of this family are significant plant pathogens causing leaf spots, fruit rots, dieback, perennial cankers, and eventual death in economically important woody perennial crops and ornamental plants as well as both in native and introduced forest tree species (Farr and Rossman, 2011). The taxonomic history of *Botryosphaeria* is complex, and the genus has been subjected to numerous taxonomic rearrangements in the systematic position of both the family and the genera included (Denman et al., 2000). Species identification in *Botryosphaeria* has been complicated due to the lack of sufficient diversity among teleomorph features of species within this genus. Additionally, the difficulty of finding teleomorphs in nature or obtaining them under laboratory conditions, has forced the identification of these fungi to be primarily based on anamorphic characters (Jacobs and Rehner, 1998; Denman et al., 2000; Phillips, 2002). Consequently, many different anamorph genera have been linked to *Botryosphaeria* and its characterization to species level has not always been accurate, which has, for many years, raised even more confusion regarding their association and pathogenicity on many hosts. The implementation of DNA-based identification techniques and phylogenetic analyses of nucleotide sequences helped to resolve some of the taxonomic conflicts previously existing in *Botryosphaeria*. In particular, a phylogenetic study based on 28S rDNA sequences showed *Botryosphaeria* to be polyphyletic comprising several phylogenetic lineages (Crous et al., 2006). Since then, *Botryosphaeria* was restricted to species with *Fusicoccum* anamorphs, which currently include *Botryosphaeria dothidea* (Mough. ex Fr.) Ces. & De Not (anamorph: *Fusicoccum aesculi* Corda), *Botryosphaeria corticis* (Demaree & M.S. Wilcox) Arx & E. Müll. (anamorph: *Fusicoccum* sp.), *Fusicoccum ramosum* (Pavlic, Burgess, M.J. Wingfield), and *Fusicoccum atrovirens* (J.W.M. Mehl & B. Slippers). However, the study could not fully resolve the

status of the *Diplodia/Lasiodiplodia* group. Two years later, Phillips et al. (2008) partially solved the *Diplodia/Lasiodiplodia* conflict based on a multigene phylogenetic analysis, which introduced four genera into this group revising the taxonomic status of numerous dematiaceous *Botryosphaeriaceae*, including some that infect grapevines. As a consequence of this and other studies (Pavlic et al., 2004; Abdollahzadeh et al., 2010), it is currently well accepted that *Lasiodiplodia* is a distinct lineage in the *Botryosphaeriaceae*. Based on these recent findings and until completion of novel taxonomic studies in *Botryosphaeriaceae*, the nomenclature proposed by both Crous et al. (2006) and Phillips et al. (2008) should be followed in order to avoid adding more confusion within this family.

1.2 Secondary metabolites in plant-microbe interactions

There are no effective fungicide controls for *Botryosphaeria* dieback. The best defense against this commonly occurring disease is to ensure plants are in optimal health by providing the appropriate cultural requirements for the particular plant species, avoiding plant stress and injury, and employing appropriate sanitation measures. For this reason a study on plant-pathogen interactions is interesting because all substances involved in this mechanism could be involved in the disease control.

They could be used:

- to understand the mechanisms of pathogenicity and virulence,
- to understand the mechanisms of action,
- in plant resistant mechanisms and possible utilization for screening of disease improved plant lines,
- as natural compounds with antimicrobial, insecticidal and herbicidal activities.

The interaction between plant pathogens and their hosts is extremely complex. There are many factors affecting the plant disease development as plant and pathogen physiology, metabolism of the host plant, physical environment and the way it impacts the plant growth and development,

biochemistry and genetics of the pathogen-plant interactions. Moreover phytopathogenic fungi employ an array of strategies to distress, weaken or kill the host plant in order to gain access to nutrients. One of these strategies is the production of secondary metabolites. They are organic compounds that are not directly involved in the normal growth, development, or reproduction of an organism but they could have an important role in the development of diseases. These toxins are compounds produced by the pathogens and their effect on plants is characterized by the appearance of specific symptoms; wilting and general growth suppression, as well as chloroses, necroses, and spotting of aerial portions are the most common. They belong to different classes of natural compounds polyketides, terpenoids, peptides, glycoproteins, polysaccharides, organic acids, fatty acids and derivatives (Berestetskiy, 2008). The role of a toxin as a disease determinant is proved by the occurrence of the toxin in an infected plant and the ability of the toxin alone to elicit at least part of the symptoms of the disease (Hamid and Strange, 2000). Some of the toxins have general phytotoxic properties and are active toward a broad range of plant species. These are non-host-specific toxins. They contribute to the virulence or symptom development in the disease in which they occur, but are not primary determinants of host range (Walton, 1996). Other toxins are host-specific ones and affect only certain plant varieties or genotypes (Osborn, 2001). The host-specific toxins (HSTs) are playing a role in determining the host range of specificity of plant pathogens and can act as an agent of virulence of those pathogens (Walton, 1996).

1.2.1. *Phytotoxin insensitivity of plants and disease resistance*

The resistance mechanism to toxin-producing fungi can be based on the ability of an R gene product to inactivate a toxin which normally induces the disease symptoms, or inhibits the induction of active defense responses (Takken et al., 2000). Genetic control of sensitivity to HSTs, and susceptibility to the producing pathogens, is highly diverse and includes dominance, semidominance, recessiveness, and maternal inheritance (Walton, 1996). Genetic and biochemical

studies revealed that toxins are the determinants of specificity. In such cases resistance or susceptibility to the fungus correlates with insensitivity or sensitivity to the toxin (Knogge, 1996). But sensitivity to the toxins and susceptibility to the pathogens are not always fully correlated. There are several possibilities for selective agents as HST's nonhost specific toxins, living pathogens and chemicals (Slavov, 2005). Two criteria must be satisfied before a toxin is used as a screening agent:

1. the toxin produced by the pathogen must be involved in the disease development;
2. the toxin must act directly at the cellular level (Hammerschlag, 1984; Yoder, 1980).

1.2.2. Mechanism of action

Some of the most potent phytotoxins are synthesized by microbes. By studies at the biochemical level important insights into the destructive modes of action of the phytotoxins have been gained (Duke et al., 2001). The strategies for exerting virulence can be manifold. In general, necrotrophic pathogens use toxins to elicit plant cell death and derive nutrition from the dead tissue, whereas biotrophic pathogens rely on living plant tissue. Phytotoxins may interact with a range of cellular targets, alter gene expression or undermine membrane integrity. A number of phytotoxins inhibit the activity of plant enzymes, thereby disrupting the biosynthesis of crucial metabolites. Other fungi interfere with the plants' physiology by producing plant hormones, such as gibberelin or gibberellic acid (Kawaide, 2006). Finally, plant cells may be damaged by the production of reactive oxygen species (ROS)(Duke et al., 2011).

Several microbial secondary compounds either inhibit an amino transferase or appear to have such a mode of action. Recently mode of action of ascaulitoxin aglycone (Table 1), was determined. It was produced by *Ascochyta caulina* (P. Karst.) Aa & Kestern, a fungus being studied as a potential mycoherbicide, is a potent phytotoxin that has profound effects on amino acid metabolism as determined by metabolic profiling (Evidente et al., 1998). Feeding treated plants

with most amino acids reversed the effects of the toxin. However, *in vitro* assays found that the toxin did not inhibit alanine aminotransferase nor alanine:glyoxylate aminotransferase, leading the authors to speculate that it might inhibit another amino transferase or one or more amino acid transporters.

Rhizobitoxine (Table 1) is a phytotoxin produced by some *Bradyrhizobium* strains (Duke et al., 2011). It inhibits β -cystathionase, which is required for methionine synthesis (Owens et al., 1968). However, it also directly inhibits production of ethylene from methionine (Owens, 1973) by inhibition of 1-aminocyclopropane-1-carboxylate synthase (Owens et al., 1971). Since synthesis of the essential plant hormone ethylene is dependent on methionine, one could assume that ethylene synthesis would be greatly inhibited in plants treated with this compound.

Acivicin (Table 1) is an analogue of glutamine and inhibits a number of glutamine-dependent enzymes, including glutamate synthase (Brunner et al., 2007). It also inhibits amidophosphoribosyltransferase, phosphoribosylformylglycinamide synthase, GMP synthase, and γ -glutamyltranspeptidase (Conti et al., 2003; Natsumeda et al., 1989; Rodriguez-Suarez et al., 2007).

Thaxtomin A (Table 1) belongs to a group of cyclic dipeptides (2,5-diketopiperazines) which arise from the condensation of 4-nitrotryptophan and phenylalanine groups. It are produced by several species of the gram-positive filamentous bacteria in the genus *Streptomyces* (e.g., *S. scabies* and *S. eubacteria*) that cause scab disease in potato and in several taproot crops. Thaxtomin A affects the formation of the cellulose synthase complexes on the outside of the plasma membrane, leading to its dissociation from the cortical microtubule cytoskeleton (King and Calhoun, 2009).

Tentoxin (Table 1), a cyclic tetrapeptide from the plant pathogen *Alternaria alternata* (Keissl.:Fr.) Beih. bot. Zbl., inhibits chloroplast development, which phenotypically manifests itself as chlorotic tissue (Bischoff et al., 2009; Halloin et al., 1970). Two fundamental processes are linked with this phenotype. This first is inhibition of energy transfer of the chloroplast-localized CF1 ATPase (Duke et al., 1982; Selman and Durbin, 1978). One would think that this process alone

could account for the chlorosis, but tentoxin also completely inhibits the transport of nuclear-coded enzyme polyphenol oxidase (PPO) into the plastid, even in etioplasts which should have no CF1 ATPase activity (Reimer and Selman, 1978). Without this processing, PPO has no enzyme activity.

The diphenyl ether compound cyperin (Table 1), a metabolite of *Preussia fleischbakkii* (Auersw.) Cain, *Phoma sorghina* (Sacc.) Boerema, Dorenb. & Kesteren and *Ascochyta cypericola* (Feld et al., 1989; Weber and Gloer, 1988; Stierle et al., 1992), inhibits plant enoyl (acyl carrier protein) reductase (ENR), which is the target site of a synthetic diphenyl ether called triclosan. Inhibition of ENR results in light-independent disruption of membrane integrity (Venkatasubbaiah et al., 1992).

Ophiobolins A (Table 1), tricyclic sesquiterpene phytotoxins from certain species of *Bipolaris* and other fungal genera (*Dechslera*), cause many symptoms on plants that were considered to be largely due to effects on the plasma membrane (Jacobellis and Bottalico, 1981). Its effects on maize root ion leakage correlate well with its direct antagonism of calmodulin (Au et al., 2000). Its effects on calmodulin cause inhibition of transport of nuclear-coded proteins into both the mitochondrion and the plastid (Kuhn et al., 2009). Recently ophiobolin displays higher *in vitro* growth-inhibitory effects in mammalian than in plant cells and displays *in vivo* antitumor activity (Bury et al., 2013).

Functional actin filaments are required for normal mitosis, as well as other cell functions related to the cell cytoskeleton. Cytochalasins (A-H) (Table 1) are actin-binding metabolites of several fungal species, such as *Phoma exigua* Sacc. and *Zygosporium masonii* Hughes (Styer and Cutler, 1984). Binding actin prevents actin polymerization into filaments, thus inhibiting the processes that require actin filaments, such as mitosis and other plant processes (Schinko et al., 2009; Wyss et al., 1980). Moreover, cytochalasins and their derivatives show *in vitro* growth inhibitory effects in cancer cells (van Goietsenoven et al., 2011).

Hydantocidin (Table 1), a spironucleoside from *Streptomyces hygrosopicus*, is highly phytotoxic (Steinberg and Burgess, 1992). It is phosphorylated *in vivo*, and the derivative, 5'-

phosphohydantocidin (5PH), inhibits adenylosuccinate synthetase (ASS) (Nakajima et al., 1991; Heim et al., 1996; Siehl et al., 1996; Fonne-Pfister et al., 1996), an enzyme required for purine synthesis. ASS converts IMP to AMP. 5PH inhibits ASS by competitively inhibiting it through binding the IMP substrate binding site, forming a dead-end complex (Cseke et al., 1996). ASS is also inhibited by ribofuranosyl triazolone, a phytotoxic product of an *Actinomadura* species (Walters et al., 1997).

Compounds with internal disulfide bridges can covalently bind proteins, sometimes inactivating the protein function. They accomplish this by reaction of the disulfide bond with the cysteine components of proteins. Some fungal phytotoxins such as sirodesmin PL from *Leptosphaeria maculans* (Sowerby) P. Karst. and gliotoxin (Table 1) have such internal disulfide bridges that conjugate proteins (Rodriguez-Foneca et al., 1995; Rouxel et al., 1998; Chai and Waring, 2000). These compounds are also implicated in generation of reactive oxygen species by redox cycling (Rouxel et al., 1998). Such compounds are generally broadly cytotoxic.

Anhydro-D-glucitol (Table 1), produced by the plant pathogenic fungus *Fusarium solani* (Mart.) Sacc., is mildly phytotoxic (Wright, 1951). When phosphorylated by the plant, it is a close analog of fructose-1,6-bisphosphate, thereby inhibiting fructose-1,6-bisphosphate aldolase activity, which is required for production of glyceraldehyde-3-phosphate and dihydroxyacetonephosphate in glycolysis (Tanaka et al., 1996).

1.3. *Botryosphaeriaceae* involved in grapevine trunk diseases (GTDs)

In recent years an increasing number of *Botryosphaeriaceae* species have been associated with grapevine decline worldwide (van Niekerk et al., 2006; Úrbez-Torres et al., 2007; Úrbez-Torres, 2001) (Table 2). Several diseases caused by these pathogens in grapevines are known, or have been known in the past, under a variety of names such as black dead arm (BDA), *Botryosphaeria* canker, excoriosis, *Diplodia* cane dieback and bunch rot (van Niekerk et al., 2006; Hewitt, 1988; Phillips, 1998; Phillips, 2002). External symptoms of these diseases include death

of the cordons, canes, shoots and buds, canker formation, stunting, delayed bud burst, bud necrosis, bleached canes, reduced bunch set and bunch rots, all of which have been extensively documented (van Niekerk et al., 2006; Hewitt, 1988; Phillips, 1998; Phillips, 2002; Larignon et al., 2001; Castillo-Pando et al., 2001; Taylor et al., 2005; Winderlich et al., 2008; Savocchia et al., 2007).

Internal symptoms on the trunks or canes of declining vines such as brown wood streaking and wedge-shaped discolourations are commonly associated with *Botryosphaeriaceae* species (van Niekerk et al., 2006; Phillips, 2002; Larignon et al., 2001; Castillo-Pando et al., 2001; Savocchia et al., 2007). Some of the symptoms, both external and internal, are shown in Figure 1.

Neofusicoccum parvum (Pennycook & Samuels) Crous, Slippers & A.J.L. Phillips isolated together other four Botryosphaeriaceous in Spain from symptomatic plants, showed to produce in liquid culture secondary metabolites (Martos et al., 2008). Four toxic metabolites were isolated from the organic extract and identified by spectroscopic and physical methods as (3R,4R)-(-)-4-hydroxy- and (3R,4S)-(-)-4-hydroxy-mellein, isosclerone, and tyrosol (Table 3). They were reported as being produced by *N. parvum* for the first time (Evidente et al., 2010). When assayed on tomato cuttings all four metabolites were toxic, producing symptoms ranging from slight to severe leaf wilting. (3R,4R)-(-)-4-Hydroxymellein and isosclerone were the most toxic (Evidente et al., 2010).

Diplodia seriata De Not., isolated from the *Vitis vinifera* L. cv. Cabernet Sauvignon, produced in liquid culture mellein, (3R,4R)-4-hydroxymellein, (3R)-7-hydroxymellein and, as new compound, (3R,4R)-4,7-dihydroxy-mellein (Djoukeng et al., 2009). A bioassay of vine cv. Gamay leaves found that (3R,4R)-4,7-dihydroxy-mellein was the most active metabolite, causing full leaf necrosis. Moreover using a HPLC DAD-MS analysis mellein detected in infected vine wood inoculated with *D. seriata* (Djoukeng et al. 2009).

1.4. *Botryosphaeriaceae* pathogen of forest plants

Different species belong to genera *Diplodia* and *Sphaeropsis* associated with disease of forestal plants. They induce heavy loss of forests and ornamental heritage, with consequent alteration of the typical landscape. These diseases are related to the production by fungi of several phytotoxins belonging to different chemical classes (Evidente et al., 2010) (Table 4).

Diplodia cupressi, A.J.L. Phillips & Alves associated with the so-called “canker” disease of species of *Cupressus* in the Mediterranean area, produced at least six tri- and tetra-cyclic unrearranged pimaranes, namely, sphaeropsidins A–F (Sparapano et al., 2004), and two phytotoxic dimedone methyl ethers, sphaeropsidone and epi-sphaeropsidone (Evidente et al., 1998). Relationships between sphaeropsidin and sphaeropsidon chemical structures and their phytotoxic and antimicrobial activities have already been extensively studied (Sparapano et al., 2004; Weber et al., 2007; Evidente et al., 2011a and b;). Moreover sphaeropsidins A-C and 10 semisynthetic derivatives were evaluated for their *in vitro* anticancer activities (Lallemand et al., 2012).

Sphaeropsis sapinea (Fr.) Dyco & Sutton, isolated from infected cypress trees, produced in liquid culture two main metabolites, named sapinofuranones A and B. They were characterised as two epimeric 2(3H)-dihydrofuranones and proved to be phytotoxic on non host plants such as tomato and on host plants as cypress and pine (Evidente et al., 1999). Successively from the same organic extract was obtained a new metabolite, namely sapinopyridione. The structure of a 3,3,6-trisubstituted-2,4-pyridione was assigned to sapinopyridione that can be formulated as the 6-methyl-2-(2-methyl-1-oxobutyl)-1-oxa-5-azaspiro[2.5]oct-6-ene-4,8-dione and its absolute configuration was also established as 2R,3R,10R (Evidente et al., 2006a).

Other strain of *S. sapinea* isolated in Sardinia from declining *Pinus radiata* L. plants showed to produce in liquid cultures well known (R)-(-)-mellein, (3R,4R)-(-) and (3R,4S)-(-)-4-hydroxymelleins. When assayed on *P. radiata* and tomato cuttings, mellein and a mixture of (3R,4R)-(-) and (3R,4S)-(-)-4-hydroxymellein in a ratio of 6.5:1 caused chlorosis and necrosis on

the needles that depend on concentration and time. The mixture showed antifungal activity when assayed on phytopathogenic species (Cabras et al., 2006)

Diplodia mutila (Fr.) Mont. and *D. corticola* (A.J.L. Phillips, A. Alves & J. Luque) are endophytic fungi, widespread in Sardinian oak forests, and considered main causes of cork oak (*Quercus suber* L.) decline (Franceschini et al., 1999). The main phytotoxic metabolite, namely diplopyrone, was isolated from *D. mutila* culture filtrates. It was characterized as new monosubstituted tetrahydropyranpyran-2-one, named diplopyrone. Diplopyrone, assayed at different concentrations, was toxic to *Q. suber* (Evidente et al., 2003). Subsequently the nonempirical assignment of its absolute configuration has been approached by two different methods and assigned as 4a(*S*), 8a(*S*), 6(*R*), 9(*S*) (Giorgio et al., 2005).

From culture filtrates of *D. corticola* was isolated two new 5'-monosubstituted tetrahydro-2*H*-bifuranyl-5-ones, named diplobifuranylones A and B, together diplopyrone, sphaeropsidins A-C, (3*S*,4*R*)-*trans*- and (3*R*,4*R*)-*cis*-4-hydroxymellein, sapinofuranone B and its (*S,S*)-enantiomer. Diplobifuranilones did not show phytotoxic and brine shrimp (*Artemia salina* L.) lethality activities (Evidente et al., 2006b). Successively other two metabolites were isolated from the same culture filtrates. They were structurally closed to sapinofuranones A and B (Table 4), and named diplofuranones A and B (Evidente et al., 2007).

Diplodia africana Damm & Crous was detected as the main pathogen involved in the aetiology of cankers and branch dieback of Phoenician juniper (*Juniperus phoenicea* L.) trees in Sardinia (Linaldeddu et al., 2011). For this pathogen, the production of two new phytotoxic dihydrofuropyran-2-ones, named afritoxinone A and B, along with six others known metabolites such as oxysporone, sphaeropsidin A, epi-sphaeropsidone, R(-) mellein, (3*R*,4*S*)-4-hydroxymellein and (3*R*,4*R*)-4-hydroxymellein was reported (Evidente et al., 2012). The phytotoxic activity of afritoxinones A and B and oxysporone was evaluated on host and non-host plant. Oxysporone proved to be the most phytotoxic compound. Recently, the absolute configuration (AC), which is strongly related with the biological activity of naturally occurring

compounds (Evidente et al., 2011; Evidente et al., 2013) was also determined for oxysporone. The AC was assigned by chiroptical methods such as optical rotatory dispersion (ORD), electronic circular dichroism (ECD) and vibrational circular dichroism (VCD) (Mazzeo et al., 2013).

2. AIM OF THESIS

The aim of the present thesis was the study of *Botryosphaeriaceae* species involved in GTDs and canker and dieback in forest plants, by chemical and biological characterization of the phytotoxins produced in order to understand the role of these natural products in the pathogenesis process and therefore to use them against specific diseases. The steps proposed to achieve this goal are summarized in the following points:

- Isolation and chemical characterization of the phytotoxic metabolites produced *in vitro* by *Neofusicoccum australe* Slippers, Crous & M.J. Wingf. (haplotypes H4), associated with grapevine cordon dieback and two different strains of *Lasiodiplodia mediterranea* Linaldedd, Deidda & Beraf-Tebbal associated with wedge-shaped lesions of the vascular tissues on grapevine.
- Isolation and chemical characterization of the phytotoxic metabolites produced *in vitro* by *Diplodia quercivora* Linaldeddu & A.J.L. Phillips found on declining *Quercus canariensis* Willd. trees in Tunisia and by *N. australe* (haplotypes H1) associated with branch dieback of Phoenician juniper.
- Isolation of oxysporone, a phytotoxic metabolite produced *in vitro* by the fungus *Diplodia africana*, pathogen of Phoenician juniper, and its structure-activity relationship study by hemisynthesis of some its derivatives for the evaluation of their phytotoxic and antifungal activities.

3. MATERIALS AND METHODS

3.1. Fungi

The species object of this thesis were isolated from wood tissues of symptomatic host plants: *Vitis vinifera*, *Juniperus phoenicea* and *Quercus canariensis*. As reported in Table 5, identified in the laboratories of Dipartimento di Agraria, Sezione di Patologia vegetale ed Entomologia, Università degli Studi di Sassari and Dipartimento di Scienze Agrarie e Forestali, Università degli Studi di Palermo (Italy). Successively they were characterized on the basis of morphological characters and analysis of Internal Transcribed Spacer (ITS) of rDNA. and part of the translation elongation factor 1- α gene (EF1-alpha). Fungal DNA extraction, PCR amplification reactions, and DNA sequencing were carried out.

Representative sequences of isolate were deposited in GenBank as reported in Table 5. Pure cultures of all strains were maintained on potato-dextrose-agar (PDA, Fluka, Sigma-Aldrich Chemic GmbH, Buchs, Switzerland) and stored at 4°C in the collection in the respective departments Table 5.

3.2. General Procedures

Melting point was measured on a Mettler Toledo FP90 Central Processor (Greifensee, Switzerland) associated with a Zeiss Axioskop microscope (Oberkochen, Germany).

Optical rotations were measured in CHCl₃, unless otherwise noted, on a Jasco P-1010 digital polarimeter, while the ECD spectra were recorded on a JASCO J-815 (Tokyo, Japan) spectrometer in EtOH; IR spectra were recorded as deposit glass film on a Thermo Electron Corporation Nicolet 5700 FT-IR spectrometer (Waltham, MA, USA) and UV spectra were measured in MeCN, unless otherwise noted, on a JASCO V-530 spectrophotometer.

¹H and ¹³C NMR spectra were recorded at 400 and 100 MHz in CDCl₃ respectively, unless otherwise noted, on on Bruker spectrometers (Karlsruhe, Germany). The same solvent was used as internal standard. Carbon multiplicities were determined by DEPT (Distortionless

Enhancement by Polarization Transfer) spectra. DEPT, COSY45 (Correlation Spectroscopy), HSQC (Heteronuclear Single Quantum Coherence spectroscopy), HMBC (Heteronuclear Multiple-Bond Correlation spectroscopy), and NOESY (Nuclear Overhauser Effect spectroscopy) experiments (Breitmaier et al., 1987) were performed using Bruker microprograms.

Coupling constants (J) are in Hertz. The following symbols were used: *s*: singlet; *brs*: broad singlet; *d*: doublet; *dd*: double doublet; *ddd*: doublet of double doublet; *t*: triplet; *q*: quartet; *m*: multiplet.

HRESI (High Resolution Electrospray Ionization Mass Spectroscopy) and ESI (Electrospray Ionization Mass Spectroscopy), and APCIMS (Atmospheric-pressure chemical ionization) spectra were recorded on Waters Micromass Q-TOF Micro (Milford, USA) and Agilent Technologies 6120 Quadrupole LC/MS instruments (Milan, Italy), respectively.

Analytical and preparative TLC were performed on silica gel (Merck, Kieselgel 60, F₂₅₄, 0.25 and 0.5 mm respectively Darmstadt, Germany), and on reversed phase (Merck, DC Kieselgel 60 RP-18, F₂₅₄, 0.20 mm) plates. The spots were visualized by exposure to UV radiation (253 nm), or by spraying first with 10% H₂SO₄ in MeOH and then with 5% phosphomolybdic acid in EtOH, followed by heating at 110 °C for 10 min.

Column chromatographic (CC) were performed on silica gel (Merck, Kieselgel 60, 0.063–0.200 mm).

4. EXPERIMENTAL SECTION

4.1. Production, extraction and purification of phytotoxins by *Neofusicoccum australe* strain BOT48.

The fungus was grown in 2 L Erlenmeyer flasks containing 400 mL of Czapek medium amended with corn meal (pH 5.7). Each flask was seeded with 5 mL of a mycelia suspension and then incubated at 25°C for 4 weeks in darkness. The culture filtrates (12 L) were acidified to pH 4 with 2 M HCl and extracted exhaustively with EtOAc. The organic extracts were combined, dried with Na₂SO₄, and evaporated under reduced pressure to give a brown-red oil residue (6 g), having a high phytotoxic activity on grapevine leaves by the puncture leaf bioassay at 4 mg/mL. The residue was submitted to a bioassay-guided fractionation through CC on silica gel eluted with CHCl₃/*i*-PrOH (95:5). Eleven homogenous fraction groups were collected (Scheme 1) and screened for their phytotoxic activity. The residue (154.1 mg) of the fifth fraction, was further purified by CC on silica gel, eluted with petroleum ether/Me₂CO (7:3). The residue (38.4 mg) of the fifth fraction was further purified by TLC on silica gel, eluent *n*-hexane/Me₂CO (7:3) yielding a homogeneous amorphous solid [**1**, 23.7 mg, *R*_f 0.53, eluent *n*-hexane/Me₂CO (7:3) and *R*_f 0.50, eluent CHCl₃/*i*-PrOH (95:5)], which was named cyclobotryoxide. The residue (100.7 mg) of the sixth fraction from the initial column was further purified by CC on silica gel, eluted with CHCl₃/MeOH (97:3). The residue (40.8 mg) of the third fraction was purified by TLC on silica gel, eluent *n*-hexane/Me₂CO (7:3) yielding a further quantity of **1** (8.7 mg, total 5.2 mg/L). The residue (20.1 mg) of the fourth fraction was purified by two successive TLC steps on silica gel, eluted with the CHCl₃/*i*-PrOH (95:5) and EtOAc/*n*-hexane (55:45), yielding a homogeneous amorphous solid identified, as 3-methylcatechol [**3**, 4.4 mg, 0.8 mg/L, *R*_f 0.50 eluent CHCl₃/*i*-PrOH (92:8) and *R*_f 0.61, eluent EtOAc/*n*-hexane (55:45)]. The residue (86.9 mg) of the eighth fraction of the initial column was purified by two successive steps using CC and TLC on silica gel, eluted both with CHCl₃/*i*-PrOH (95:5), yielding a homogeneous amorphous solid identified

as tyrosol [**4**, 1.7 mg, 0.31 mg/L, R_f 0.23 eluent $\text{CHCl}_3/i\text{-PrOH}$ (95:5) and R_f 0.48, eluent $\text{EtOAc}/n\text{-hexane}$ (6:4)].

4.1.1. *Cyclobotryoxide* (**1**)

Cyclobotryoxide (**1**, Figure 2) obtained as homogeneous amorphous solid had: $[\alpha]_D^{25}$ -73 ($c = 0.3$); ECD ($c = 6.5 \times 10^{-4}$ M) $\Delta\epsilon$ -74.4 (310), +14,73 (276); UV λ_{max} nm ($\log \epsilon$) 272 (4.02); $\text{IR}_{\nu_{\text{max}}}$ cm^{-1} 3346, 1712, 1640, 1613, 1462, 1243; ^1H and ^{13}C NMR: Table 6. HRESIMS(+) m/z : 193.1509 [$\text{C}_8\text{H}_{10}\text{O}_4\text{Na}$, calcd. 193.1518, $\text{M}+\text{Na}$] $^+$; ESIMS (-) m/z : 169 [$\text{M}+\text{H}$] $^-$

4.1.2. *3-Methylcatechol* (**3**)

3-Methylcatechol (**3**, Figure 2) obtained as homogeneous amorphous solid had: UV λ_{max} nm ($\log \epsilon$) 292 (3.59); $\text{IR}_{\nu_{\text{max}}}$ cm^{-1} 3318, 1503, 1201; ^1H and ^{13}C NMR were similar to those reported (Ahamad et al., 2001). ESIMS (+) m/z : 147 [$\text{M}+\text{Na}$] $^+$; ESIMS (-) m/z : 123 [$\text{M}-\text{H}$] $^-$.

4.1.3. *Tyrosol* (**4**)

Tyrosol (**4**, Figure 2) obtained as homogeneous amorphous solid had: ^1H NMR was similar to data reported (Capasso et al., 1992). ESIMS (+) m/z : 161 [$\text{M}+\text{Na}$] $^+$; ESIMS (-) m/z : 137 [$\text{M}-\text{H}$] $^-$.

4.1.4. *Acetylation of cyclobotryoxide* (**2**)

Cyclobotryoxide (**1**, 5.0 mg), dissolved in pyridine (30 μL), was converted into the corresponding 5-*O*-acetyl derivative by acetylation with Ac_2O (30 μL) at room temperature for 10 min. The reaction was stopped by addition of MeOH and an azeotrope formed by addition of benzene was evaporated in a N_2 stream. The oily residue (6.0 mg) was purified by TLC on silica gel, eluent $n\text{-hexane}/\text{Me}_2\text{CO}$ (6:4) yielding derivative **2** (Figure 2) as a homogeneous solid (4.1

mg, R_f 0.39). It had: UV λ_{\max} nm ($\log \epsilon$) 272 (3.98); IR ν_{\max} cm^{-1} 1747, 1654, 1624, 1240, 1207; ^1H NMR δ : 6.18 (1H, br s, H-5), 3.76 (3H, s, OCH_3), 3.63 (1H, dd, $J=1.8$ and 1.0 Hz, H-6), 3.50 (1H, d, $J=1.8$ Hz, H-1), 2.19 (3H, s, MeCO), 1.76 (3H, br s, Me); ESIMS (+) m/z : 235 $[\text{M}+\text{Na}]^+$.

4.2. Production, extraction and purification of phytotoxins by *Lasiodiplodia mediterranea* strain BL101.

The fungus was grown as previously reported in paragraph 4.1. In this case, 3L of culture filtrates were acidified to pH 2 with 2 M HCl and extracted as as previously reported in paragraph 4.1. The phytotoxic extract (2.3 g, brown-red oil) of *L. mediterranea* strain BL101, was obtained as previously reported in paragraph 4.1. The residue was submitted to a bioassay-guided fractionation through CC on silica gel, eluted with CHCl₃/*i*-PrOH (95:5). Height homogenous fraction groups were collected (Scheme 2) and screened for their phytotoxic activity. The residue (18.7 mg) of the first fraction was purified by TLC on silica gel eluted with *n*-hexane/Me₂CO (95:5) yielding a uncolored oil identified as (1*R*,2*R*)-methyl ester of jasmonic acid [**11**, Figure 3, 3.4 mg, 1.1 mg/L, *R_f* 0.81 eluent CHCl₃/*i*-PrOH (95:5) and *R_f* 0.13 eluent *n*-hexane/Me₂CO (95:5)]. The residue of the active second fraction (27.7 mg) was purified by TLC on reversed phase eluted with EtOH/H₂O (6:4) to give three main bands. The first band obtained as an uncoloured oil [1.6 mg, 0.6 mg/L, *R_f* 0.30 eluent EtOH/H₂O (6:4)], was characterized as lasiojasmonates B and C (**8** and **9**, Figure 4), obtained as an inseparable mixture. The second band corresponded to another uncolored oil [5.2 mg, 1.7 mg/L, *R_f* 0.40 eluent EtOH/H₂O (6:4)] was characterized as lasiojasmonate A (**5**, Figure 4). The third band corresponded to an amorphous solid [5.2 mg, 1.7 mg/L, *R_f* 0.50 eluent EtOH/H₂O (6:4)], was characterized as 16-*O*-botryosphaerilactone A and C acetylates (**6** and **7**, Figure 3). The residue (587.4 mg) of the third fraction of the original column appeared to be the main metabolite, obtained as a pure yellow oil [*R_f* 0.43 eluent CHCl₃/*i*-PrOH (95:5) and *R_f* 0.50, TLC on reversed phase, eluent EtOH/H₂O (6:4)]. It was identified as (1*R*,2*R*)-jasmonic acid (**10**, Figure 3). The residue (294.4 mg) of the fourth fraction was dissolved in EtOAc and then washed with a saturated solution of NaHCO₃ to remove jasmonic acid (110.3 mg, 236.6 mg/L). The organic phase was dried with Na₂SO₄, and evaporated under reduced pressure affording a brown oil residue (175.8 mg). This residue was further purified by CC on silica gel, eluted with solvent CHCl₃/MeOH (93:7), yielding six

homogeneous fraction groups. The residue (48.3 mg) of the second fraction was purified by TLC on reversed phase eluted with EtOH/H₂O (6:4), yielding an amorphous white solid [6.6 mg, 2.2 mg/L, *R_f* 0.68 eluent EtOH/H₂O (6:4)], which was characterized as (3*R*,4*S*)-botryodiplodin (**14**, Figure 3), and an uncolored oil [27.6 mg, 9.2 mg/L, *R_f* 0.64 eluent EtOH/H₂O (6:4)], which was characterized as botryosphaerilactone A (**12**, Figure 3). The residue (18.3 mg) of the fifth fraction of the same column was purified by TLC on reversed phase eluted with EtOH/H₂O (6:4) yielding a homogeneous amorphous solid [4.4 mg, 1.7 mg/L, *R_f* 0.76 eluent EtOH/H₂O (6:4)], which was identified as the (3*S*,4*R*,5*R*)-4-hydroxymethyl-3,5-dimethyldihydro-2-furanone (**13**, Figure 3).

4.2.1. *Lasiojasmonate A* (**5**)

Compound **5**, obtained as uncolored oil, had: $[\alpha]_D^{25}$ -15 ($c = 0.4$); UV λ_{\max} nm (log ϵ) 204 (3.98); IR ν_{\max} cm⁻¹ 1747, 1695, 1634, 1240, 1207; ¹H and ¹³C NMR spectra: Table 7; HRESIMS (+) m/z : 359.1913 [M+Na]⁺ (calcd. for C₁₉H₂₈NaO₅ 359.1834); APCIMS (+) m/z : 337 [M+H]⁺.

4.2.2. *16-O-Acetylbotryosphaerilactones A and C* (**6** and **7**)

Compounds **6** and **7**, obtained as inseparable mixture and as amorphous solids, had: UV λ_{\max} nm (log ϵ) 203 (4.01); IR ν_{\max} cm⁻¹ 1764, 1731, 1681, 1438, 1379; ¹H NMR: Table 8; ESIMS (+) m/z : 651 [2M+Na]⁺, 314 [M+Na]⁺; APCIMS (+) m/z : 172 [C₉H₁₆O₃]⁺, 145 [C₇H₁₃O₃]⁺, 127 [C₇H₁₁O₂]⁺, 113 [C₇H₁₃O]⁺.

4.2.3. *Lasiojasmonates B and C* (**8** and **9**)

Compounds **8** and **9**, obtained as an inseparable mixture and as uncolored oil, had: UV λ_{\max} nm (log ϵ) 205 (4.00); IR ν_{\max} cm⁻¹ 1765, 1701, 1624, 1238, 1211; ¹H NMR: Table 9; ESIMS (+) m/z : 487.1682 [M+Na]⁺ (calcd. for C₂₆H₄₀NaO₇ 487.2672); APCIMS (+) m/z : 482 [M+H₂O]⁺, 465 [M+H]⁺, 322 [C₁₉H₃₀O₄]⁺, 145 [C₇H₁₃O₃]⁺, 127 [C₇H₁₁O₂]⁺, 113 [C₇H₁₃O]⁺.

4.2.4. (1R,2R)-Jasmonic acid (**10**)

Compound **10**, obtained as yellow oil, had: $[\alpha]_{\text{D}}^{25}$ -75 ($c = 0.3$, MeOH); UV λ_{max} nm (log ϵ) 206 (3.72); IR ν_{max} cm^{-1} 3571, 1749, 1707, 1636, 1259; [lit, Aldridge et al., 1971: $[\alpha]_{\text{D}}^{25}$ -73 ($c = 0.1$, MeOH); lit, Nielsen and Smedsgaard, 2003: UV absorption (nm) in % of UV-max (MeOH) end; lit, Husain et al., 1993: ν_{max} cm^{-1} 1740, 1700]; ^1H and ^{13}C NMR were similar to data previously reported (Husain et al., 1993); ESIMS (+) m/z : 233 $[\text{M}+\text{Na}]^+$; APCIMS (+) m/z : 211 $[\text{M}+\text{H}]^+$.

4.2.5. (1R,2R)-Methyl jasmonate (**11**)

Compound **11**, obtained as uncolored oil, had: $[\alpha]_{\text{D}}^{25}$ -58 ($c = 0.4$); UV λ_{max} nm (log ϵ) 205 (3.67); IR ν_{max} cm^{-1} 1754, 1678, 1426, 1165; [lit, Nishida et al., 1985: $[\alpha]_{\text{D}}^{25}$ -58 ($c = 0.2$, MeOH); lit, Nielsen and Smedsgaard, 2003: UV absorption (nm) in % of UV-max (MeOH) end; lit, Takeda et al., 2006: IR (neat) ν_{max} : 1738, 1438, 1198, 1160 cm^{-1}]; ^1H NMR spectrum was similar to data reported (Takeda et al., 2006); ESIMS (+) m/z : 247 $[\text{M}+\text{Na}]^+$; APCIMS (+) m/z : 225 $[\text{M}+\text{H}]^+$.

4.2.6. Botryosphaerilactone A (**12**)

Compound **12**, obtained as uncolored oil, had: $[\alpha]_{\text{D}}^{25}$ -4.0 ($c = 0.3$, MeOH); UV λ_{max} nm (log ϵ) 209 (3.81); IR ν_{max} cm^{-1} 3458, 1764, 1678, 1613, 1453, 1187; [lit: $[\alpha]_{\text{D}}^{25}$ -1.2 ($c = 0.77$, MeOH); UV (MeOH) λ_{max} (log ϵ) 286 (1.30) nm; IR (neat) ν_{max} 3438, 1770 cm^{-1} (Rukachaisirikul et al., 2009)]; ^1H and ^{13}C NMR were very similar to those reported previously (Rukachaisirikul et al., 2009); ESIMS (+) m/z : 567 $[2\text{M}+\text{Na}]^+$, 295 $[\text{M}+\text{Na}]^+$; ESIMS (-) m/z : 271 $[\text{M}-\text{H}]$; APCIMS (+) m/z : 145 $[\text{C}_7\text{H}_{13}\text{O}_3]^+$, 129 $[\text{C}_7\text{H}_{13}\text{O}_2]^+$, 127 $[\text{C}_7\text{H}_{11}\text{O}_2]^+$, 111 $[\text{C}_7\text{H}_{11}\text{O}]^+$.

4.2.7. (3S,4R,5R)-4-Hydroxymethyl-3,5-dimethyldihydro-2-furanone (**13**)

Compound **13**, obtained as homogeneous amorphous solid, had: $[\alpha]_{\text{D}}^{25}$ -18 ($c = 0.3$); UV λ_{max} final absorption; IR ν_{max} cm^{-1} 3427, 1747, 1635; 1456, 1385, 1183; [lit, Ravi et al., 1979: IR λ_{max} cm^{-1} 3400, 1770; ^1H NMR spectrum was similar to data previously reported]; ^{13}C NMR δ : 179.0 (s, C-

2), 76.1 (d, C-5), 60.7 (t, C-8), 52.7 (d, C-4), 37.6 (d, C-3), 20.1 (q, C-6), 14.2 (q, C-7); ESIMS (+) m/z : 167 [M+Na]⁺; ESIMS (-) m/z : 143 [M-H]⁻.

4.2.8. (3R,4S)-Botryodiplodin (**14**)

Compound **14**, obtained as amorphous white solid, had: UV λ_{\max} nm (log ϵ) 205 (3.92); IR ν_{\max} cm⁻¹ 3457, 1707, 1467, 1343; ¹H NMR was similar to data previously reported (Ramezani et al., 2007); ESIMS (+) m/z : 167 [M+Na]⁺; APCIMS (+) m/z : 145 [M+H]⁺, 127 [M-OH]⁺.

4.2.9. Acetylation of botryosphaerilactone A (**6** and **7**)

Botryosphaerilactone A (**12**, Figure 3, 5.0 mg), was converted into the corresponding 16-*O*-acetyl derivatives by acetylation as previously reported in paragraph 4.1.4. The oily residue (6.0 mg) was purified by TLC on silica gel, eluted with *n*-hexane/Me₂CO (6:4), yielding a mixture of α and β anomers acetyl derivatives [**6** and **7**, Figure 3, 4.1 mg, *R_f* 0.39 eluent *n*-hexane-Me₂CO (6:4)], in a ratio of α/β 90:10.

4.2.10. Acetylation of (3R,4S)-botryodiplodin (**14a**)

(3R,4S)-botryodiplodin (**14**, 2.0 mg) was acetylated with pyridine (35 μ L) and Ac₂O (35 μ L) in the same conditions previously reported (par. 4.1.4). The residue (2.4 mg) was purified by TLC on silica gel, eluent CHCl₃/*i*-PrOH (95:5), to give 2,3-*trans*-botryodiplodin acetate [0.8 mg, *R_f* 0.88 eluent CHCl₃/*i*-PrOH (95:5)], whose physic and spectroscopic data were very similar to those previously reported (Arsenault and Althaus, 1969).

4.2.11. Alkaline hydrolysis of lasiojasmonates A-C

Lasiojasmonate A (**5**, 3.0 mg) was dissolved in MeOH (200 μ L) and H₂O (10 μ L) and hydrolysed with K₂CO₃ (6.0 mg). The mixture was stirred at 60 °C for 2h to the procedure previously reported (Farmer et al., 1992). Then the mixture was diluted with H₂O (2 mL) and

acidified to pH 4.0 with 2 M HCl and extracted with EtOAc (2 mL x3). The organic extracts were combined, dried (Na₂SO₄) and evaporated under reduced pressure. The residue (2.8 mg) was purified by TLC on silica gel, eluent CHCl₃/*i*-PrOH (95:5). Jasmonic acid (0.8 mg) was compared by TLC, OR and ¹H NMR with the authentically sample of (1R,1R)-jasmonic acid. Jasmonates B and C (**8** and **9**) were hydrolyzed in the same conditions used to treat **5**, yielding (1R,1R)-jasmonic acid ascertained as above reported.

4.3. Production, extraction and purification of metabolites by *Lasiodiplodia mediterranea* strain B6.

The fungus was grown in 1L Roux flasks containing 250 mL of Czapek medium amended with 2% corn meal (pH 5.7). Each Roux was inoculated with about 5 mL of a mycelial suspension and incubated at 25°C for 21 days in darkness. The culture filtrates were obtained by sterile-filtering the culture in a vacuum on a 500 ml Stericup (0.45 µm HV Durapore membrane, Millipore) and stored at -20°C

The phytotoxic extract (989.8 mg, brown oil) was obtained as previously reported (par.4.1) from 5 L of culture filtrates and submitted to a bioassay-guided fractionation through CC on silica gel, eluted with CHCl₃/*i*-PrOH (95:5) to give seven homogeneous fractions (Scheme 3). The residue of the second fraction, major bioactive, (603.5 mg) was submitted to CC on silica gel eluted with CHCl₃/*i*-PrOH (95:5) witch afforded six fractions. The third fraction of this column (323.0 mg) was further purified by CC on silica gel eluted with *n*-hexane-EtOAc (1:1) to furnish six homogenous fractions. The residue of the second fraction (150.3 mg)of the last column was purified by preparative TLC on silica gel eluted with CHCl₃/*i*-PrOH (93:7) yieldind two main fractions. The residue of the first fraction (21.3 mg) was further purified by TLC on silica gel eluted with *n*-hexane/Me₂CO (7:3 3x) to give two pure compounds as uncoloured oil [**17**, Figure 5, 5.8 mg/L, R_f0.24 eluent *n*-hexane/Me₂CO (7:3 3x) and R_f0.41 eluent CHCl₃/*i*-PrOH (92:8)] and [**18**, Figure 5, 0.8 mg/L, R_f 0.20 eluent *n*-hexane/Me₂CO (7:3 3x), and R_f 0.35 eluent

CHCl₃/*i*-PrOH (92:8)] identified as botryosphaerodiplodin and (5*R*)-5-hydroxyIASIodiplodin respectively.

The residue of the second fraction (65.3 mg) was subsequently purified by preparative TLC on silica gel eluted with CHCl₃/*i*-PrOH (92:8) yielding a homogeneous amorphous solid [**14**, Figure 5, 6.4 mg/L, *R_f* 0.62 eluent CHCl₃/*i*-PrOH (92:8) and *R_f* 0.76, TLC on reversed phase, eluent EtOH/H₂O (6:4)] identified as (3*R*,4*S*)-botryodiplodin.

The residue of the fourth fraction of the first column (130.5 mg) was purified by preparative TLC on silica gel eluted with CHCl₃/*i*-PrOH (92:8) to give an homogenous oil, [**15** and **16**, Figure 6, 4.5 mg/L, *R_f* 0.31 eluent CHCl₃/*i*-PrOH (92:8) and *R_f* 0.12 eluent *n*-hexane/EtOAc (1:1)] as an inseparable mixture and jasmonic acid [**10**, Figure 5, 3.4 mg/L, *R_f* 0.45 eluent CHCl₃/*i*-PrOH (92:8) and *R_f* 0.50, TLC on reversed phase, eluent EtOH/H₂O (6:4)].

4.3.1. *Lasiolactols A and B (15 and 16)*

Compounds **15** and **16** (Figure 6), obtained as homogenous oil, had: $[\alpha]_D^{25} +9$ ($c = 0.2$); UV λ_{\max} : end absorbtion. IR ν_{\max} cm⁻¹ 3300, 1651, 1637, 1541, 1085; ¹H and ¹³C NMR: Table10.; HRESIMS: Table 11.

4.3.2. *Botryosphaeriodiplodin (17)*

Compound **17** (Figure 5), obtained as uncoloured oil. had: $[\alpha]_D^{25} -12$ ($c = 0.2$); UV λ_{\max} nm (log ϵ) 205 (3.70), 247 (2.61), 283 (2.43); IR ν_{\max} cm⁻¹ 3350, 1697, 1602, 1469, 1273 [lit, Rukachaisirikul et al., 2009: $[\alpha]_D^{26} -9.8$ ($c = 0.7$); UV (MeOH) λ_{\max} nm 205 (3.20), 247 (2.44), 283 (2.19); IR ν_{\max} cm⁻¹ (neat): 3440, 1684]; ¹H and ¹³C NMR were very similar those reported (Rukachaisirikul et al., 2009); ESIMS (+) m/z : 639 [2M+Na]⁺, 347[M+K]⁺, 331 [M+Na]⁺, 309 [M+H]⁺.

4.3.3. *(5R)-5-HydroxyIASIodiplodin (18)*

Compound **18** (Figure 5), obtained as uncolored oil, had: $[\alpha]_{\text{D}}^{25}$ -12 ($c = 0.2$); UV λ_{max} nm 205 (3.70), 247 (2.61), 283 (2.43); IR ν_{max} cm^{-1} 3350, 1697, 1602, 1469, 1273 [lit, Rukachaisirikul et al., 2009]; $[\alpha]_{\text{D}}^{26}$ -9.8 ($c = 0.7$); UV (MeOH) λ_{max} nm 204 (3.20), 245 (2.44), 284 (2.19); IR ν_{max} cm^{-1} 3440, 1684; ^1H and ^{13}C NMR were very similar those reported (Rukachaisirikul et al., 2009); ESIMS(+) 639 $[\text{M}+\text{Na}]^+$, 347 $[\text{M}+\text{K}]^+$, 331 $[\text{M}+\text{Na}]^+$, 309 $[\text{M}+\text{H}]^+$.

4.3.4. Methylation of botryodiplodin

At botryodiplodin (**17**, 3.7 mg) dissolved in MeOH (1.0 mL) was added an ethereal solution of CH_2N_2 . The reaction mixture was left at room temperature for 6 h. The solvent was evaporated under a N_2 stream giving a oil residue (3.8 mg). This latter was purified by preparative TLC on silica gel eluted with $\text{CHCl}_3/i\text{-PrOH}$ (95:5) to give 13-*O*-methylbotryosphaeriodiplodin (**19**, Figure 7, 3.5 mg, R_f 0.69 eluent $\text{CHCl}_3/i\text{-PrOH}$ (95:5) as uncolored oil. It had: UV λ_{max} nm ($\log \epsilon$) 206 (3.13), 249 (2.52), 282 (2.29); IR ν_{max} cm^{-1} 3370, 1715, 1700, 1697, 1451, 1260; ^1H NMR: Table 12; ESIMS (+) m/z 361 $[\text{M}+\text{K}]^+$, 345 $[\text{M}+\text{Na}]^+$, 323 $[\text{M}+\text{H}]^+$.

4.3.5. 7-*O*-(*S*)- α -Methoxy- α -trifluoromethyl- α -phenylacetate (MTPA) ester of 13-*O*-Methylbotryosphaeriodiplodin (**20**)

(*R*)-(-)-MPTA-Cl (20 μL) was added to **19** (1.0 mg) dissolved in dry pyridine (20 μL). The reaction was stirred at room temperature over night, and then stopped by adding MeOH. Pyridine was removed by a N_2 stream. The residue (7.3 mg) was purified by preparative TLC on silica gel eluted with $\text{CHCl}_3/i\text{-PrOH}$ (98:2) to give 7-*O*-(*S*)- α -methoxy- α -trifluoromethyl- α -phenylacetate ester of **19** (**20**, Figure 7, 0.9 mg, R_f 0.66 eluent $\text{CHCl}_3/i\text{-PrOH}$ (98:2) as homogeneous oil. It had: UV λ_{max} nm ($\log \epsilon$) 206 (3.58), 249 (2.42), 282 (2.16); IR ν_{max} cm^{-1} 1742, 1646, 1453, 1257, 1154; ^1H NMR: Table 12; ESIMS (+) m/z 577 $[\text{M}+\text{K}]^+$, 561 $[\text{M}+\text{Na}]^+$, 539 $[\text{M}+\text{H}]^+$.

4.3.6. 7-O-(R)- α -Methoxy- α -trifluoromethyl- α -phenylacetate (MPTA) ester of 13-O-Methylbotryosphaeriodiplodin (**21**)

(S)-(+)-MPTA-Cl (20 μ l) was added to **19** (1.0 mg) dissolved in dry pyridine (20 μ l). The reaction was carried out under the same conditions used for preparing **20** from **19**. The residue (8.1 mg) was purified by preparative TLC on silica gel eluted with CHCl₃/*i*-PrOH (98:2) to give 7-O-(R)- α -methoxy- α -trifluoromethyl- α -phenylacetate ester of **19** (**21**, Figure 7, 1.2 mg, *R_f* 0.66 eluent CHCl₃/*i*-PrOH (98:2) as homogeneous oil. It had: UV λ_{\max} nm (log ϵ) 206 (3.56), 250 (2.40), 281 (2.16); IR ν_{\max} cm⁻¹ 1751, 1587, 1461, 1265, 1168; ¹H NMR: Table 12; ESIMS (+) *m/z* 577 [M+K]⁺, 561 [M+Na]⁺, 539 [M+H]⁺.

4.4. Production, extraction and purification of phytotoxins by *N. australe* strain BL24

The fungus was grown as previously reported in paragraph 4.1. The phytotoxic extract (400 mg, brown oil) was obtained as previously reported (par.4.1) from 7 L of culture filtrates and submitted to a bioassay-guided fractionation through CC on silica gel, eluted with CHCl₃/*i*-PrOH (95:5) to give ten homogeneous fractions (Scheme 4). The residue (11.3 mg) of sixth fraction, was purified by TLC on silica gel, eluent CHCl₃/*i*-PrOH (95:5), yielding a homogeneous amorphous solid identified as tyrosol [**4**, Figure 8, 2.8 mg, 0.4 mg/L *R_f* 0.23 eluent CHCl₃/*i*-PrOH (95:5), *R_f* 0.48 eluent EtOAc/*n*-hexane (6:4)]. The residue (20.6 mg) of the seventh fraction was further purified by two successive steps by TLC on silica gel, eluent CHCl₃/*i*-PrOH (95:5) and by reversed phase TLC, eluent EtOH/H₂O (6:4), yielding two homogeneous amorphous solids identified as botryosphaerone D [**22**, Figure 8, mg 4.8, 0.7 mg/L *R_f* 0.24 eluent CHCl₃/*i*-PrOH (95:5) and *R_f* 0.56, TLC on reversed phase, eluent EtOH/H₂O (6:4)] and (3*S*,4*S*)-3,4,8-trihydroxy-6-methoxy-3,4-dihydro-1(2*H*)-naphthalenone [**23**, Figure 8, 1.5 mg, 0.2 mg/L, *R_f* 0.24 eluent CHCl₃/*i*-PrOH (95:5) and *R_f* 0.65, TLC on reversed phase, eluent EtOH/H₂O (6:4)].

4.4.1. *Botryosphaerone D (22)*

Botryosphaerone D, obtained as homogeneous amorphous solid, had: $[\alpha]_{\text{D}}^{25} +18$ ($c = 0.2$); ECD ($c = 5.16 \cdot 10^{-4}$ M) $\Delta\epsilon$: +17.7 (286), +8.5 (239), -46.2 (214); UV (CH₃OH) λ_{max} nm (log ϵ): 222 (4.27), 288 (4.19); IR ν_{max} cm⁻¹ 3307, 1622, 1310, 1126; [for the botryosphaerone D (Xu et al., 2011), $[\alpha]_{\text{D}}^{25} +13$ (c 2.0, MeOH); UV (MeOH) λ_{max} nm (log ϵ): 230 (2.19), 297 (2.78); IR (KBr) ν_{max} cm⁻¹ 3428, 1626, 1311, 1126]; ¹H and ¹³C NMR data were very similar to those already report (Xu et al., 2011); ESIMS (-) m/z : 251 [M-H]⁻, 233 [M-H₂O-H]⁻, APCIMS (+) m/z : 253 [M+H]⁺.

4.4.2. *3,4,8-Trihydroxy-6-methoxy-3,4-dihydro-1(2H)-naphthalenone (23)*

The compound **23**, obtained as homogeneous amorphous solid, had: $[\alpha]_{\text{D}}^{25} +53$ ($c = 0.2$); ECD ($c = 5.8 \cdot 10^{-4}$ M) $\Delta\epsilon$: +11.1 (280), +7.6 (238), -38.6 (214); UV (MeOH) λ_{max} nm (log ϵ): 214 (4.26), 230 (4.09), 238 (4.04), 280 (4.14), 317 (3.79); IR ν_{max} cm⁻¹ 3384, 1739, 1625, 1362, 1169; [lit, Pittayakhajonwut et al., 2008: $[\alpha]_{\text{D}}^{25} +49.38$ ($c = 0.048$, MeOH); UV (MeOH) λ_{max} nm (log ϵ): 216 (4.21), 230 (4.04); 237 (3.95), 281 (4.10), 321 (3.82); IR (KBr) ν_{max} cm⁻¹ 3494, 3405, 2958, 2927, 2855, 1729, 1636, 1578, 1459, 1432, 1403, 1375, 1360, 1291, 1164, 1128, 1075, 1031, 843); ¹H and ¹³C NMR data very similar to those already report]; ESIMS (-) m/z : 223 [M-H]⁻, 207 [M-OH]⁻, APCIMS (+) m/z : 225 [M+H]⁺.

4.5. Production, extraction and purification of phytotoxins by *Diplodia quercivora* strain BL9.

The fungus was grown as previously reported in paragraph 4.1. The phytotoxic extract (11.5 g, brown-red oil) of *D. quercivora* strain BL9, was obtained as previously reported in paragraph 4.1 from 21.6 L of culture filtrate. The residue was submitted to a bioassay-guided fractionation through CC on silica gel, eluted with *n*-hexane/Me₂CO (8:2). Eight homogeneous fraction groups were collected (Scheme 5). The residue of the third fraction (1.03 g) was purified by CC on silica gel eluted with CHCl₃/*n*-hexane/Me₂CO (4.5:4.5:1) yielding five homogeneous fractions. The residue of the third fraction of this column (323.0 mg) was crystallized with

EtOAc/*n*-hexane (1:5) to give white crystals, which being a new compound was named diplopimarane [24, Figure 9, 142.7 mg, 6.6 mg/L, *R_f* 0.7 eluent *n*-hexane/EtOAc (7:3)]. The residue of the fourth fraction of the first column (2.938 g) was crystallized with EtOAc/*n*-hexane (1:5) to give sphaeropsidin A [32, Figure 10, 2.081 g, *R_f* 0.5 eluent *n*-hexane/Me₂CO (7:3) and *R_f* 0.7 eluent *n*-hexane/EtOAc (6:4)] as white crystals. The residue of the fifth fraction of the same CC (2.567 g) was purified by CC on silica gel eluted with CHCl₃/*i*-PrOH (95:5) yielding five homogeneous fractions. The residue of the second fraction of the last CC (421.8 mg) was crystallized with EtOAc/*n*-hexane (1:5) giving further quantities of sphaeropsidin A (278.7 mg). The residue of the fourth fraction (689.1 mg) was purified by CC on silica gel, eluent *n*-hexane/EtOAc/ Me₂CO (6:2.5:1.5) giving three main metabolites as white solids identified as (+)-epiepoformin [34, Figure 10, 301.2 mg, 13.9 mg/L, *R_f* 0.42 eluent *n*-hexane/EtOAc/ Me₂CO (6:2.5:1.5) and *R_f* 0.44 eluent *n*-hexane/EtOAc (6:4)], sphaeropsidin C [33, Figure 10, 53.3 mg, 2.46 mg/L, *R_f* 0.52 eluent *n*-hexane/EtOAc/ Me₂CO (6:2.5:1.5) and *R_f* 0.63 eluent *n*-hexane/EtOAc (6:4)] and a further quantity of sphaeropsidin A (32, 203.2 mg, total yield 119.0 mg/L).

4.5.1. Diplopimarane (24)

Compound 24, obtained as white crystals, had: Mp 136 °C; [α]_D²⁵ +25.8 (*c* = 0.6); UV λ_{\max} nm (log ϵ) 285 (3.34), 228 sh (3.90); IR ν_{\max} cm⁻¹ 3497, 3457, 3239, 1609, 1571, 1440, 1342, 1289, 1205; ¹H and ¹³C NMR: Table 13; HRESIMS (+) spectrum *m/z*: 325.1785 [C₁₉H₂₆O₃Na, calcd. 325.1780, M+Na]⁺; ESIMS (+) *m/z*: 623 [2M-4H+Na]⁺, 339 [M-2H+K]⁺, 325 [M+Na]⁺, 323 [M-2H+Na]⁺; ESIMS(-) *m/z*: 301 [M-H]⁻; APCIMS (+) *m/z*: 285 [M-OH+H]⁺, APCIMS (-) *m/z*: 301 [M-H]⁻.

4.5.2. 6-O-Methyl and 6,7-O,O'-Dimethyldiplopimarane (**25** and **26**).

To compound **24** (12.0 mg) dissolved in MeOH (1.5 mL), was slowly added an ethereal solution of CH₂N₂ until a yellow color was persistent. The reaction mixture was left at room temperature for 78h. The solvent was evaporated under a N₂ stream giving a oil residue (12.4 mg). This latter was purified by preparative TLC on silica gel, eluent *n*-hexane/EtOAc (8:2) to give **25** and **26** as uncoloured oils (3.5 and 3.9 mg, R_f 0.3 and 0.5, respectively). 6-O-methyldiplopimarane (**25**, Figure 9) had: UV λ_{max} nm (log ε) 227sh (3.80), 281 (3.35); IR ν_{max} cm⁻¹ 3502, 1731, 1640, 1429; ¹H NMR: Table 14; ESIMS (+) *m/z* 655 [2M+Na]⁺, 355 [M+K]⁺, 339 [M+Na]⁺; APCIMS (-) *m/z* 315 [M-H]⁻, 301 [M-Me]⁻. 6-O-O-dimethyldiplopimarane (**26**, Figure 9) had: UV λ_{max} nm (log ε) 228 sh (3.00), 280 (3.02); IR ν_{max} 3497, 1730, 1628, 1576, 1451 cm⁻¹; ¹H NMR: Table 14; ESIMS (+) *m/z* 369 [M+K]⁺, 353 [M+Na]⁺; APCIMS (+) *m/z* 331 [M+H]⁺.

4.5.3. 6,7,14-O,O',O''-Triacetyldiplopimarane (**27**)

Diplopimarane **24** (2.3 mg), dissolved in pyridine (30 μL), was converted into the corresponding 6,7,14-O,O',O''-triacetyl derivative (**27**, Figure 9) by acetylation with Ac₂O (30 μL) at room temperature for 1 h. The reaction was workup as previously reported (par. 4.3.4.). The oily residue (2.5 mg) was purified by TLC on silica gel, *n*-hexane/EtOAc (8:2) yielding derivative **27** [1.0 mg, R_f 0.6 eluent *n*-hexane/EtOAc (8:2)] as a uncolored oil. Triacetyldiplopimarane had: UV λ_{max} nm (log ε) 222 sh (3.81), 271 (3.43); IR ν_{max} cm⁻¹ 1773, 1725, 1626, 1423, 1374; ¹H NMR: Table 14; ESIMS (+) *m/z* 467 [M+K]⁺, 451 [M+Na]⁺; APCIMS (+) *m/z* 429 [M+H]⁺.

4.5.4. 6-O-*p*-Bromobenzoyl Ester of Diplopimarane (**28**)

To diplopimarane **24** (5.0 mg), dissolved in CH₃CN (750 μL), DMAP (7.3 mg) and *p*-bromobenzoyl chloride (7.0 mg) were added. The reaction mixture was stirred at room temperature for 2 h, and then evaporated under reduced pressure. The residue (20.0 mg) was purified by TLC on silica gel, eluent CHCl₃/*i*-PrOH (97:3) giving **28** [Figure 9, 1.0 mg, R_f 0.8

eluent $\text{CHCl}_3/i\text{-PrOH}$ (97:3)] as uncoloured oil. It had: UV λ_{max} nm (log ϵ) 203 (3.57), 245 (3.65), 280 (3.31); IR ν_{max} cm^{-1} 3464, 3406, 1727, 1583, 1437, 1269, 1010; ^1H NMR: Table 14; ESIMS (+) m/z 525 $[\text{M}+2+\text{K}]^+$, 523 $[\text{M}+\text{K}]^+$, 509 $[\text{M}+2+\text{Na}]^+$, 507 $[\text{M}+\text{Na}]^+$; ESIMS (-) m/z 485 $[\text{M}+2-\text{H}]^-$, 483 $[\text{M}-\text{H}]^-$, 301 $[\text{M}-p\text{-BrC}_6\text{H}_4\text{-CO}]^-$; APCIMS (+) m/z 469 $[\text{M}+2+\text{H}-\text{H}_2\text{O}]^+$, 467 $[\text{M}+\text{H}-\text{H}_2\text{O}]^+$, 285 $[\text{M}-p\text{-BrC}_6\text{H}_4\text{CO}_2]^+$; APCIMS (-) m/z 485 $[\text{M}+2-\text{H}]^-$, 483 $[\text{M}-\text{H}]^-$, 285 $[\text{M}-p\text{-BrC}_6\text{H}_4\text{-CO}_2]^+$, 314 $[\text{M}-p\text{-BrC}_6\text{H}_4]^-$; 301 $[\text{M}-p\text{-BrC}_6\text{H}_4\text{-CO}]^-$.

4.5.5. 15,16-Dihydrodiplopimarane (29)

Diplopimarane **24** (5.8 mg) dissolved in MeOH (200 μL) was added to a presaturated suspension of 10% Pd/C in MeOH (600 μL). Hydrogenation was carried out at room temperature and atmospheric pressure with continuous stirring over night. The reaction was stopped by filtration, and the clear solution evaporated under a N_2 stream. The residue (6.1 mg) was purified by preparative TLC on silica gel, eluted with *n*-hexane/EtOAc (8:2), to yield 5.0 mg of **29** (Figure 9) as yellow oil [R_f 0.7 eluent *n*-hexane/EtOAc (8:2)]. It had: UV λ_{max} nm (log ϵ) 225 sh (3.81), 312 (3.38); IR ν_{max} cm^{-1} 3643, 3239, 3498, 1728, 1691, 1556, 1456; ^1H NMR: Table 14; ESIMS (+) m/z 595 $[2\text{M}-2\text{H}_2\text{O}+\text{Na}]^+$, 309 $[\text{M}-\text{H}_2\text{O}+\text{Na}]^+$, 287 $[\text{M}-\text{H}_2\text{O}+\text{H}]^+$.

4.5.6. 14-O-(S)- α -Methoxy- α -trifluoromethyl- α -phenylacetate (MTPA) ester of 6,7-O,O'-Dimethyldiplopimarane (30)

(R)-(-)-MPTA-Cl (20 μL) was added to **26** (1.5 mg) dissolved in dry pyridine (20 μL). The reaction was stirred at room temperature for 2 h and then stopped by adding MeOH. Pyridine was removed by a N_2 stream. The purification of the crude residue (7.3 mg) by preparative TLC on silica gel, eluted with *n*-hexane/EtOAc (9:1) gave **30** (Figure 11) as homogeneous oil [0.7 mg, R_f 0.83 eluent *n*-hexane/EtOAc (9:1)]. It had: UV λ_{max} nm (log ϵ) 207 (3.98), 233 (4.22), 281

(3.16); IR ν_{\max} cm^{-1} 1742, 1646, 1453, 1257, 1154; ^1H NMR: Table 15; ESIMS (+) m/z 569 $[\text{M}+\text{Na}]^+$, 585 $[\text{M}+\text{K}]^+$.

4.5.7. *14-O-(R)- α -Methoxy- α -trifluoromethyl- α -phenylacetate (MTPA) ester of 6,7-O'-Dimethyldiplopimarane (31)*

(S)-(+)-MPTA-Cl (20 μl) was added to **26** (1.5 mg) dissolved in dry pyridine (20 μl). The reaction was carried out under the same conditions used for preparing **30** from **26**. The purification of the crude residue (8.1 mg) by preparative TLC on silica gel, eluted with *n*-hexane/EtOAc (9:1) gave **31** (Figure 11) as homogeneous oil [1.2 mg, R_f 0.83 *n*-hexane/EtOAc (9:1)]. It had: UV λ_{\max} nm (log ϵ) 208 (3.98), 231 (4.22), 281 (3.16); IR ν_{\max} cm^{-1} 1751, 1649, 1461, 1265, 1168; ^1H NMR: Table 15; ESIMS (+) m/z 569 $[\text{M}+\text{Na}]^+$, 585 $[\text{M}+\text{K}]^+$.

4.5.8. *Conversion of Sphaeropsidin A into Diplopimarane.*

Within a solution of sphaeropsidin A (60 mg) in dry MeOH (30 mL) at 0 $^\circ\text{C}$, gaseous HCl, generated *in situ* by reaction of 96% H_2SO_4 and NaCl, was gurgled. The reaction was stopped after 12 h by neutralization with 1N NaOH. The solution was extracted with EtOAc (3x 50 mL) and the organic extracts combined, dried and evaporated under reduced pressure. The residue (58 mg) was purified by TLC on silica gel eluent *n*-hexane/EtOAc (7:3), giving the mixture of **24** and its C-14 epimer (16.3 mg) as the main product.

4.5.9. *Sphaeropsidin A and C (32 and 33).*

The ^1H and ^{13}C NMR and optical properties, recorded in the same condition were identical to those previously reported (Evidente et al., 1996 and 1997). Sphaeropsidin A had: ESIMS (+) m/z 715 $[2\text{M}+\text{Na}]^+$; 369 $[\text{M}+\text{Na}]^+$; ESIMS (-) m/z 345 $[\text{M}-\text{H}]^-$; APCIMS (+) m/z 347 $[\text{M}+\text{H}]^+$; APCIMS (-) m/z 345 $[\text{M}-\text{H}]^-$. Sphaeropsidin C had: ESIMS (+) m/z 371 $[\text{M} + \text{K}]^+$; 355 $[\text{M} +$

Na]⁺; ESIMS (-) m/z 331 [M-H]⁻; APCIMS (+) m/z 333 [M+H]⁺; 315 [M-OH]⁺; APCIMS (-) m/z 331 [M-H]⁻.

4.5.10. (+)-*Epiepoformin* (**34**)

Compound **34**, obtained as white amorphous solid, had: $[\alpha]_D^{25}$ +243 (c = 0.4, EtOH); ECD (c = 0.01, EtOH): $[\theta]^{25}$ +6100 (340), +220 (282), 12,530 (254); UV λ_{\max} nm (log ϵ) 210 (3.49), 238 (3.51); IR ν_{\max} cm⁻¹ 3408, 1664, 1439, 1371, 1271, 1033; [lit, Nagasawa et al., 1978]: IR ν_{\max} cm⁻¹: 3440 (OH), 1668 (C-O), 1282, 1042 (C-O), 830, 727. UV (EtOH) λ_{\max} nm (log ϵ): 237 (3.65); λ_{\max} 10 % NaOH in EtOH nm (log ϵ): 232sh (3.82), 262 (3.53), 324sh (2.94). CD (c = 0.01, dioxane) $[\theta]^{25}$ (nm): 0 (385), +6300 (340), +140 (282), +11,600 (254); MS m/z 140.0448 (M⁺, 140.0472 calcd for C₇H₈O₈), 112, 111, 97, 83, 71]; ESIMS (-) m/z 139 [M-H]⁻; APCIMS (-) m/z 139 [M-H]⁻.

4.5.11. Crystal Structure Determination of *Diplopimarane* (**24**)

Yellow, block-shaped single crystals of **24** were obtained by slow evaporation of a EtOAc-*n*-hexane (1:3) solution at ambient temperature. X ray data collection was performed at 298 K on a Bruker-Nonius Kappa CCD diffractometer equipped with graphite-monochromated MoK_α radiation (λ = 0.71073 Å, CCD rotation images, thick slices, φ and ω scans to fill asymmetric unit). Unit cell parameters were obtained from a least-squares fit of the θ angles of 79 reflections in the range $4.217^\circ \leq \theta \leq 19.663^\circ$. A semiempirical absorption correction (multiscan, SADABS) was applied. The structure was solved by direct methods using SIR97 package (Altomare et al., 1999) and refined by the full matrix least-squares method on F² against all independent measured reflections using SHELX97 software package (Sheldrick et al., 2008). All non-hydrogen atoms were refined anisotropically. Hydroxy hydrogen atoms were found in difference Fourier maps, all the other H atoms were placed in calculated positions and refined according to a riding model (C-H in the 0.93-0.96 Å range; $U_{\text{iso}}(\text{H}) = 1.2 \cdot U_{\text{eq}}(\text{C}_{\text{Ar}})$, $U_{\text{iso}}(\text{H}) =$

1.5·Ueq (C_{Me}) of the carrier atom). The final refinement converged to $R1 = 0.0591$, $wR2 = 0.1372$ for 2495 observed reflections having $I > 2\sigma(I)$. Minimum and maximum residual electronic density was -0.314 and $0.366 \text{ e}\text{\AA}^{-3}$. Crystal data for **24**: empirical formula: $C_{19}H_{26}O_3$; formula weight $302.40 \text{ g mol}^{-1}$; crystal system: monoclinic; space group: $P 2_1$; unit cell dimensions: $a = 6.0156(7)$, $b = 8.8811(11)$, $c = 15.2432(10)\text{\AA}$, $\beta = 95.315(7)^\circ$; reflections collected/unique: 8445/3426 [$R(\text{int}) = 0.0390$]; data/restraints/parameters: 3426/1/211; goodness of fit on F^2 : 1.077 ; final R indices [$I > 2\sigma(I)$]: $R1 = 0.0591$, $wR2 = 0.1372$; R indices (all data): $R1 = 0.0907$, $wR2 = 0.1528$; largest diff. peak and hole ($\text{e}/\text{\AA}^3$): 0.366 and -0.314 .

4.6. Production, extraction and purification of oxysporone (35)

Oxysporone (**35**, Figure 12) was isolated from culture filtrate of *D. africana* strain DA1 grown on a mineral defined liquid media named M1-D (Pinkerton and Strobel, 1976) as recently reported in details (Evidente et al., 2012). The purification of the organic extract obtained by its culture filtrate (12 L), carried out as previously described (Evidente et al., 2012), allowed to obtain oxysporone (**35**) as homogeneous oils (357.6 mg, 29.7 mg/L).

4.6.1 Preparation of oxysporone derivatives

4.6.2. 4-O-Acetyloxysporone (38)

Oxysporone (**35**, 30.5 mg), dissolved in pyridine (60 μL), was converted into the corresponding 4-O-acetyl derivative (**38**) by acetylation with Ac_2O (60 μL) at room temperature for 2 h. The reaction was workup as previously reported (par.4.3.4.). The oily residue (38.2 mg) was purified by TLC on silica gel, eluent $\text{CHCl}_3/i\text{-PrOH}$ (95:5), yielding derivative **38** [Figure 13, 25.8 mg, R_f 0.7 eluent $\text{CHCl}_3/i\text{-PrOH}$ (95:5)] as a homogeneous oil. It had: UV λ_{max} nm ($\log \epsilon$) 206 (3.00); IR ν_{max} cm^{-1} 1789, 1731, 1652, 1230 1011; ^1H NMR: Table 16; ESIMS (+) m/z 221 $[\text{M}+\text{Na}]^+$.

4.6.3. 2,3-Dihydrooxysporone (39)

Oxysporone (**35**, 15.0 mg), dissolved in MeOH (750 μ L), was added to a presaturated suspension of Pt (5%) in MeOH (750 μ L). Hydrogenation was carried out at room temperature and atmospheric pressure under stirred conditions. After 4 h the reaction was stopped by filtration and the clear solution then evaporated under reduced pressure. The residue (17.4 mg) purified by preparative TLC on silica gel, eluent CHCl₃/*i*-PrOH (93:7), giving **39** [Figure 13, 11.0 mg, *R_f* 0.3 eluent CHCl₃/*i*-PrOH (93:7)] as homogeneous solid. It had: UV λ_{\max} nm (log ϵ): 205 (2.91); IR ν_{\max} cm⁻¹ 3426, 1767, 1165; ¹H NMR: Table 16; ESIMS (+) *m/z*: 339 [2M+Na]⁺, 181 [M+Na]⁺.

4.6.4. 4,0-Dehydrooxysporone (**40**)

To oxysporone (**35**, 15.1 mg), dissolved in CH₂Cl₂ (3.0 mL), Corey's reagent (Corey and Suggs, 1975) (75.1 mg) was added and the reaction mixture was stirred at room temperature for 1 h. The reaction was then stopped by filtration on a glass fennel and the clear solution obtained evaporated under reduced pressure. The residue (36.5 mg) purified by preparative TLC on silica gel, eluent CHCl₃/*i*-PrOH (93:7), giving **40** [Figure 13, 4.3 mg, *R_f* 0.36 eluent CHCl₃/*i*-PrOH (93:7)] as a homogeneous solid. It had: UV λ_{\max} nm (log ϵ) 205 (3.77); IR ν_{\max} cm⁻¹ 1794, 1738, 1681, 1005; ¹H NMR: Table 16; APCIMS (+) *m/z*: 155 [M+H]⁺; APCIMS (-) *m/z*: 153 [M-H]⁻.

4.6.5. 4-*O*-*p*-Bromobenzoyloxysporone (**41**)

To oxysporone (**35**, 10.0 mg) dissolved in CH₃CN (1.0 mL), DMAP (23.0 mg) and *p*-bromobenzoyl chloride (25.0 mg) were added. The reaction mixture was stirred at room temperature for 4 h, and then evaporated under reduced pressure. The residue (43.2 mg) was purified by TLC on silica gel, eluent CHCl₃/*i*-PrOH (97:3), giving **41** [Figure 13, 10.6 mg, *R_f* 0.8, eluent CHCl₃/*i*-PrOH (97:3)] as a white solid. It had: UV λ_{\max} nm (log ϵ): 203 (4.42), 245 (4.28); IR ν_{\max} cm⁻¹ 1798, 1715, 1655, 1619, 1266, 1013; ¹H NMR: Table 16; ESIMS (+) *m/z*: 378

$[M+2+K]^+$, 376 $[M+K]^+$, 362 $[M+2+Na]^+$, 360 $[M+Na]^+$; ESMS (-) m/z 338 $[M+2-H]^-$, 336 $[M-H]^-$, 201 $[p\text{-BrC}_6\text{H}_4\text{-CO}_2+2]^-$, 199 $[p\text{-BrC}_6\text{H}_4\text{-CO}_2]^-$.

4.6.6. 2-(4-Pyronyl)acetic acid (42)

To oxysporone (**35**, 10.0 mg), dissolved in Me₂CO (2.0 mL), at 0 °C, Jones's reagent (Bowers et al., 1953) was added under stirring until to have a orange supernatant. After 10 min the reaction was stopped by addition of *i*-PrOH and ice. The suspension was diluted with iced H₂O to obtain a brilliant green solution, which was extracted with EtOAc (3x 2mL). The organic extracts were combined, dried (Na₂SO₄), filtered and evaporated under reduced pressure. The residue (33.1 mg) was purified by TLC on reverse phase, eluent MeOH/H₂O (1:1), giving **42** [Figure 13, 4.1 mg, *R_f* 0.78 eluent MeOH/H₂O (1:1)] as amorphous solid. It had: UV λ_{max} nm (log ϵ): 204 (3.56), 251 (3.51); IR ν_{max} cm⁻¹ 3400, 1740, 1653, 1082; [lit, Nagata and Ando, 1989: ν_{max} (KBr)/cm⁻¹ 3600-3300, 1725 and 1638]; ¹H NMR was similar to that previously reported in D₂O (Salvatore et al., 1994). ¹H NMR: Table 16; ESIMS (+) m/z 177 $[M+Na]^+$; APCIMS (+) m/z 155 $[M+H]^+$; APCIMS (-), m/z 153 $[M-H]^-$.

4.6.7. 4-O-Acetyl-2,3-dihydrooxysporone (43)

Compound **38** (15.0 mg) dissolved in MeOH (750 μ L), was added to a presaturated suspension of Pt (5%) in MeOH (750 μ L). Hydrogenation was carried out at room temperature and atmospheric pressure under stirred conditions. After 5 h the reaction was stopped by filtration and clear solution was then evaporated under reduced pressure. The residue (18.5 mg) was purified by preparative TLC on silica gel, eluent CHCl₃/*i*-PrOH (97:3), giving **43** [Figure 13, 8.1 mg *R_f* 0.4 eluent CHCl₃/*i*-PrOH (97:3)] as a homogeneous solid. It had: UV λ_{max} nm (log ϵ): 203 (4.01); IR ν_{max} cm⁻¹ 1733, 1243; ¹H NMR: Table 16; ESIMS (+) m/z 223 $[M+Na]^+$.

4.6.8. 2-(2,3-Dihydro-4-pyronyl)acetic acid (44)

To compound **39** (5.0 mg) in Me₂CO (1.0 mL), at 0 °C, Jones's reagent (Bowers et al., 1953) was added under stirring as previously reported to convert **35** into **42**. The residue (13.2 mg) of the work-up reaction was purified by TLC on reverse phase, eluent MeOH/H₂O (1:1), giving **44** [Figure 13, 1.4 mg, *R_f* 0.70 eluent MeOH/H₂O (1:1)] as amorphous solid. It had: UV λ_{\max} nm (log ϵ): 268 (3.72); IR ν_{\max} cm⁻¹ 3416, 1725, 1659, 1612, 1601; [lit, Scott et al., 1972: λ_{\max} (EtOH) 267 nm (ϵ 7960); IR ν_{\max} (CHCl₃) 3510, 1718, 1672, 1621]; ¹H NMR: Table 16; ESIMS (+) *m/z* 179 [M+Na]⁺; ESIMS (-) *m/z* 155 [M-H]⁻; APCIMS (+) *m/z* 157 [M+H]⁺; APCIMS (-) *m/z* 155 [M-H]⁻.

4.6.9. Methyl ester of 2-(4-pyronyl)acetic acid (**45**)

To compound **42** (2.5 mg) dissolved in MeOH (1.0 mL), was slowly added an ethereal solution of CH₂N₂ until a yellow colour was persistent. The solvent was evaporated under a N₂ stream and the residue (3.1 mg) purified by preparative TLC on silica gel, eluent CHCl₃/*i*-PrOH (93:7), giving **45** [Figure 13, 1.2 mg, *R_f* 0.5 eluent CHCl₃/*i*-PrOH (93:7)] as a white solid. It had: UV λ_{\max} nm (log ϵ): 205 (2.91), 248 (2.95); IR ν_{\max} cm⁻¹ 1731, 1650, 1610, 1438; ¹H NMR: Table 16; ESIMS (+) *m/z* 191 [M+Na]⁺; APCIMS (+) *m/z* 169 [M+H]⁺, 137 [M+CH₃O]⁺.

4.7. Biological assays

4.7.1. Phytotoxic activity

Phytotoxic activity was tested on weedy plants: *Quercus ilex* L., *Quercus suber* L., *Vitis vinifera* L., and *Lycopersicon esculentum* L. The culture filtrates were assayed as such as. Organic extracts, chromatographic fractions and pure compounds were tested in a range of concentration from 4 to 0.1 mg/mL. Samples were dissolved in a small amount of MeOH and diluted with distilled H₂O up to the assay concentrations (the final content of MeOH was 4%).

4.7.1.1. Leaf puncture assays

Young holm oak, cork oak and tomato leaves were utilized for this assay. Compounds were first dissolved in MeOH, and then a stock solution with sterile distilled water was made. A droplet (20 µL) of test solution was applied on the adaxial sides of leaves that had previously been needle punctured. Droplets (20 µL) of MeOH in distilled water (4%) were applied on leaves as control. Each treatment was repeated three times. The leaves were kept in a moist chamber to prevent the droplets from drying. Leaves were observed daily and scored for symptoms after 7 days. The effect of the samples on the leaves, consisting in necrotic spots surrounding the puncture, were observed up to 15 days after droplet application. Lesions were estimated using APS Assess 2.0 software (Lamari, 2002) following the tutorials in the user's manual. The lesion size was expressed in mm².

4.7.1.2. Cutting assays

Detached leaves of grapevine with their petioles were immersed in 2 mL toxic solution until complete absorption and then transferred to distilled water. Toxicity symptoms were recorded 48 h later up to 7 days.

Tomato cuttings were taken from 21 day old seedlings and each compound was assayed at 0.05, 0.1 and 0.2 mg/mL. Cuttings were placed in the test solutions (2 mL) for 72 h and then transferred to distilled water. Symptoms were visually evaluated up to 7 days.

4.7.2. Zootoxic activity assays

Compounds were assayed on brine shrimp larvae (*Artemia salina* L.). The assay was performed in cell culture plates with 24 cells (Corning) as already described (Favilla et al., 2006). The metabolites were dissolved in methanol and tested at 50 µg/mL. Tests were performed in quadruplicate. The percentage of larval mortality was determined after incubation for 24 and 36 h at 27 °C in the dark.

4.7.3. Antifungal activity

Antifungal activity was tested on the following species: *Diplodia corticola* A.J.L. Phillips, A. Alves & J. Luque (Ascomycetes), *Athelia rolfsii* (Curzi) C.C. Tu & Kimbr. (Basidiomycetes), *Diplodia seriata*, *Neofusicoccum parvum*, *N. vitifusiforme* van Niekerk & Crous, Slippers & A.J.L. Phillips and three Oomycetes: *Phytophthora cinnamomi* Rands, *Phytophthora plurivora* T. Jung & T.I. Burgess and *Phytophthora citrophthora* (R.E. Sm. & E.H. Sm.) Leonian. The sensitivity of all species to compounds was evaluated by transferring mycelial plugs (6-mm diameter) of each isolate, taken from the margin of actively growing 3-day-old colonies, to carrot agar medium supplemented with 100 µg/mL of each compound. Each disk was placed in the centre of a Petri dish with mycelia in contact with the medium. The plates were incubated at 20 or 25 °C depending on the pathogen in the dark until the target fungi used as negative control covered the plate's surface. Then the two perpendicular diameters of all fungi were measured and the results were reported as inhibition of growth. Three replicates were tested for each isolate and each assay was performed twice. Metalaxyl-M (mefenoxam; p.a. 43.88%; Syngenta) was used as positive control for Oomycetes, while PCNB (Pentachloronitrobenzene), was used as positive control for Ascomycetes and Basidiomycetes. MeOH (0.5% v/v) were used as a negative control. Three

replicate Petri dishes were used for each treatment. The dishes were inoculated, incubated and colony growth was determined as described above.

4.7.4. Analysis of data

Each experiment was repeated twice with three replicates. All data were processed with XLSTAT software (Addinsoft, Damrémont, Paris, France). Probit analysis was used to calculate the effective concentration values that inhibited mycelial growth by 50% (EC₅₀).

5. RESULTS AND DISCUSSION

5.1. Chemical and biological characterization of phytotoxins from *Neofusicoccum australe* strain BOT48.

The strain *N. australe* was associated with grapevine cordon dieback in Sardinia (Linaldeddu et al., 2010) as showed in Figure 14. The lack information on secondary metabolites produced by *N. australe* involved in grapevine dieback, suggested to evaluate its ability to produce in vitro phytotoxins potentially involved in the pathogenesis process. For this reason the fungus was grown in liquid cultures and the organic extract, showing a high phytotoxic activity was purified by a combination of CC and TLC as detailed in the experimental section (par.4.1) yielding three metabolites (Figure 2). Metabolites were isolated as homogeneous amorphous solids and by preliminary ^1H NMR investigation appeared to belong to different classes of natural compounds.

Main metabolite, named cyclobotryoxide (**1**), had a molecular weight of 170 as deduced from its HRESIMS spectrum corresponding to a molecular formula of $\text{C}_8\text{H}_{10}\text{O}_4$, indicating four hydrogen deficiencies. The same spectrum showed the sodium cluster $[\text{M}+\text{Na}]^+$ at m/z 193.1509 and when the same spectrum was recorded in negative mode the pseudomolecular ion $[\text{M}-\text{H}]^-$ at m/z 169. The UV spectrum (Figure 15) showed an absorption maximum at 275 nm, consistent with the theoretical one (272) calculated applying the Woodward rules for compound containing a suitable α,β,γ -trisubstituted α,β -unsaturated carbonyl group (Pretsch et al., 2000). IR spectrum showed bands characteristic of hydroxy and conjugated carbonyl groups (Nakanishi and Solomon, 1977).

The ^1H NMR spectrum of **1** (Figure 16) showed the presence of a doublet of doublets ($J = 3.0$ and 1.0 Hz) and a doublet at δ 3.79 and 3.45 ($J = 3.0$ Hz), respectively, typical of the protons (H-6 and H-1) of a *cis*-disubstituted oxirane ring (Pretsch et al.,2000). The resonance at δ 4.88 was assigned to a proton (H-5) of a secondary hydroxylated carbon. It coupled in the COSY spectrum (Berger et al.,2004) with the geminal hydroxy group observed as a doublet ($J = 11.0$ Hz) at δ 3.60, with H-6 and long range ($J < 1\text{Hz}$) with a vinyl methyl group $[\text{CH}_3\text{-C}(4)]$ (Figure 17).

The latter was observed as a broad singlet at δ 1.26. Furthermore, the ^1H NMR spectrum showed a singlet at δ 4.05 assigned to a methoxy group (Pretsch et al.,2000).

These partial structures were confirmed by data of the ^{13}C NMR spectrum (Figure 18) which showed the presences of signals due to an α,β -unsaturated α -oxygenated carbonyl group (δ 194.3, 165.5, 112.0), for the carbonyl (C-2) and two quaternary olefinic (C-3 and C-4) carbons. The methoxy and methyl groups resonated at δ 56.1 and 7.9, and were located at C-3 and C-4, respectively on the basis of the couplings observed in the HMBC spectrum (Figure 19)(Berger et al.,2004). The three oxygenated secondary carbons were observed at typical chemical shift values of δ 60.9, 54.2, 52.1, and they were assigned by the coupling observed in the HSQC spectrum (Figure 20) (Berger et al.,2004) to C-5, C-6 and C-1, respectively (Breitmaier et al., 1987).

Thus, chemical shifts were assigned to all the protons and carbons and cyclobutryoxide was formulated as 5-hydroxy-3-methoxy-4-methyl-7-oxabicyclo[4.1.0]hept-3-en-2-one.

This structure was confirmed by all the couplings and correlations observed in the HMBC and NOESY(Berger et al., 2004) spectra. The NOESY spectrum (Figure 21)showed, besides the expected correlations between H-1 and H-6 and the methoxy and the methyl groups, also those between the latter and the proton of hydroxy group at C-5 and between H-5 and H-6. The latter correlation was in agreement with an inspection of a Dreiding model of **1** as both relative configurations of C-5 (R^* or S^*) could generate an nOe effect between H-6 and H-5. However, only the relative R^* configuration could be assigned to C-5 as it is consistent with the dihedral angle near 90° observed between H-5 and H-6, which, in agreement to the literature, was a very low value (1.0 Hz) measured for their coupling in the ^1H NMR spectrum(Pretsch et al.,2000).

The absolute configuration of **1** was determined by comparison of its ECD spectrum with those of the structurally related epoxycyclohexenones (Mennucci et al., 2007). In fact, its ECD spectrum (Figure 22) showed negative and positive Cotton effects at 310 and 270 nm, respectively. These effects were similar to related epoxycyclohexenones such as sphaeropsidone, terreminin, and panepoxydon (Mennucci et al., 2007; Evidente et al.,1998).

On the basis of these results **1** was formulated as (1*S*,5*R*,6*S*)-5-hydroxy-3-methoxy-4-methyl-7-oxabicyclo[4.1.0]hept-3-en-2-one.

The structure assigned to cyclobotryoxide was further supported by preparation of derivative **2** by acetylation. The spectroscopic data of this derivative were fully consistent with the structure assigned to **1**. The IR spectrum of **2** showed the absence of a hydroxy group and the presence of a band typical of an acetyl carbonyl group at 1747 cm⁻¹ (Nakanishi et al., 1977). Its ¹H NMR (Figure 23) spectrum differed from that of **1** essentially in the downfield shift ($\Delta\delta$ 1.30) of H-5 observed as broad singlet at δ 6.18, and the absence of the doublet at δ 3.60 of the hydroxy proton, and the presence of the singlet of the acetyl group at δ 2.19. The ESIMS spectrum of **2** recorded in the positive mode showed the sodium cluster [M+Na]⁺ at m/z 235.

Cyclobotryoxide was characterized as a new naturally occurring compound belonging to a family of epoxycyclohexenones which have been isolated from bacteria, fungi, higher plants, and molluscs. These compounds have shown interesting biological properties such as antifungal, antibacterial, antitumoral, phytotoxic, and enzyme inhibitory activities (Mennucci et al., 2007). Furthermore, sphaeropsidone and *epi*-sphaeropsidone, belonging to the same family of natural compounds were previously isolated from *Diplodia cypressi*, (Evidente et al., 2011) a pathogenic fungus of cypress.

Metabolites **3** was identified as 3-methylcatechol on the basis of its spectroscopic data which were the same as previously reported (Ahamad et al., 2001). 3-methylcatechol, a minor metabolite of toluene, showed toxicity in human and mammal cells (Shen et al., 1998 and Nakai et al., 2003). It was also isolated, together with other phenolic compounds, from the fermentation liquid of the endophytic fungus *Penicillium* sp. GT6105 from *Kandelia candel*. (Li et al., 2007).

Metabolite **4** was identified as tyrosol, on the basis of its spectroscopic data, which was similar to that previously reported (Capasso et al., 1992). Tyrosol is a phytotoxic metabolite produced by plants and fungi including *Botryosphaeriaceae* species (Venkatasubbaiah et al., 1991; Capasso et al., 1992). Recently, tyrosol was also identified as a phytotoxic metabolite produced by

N. parvum (Evidente et al., 2010). This fungus was isolated together with four other *Botryosphaeriaceae* from declining grapevines in Spain (Martos et al., 2008).

When assayed on the leaves of different plant species at different concentrations as previously reported in experimental section, compounds **1**, **3** and **4** showed varying degrees of phytotoxicity. The toxicity data obtained in the leaf-puncture bioassay on holm oak, cork oak, and grapevine cv. Cannonau leaves, are summarized in Table 17. Cyclobotryoxide (**1**) appeared to be the most active metabolite.(Figure 24). It had remarkable toxicity in a range of concentrations from 0.25 to 1.0 mg/mL, causing necrotic lesions to leaves of all species tested. At the lower concentrations its toxicity was progressively reduced. A marked decrease of activity was observed for its acetyl derivative (**2**) even at the highest concentration (1 mg/mL) tested, confirming that structural modifications could alter biological activity. At the lower doses, compound **2** was inactive on cork and holm oak. Compound **3** showed moderate activity on grape leaves, while on the other species tested it was weakly active or inactive. Compound **4**, exhibited moderate phytotoxicity on grapevine leaves, whereas on the other species tested it was weakly active or inactive.

Compounds **1** and **4** were also tested on grapevine detached leaves at 0.25 and 0.5 mg/mL. In this bioassay cyclobotryoxide caused symptoms at 0.5 mg/mL on the foliar lamina consisting in irregular internerval or marginal necrotic spots, slowly becoming coalescent, followed by distortion and withering of the leaf lamina. No visible symptoms were induced by tyrosol.

5.2. Purification and chemical characterization of phytotoxins by *Lasiodiplodia mediterranea* strain BL101 .

Lasiodiplodia mediterranea is a new specie recently characterized (Linaldeddu et al., 2014) associated with wedge-shaped lesions of the vascular tissues on grapevine in Sardinia (Linaldeddu et al., 2012).

The nature of symptoms caused by this new species of *Lasiodiplodia* on grapevine (Figure 25) suggests that phytotoxic metabolites may be involved in the host-pathogen interaction. On the other hand, it is well-known that *L. theobromae* which is considered the type species of the *Lasiodiplodia* genus, biosynthesizes a variety of lipophilic and hydrophilic metabolites that exhibit interesting biological activities (Aldridge et al., 1971; Husain et al., 1993; Nakamori et al., 1994; Matsuura et al., 1998; Yang et al., 2000; He et al., 2004; Miranda et al., 2008; Kitaoka et al., 2009; Pandi et al., 2010).

Therefore the study of secondary metabolites was carried out on strain BL101. Its organic extracts were purified as detailed reported in the experimental section, yielding 10 metabolites (Figures 3 and 4). The preliminary ¹H NMR investigation showed that the metabolites belong to different classes of natural compounds. The structures of the known compounds (Figure 3) were confirmed by physical and spectroscopic methods (OR, IR, UV, ¹H and ¹³C NMR, ESI and/or APCIMS) and by comparison of the obtained data with those reported in the literature for (1*R*,2*R*)-jasmonic acid and its methyl ester (**10** and **11** Figures 26 and 27) (Husain et al., 1993; Yukimune et al., 2000), botryosphaerilactone A (**12**, Figure 28) (Rukachaisirikul et al., 2009), (3*S*,4*R*,5*R*)-4-hydroxymethyl-3,5-dimethyldihydro-2-furanone (**13**, Figure 29) (Ravi et al., 1979), and (3*R*,4*S*)-botryodiplodin (**14**, Figure 30) (Ramezani et al., 2007). Some other new spectroscopic data as ESI and/or APCI spectra and in particular the ¹³C NMR data for the trisubstituted dihydrofuranone **13** were detailed reported in the corresponding paragraphs of experimental section. In addition, the identification of **12** was also supported by data from its COSY, HSQC and HMBC spectra. Finally, as (3*R*,4*S*)-botryodiplodin (**14**) was obtained as an inseparable anomeric mixture (α/β , 65:35), its structure was confirmed by acetylation carried out in the usual conditions. In fact, this reaction yielded only the 2,3-*trans*-botryodiplodin acetate, whose physic and spectroscopic data were very similar to those previously reported (Arsenault and Althaus, 1969).

Furthermore, the preliminary ^1H and ^{13}C investigation of **5** showed its close correlation with both jasmonic acid and 3,4,5-trisubstituted dihydrofuranone **13** and, being a new compound as described below, it was named lasiojasmonate A (Figures 31 and 32). These suggestions were also confirmed by the band typical of ketone ester and olefinic groups (Nakanishi and Solomons, 1977) and the end absorption maximum (Scott, 1964) observed in the IR and UV spectra, respectively (Figures 33 and 34). It showed a molecular weight of 336 associated to the molecular formula of $\text{C}_{19}\text{H}_{28}\text{O}_5$ with six hydrogen deficient as deduced from the HRESIMS spectrum. The ^1H NMR spectrum, also compared to that of jasmonic acid (Husain et al., 1993) and of standard commercially sample, showed the signal patterns of the jasmonyl residue. For the 2-pentenyl moiety the multiplets of the protons (H-10 and H-9) of the *cis* double bond, the two allylic methylene groups (H₂-8 and H₂-11) and the triplet ($J = 7.4$ Hz) of the terminal methyl group (Me-12) were observed at δ 5.45, 5.26, 2.37, 2.04 and 0.9, respectively. For the 2,3-disubstituted cyclopentanone residue the multiplets of H-1 and H-2, the double doublet ($J = 20.0$ and 8.2 Hz) and the multiplet, and the multiplets of H₂C-4 and H₂C-5 were observed at δ 2.10, 1.90, 2.74 and 2.37, and 2.33 and 1.50 respectively (Pretsch et al, 2000).

As regard the signal system of the 4-hydroxy-3,5-dimethyl-3,4-dihydrofurane residue, which were also compared to those reported in literature (Ravi et al., 1979) (Figure 31) the protons of hydroxymethylene H₂C-8' showed, in particular, the typical AB system appearing as a multiplet and double doublet ($J = 11.0$ and 5.7 Hz) at δ 4.26 and 4.21 significantly downfield shifted ($\Delta\delta$ 0.43 and 0.46) at δ 4.26 and 4.21, as consequence of the esterification with the jasmonic acid. The other signals of the same moiety appeared as a double quartet ($J = 11.0$ and 7.1 Hz) for H-3', two multiplets for H-4' and H-5' (the latter being overlapped with the signal of H-8'A) and two doublets ($J = 6.1$ and 7.1 Hz) for the two secondary methyl groups (Me-6' and Me-7') at δ 2.49, 2.04, 4.26, and 1.47 and 1.28, respectively (Pretsch et al., 2000). All these attributions were confirmed by the coupling observed in the COSY and HSQC spectra (Figures 35 and 36) (Berger and Braun, 2004), with the last that also contributed to assign the chemical shifts of protonated

carbons in the ^{13}C NMR spectrum as reported in Table 7. The signals of the remaining quaternary carbons observed at δ 218.3 177.6 and 171.7 typical of a ketone and two ester carbonyl groups (Breitmaier and Voelter, 1987) were assigned to C-3, C-2' and C-7 with the last two attributed on the basis of the couplings observed in the HMBC spectrum (Table 37) (Berger and Braun, 2004) between C-2' with H-3', Me-7' and H-8'B and C-7 with H₂C-5, H₂C-6 and H₂C-8'. Very significant to support the jasmonate esterification of the 4-hydroxymethyl-3,5-dimethyl-3,4-dihydrofuranone was the coupling observed in the HMBC spectrum between C-7 with H₂C-8'. On the basis of these results lasiojasmonate A was formulated as 4-hydroxymethyl-3,5-dimethyldihydro-2-furanone jasmonate (**5**).

The structure of **5** was confirmed by all the other couplings observed in the HMBC spectrum and by data from the HRESI and APCIMS spectra which showed, respectively, the sodium cluster $[\text{M}+\text{Na}]^+$ and the pseudomolecular ion $[\text{M}+\text{H}]^+$ at m/z 359.1913 and 337.

The relative stereochemistry of **5** as depicted in Figure 4 was deduced by the comparison of the couplings constant measured in its ^1H NMR spectrum with those reported for (1*R*,2*R*)-jasmonic acid (Husain et al., 1993) and (3*S*,4*R*,5*R*)-4-hydroxymethyl-3,5-dimethyldihydro-2-furanone. This stereochemistry was also confirmed by the correlations observed in the NOESY spectrum (Berger and Braun, 2004). In fact, this spectrum showed the correlations between the protons of the *cis* double bond H-10 and H-9 and that this latter with the protons of allylic methylene H₂-8, and that of H-3' with H-5'. Thus, lasiojasmonate A can be formulated as (1*R**,2*R**,3'*S**,4'*R**,5'*R**)-4-hydroxymethyl-3,5-dimethyldihydro-2-furanone jasmonate.

Compounds **6** and **7** being two epimeric acetals showed both a molecular weight of 314, as deduced from their ESIMS. They were obtained as an inseparable mixture (α/β , 45:55). All the attempts done, using different chromatographic methods on direct and reverse phase and different solvent mixtures, failed. Their ^1H NMR spectra (Figure 38) showed the presence of two doublets ($J=2.3$ and 4.6 Hz) typical of anomeric protons (H-10) for the β and α isomers at δ 4.67 and 4.79, respectively. The comparison of this spectrum with that of botryosphaerilactone **12**

(Rukachaisirikul et al., 2009) indicate that **6** and **7** were the acetyl derivatives of botryosphaeriolactones A and C, or of their respective enantiomers. In fact, their ^1H NMR spectra (Table 8) differed from that of **12** and botryosphaerilactone C (Rukachaisirikul et al, 2009) essentially for the downfield shift of $\text{H}_2\text{C}-16$ ($\Delta\delta$ 0.46 and 0.35; and 0.41 and 0.40, for β and α isomers respectively) resonating as two double doublets for β anomer (**6**) at δ 4.15 and 4.04 ($J=11.0, 5.6$ and $11.0, 7.9$ Hz), while for the α anomer (**7**) at δ 4.21 and 4.06 ($J=11.3, 4.5$ and $11.3, 7.6$ Hz). Furthermore, two singlets of the acetyl groups resonated at δ 2.06 and 2.07 for **6** and **7** respectively. The chemical shifts of all protons of two anomers were assigned (Table 8) by comparison of their ^1H NMR spectra with that of **12**. The epimeric nature of **6** and **7** was also confirmed by usual acetylation of botryosphaerilactone A with pyridine and acetic anhydride. As expected this reaction yielded both the β and α anomers being the latter (**7**) the main product of the reaction.

The structures assigned to **6** and **7** were also confirmed by data of both ESI and APCI spectra. The ESIMS spectrum showed dimeric sodiated form $[2\text{M}+\text{Na}]^+$ and the sodium cluster $[\text{M}+\text{Na}]^+$ at m/z 651 and 314. The APCIMS spectrum showed ions originated from the pseudomolecular ion $[\text{M}+\text{H}]^+$ recorded at m/z 337 by fragmentation mechanisms typical of asymmetrical ethers (Pretsch et al 2000) as reported in Figure 39. In fact, the pseudomolecular ion by cleavage of the acetalic bond C(10)-O (mechanism a) originated the γ -lactonyl and the trisubstituted tetrahydrofurane ions recorded at m/z 145 and 172, respectively. This latter, by loss of AcOH generated a fragment ion at m/z 113 (Figure 39). Furthermore, the pseudomolecular ion by the alternative cleavage of the acetalic bond C(8)-O (fragmentation mechanism b) generated the γ -lactonyl fragment ion observed at m/z 127 (Figure 39).

Compounds **8** and **9** showed a molecular weight of 464, as deduced from their HRESIMS spectrum recorded in positive mode associated to the molecular formula of $\text{C}_{26}\text{H}_{40}\text{O}_7$. They were obtained as an inseparable epimeric mixture (α/β , 30:70). As above reported for **6** and **7**, all the attempts made using different chromatographic methods failed. By preliminary ^1H NMR

investigation, they appeared closely relate to both botryosphaeriolactones A and C and jasmonic acid, suggesting for **8** and **9** a structure of jasmonate esters and therefore were named lasiojasmonate B and C. Their ^1H NMR spectra (Figure 40) showed the presence of two doublets ($J=2.0$ and 4.5 Hz) typical of anomeric protons (H-10') at δ 4.68 and 4.80 for the β and α isomers, respectively. Significant differences from the ^1H NMR spectra of botryosphaerilactones A and C were observed for the protons of the ABX systems HC-(13')-H₂C-(16'). As expected the H₂-16' protons were downfield shifted ($\Delta\delta$ 0.48, 0.41, and 0.43, 0.41 for **8** and **9**) with respect to the values reported for the same protons in botryosphaerilactones A and C (Rukachaisiriku et al., 2009). These protons appears as doublet of doublets ($J=11.0$, 7.2, and 6.9) and ($J=11.0$, 5.8 and 11.3, 4.5) at δ 4.10 and 4.17, and δ 4.07 and 4.23 for **8** and **9**. Thus, all the chemical shifts of all protons were assigned to **8** and **9** in comparison to those reported for **6** and **7** and jasmonic acid as reported in Table 9. Therefore, **8** and **9** can be formulated as (1R*,2R*,3'S*,4'R*,5'R*,10'R*,12'R*,13'R*,14'S*)- and (1R*,2R*,3'S*,4'R*,5'R*,10'S*,12'R*,13'R*,14'S*)-4-(4-hydroxymethyl-3,5-dimethyltetrahydrofuran-2-ylloxymethyl)-3,5-dimethyldihydro-2 furanone jasmonates.

These structures were confirmed through fragmentation ions observed in APCIMS spectrum recorded in positive mode. Also in this case the spectrum exhibited ions originated by pseudomolecular ion by two different fragmentation mechanisms generated by the cleavage of the acetalic bond as reported in Figure 39. The cleavage of the bond C(8')-O (mechanism c) generated the fragment ion m/z 127 and the 4-hydroxy-3,5-dimethyl-4-hydroxy jasmonate esters. This latter, generated jasmonic acid and fragment ion m/z 113 and H₂O (mechanism e). Alternatively, the pseudomolecular ion by cleavage of the acetalic bond C(10')-O (mechanism d) generated two fragment ions recorded at m/z 145 and 322.

The presence in lasiojasmonates A-C of (1R,2R)-jasmonic acid was confirmed by their mild alkaline hydrolysis carried out according Farmer et al. (1992). In fact jasmonic acid obtained from **5**, **8** and **9**, as detailed report in the Experimental section, and **10** showed the same R_f by

TLC analysis (silica gel eluent CHCl₃/*i*-PrOH (95:5) *R_f* 0.43, and on reversed phase eluent EtOH/H₂O (6:4) *R_f* 0.50) also by co-injection and OR and ¹H NMR recorded in the same conditions.

In addition the keto-enolization process of C-2 of jasmonic acid, as report in literature by Miersch et al., (1987), was ruled out for the compounds **5,8-11** isolated from *Lasiodiplodia* sp. as resulted by their optical (OR) and/or spectroscopic (essential ¹H NMR) properties. So that compounds **5, 8-11** are not artefact.

Pathogenicity of the new species of *Lasiodiplodia* was verified by wound inoculation of excised canes under controlled laboratory conditions. Fifty days after inoculation, the lignified canes inoculated with the pathogen displayed dark-brown to black discoloration on bark and vascular tissues, measuring 7.4±2.7 cm (mean ± S.D.). In cross section all canes showed a wedge-shaped necrotic sector. The pathogen was successfully re-isolated from the margin of symptomatic tissues, thus fulfilling Koch's postulates. Artificially obtained symptoms were congruent with field observations. Control canes inoculated with sterile PDA plugs remained symptomless.

The phytotoxicity data obtained in the leaf-puncture assay on cork oak and grapevine leaves showed that (1*R*,2*R*)-jasmonic acid (**10**) was the only active metabolite. It had remarkable toxicity at 1.0 mg/mL causing necrotic lesions to leaves of both species tested (necrosis area: 7.04 and 11.96 mm² on grapevine and cork oak, respectively). All the other metabolites tested did not show any effect in this bioassay.

All compounds, except **8** and **9**, were also tested on grapevine detached leaves at 0.25 and 0.5 mg/mL. In this bioassay only jasmonic acid caused veins necrosis, slowly diffusing to large areas of the leaf lamina at 0.5 mg/mL. When assayed on tomato cuttings at 0.1 mg/mL jasmonic acid caused withering within 7 days from treatment. None of the compounds showed activity in the assay performed for zootoxicity (*Artemia salina*) at 50 µg/mL.

Jasmonic acid is the basic structure of a naturally occurring family of compounds named jasmonates which regulate many aspects of growth, development and defence, activating responses to wounding, herbivores and necrotrophic pathogens. Compound **10** and related compounds were also produced by fungi (Miersch et al., 1999b and literature cited). In particular, *Lasiodiplodia* spp. are among the few fungal species which synthesize enantiomeric pure form of the different enantiomers as (1*R*,2*S*) diastereomer, called also (+)-7-iso-jasmonic acid, isolated from *L. theobromae* (Miersch et al., 1987). Jasmonic acid is biosynthesised by the octadecanoid pathway in plants (Schaller and Stinzi, 2009) and fungi (Tsukada et al., 2010). Recently jasmonate biosynthesis by a linolenate 9*R*-dioxygenase and an allene oxide synthase has been described in *L. theobromae* (Jernerèn et al., 2012).

Botryosphaerilactone **A** and (3*S*,4*R*,5*R*)-4-hydroxymethyl-3,5-dimethyl-dihydro-2-furanone (**12** and **13**) were recently reported as secondary metabolites of the endophytic fungus *L. theobromae* (synonym. *Botryosphaeria rhodina*) PSU-M35 and PSU-M114 isolated from leaves of *Garcinia mangostana* L. (Rukachaisirikul et al., 2009). When they were assayed against *Staphylococcus aureus* they did not show antibacterial activity (Rukachaisirikul et al., 2009).

(3*R*,4*S*)-Botryodiplodin was first isolated from cultures of *L. theobromae* Pat. the causal agent of fruit rot in tropical fruits trees (Gupta et al., 1966). Subsequently, it was found in other cultures of phytopathogenic fungal species such as *Penicillium roqueforti* Thom strains (Nielsen et al., 2006), *Penicillium stipitatum* Thom (Fuska et al., 1988) and *Macrophomina phaseolina* (Cooke) Wint. (Ramezani et al., 2007).

(3*R*,4*S*)-Botryodiplodin exhibits anticancer, antibacterial, antifungal, phytotoxic, mitogenic, and antifertility activities, and may play a role in plant diseases. Unusual structural properties allow oligomerization of (-)-botryodiplodin to pigments and cross-linking agents, which may be responsible for some of its biological activities (Shier et al., 2007).

5.3. Chemical and biological characterization of phytotoxins by *Lasiodiplodia mediterranea* strain B6.

A strain of *L. mediterranea* associated with dieback of grapevine in Sicily (Figure 41)(Burruano et al., 2008; Mondello et al.,2013) was grown. For the same reasons previously reported (par.5.2), a study of secondary metabolites was performed. The organic extracts were purified as detailed reported in the experimental section (par.4.3), yielding six metabolites (**10**, **14-18**, Figures 5 and 6). The structures of the known compounds (Figure 5) were confirmed by physical and spectroscopic methods (OR, IR, UV, ^1H and ^{13}C NMR, ESI MS) and by comparison of the obtained data with those reported in the literature for, botryosphaeriodiplodin **17** (Figure 42, Rukachaisirikul et al., 2009), (5R)-5-hydroxylasiodiplodin **18** (Figure 43, Matsuura et al.,1998), (1R,2R)-jasmonic acid **10** (Figure 26, Husain et al., 1193; Yukimune et al., 2000), (3S,4R,5R)-4-hydroxymethyl-3,5-dimethyldihydro-2-furanone **13** (Figure 29, Andolfi et al., 2014). Furthermore, the preliminary ^1H - and ^{13}C -NMR investigation of **15** and **16** (Figures 44 and 45) showed its close correlation with botryosphaeriolactones A and C (Rukachaisirikul et al., 2009), and, being new compounds as described below, were named lasiolactols A and B.

Compounds **15** and **16** were obtained as homogenous oil and as an inseparable mixture of two epimeric lactons in a ratio of β/α 75:25. Their molecular formulas were $\text{C}_{14}\text{H}_{26}\text{O}_5$ with two degrees of unsaturation, as deduced from HRESIMS [m/z 313.1456 $[\text{M}+\text{K}]^+$, and 297.1649 $[\text{M}+\text{Na}]^+$] (Table 11). The IR spectrum (Figure 46)exhibited absorption band of OH groups (3300 cm^{-1}) (Nakanishi and Solomon, 1977). The UV spectrum (Figure 47) showed the absence of chromophores (Scott, 1964). The ^1H -NMR spectrum (Figure 44) showed the presence of a broad singlet and of a doublet ($J=4.1\text{ Hz}$) typical of acetalic protons (H-2) for the **15** and **16** compounds at δ 5.06 and 5.24 of lactols ring, resp. (Rukachaisirikul et al., 2009). Same spectrum displayed a double quartets at δ 4.20 ($J=7.0, 6.1, \text{H-5}$), a doublet of doublet quartet at δ 2.10 ($J=8.5, 7.2, 6.0 \text{H-3}$), and a multiplet at δ 1.56 (H-4) attributed to **15** (Table 10). Moreover two secondary Me groups were inferred from two 3-H doublets at δ 1.14 ($J=7.2, \text{H}_3\text{-7}$), and 1.33

($J=6.1$, H₃₋₆) (Table 10). The ¹³C-NMR spectrum (Figure 45) exhibited for **15** seven C-atom resonances of four CH (one of acetalic proton) at δ 103.8 (C-2), 43.9 (C-3), 54.9 (C-4), 76.5 (C-5), one CH₂ at δ 62.7 (C-8) O-bearing, and two Me at δ 21.4 (C-6), and 19.2 (C-7) groups (Table 10). Comparative analysis of ¹H- and ¹³C-NMR data with those of botryosphaeriolactones A and C suggested for **15** the presence of γ -lactol moiety (Andolfi et al., 2014). These data allowed to assign for **15** a partial structure of 4-hydroxymethyl-3,5-dimethyl-tetrahydrofuran-2-ol. The 2D NMR spectra data supported this hypothesis. In fact the COSY spectrum (Figure 48) exhibited correlations of the signal at δ 5.06 (H-2) with that at δ 2.10 (H-3), with this last with those at δ 1.56 (H-4), and 1.14 (Me-7); of the signal at δ 1.56 (H-4) with those at δ 3.75-3.71 (CH₂-8), and 4.20 (H-5), and finally with this last with that at δ 1.33 (Me-6). The key HMBs δ 103.8 (C-2) with those at δ 2.10 (H-3) and 1.14 (H-7), δ 43.9 (C-3) with those at δ 1.56 (H-4) and 4.20 (H-5), δ 54.9 (H-4) with those at δ 3.75 and 3.71 (CH₂-8), and δ 76.5 (C-5) with those at δ 2.10 (H-3), 1.56 (H-4) and 1.33 (H-6) further supported this assignment.

The ¹H-NMR and ¹³C-NMR spectra in addition to the signals of acetalic methine, previously reported, showed the presence of signals attributed to **16** as report in Table 10. Therefore its structure was assigned on the basis of 2D NMR spectra and in comparison with that of **15**.

The structure of dimer γ -lactol was formulated for **15** and **16**, considering HRESIMS data, below reported (Table 11), that gave a molecular formula containing twice the number of carbon and hydrogen atoms. Moreover the same spectrum exhibited ions originating by pseudomolecular ion through mechanism generated by fragmentation mechanisms typical of asymmetrical ethers (Pretsch et al., 2000). In particular the cleavage of the acetalic bond C(2)-O, by as previous report for 16-O-acetylbotryosphaerilactones A and C (Andolfi et al., 2014), originated 4-hydroxymethyl-3,5-dimethyl-tetrahydro-furan-2-ol (m/z 169.0818 [$M-C_7H_{13}O_2+H+Na$]⁺) corresponding at molecular formula C₇H₁₄NaO₃ and (2,4-dimethyl-

tetrahydro-furan-3-yl)-methanol (m/z 129.0897 [$M-C_7H_{13}O_3$]⁺) corresponding at molecular $C_7H_{13}O_2$ (Table 11).

The relative stereochemistry of **15** as depicted in Figure 6 was deduced by the comparison of the couplings constant measured in its ¹H-NMR spectrum with those reported for same moiety in the botryosphaeriolactone A (Rukachaisirikul et al., 2009). This stereochemistry was also confirmed by the correlations observed in the NOESY spectrum (Figure 49, Berger and Braun, 2004). In fact, this spectrum showed the correlations between acetalic protons H-2 and H-3. So that a (2*S*,3*S*,4*R*,5*R*,2'*S*,3'*S*,4'*R*,5'*R*)-**15** relative configuration was established.

The relative stereochemistry of **16** was also confirmed by the correlations observed in the NOESY spectrum (Berger and Braun, 2004). In this case, NOESY spectrum didn't show the correlations between acetalic protons H-2 and H-3. Therefore a (2*R*,3*S*,4*R*,5*R*,2'*R*,3'*S*,4'*R*,5'*R*)-**2** relative configuration was established.

Compound **17**, as previous report, was identified as botryosphaeriodipodin by comparison of their spectroscopic and optical proprieties with those report by (Rukachaisirikul et al., 2009). This compound was recently isolated from mycelia extract of endophytic fungus *Botryosphaeria rhodina* (PSU-M35) together other known lasiodiplodins (Rukachaisirikul et al., 2009). In this case the authors did not assign relative configuration at secondary hydroxylated C-7 of macrocyclic ring using NOEDIFF data because it was inadequate. Moreover, analysis of the absolute configuration of the same carbon was not performed as botryosphaeriodiplodin was obtained in low amount (Rukachaisirikul et al., 2009).

The absolute configuration at C-7 of **17** was established for its 13-*O*-methyl derivative (**19**) by an advanced Mosher method (Ohtani et al., 1991). Analysis of differences in proton chemical shifts between the (*S*)- and (*R*)-MTPA ester of **19**. This derivative was obtained by usually methylation of phenolic proton with ethereal solution of CH₂N₂.(Figure 7) Its ¹H-NMR spectrum (Figure 50) essentially differed from that of **17** only for the presence of other one methoxy group resonating as singlet at δ 3.78. ESIMS spectrum of **17**, recorded in positive mode, showed the

sodium cluster and pseudomolecular ion $[M + Na]^+$ and $[M + H]^+$ at m/z 345 and 323, respectively. **19** was converted to (S)- and (R)-MPTA esters (**20** and **21**) esters by reaction with R-(-)- α -methoxy- α -trifluoromethylphenylacetyl (MPTA) and S-(+)-MPTA chlorides, respectively. The chemical shift differences between **20** and **21** ($\Delta\delta_H = \delta_S - \delta_R$, Figures 51-53) indicated an R configuration at C-7. The relative configuration at C-3 was assumed to be identical to that lasiodiplodin (Sultan et al., 2014). Thus, the structure of **17** was assigned to be (3R,7R)-7-hydroxylasiodiplodin.

The toxicity of compounds **15-17**, **10** and **13** used in the leaf-puncture assay on grapevine leaves showed different values depending on the kind of compound, its concentration and their interaction. In particular, the phytotoxicity of all compounds has grown according to the concentration increase; moreover, the compound **10** resulted more toxic than the others. Its produced necrotic area of 5.3 mm². Differences between toxicity values were resulted statistically significant (Figure 54). The compounds **15-17**, **10** and **13** did not show *in vitro* antifungal and antioomycete activity against four assayed phytopathogens. Only Ridomil Gold SL completely inhibited the mycelial growth of *Phytophthora citrophthora*.

5.4. Purification and chemical characterization of phytotoxins by *Neofusicoccum australe* strain BL24.

Another strain of *N. australe* isolated from symptomatic juniper in Sardinia, strain BL24, (Figure 55) was grown and its secondary metabolites were purified as detailed in the experimental section (par.4.4), yielding two well know metabolites (**22** and **23**) and tyrosol identified as described in paragraph 5.1. (Figure 8).

The molecular weights of **22** and **23** were determined to be 252 and 224, respectively, as deduced from their ESI and APCIMS spectra recorded, respectively, in the positive and negative modes.

The chemical shifts and multiplicities of all protons and corresponding carbons of **22** and **23** were assigned by the couplings observed in their NMR, COSY, HMBC, and HSQC spectra (Figures 56 and 57). Comparison of these and reported data identified **22** and **23** as botryosphaerone D (Xu et al., 2011) and (3*S*,4*S*)-3,4,8-trihydroxy-6-methoxy-3,4-dihydro-1(2*H*)-naphthalenone (Pittayakhajonwut et al., 2008).

The absolute configuration of botryosphaerone D (**22**), not previously reported, was also determined. Its ECD spectrum (Figure 58) was recorded under the same conditions and compared to that of **23** (Pittayakhajonwut et al., 2008). On the basis of coincident negative and positive Cotton effect at 214, and 230, and 280 nm, compound **22** was formulated as (3*S*,4*S*)-7-ethyl-3,4,8-trihydroxy-6-methoxy-3,4-dihydro-1(2*H*)-naphthalenone. Botryosphaerone D (**22**), together with three other new naphthalenone polyketides, had previously been isolated from *N. australe* strain ZJ12-1A, a fungus obtained from sterilized root epidermis of *Sonneratia apetala* in China. This compound did not show any antimicrobial and cytotoxic activities (Xu et al., 2011). Finally, (3*S*,4*S*)-3,4,8-trihydroxy-6-methoxy-3,4-dihydro-1(2*H*)-naphthalenone (**23**) was reported as new naphthalenone produced from wood-decaying fungus *Phaeosphaeria* sp. (Pittayakhajonwut et al., 2008).

The isolation of naphthalenone polyketides as **22** and **23** was not a surprise. In fact, they belong to a group of well known phytotoxins produced by pathogenic fungi for different agrarian crops such as scytalone, isosclerone, botrytone, and *cis*- and *trans*-3,4-dihydro-2,4,8-trihydroxynaphthalenones etc (Andolfi et al., 2011; Cimmino et al., 2011).

When assayed by leaf-puncture bioassay on holm oak, cork oak, and grapevine cv. Cannonau leaves at different concentrations compounds **22**, isolated as the main metabolite, appeared to be slightly toxic, even at the highest concentration. In addition, compound **23** did not show any phytotoxicity either (Table 18).

5.5 Purification and chemical characterization of phytotoxins from *Diplodia quercivora* strain BL9.

The strain of *Diplodia quercivora* (BL9) was recently described oak pathogen originally found on declining *Quercus canariensis* trees in Tunisia (Linaldeddu et al., 2013) (Figure 59). Given the great ecological impact of *D. quercivora* on oak trees worldwide, we decided to explore the secondary metabolite pattern of this pathogen for which there is no information on its ability to secrete in vitro metabolites which could play a crucial role in its interaction with host plants.

The organic extract having a high phytotoxic activity, was bioguided purified as reported in detail in the experimental (par.4.5) yielding a new *nor-ent*-pimarane, named diplopimarane (**24**, Figure 9), along with the well known sphaeropsidins A and C, and (+)-epiepoformin (**32-34**, Figure 10).

The identification of the well known phytotoxic metabolites sphaeropsidins A and C and (+)-epiepoformin was carried out by comparing their spectroscopic (essentially ^1H and ^{13}C NMR) and optical properties (OR) with those previously reported in literature for **32** (Evidente et al., 1996), **33** (Evidente et al., 1997) and **34** (Nagasawa et al., 1978), respectively. The data of ESI and APCI spectra, are detailed reported in the experimental and are in full agreement to those of EI MS reported in literature (Evidente et al., 1996; 1997; Nagasawa et al., 1978).

Sphaeropsidins A and C were isolated from *Diplodia cupressi*, a canker causing agent of Mediterranean cypress, together with other minor ones B (Evidente et al., 1997), D, E (Evidente et al., 2002), and F (Evidente et al., 2003). Sphaeropsidin A was also isolated from *Smardaea* sp., a fungal endophyte of the Moss *Ceratodonn purpureus* (Hedw.) Brid., along with five isopimarane diterpenes, smardaesidins A-E, two new 20-*nor*-isopimarane diterpenes, and sphaeropsidins C-F (Wang et al., 2011). Studies on structure-activity relationships were also carried out by testing the natural sphaeropsidins and some their key hemisynthetic derivatives for their phytotoxic and antimicrobial activities (Sparapano et al., 2004 Evidente et al., 2011). More recently the anticancer activity of sphaeropsidin A was reported (Lallemand et al., 2012; Wang et al., 2011).

Epiepoformin was isolated together with (+)-epiepoxydon from the culture filtrate of an unidentified fungus isolated from a diseased leaf of crape-myrtle (*Lagerstroemia indica* L. Pers.) showing marked inhibition activity against the germination of lettuce seeds (Nagasawa et al., 1978). Moreover, it has been the subject of several synthetic attempts (Barreros et al., 2005; Carreno et al., 2005; Okamura et al., 2003; Tachihara and Kitahara, 2003), and its absolute configuration was also determined by time dependent density functional theory calculation of the optical rotation (Mennucci et al., 2007).

Diplopimarane (**24**) showed a molecular formula of $C_{19}H_{26}O_3$, as deduced from its HRESIMS, which was consistent with seven hydrogen deficiencies. The preliminary investigation of its 1H and ^{13}C NMR spectra (Figures 60 and 61), in agreement with its MS data, and by comparison with those of sphaeropsidin A (**9**), (Evidente et al., 1996) showed that it could be a *nor-ent*-pimarane. In fact, a successive detailed investigation of its 1H NMR spectrum (Figure 60) showed, as in sphaeropsidin A, the significant presence of the double doublet ($J = 17.6$ and 11.0 Hz) and the two broad doublets ($J = 11.0$ and 17.6 Hz), and the singlet of the vinyl and the tertiary methyl groups at C-13 at δ 6.04 and 5.34 and 5.31, and 1.25, respectively (Pretsch et al., 2000). In the same spectrum, two singlets resonating at δ 1.45 and 1.42 and due to the geminal methyls groups (Me-19 and Me-18) at C-4, were also present. The latter two methyls represent the head of the diterpenoid biosynthetic precursor. These results were confirmed by the couplings observed in the COSY spectrum, (Figure 62, Berger et al., 2004) as well as those observed in the HMBC spectrum (Figure 63, Berger et al., 2004) between C-13 with the protons (H-15 and H-16) of the vinyl group and H-14, C-12 and C-14 with Me-17, and C-4 with both Me-18 and Me-19. The couplings observed in the HSQC spectrum (Figure 64, Berger et al., 2004) allowed us to assign the chemical shifts to the corresponding carbons (Figure 61) at δ 139.1, 118.7, 28.6, 27.6 and 23.2 for C-15, C-16, C-19, C-18 and C-17, respectively (Breitmaier et al., 1987). The most significant differences between **24** and sphaeropsidin A were the absence in the 1H NMR spectrum of the singlet of H-5, the proton of one of headbridge carbons between rings

A and B, as well as the absence of the tertiary hydroxylated carbon (C-9), the ketone carbonyl (C-7) and the carboxyl group (C-20) in the ^{13}C NMR spectrum. The latter in **32** also lactonized the hemiketal hydroxy group at C-6 generating ring D, which is obviously absent in **24**. Thus, diplopimarane appeared to be a *nor*-pimarane. Furthermore, the ^1H and ^{13}C NMR spectra showed the significant presence of a secondary hydroxylated carbon (C-14) at δ 4.70 (d, $J = 9.9$ Hz) and 76.0. This latter in the HMBC spectrum significantly coupled with H₂-12, H-15 and Me-17. The other couplings observed in the COSY, HSQC and HMBC spectra also allowed us to assign chemical shifts to the protons and the carbons of the five methylene groups belonging to, respectively, three to A and two to C rings (Table 13). Considering the remaining three unsaturations and the presence of six quaternary aromatic carbons, two of which bear hydroxy groups, ring B appeared to be aromatized. The couplings observed in the HMBC spectrum confirmed the location of the two phenolic hydroxy groups at C-6 and C-7 and allowed us to assign the chemical shifts at δ 142.2, 141.5, 131.2, 127.0, 124.5 and 119.5 to C-6, C-7, C-8, C-10, C-9 and C-5, and to all the protons and carbons of diplopimarane, as reported in Table 13. On the basis of these results diplopimarane could be formulated as 2,8,8-trimethyl-2-vinyl-1,2,3,4,5,6,7,8-octahydrophenanthrene (**24**).

The structure assigned to **24** was supported by the data observed in its HRESIMS spectrum which showed the sodium cluster $[\text{M}+\text{Na}]^+$ at m/z 325.1785, while the APCIMS spectrum showed the significant fragmentation ion $[\text{M}-\text{H}_2\text{O}]^+$ at m/z 285 generated by the molecular ion by loss of water. When both the ESI and APCIMS spectra were recorded in negative mode the pseudomolecular ion $[\text{M}-\text{H}]^-$ was observed at m/z 301.

The structure assigned to **24** was also supported by the preparation of some key derivatives (**25-29**, Figure 9). In particular, derivative **26** was also essentially prepared to convert it into the diastereomeric R and S MPTA (α -methoxy- α -trifluoromethylphenylacetyl) esters to assign the absolute configuration to **24** as below detailed reported. By treatment with ethereal solution of diazomethane, diplopimarane was converted into the 7-O-methyl and 6,7-O,O'-dimethyl ether

derivatives (**25** and **26**, Figure 9), **26** being the main reaction product. Their ^1H NMR spectra (Figures 65 and 66) essentially differed from that of **24** only for the presence of one and two methoxy groups resonating at δ 3.88 and 3.88 and 3.86. ESIMS spectrum of **25**, recorded in positive mode, showed the sodiated dimeric form $[\text{2M}+\text{Na}]^+$, the potassium and sodium clusters $[\text{M}+\text{K}]^+$, $[\text{M}+\text{Na}]^+$ and $[\text{M}+\text{H}]^+$ at m/z 655, 355, 339. The APCIMS spectrum recorded in negative mode showed the pseudomolecular ion $[\text{M}-\text{H}]^-$ at m/z 315 and fragmentation ion $[\text{M}-\text{Me}]^-$ at m/z 301 generated from the molecular ion by loss of methyl group. The ESI and APCIMS spectra of **26**, recorded in positive mode showed the potassium and sodium clusters $[\text{M}+\text{K}]^+$, $[\text{M}+\text{Na}]^+$, and the pseudomolecular ion $[\text{M}+\text{H}]^+$ at m/z 369, 353, and 331, respectively. Furthermore, **24** was also converted into the 6,7,14-*O,O',O''*-triacetyl, and 7-*O-p*-Br-benzoyl (**27** and **28**, Figure 9) esters by the reaction with anhydride acetic and pyridine and DMAP and *p*-Br-benzoyl chloride, respectively. The IR of **27** significantly differed from that of **24** for the absence of hydroxy group and the presence of bands due to the ester groups (Nakanishi et al., 1977), Its ^1H NMR spectrum (Figure 67) differed from that of **24** for the significant downfield shift of H-14 ($\Delta\delta$ 1.10), appearing as expected as a broad singlet at δ 5.80 and for the presence of the typical three singlets of the acetyl groups at δ 2.29, 2.24 and 1.92. Its ESI and APCIMS spectra, recorded in positive mode, showed the potassium and the sodium clusters $[\text{M}+\text{K}]^+$, $[\text{M}+\text{Na}]^+$ and the pseudomolecular ion $[\text{M}+\text{H}]^+$ at m/z 467, 451, and 429, respectively. The IR spectrum of **28** showed the presence of a signal due to the ester group while its ^1H NMR spectrum (Table 68) differed from that of **24** for the typical signal pattern of the *p*-Br-benzoyl residue which resonated as two couples of doublets ($J = 8.4$ Hz) at δ 8.81 (2', 6') and 7.65 (3', 5'). Its ESIMS spectrum, recorded in positive mode showed the typical isotopic bromine peaks for the potassium and sodium clusters $[\text{M}+2+\text{K}]^+$, $[\text{M}+\text{K}]^+$, $[\text{M}+2+\text{Na}]^+$, $[\text{M}+\text{Na}]^+$ at m/z 525, 523, 509 and 507. The APCIMS spectrum, recorded in the same mode, gave fragmentation peaks generated from the pseudomolecular ion and its isotopic peak by loss of H_2O $[\text{M}+\text{H}-\text{H}_2\text{O}]^+$, and $[\text{M}+2+\text{H}-\text{H}_2\text{O}]^+$ at m/z 467 and 469 and also the peak generated from the molecular ion by the loss of the *p*-Br-

benzoate $[M-p\text{-BrC}_6\text{H}_4\text{CO}_2]^+$ at m/z 285. The ESIMS spectrum, recorded in negative mode, showed the pseudomolecular ion and its isotopic ions $[M-H]^-$ and $[M+2-H]^-$ at m/z 483 and 485 and the ion generated from the molecular ion by loss of the *p*-Br-benzoyl group $[M-p\text{-BrC}_6\text{H}_4\text{CO}]^-$ at m/z 301. The APCIMS spectrum, recorded in the same mode, gave the pseudomolecular ion and its isotopic ion $[M-H]^-$ and $[M+2-H]^-$ at m/z 483 and 485 and the peaks generated from the molecular ion by loss of *p*-Br-benzoate $[M-p\text{-BrC}_6\text{H}_4\text{CO}_2]^-$, *p*-Br-benzoyl $[M-p\text{-BrC}_6\text{H}_4\text{CO}]^-$ and the *p*-Br-phenyl $[M-p\text{-BrC}_6\text{H}_4]^-$ at m/z 285, 301 and 314, respectively. Finally **24** was converted into 15,16-dihydro derivative (**29**) by catalytic hydrogenation. The ^1H NMR spectrum (Figure 69) of **29** differed from that of **24** essentially for the absence of the signals of the vinyl group at C-13 while the signals of the corresponding ethyl group were observed as a triplet (CH_3 -16) and a quartet (CH_2 -15) ($J= 7.4$ Hz,) at δ 0.71 and 1.04, respectively (Pretsch et al., 2000). Its ESIMS spectrum, recorded in positive mode, showed ions generated from the sodiated dimeric form, the sodium cluster and the pseudomolecular ion by loss of water $[2M-2\text{H}_2\text{O}+\text{Na}]^+$, $[M-\text{H}_2\text{O}+\text{Na}]^+$ $[M-\text{H}_2\text{O}+\text{H}]^+$ at m/z 595, 309, and 287, respectively.

The relative configuration of diplopimarane was determined by X-ray diffractometric analysis of its suitable crystal obtained by a slow evaporation of EtOAc-*n*-hexane (1:3) solution. This stereochemistry, reported in the ORTEP view of **24** (Figure 70) allowed us to axially and equatorially locate the vinyl group at C-13 and the hydroxy group at C-14, respectively, in the C-ring which assumes a half-chair conformation.

Compound **24** crystallizes in the monoclinic $P 2_1$ space group with one molecule in the asymmetric unit. All bond lengths are in the normal range. The molecule consists of three condensed rings. The central ring B is planar and exhibit C-C distances typical of a fully substituted benzene ring. Accordingly with the minimum energy conformation for cyclohexene rings, both the two condensed rings (A and C) adopt the half-chair conformation. In the ring C the vinyl group at C-13 is located in the axial position, while the hydroxy group at C-14 is in the

equatorial position. In the crystal packing the hydroxy groups are involved in intra and intermolecular OH...O hydrogen bonds affording chains of molecules along **b** axis direction.

The relative configuration of **24** was confirmed by the correlations observed in the NOESY spectrum (Berger et al., 2004) (Figure 71) between Me-17 and H-14, H-14 and H-12b, and H-15 with H-12a.

The absolute configuration of **24** was determined by applying a modified Mosher's method (Othani et al., 1989). Diplopimarane 6,7-*O,O'*-dimethyl ether (**26**) was converted into the corresponding *S*-MTPA and *R*-MTPA monoesters at C-14 (**30** and **31**, Figure 11) by reaction with *R*-(-)- α -methoxy- α -trifluoromethylphenylacetyl (MTPA) and *S*-(+)- MTPA chloride, whose spectroscopic data (Figures 72 and 73) were consistent with the structure assigned to **24**. Subtracting the chemical shifts of the protons (Table 15) of 14-*O-R*-MTPA (**31**) from those of 14-*O-S*-MTPA (**30**) esters, the $\Delta\delta$ (**30-31**) values for all the protons were determined as reported in Figure 74. The positive $\Delta\delta$ values are located on the right-hand side, and the negative values on the left-hand side of model A as reported in Othani et al. (1989). This model allowed the assignment of the *S* configuration to C-14 and consequently a *R* configuration to C-13. Thus, **24** was formulated as (1*S*,2*R*)-2,8,8-trimethyl-2-vinyl-1,2,3,4,5,6,7,8-octahydro-phenanthrene-1,9,10-triol.

That diplopimarane belongs to the *ent*-pimarane subgroup of diterpens was also confirmed by conversion of sphaeropsidin A (**32**) into **24** by gaseous HCl treatment in MeOH at 0 °C. Different reaction products were obtained and, among them, **24** and its C-14 epimer were also obtained as an inseparable mixture. However, investigation of the ¹H NMR spectrum of this mixture showed clearly the significant signals of diplopimarane at the chemical shifts reported in Table 13 together with those of its corresponding 14-epimer. In fact, this spectrum also showed six other singlets at δ 8.65, 5.83, 4.89, 1.44, 1.43 and 1.06 due to HO-6, HO-7, H-14 and Me-19, Me-18 and Me-17, and a doublet of doublets ($J=15.0, 10.7$ Hz) at 5.83 due to H-15 of 14-*epi*-diplopimarane. Previously a similar conversion of the antibiotic LL-S491 β then later turned out

to be sphaeropsidin A, (Evidente et al., 1996) was reported but no detailed reaction conditions, products and stereochemistry at C-14 were indicated (Ellestad et al., 1972).

Considering the structure of **24** and its formation by acid conditions from sphaeropsidin A, which is the main phytotoxic metabolite produced by *D. quercivora*, a probable mechanism of this conversion was reported in Figure 75. The first step could be the hydrolysis of the lactone D ring which generated the carboxylic group at C-10 and the ketone group at C-6. The protonation of the tertiary hydroxy group at C-9 and the successive elimination of water and CO₂ generated the double bond between C-9 and C-10. Successively, the protonation of the ketone at C-7 and the non- stereoselective addition of water at C-14 of the double bond C-8 and C-14, followed by deprotonation generated the corresponding diol. Finally, keto-enol equilibrium between C-5 and C-6 generated **24** and its C-14 epimer.

Two bioassays were used to investigate the phytotoxic activity of diplopimarane (**24**), its derivatives (**25-29**), sphaeropsidin A (**32**), sphaeropsidin C (**33**) and (+)-epiepoformin (**34**) as described in the experimental section. In the leaf-puncture bioassay, the phytotoxicity was evaluated on holm oak, cork oak, and tomato leaves. As shown in Table 19, none of these compounds, except **32** and **34**, were active in this assay. Specifically, sphaeropsidin A (**32**) caused necrotic lesions on holm and cork oak (area lesion sizes of 10.85 and 15.03 mm², respectively), whereas the lesions on tomato leaves appeared as dark green water-soaked spots surrounded by a yellow halo (area lesion sizes of 120.92 mm²). Epiepoformin exhibited similar activity to **32** on holm and cork oak (area lesion sizes of 6.68 and 9.49 mm², respectively). When applied on detached leaves of tomato, **34** caused irregular necrotic lesions (13.49 mm² area).

In tomato cuttings bioassay, the compounds **24**, **25**, **29**, **32** and **34** were active. Diplopimarane (**24**) caused stewing on stem within 48 h from the application at 0.2 and 0.1 mg/mL. Both its derivatives **25** and **29** caused, to different extents, stewing on stem at 0.2

and 0.1 mg/mL. Stewing and/or wilting symptoms were observed with sphaeropsidin A and C (**32** and **33**, respectively) and (+)-epiepoformin (**34**) at 0.2 and 0.1 mg/mL.

The compounds **24**, **32**, **33** and **34** were preliminarily screened for antifungal and antioomycete activity *in vitro* against four plant pathogens at 100 µg/mL (see par.4.7.3.). Two synthetic fungicides: Metalaxyl-M and PCNB to which *Oomycetes*, *Ascomycetes* and *Basidiomycetes* are sensitive were used as positive control. The mycelial growth inhibition (as a percentage) was listed in Table 20. The compounds **24** and **32-34** showed a different spectrum of activity. Among the tested pathogens, *P. cinnamomi* and *P. plurivora* seem to be the most sensitive target organisms followed by *A. rolfsii*, whereas *D. corticola* was shown to be the most resistant one. Among the tested compounds, **32** showed high activity against *P. cinnamomi*, *P. plurivora* and *A. rolfsii*. In particular, it completely inhibited the mycelial growth of both oomycetes showing the same effectiveness of metalaxyl-M at 100 µg/mL. It also induced 83.2% inhibition of *A. rolfsii* and its effect magnitude is comparable to that of PCNB at 100 µg/mL. In addition, compound **32** exhibited negligible activity against *D. corticola* (19.8% inhibition growth). Moreover, the mycelial growth of *D. corticola* was only slightly inhibited by compound **24** (54.5 inhibition percentage) and **34** (39.7 inhibition percentage). No antifungal and antioomycete activity was significantly shown by compound **33** at the concentration used.

In the *Artemia salina* bioassay, diplopimarane (**24**), its derivatives (**25-27**, **29**), sphaeropsidin A (**32**) and (+)-epiepoformin (**34**) caused more than 50% larval mortality at 200 µg/mL after 36 h of exposure to the metabolites (Table 19). Sphaeropsidin C (**33**) was inactive. On the basis of these preliminary results, it could envisage a LC₅₀ value of less than 200 µg/mL. Thus, each of these metabolites, in particular **24** and its derivatives **25** and **29**, could be screened against tumor cell lines and evaluated in more specific antitumor systems. Moreover, previous studies have shown significant cytotoxic activity of sphaeropsidin (Evidente et al., 1996; Wang et al., 2011). Interestingly, it inhibits not only cancer cell proliferation but also migration of metastatic breast cancer cell line.

5.6 Synthesis and chemical characterization of oxysporones derivatives

Eight derivatives of oxysporone were hemisynthesized in order to carry out a structure-activity relationships study aimed to obtain compounds with improved activities and specificity. Firstly **35** was converted into the corresponding 4-O-acetyl derivative (**38**, Figure 13) by usual acetylation carried out with acetic anhydride and pyridine; **38** showed the reversible modification of the hydroxy group at C-4 of dihydropyran ring. A different modification of the same hydroxy group was obtained by conversion of **35** into the corresponding 4-O-p-bromobenzoyl derivative (**41**, Figure 13) by reaction with p-bromobenzoyl chloride carried out in CH₃CN. **41** differed from **38** for the aromatic and bulky nature of the acyl group.

The dihydropyran ring was modified by catalytic hydrogenation of its double bond. The reaction was carried out both on oxysporone (**35**) and on its acetylated derivative (**38**), yielding the corresponding 2,3-dihydroderivative **39** and **43** (Figure 13). Oxysporone showed a different reactivity in respect to some oxidant reagents. In fact, when the reaction was conducted with Corey's reagent (Corey and Suggs, 1975), the expected oxidation of secondary hydroxy group at C-4 was observed, yielding the corresponding α,β -unsaturated ketone (**40**, Figure 13). Instead, when the reaction was performed with Jones's reagent (Bowers et al., 1953), the derivative **40** was not obtained and the only product of the oxidation was 2-(4-pyronyl) derivative of acetic acid (**42**, Figure 13). A probable reaction mechanism, which justify the conversion of **35** into **42**, is in agreement with the literature data (Edwards et al., 2001). The strong acid conditions probably induced the enolization of the ketone group at C-4 of **6** and the protonation of the carbonyl of the furanone ring (Figure 76). This latter rearranged into the 2-(4-pyronyl)acetic acid (**42**) being the driving force the stability of the 4-pyrone ring. This compound, named xylaric acid, had been firstly isolated from *Xylaria* spp. (Salvatore et al., 1994). Then it was also isolated from *Xylaria grammica* (Mont.) Fr. along with grammicin (Edwards et al., 2001) and from *Pestalotiopsis* sp. HC02 isolated from *Chondracris rosea* L. gut together pestalotines A and B (Zhang et al., 2008). The acid

42 was converted into the corresponding methyl ester **45** (Figure 13) by reaction with an ethereal solution of diazomethane.

As already observed for oxysporone, the oxidation conducted with Jones's reagent on the 2,3-dihydrooxysporone (**39**, Figure 13) gave the expected 2-(2,3-dihydro-4-pironyl)acetic acid (**44**), probably through a reaction mechanism similar to that hypothesized for formation of **42**, **44**, also known as desoxyapatulinic acid, was previously obtained by synthesis (Woodward and Singh, 1950) and by hydrogenation of patulin (Engel et al., 1949). It was also successively isolated from cultures of *Penicillium patulum* (Scott et al., 1972) and from an unidentified marine fungus reported as *Penicillium* sp. (Wu et al., 2010). The structures of all derivatives **38-45** were determined by comparing their spectroscopic data, essentially ¹H NMR (Figures 77-85) and ESI and/or APCIMS, with those of oxysporone. Two bioassays were used to investigate the phytotoxic activity of oxysporone (**35**), its derivatives (**35-45**). In the leaf-puncture bioassay, the phytotoxicity was evaluated on holm oak, cork oak and grapevine leaves. As shown in Table 21, oxysporone (**35**) confirmed its strong toxicity on all species tested causing necrotic lesions ranging from 15.81 mm² on cork oak leaves to 23.04 mm² on grapevine leaves. Among oxysporone (**35**) derivatives compounds **38** and **40** retained the phytotoxicity, whereas the derivatives **39**, **41-45** were inactive. Specifically, the monoacetyl derivative (**38**) of oxysporone exhibited the same moderate activity as that shown by **40** on all plant species tested (lesion sizes ranging from 3.50 to 7.83, and from 4.28 to 7.86 mm², respectively). In tomato cuttings bioassay, the compounds **35**, **38**, and **40** were active. Oxysporone (**35**) caused wilting within 48 h from the application at 0.2 mg/mL. Stewing or wilting symptoms were also observed with this compound at 0.1 and 0.05 mg/mL. Both **38** and **40** caused stewing on stem at 0.2 and 0.1 mg/mL. None of the other compounds caused any visible symptoms in this bioassay at the highest concentration used. From the analysis of the structures and the activities displayed by all compounds, structure-activity relationships and some structural features related to the phytotoxic activity can be extracted.

The dihydrofuropyran carbon skeleton is a structural feature important for the activity considering that the oxidative opening of the dihydrofuran ring into the corresponding 2-substituted acetic acid joined with the conversion of the pyran ring into the corresponding semiquinone as in **42** and **45** and the corresponding 2,3-dihydro derivative **44** determine the complete loss of activity. The double bond of the dihydropyran ring present in **35** appears to be also an important structural feature for phytotoxic activity. In fact, derivatives as **39** and **43** lacking this double bond were inactive. This was also confirmed by the inactivity of derivative **43**. The hydroxy group at C-4 seems also to be somehow associated with the phytotoxic effects. In fact, the acetylation of this functional group as in derivative **38** led to a decrease of activity, and the introduction of a bulky substituent in the same position as in derivative **41** resulted in the total loss of activity. The oxidation by Corey's reagent of hydroxy group at C-4 seems only to decrease the bioactivity of **35** as observed testing derivatives **40**. All compounds, with the exception of **44** and **45**, obtained in small quantities, were preliminary screened for antifungal activities in vitro against four plant pathogens at 100 mg/mL (see experimental). The results summarized in Table 21 showed that among all the tested compounds only compound **41** displayed significant activities (35.6–100% inhibition rates) against all pathogens tested at 100 mg/mL. Oxysporone, the other derivatives **38-40** and **42-43** were inactive at the same concentration. Fungal sensitivity to **41** varied according to the species. *Athelia rolfsii* and *Phytophthora plurivora* appeared to be more sensitive (100% inhibition) to this compound. *Diplodia corticola* showed to be less sensitive (inhibition <40%), whereas on *P. cinnamomi* the inhibition rate was of 77.2%. In order, to more fully understand the activity of the active compound **41**, its EC₅₀ was further evaluated (concentration which inhibits mycelial growth by 50%) towards the same pathogens used in the preliminary test, except *D. corticola*, in comparison with three specific commercial fungicides namely toclofos-methyl, PCNB and metalaxyl-M. As shown in Table 22, derivative **41** gave the highest activity against *P. plurivora* with EC₅₀ value of 29.47 mg/mL, whereas it showed the lowest activity against *P. cinnamomi* with EC₅₀ value of 43.5 mg/mL.

Nevertheless, each fungal species showed sensitivity levels to compound **41** that were one or two orders of magnitude lower than those recorded for the commercial fungicides (Table 22).

6. CONCLUSION

- A new phytotoxic cyclohexenone, namely cyclobotryoxide was isolated from *Neofusicoccum australe* strain BOT48.
- From the culture filtrates of *Lasiodiplodia mediterranea* strain BL101 were isolated and characterized three new jasmonic acid esters, namely lasiojasmonates A-C, and for the first time 16-O-acetyl derivatives of botryosphaerilactones A and C. Moreover (1R,2R)-jasmoic and its methyl ester, botryosphaerilactone A and (3S,4R,5R)-4-hydroxymethyl-3,5-dimethyl-dihydro-2-furanon and (3R,4S)-botryodiplodin were isolated and identified.
- From the culture filtrates of *Lasiodiplodia mediterranea* strain B6 two new dimeric γ -lactols namely lasiolactols A and B were isolated and characterized. Moreover botryosphaeriodiplodin, (5R)-5-hydroxylasiodiplodin, (1R,2R)-jasmoic and (3S,4R,5R)-4-hydroxymethyl-3,5-dimethyl-dihydro-2-furanon were isolated and identified.
- *Neofusicoccum australe* strain BL24 showed produced three known metabolites: tyrosol, botryosphaerone D and (3S,4S)-3,4,8-trihydroxy-6-methoxy-3,4-dihydro-1(2H)-naphthalenone.
- A new 20-nor-ent-pimarane, named diplopimarane, having antifungal activity, was isolated together with sphaeropsidins A and C, and (+)-epiepoformin from organic crude extracts of *Diplodia quercivora*.
- Structure-activity study on oxysporone showed that dihydrofuopyranone carbon skeleton and both the double bond the hydroxy group of dihydropyran ring appeared to be structural features important in conferring activity.
- New derivative with antifungal activity was prepared from oxysporone

7. REFERENCES

1. Ahamad, P. Y. A.; Kunhi, A. A. M.; Divakar, S. *J. Microbiol Biotechnol.* **2001**, *17*, 371-377.
2. Aldridge, D.C., Galt, S., Giles, D., Turner, W.B. *J. Chem. Soc.* **1971**, C 1623-1627.
3. Altomare, A.; Burla, M. C., Cavalli, M., Cascarano, G. L., Giacovazzo, C., Guagliardi, A., Moliterni, A. G. G., Polidori G., Spagna R. *J. Appl. Crystall.* **1999**, *32*, 115–119.
4. Andolfi, A.; Mugnai, L.; Luque, J.; Surico, G., Cimmino, A.; Evidente, A. *Toxins* **2011**, *3*, 1569-1605.
5. Andolfi, A., Maddau, L., Cimmino, A., Linaldeddu, B.T., Franceschini, A., Serra, S., Basso, S., Melck D., Evidente A. *J. Nat. Prod.* **2012**, *75*, 1785-1791.
6. Arsenault, G.P., Althaus, J.R. *J. Chem. Soc.* **1969**, (D), *Chem. Commun.*, 1414-1415.
7. Au, T.K., Wallace, S.H.C., Leung, P.C. *Plant Physiol.* **1985**, *77*, 303-308.
8. Au, T. K., Wallece, S.H.C., Leung, P.C. *Life Sci.* **2000**, *67*, 733-742.
9. Barros, M. T., Maycock, C. D., Ventura, M. R. *Chem. Eur. J.* **2000**, *6*, 3991–3996.
10. Berestetskiy, A. O. *App. Biochem.Microbiol.* **2008**, *44*, 453-465.
11. Berger, S., Braun, S. In *200 and More Basic NMR Experiments: A Practical Course*, first ed. Wiley-VCH, Weinheim, **2004**.
12. Bischoff, V., Cookson, S.J., Wu, S., Scheible, W.R. *J. Exp. Bot.* **2009**, *60*, 955-965.
13. Bowers, A., Halsall, T.G., Jones, E.R.H., Lemin, A.J., 1953. In *The chemistry of the triterpenes and related compounds. Part XVIII.* J. Chem. Soc. 2548-2560.
14. Breitmaier, E.; Voelter, In *Spectroscopy* VCH: Weinheim, **1987**, pp 183-280.

15. Brunner, H.G., Chemla, P., Dobler, M.R., O'Sullivan, A.C., Pachlatko, P., Pillonel, C., Stierli, D. *Am. Chem. Soc. Ser.* **2007**, *948*, 121-135.
16. Burruano, S., Mondello, V., Conigliano, G., Alfonso, A., Spagnolo, A., Mugnai, L., *Phytopathol. Mediterr.* **2008**, *47*, 132.
17. Bury, M., Novo-Uzal, E., Andolfi, A., Cimini, S., Wauthoz, N., Heffeter, P., Lallemand, B., Avolio, F., Delporte, C., Cimmino, A., Dubois, J., Van Antwerpen, P., Zonno, M.C., Vurro, M., Poumay, Y., Berger, W., Evidente, A., De Gara, L., Kiss, R., Locato V. *Int. J. Oncol.* **2013**, *43*, 575-585.
18. Cabras A., Mannoni, M.A., Serra, S., Andolfi, A., Fiore, M., Evidente. A. *Eur. J. Plant Pathol.* **2006**, *115*, 187-193.
19. Capasso, R.; Cristinzio, G.; Evidente, A.; Scognamiglio, F. *Phytochemistry* **1992**, *31*, 4125–4128.
20. Carreno, M. C., Merino, E., Ribagorda, M., Somoza, A., Urbano, A. *Org. Lett.* **2005**, *7*, 1419–1422.
21. Castillo-Pando, M., Somers, A., Green, C.D., Priest, M., Sriskanthades, M. *Australas. Plant Pathol.* **2001**, *30*, 59-63.
22. Chai, C.L.L., Waring, P. *Redox Rep.* **2000**, *5*, 257-264.
23. Cimmino, A.; Villegas-Fernández, A. M.; Andolfi, A.; Melck, D.; Rubiales, D.; Evidente, A. *J. Agric. Food Chem.* **2011**, *59*, 9201-9206.
24. Cimmino, A., Andolfi, A., Zonno, M.C., Avolio, F., Santini, A., Tuzi, A., Berestetskiy, A., Vurro, M., Evidente, A. *J. Nat. Prod.* **2013**, *76*, 1291–1297.
25. Cimmino, A., Andolfi, A., Zonno, M.C., Avolio, F., Berestetskiy, A., Vurro, M., Evidente, A., *Phytochemistry* **2013**, *96*, 208–213.
26. Conti, P., Roda, G., Stabile, H., Vanoni, M.A., Curti, B., De Amici, M. *Farmaco* **2003**, *58*, 683-690.
27. Corey, E.J., Suggs, J.W., *Tetrahedron Lett.* **1975**, *31*, 2647-2650.

28. Crous, P.W., Slippers, B., Wingfield, M.J., Rheeder, J., Marasas, W.F.O., Phillips, A.J.L., Alves, A., Burgess, T Barber, P., Groenewald, J.Z.. *Stud. Mycol.* **2006**, *55*, 235-253.
29. Cseke, C., Gerwick, B.C., Crouse, G.D., Murdoch, M.G., Green, S.B., Heim, D.R. *Pestic. Biochem. Physiol.* **1996**, *55*, 210-217.
30. Denman, S., Crous, P.W., Taylor, J.E., Kang, J.Ch., Pascoe, I., Wingfield, M.J. *Stud. Mycol.* **2000**, *45*, 129-140.
31. Djoukeng, J.D., Polli, S., Larignon, P., Mansour, E.A. *Eur. J. Plant Pathol.* **2009**, *124*, 303-308.
32. Duke, S.O., Wickliff, J.L., Vaughn, K.C., Paul, R.N. *Physiol. Plant.* **1982**, *56*, 387-398.
33. Duke, S.O., Evidente, A., Fiore, M., Rimando, A.M., Vurro, M., Chistiansen, N., Looser, R., Grossmann, K. *Pestic. Biochem. Physiol.* **2011**, *100*, 41-50.
34. Edwards, R. L., Maitland, D. J., Pittayakhajonwut, P., Whalley A.J.S., *J. Chem. Soc.* **2001**, *1*, 1296-1299.
35. Ellestad, G. A., Kunstmann, M. P., Mirando, P., Morton, G. O. *J. Am. Chem. Soc.* **1972**, *94*, 6206-6208.
36. Engel, B.G., Brzeski, W., Plattner, P.A., *Helv. Chim. Acta* **1949**, *32*, 1166-1175.
37. Evidente, A., Sparapano, L., Motta, A., Giordano, F., Fierro, O., Frisullo, S. *Phytochemistry* **1996**, *42*, 1541-1546.
38. Evidente, A., Sparapano, L., Giordano, F., Fierro, O., Motta, A. *Phytochemistry* **1997**, *45*, 705-713.
39. Evidente, A.; Sparapano, L.; Fierro, O.; Bruno, G.; Giordano, F.; Motta, A. *Phytochemistry* **1998**, *48*, 1139-1143.
40. Evidente, A., Capasso, R., Cutignano, A., Taglialatela-Scafati, O., Vurro, M., Zonno, M.C., Motta, A. *Phytochemistry* **1998**, *48*, 1131-1137.

41. Evidente, A, Sparapano, L, Fierro, O., Bruno, G., Motta, A. *J. Nat. Prod.*, **1999**, *62*, 253-256.
42. Evidente, A., Sparapano, L., Fierro, O., Bruno, G., Giordano, F., Motta, A. *Phytochemistry* **2002**, *59*, 817-823.
43. Evidente, A., Maddau, L., Spanu, E., Franceschini, A., Lazzaroni, S., Motta, A. *J. Nat. Prod.* **2003**, *66*, 313-315.
44. Evidente, A., Sparapano, L., Andolfi, A., Bruno, G., Motta, A. *Austral. J. Chem.* **2003**, *56*, 615-619.
45. Evidente, A, Maddau, L, Spanu, E, Franceschini, A, Lazzaroni, S, Motta, A. *J. Nat. Prod.*, **2003**, *66*, 313-315.
46. Evidente, A., Fiore, M., Bruno, G., Sparapano, L., Motta, A. *Phytochemistry* **2006a**, *67* (10), 1019-1028.
47. Evidente A., Andolfi, A., Fiore, M., Spanu, E., Maddau, L., Franceschini, A., Marras, F., Motta, A. *J. Nat. Prod.* **2006b**, *69*, 671-674.
48. Evidente A., Andolfi, A., Fiore, M., Spanu, E., Franceschini, A., Maddau, L. *Archivok* **2007**, *7*, 318-328.
49. Evidente, A.; Punzo, B.; Andolfi, A.; Cimmino, A.; Melck, D.; Luque, J. *Phytopathol. Mediterr.* **2010**, *49*, 74-79.
50. Evidente, A., Andolfi, A., Cimmino, A., Abouzeid, M. A. In: *Sustainable Agriculture: Technology, Planning and Management* (Salazar, A., Rias, I. Eds.), Nova Science Publishers Inc. ISBN: **2010**, 978-1-60876-269-9 pp.177-234.
51. Evidente, A., Punzo, B., Andolfi, A., Cimmino, A., Melck, D., Luque, J. *Phytopathol. Mediterr.* **2010**, *49*, 74-79.
52. Evidente, A., Andolfi, A., Cimmino, A., Abouzeid, A. M. In *Sustainable Agriculture: Technology, Planning and Management* (Salazar, A., Rias, I. Eds.) Nova Science Publishers Inc. New York **2010**, pp. 145-176.

53. Evidente, A., Andolfi, A., Cimmino, A. *Chirality* **2011**, *23*, 674-693.
54. Evidente, A., Maddau, L., Scanu, B., Andolfi, A., Masi, M., Motta, A., Tuzi, A. *J. Nat. Prod.* **2011**, *74*, 757-763.
55. Evidente A., Venturi V., Masi M., Degrassi G., Cimmino A., Maddau L., Andolfi A. *J. Nat. Prod.* **2011a**, *74*, 2520-2525.
56. Evidente, A., Maddau, L., Scanu, B., Andolfi, A., Masi, M., Motta, A., Tuzi, A. *J. Nat. Prod.* **2011b**, *74*, 757-763.
57. Evidente, A., Masi M., Linaldeddu, B. T., Franceschini, A., Scanu, B., Cimmino, A., Andolfi, A., Motta, A., Maddau, L. *Phytochemistry* **2012**, *77*, 245-250.
58. Evidente, A., Cimmino, A., Andolfi A. *Chirality* **2013**, *25*, 59-78.
59. Farmer, E.E., Johnson, R.R., Ryan, C.A. *Plant. Physiol.* **1992**, *98*, 995-1002.
60. Farr, D.F., Rossman, A.Y. **2011**. *Fungal Databases, Systematic Mycology and Microbiology Laboratory, ARS, USDA*. Retrieved May 20, 2011, from [http:// nt.ars-grin.gov/fungaldatabases/fungushost/fungushost.cfm](http://nt.ars-grin.gov/fungaldatabases/fungushost/fungushost.cfm).
61. Favilla, M., Macchia, L., Gallo, A., Altomare, C. *Food Chem. Toxicol.* **2006**, *44*, 1922-1931.
62. Feld, A., Kobek, K., Litchenthaler, H.K. *Brighton Crop Prot. Conf. Weeds* **1989**, *2*, 479-486.
63. Fonne-Pfister, R., Chemla, P., Ward, E., Girardet, M., Kreuz, E., Honzatko, R.B., Fromm, H.J., Schar, H.P., Grutter, M.G., Cowan-Jacob, S.W. *Proc. Natl. Acad. Sci. USA* **1996**, *93*, 9431-9436.
64. Franceschini, A., Corda, P., Maddau, L., Marras, F. *IOBC Bulletin*, **1999**, *22*, 5-12.
65. Frisvad, J. C., Andersen, B., Thrane, U. *Mycol. Res.* **2008**, *112*, 231-240.
66. Fuska, J., Proksa, B., Uhrin, D., *Folia Microbiol.* **1988**, *33*, 238-240.

67. Giorgio E., Maddau L., Spanu E., Evidente A., Rosini C. *J. Org. Chem.* **2005**, *70*, 7-13.
68. Gupta, R.S., Chandran, R.R., Divekar, P.V. *Indian J. Exp. Biol.* **1966**, *4*, 152-153.
69. Halloin, J.M., De Zoeten, G.A., Gaard, G.R., Walker, J.C. *Plant Physiol.* **1970**, *45*, 310-314.
70. Hamid, K., Strange, R.N. *Physiol. Mol. Plant Pathol.* **2000**, *56*, 235-244.
71. Hammerschlag F.A. In: *Advances in agricultural Biotechnology* (G.B. Collins, J.G. Petolino, Eds.). Martinus Nijhoff/Dr W. Junk Publishers, **1984**, 453-489.
72. Hassal, K.A. In *Biochemistry and Use of Pesticides*. Verlag Chemie, Weinheim, **1990**, pp. 58, 72, 304, 429, and 497.
73. He, G., Matsuura, H., Yoshihara, T. *Phytochemistry* **2004**, *65*, 2803-2807.
74. Heim, D.R., Cseke, C., Gerwick, B.C., Murdoch, M.G., Green, S.B. *Pestic. Biochem. Physiol.* **1996**, *55*, 210-217.
75. Hewitt, R.D. In *Compendium of Grape Diseases*; The American Phytopathological Society (APS) Press: St. Paul, MN, USA, **1988**; pp. 25-26.
76. Husain, A., Ahmad, A., Agrawal, K. P. *J.Nat. Prod.* **1993**, *56*, 2008-2011.
77. Iacobellis, N.S., Bottalico, A. *Phytopathol. Medierr.* **1981**, *20*, 129-132.
78. Isaka, M., Yangchum, A., Auncharoen, P., Srichomthong, K., Srikitikulchai, P. *J. Nat. Prod.* **2011**, *74*, 300-302.
79. Jacobs, K.A., Rehner, S.A. *Mycologia* **1998**, *90*, 601-610.
80. Jernerèn, F., Eng, F., Hamberg, M., Oliw E. H., *Lipids* **2012**, *47*, 65-73.
81. Kawaide H. *Biosci. Biotechnol. Biochem.* **2006**, *70*, 583-590.
82. King, R.R., Calhoun, L.A. *Phytochemistry* **2009**, *70*, 833-841.
83. Kitaoka, N., Nabeta, K., Matsuura, H. *Biosci. Biotechnol. Biochem.* **2009**, *73*, 1890-1892.
84. Knogge, W. *The Plant Cell.* **1996**, *8*, 1711-1722.

85. Kuhn, S., Bussemer, J., Chigri, F., Vothknecht, U.C. *Plant J.* **2009**, *58*, 694-705.
86. Xu, Y.X., Lu, C.H., Zheng, Z.H., Shen, Y.N. *Helv. Chim. Acta* **2011**, *94*, 897-902.
87. Lallemand, B., Masi, M., Maddau, L., De Lorenzi, M., Damd, R., Cimmino, A., Moreno y Banuls, L., Andolfi, A., Kiss, R., Mathieu, V., Evidente, A. *Phytochem. Lett.* **2012**, *5*, 770-775.
88. Lamari, L. In *Assess Image Analysis Software for Plant Disease Quantification*, APS Press: St. Paul, MN, **2002**.
89. Larignon, P., Fulchic, R., Cere, L., Dubos, B. *Phytopathol. Mediterr.* **2001**, *40*, S336-S342.
90. Li, X., Yao, Y.H., Zheng, Y.N., Lin, W.H., Sattler, I., Deng, Z.W. *Zhongguo Tianran Yaowu* **2007**, *5*, 20-23.
91. Linaldeddu, B.T., Scanu, B., Schiaffino, A., Serra, S. *Phytopathol. Mediterr.* **2010**, *49*, 417-420.
92. Linaldeddu, B.T., Scanu, B., Maddau, L., Franceschini, A., *Phytopathol. Mediterr.* **2011**, *50*, 473-477.
93. Linaldeddu, B.T., Franceschini, A., Alves, A., Phillips, A. J. L. *Mycologia* **2013**, *105*, 1266-1274.
94. Linaldeddu, B.T., Deidda, A., Scanu, B., Franceschini, A., Serra, S., Berraf-Tebbal, A., Zauaoui Boutiti, M., Ben Jamâa, M.L., Phillips, A.J.L. *Fungal Divers.* **2014**, DOI 10.1007/s13225-014-0301-x.
95. Martos, S., Andolfi, A., Luque, J., Mugnai, L., Surico, G., Evidente, A. *Eur. J. Plant Pathol.* **2008**, *121*, 451-461.
96. Matsuura, H., Nakamori, K., Omer, E.A., Hatakeyama, C., Yoshihara, T. *Phytochemistry* **1998**, *49*, 579.

97. Mazzeo, G., Santoro, E., Andolfi, A., Cimmino, A., Troselj, P., Petrovic, A. G., Superchi, S., Evidente, A., Berova, N. *J. Nat. Prod.* **2013**, *76*, 588-599.
98. Mennucci, B., Claps, M., Evidente, A., Rosini, C. *J. Org. Chem.* **2007**, *72*, 6680-6691.
99. Miersch, O., Preiss, G.S., Schreiber, K. *Phytochemistry* **1987**, *26*, 1037-1039.
100. Miersch, O., Kramell, R., Parthier, B., Wasternack, C. *Phytochemistry* **1999a**, *50*, 353-361.
101. Miranda, C.C.B.O., Dekker, R.F.H., Serpeloni J.M., Fonseca, E.A.I., Cólus, I.M.S., Barbosa A.M. *Int. J. Biol. Macrom.* **2008**, *42*, 172-177.
102. Mondello, V., Lo Piccolo, S., Conigliano, G., Alfonso, A., Torta, L., Burrano, S., *Phytopathol. Mediterr.* **2013**, *52*, 388.
103. Nagasawa, H., Suzuki, A., Tamura, S. *Agr. Biol. Chem.* **1978**, *42*, 1303-1304.
104. Nagata, T., Ando, Y. *Agric. Biol. Chem.* **1989**, *53*, 2811.
105. Nakajima, M., Itoi, K., Takamatsu, Y., Kinoshita, T., Okazaki, T., Kawakubo, K., Shindo, M., Honma, T., Tohjigamori, M., Haneishi, T. *J. Antibiot.* **1991**, *44*, 293-300.
106. Nakamori, K., Matsuura, H., Yoshihara, T., Ichihara, A., Koda Y. *Phytochemistry* **1994**, *35*, 835-839.
107. Nakanishi, K., Solomon, P.H. In *Infrared Absorption Spectroscopy* (Holden Day: Oakland, Eds.II) **1977**, pp 17-44.
108. Nakai, N., Murata, M., Nagahama, M., Hirase, T., Tanaka, M., Fujikawa, T., Nakao, N., Nakashima, K., Kawanishi, S. *Free Radic. Res.* **2003**, *37*, 69-76.
109. Natsumeda, Y., Ikegami, T., Olah, E., Weber, G. *Cancer Res.* **1989**, *49*, 88-92.
110. Nielsen, K. F., Sumarah, M. W., Frisvad, J. C., Miller, J. D. *J. Agric. Food Chem* **2006**, *54*, 3756-3763.
111. Okamura, H., Shimizu, H., Yamashita, N., Iwagawa, T., Nakatani, M. *Tetrahedron* **2003**, *59*, 10159-10164.
112. Osbourn A.E. *PNAS*, **2001**, *98(25)*, 14187-14188.

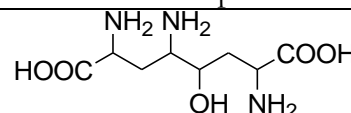
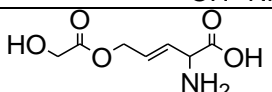
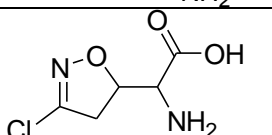
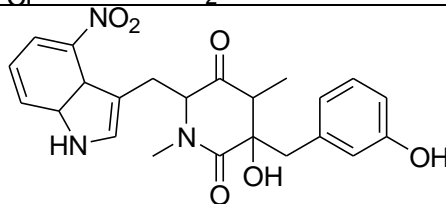
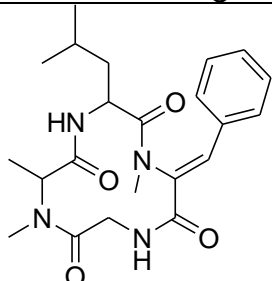
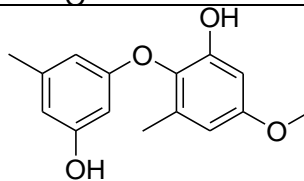
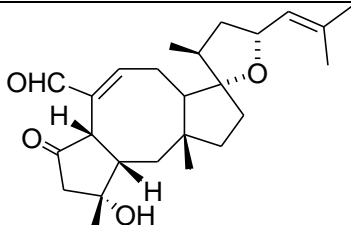
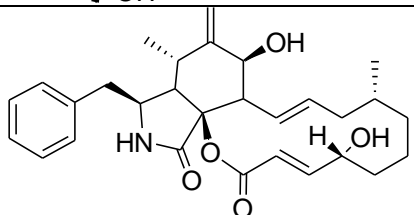
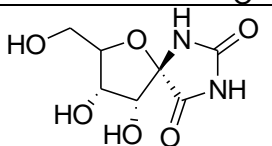
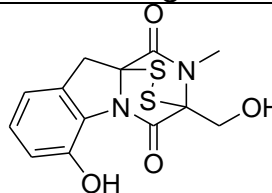
113. Othani, I., Kusumi, T., Ishitsuka, M.O., Kakisawa, H. *Tetrahedron Lett.* **1989**, *30*, 3147-3150.
114. Ohtani, I., Kusumi, T., Kashman, Y., Kakisawa, H. *J. Am. Chem. Soc.* **1991**, *113*, 4092.
115. Owens, L.D., Guggenheim, S., Hilton, J.L. *Biochim. Biophys. Acta* **1968**, *158*, 219-225.
116. Owens, L.D., Lieberman, M., Kunishi, A. *Plant Physiol.* **1971**, *48*, 1-4.
117. Owens, L.D. *Weed Sci.* **1973**, *21*, 63-66.
118. Pandi, M., Manikandan, R., Muthumary, J. *Biomed. Pharmacol.* **2010**, *64*, 48-53.
119. Pavlic, D., Slippers, B., Coutinho, T.A, Gryzenhout, M., Wingfield, M.J. *Stud. Mycol.* **2004**, *50*, 313-322.
120. Phillips, A.J.L. *Phytopathol. Mediterr.* **2002**, *41*, 3-18.
121. Phillips, A.J.L., Pennycook, S.R., Johnston, P.R., Ramaley, A., Akulov, A., Crous, P.W. *Persoonia* **2008**, *21*, 29-55.
122. Pinkerton, F., Strobel, G. *Proc. Natl. Acad. Sci. USA* **1976**, *73*, 4007-4011.
123. Phillips, A.J.L. *J. Phytopathol.* **1998**, *146*, 327-332.
124. Phillips, A.J.L. *Phytopathol. Mediterr.* **2002**, *41*, 3-18.
125. Pittayakhajonwut, P., Sohsomboon, P., Dramaee, A., Suvannakad, R., Lapanun, S., Tantichareon, M. *Planta Med.* **2008**, *74*, 281-286.
126. Pretsch, E.; Bühlmann, P.; Affolter, C. In *Structure Determination of Organic Compounds-Table of Spectral Data* (Springer-Verlag: Berlin Eds.III) **2000**, pp, 161-243, 385-404.
127. Ramezani, M., Shier, W.T., Abbas, H.K., Tonos, J.L., Baird, R.E., Sciumbato, G.L. *J. Nat Prod.* **2007**, *70*, 128-129.
128. Ravi, B.N., Armstrong, R.W., Faulkner, D.J. *J. Org. Chem* **1979**, *44*, 3109-3113.
129. Reimer, S., Selman, B.R. *J. Biol. Chem.* **1978**, *253*, 7249-7255.
130. Rodriguez-Foneca, C., Amils, R., Garrett, R.A. *J. Mol. Biol.* **1995**, *247*, 224-235.
131. Rodriguez-Suarez, R., Xu, D., Veillette, K., Davison, J., Sillaots, S., Kauffman, S., Hu, W., Bowman, H., Martel, N., Trosok, S., Wang, H., Zhang, L., Huang, LY., Li, Y.,

- Rahkhooadee, F., Ransom, T., Gauvin, D., Douglas, C., Youngman, P., Becker, J., Jiang, B., Roemer, T. *Chem. Biol.* **2007**, *14*, 1163-1175.
132. Rouxel, T., Chupeau, Y., Fritz, R., Kollmann, A., Blouquet, J.F. *Plant Sci.* **1988**, *57*, 45-53.
133. Rukachaisirikul, R., Arunpanichlert, J., Sukpondma, Y., Phongpaichit, S., Sakayaroj, J. *Tetrahedron* **2009**, *65*, 10590-10595.
134. Sakalidis, M. L.; Hardy, G. E. St. J.; Burgess, T. I. *Australas. Plant Pathol.* **2011**, *40*, 510-521.
135. Salvatore, M.J., Hensens, O.D., Zink, D.L., Liesch, J., Dufresne, C., Ondeyka, J.G., Jürgens, T.M., Borris, R.P., Raghoobar, S., McCauley, E., Kong, L., Gartner, S. E., Koch, G. E., Peláez, F., Diez, M.T., Cascales, C., Martin, I., Polishook, J.D., Balick, M.J., Beck, H.T., King, S.R., Hsu, A., Lingham R.B. *J. Nat. Prod.* **1994**, *57*, 755-760.
136. Savocchia, S., Steel, C.C., Stodart, B.J., Somers, A. *Vitis* **2007**, *46*, 27-32.
137. Schinko, E., Schad, K., Eys, S., Keller, U., Wohlleben, W. *Phytochemistry* **2009**, *70*, 1787-1800.
138. Scott, P. M., Kennedy, B., van Walbeek, W. *Experientia* **1972**, *28*, 1252.
139. Scott A.I. In *Interpretation of Ultraviolet Spectra of Natural Products* Pergamon Press LTD Oxford, **1964**, pp. 15-162.
140. Schaller, A., Stinzi, A. *Phytochemistry*, **2009**, *70*, 1532-1538.
141. Selman, B.R., Durbin, R.D. *Biochim. Biophys. Acta* **1978**, *502*, 29-37.
142. Sheldrick, G. M. *Acta Crystallogr.* **2008**, *A64*, 112-122.
143. Shen, Y. *Arch. Environ. Contam. Toxicol.* **1998**, *34*, 229-34.
144. Shier, W. T., Abbas, H., Baird, R., Ramezani, M., Sciumbato, G. *Toxin Rev.* **2007**, *26*, 343-386.

145. Siehl, D.L., Subramanian, M.V., Walters, E.W., Lee, S.F., Anderson, R.J., Toschi, A.G. *Plant Physiol.* **1996**, *110*, 753-758.
146. Slavov, S. *Biotechnol. Biotec. Eq.* **2005**, *19: sup3*, 48-55.
147. Sparapano, L., Bruno, G., Fierro, O., Evidente, A. *Phytochemistry* **2004**, *65*, 189-198.
148. Steinberg, T.H., Burgess, R.R. *J. Biol. Chem.* **1992**, *267*, 20204-20211.
149. Stierle, A., Upadhyay, R., Strobel, G. *Phytochemistry* **1992**, *30*, 2191-2192.
150. Styer, C.H., Cutler, H.G. *Plant Cell Physiol.* **1984**, *25*, 1077-1082.
151. Sultan, S., Sun, L., Blunt, J.W., Cole, A.L.J., Munro, M.H.G., Ramasamy, K., Weber, J.F.F. *Tetrahed. Lett.* **2014**, *55*, 453.
152. Tachihara, T., Kitahara, T. *Tetrahedron*, **2003**, *59*, 1773-1780.
153. Takken, F.L.W., Joosten, M.H.A.J. *Eur. J. Plant Pathol.* **2000**, *106*, 699-713.
154. Tanaka, T., Hanato, K., Watanabe, M., Abbas, H.K. *J. Nat. Toxins* **1996**, *5*, 317-329.
155. Taylor, A., Hardy, G.E.S., Wood, P., Burgess, T. *Australas. Plant Pathol.* **2005**, *34*, 187-195.
156. Tsukada, K., Takahashi, K., Nabeta, K. *Phytochemistry* **2010**, *71*, 2019-2023.
157. Turner, J.G. In *Plant diseases: infection, damage and loss* (Wood, R.K.S., Jellis, G.J. Eds.), Blackwell Scientific Publications, Oxford, **1984**, 3-12.
158. Úrbez-Torres, J.R., Gubler, W.D., Luque, J. *Plant Dis.* **2007**, *91*, doi:10.1094/PDIS-91-6-0772C.
159. Úrbez-Torres, J.R. *Phytopathol. Mediterr.* **2011**, *50*, S5-S45.
160. Van Goietsenoven, G., Mathieu, V., Andolfi, A., Cimmino, A., Lefranc, F., Kiss, R., Evidente, A. *Planta Med.* **2011**, *77*, 711-717.
161. Van Niekerk, J.M., Fourie, P.H., Halleen, F., Crous, P.W. *Phytopathol. Mediterr.* **2006**, *45*, S43-S54.

162. Venkatasubbaiah, P., Sutton, T.B., Chilton, W.S. *Phytopathology* **1991**, *81*, 243-247.
163. Venkatasubbaiah, P., van Dyke, C.G., Chilton, W.S. *Mycologia* **1992**, *84*, 715-723.
164. Walters, E.W., Lee, S.F., Niderman, T., Bernasconi, P., Subramanian, M.V., Siehl, D.L. *Plant Physiol.* **1997**, *114*, 549-555.
165. Walton, J.D. *Plant Cell.* **1996**, *8*, 1723-1733.
166. Wang, X.N., Bashyal, B.P., Wijeratne, E.M.K., U'Ren, J.M., Liu, M.X., Gunatilaka, M.K., Arnold, A.E., Gunatilaka, A.A.L. *J. Nat. Prod.* **2011**, *74*, 2052-2061.
167. Weber, H.A., Gloer, J.B. *J. Nat. Prod.* **1988**, *51*, 879-883.
168. Weber, R.W., Kappe, R., Paululat, T., Mosker, E., Anke, H. *Phytochemistry* **2007**, *68*, 886-889.
169. Woodward, R.B., Singh, G. *Nature* **1950**, *165*, 928-930.
170. Wright, J.M. *Ann. Bot.* **1951**, *15*, 493-499.
171. Wu, H.H., Tiam, L., Feng, B.M., Li, Z.F., Zhang, Q.H., Pei, Y.H. *J. Asian Nat. Prod. Res.* **2010**, *12*, 15-19.
172. Wunderlich, N., Steel, C.C., Ash, G., Raman, H., Savocchia, S. In *Proceedings of the 6th International Workshop on Grapevine Trunk Diseases*, Florence, Italy, 1-3 September **2008**.
173. Wyss, R., Tamm, C., Vederas, J.C. *Helv. Chim. Acta* **1980**, *63*, 1538-1541.
174. Xu, Y.X., Lu, C.H., Zheng, Z.H., Shen, Y.N. *Helv. Chim. Acta* **2011**, *94*, 897-902.
175. Yang, Q., Asai, M., Matsuura, H., Yoshihara, T. *Phytochemistry* **2000**, *54*, 489-494.
176. Yoder, O.C. *Ann. Rev. Phytopathol.* **1980**, *18*, 103-129.
177. Yukimune, Y., Hara, Y., Nomura, E., Seto, H., Yoshida, S. *Phytochemistry* **2000**, *54*, 13-17.
178. Zhang, Y.L., Ge, H.M., Li, F., Song, Y.C., Ta

Table 1. Modes of action of microbially-produced phytochemicals

Name	Compound	Source	Action mechanism
Ascaulitoxin aglycone		<i>Ascochyta caulina</i>	Aminotransferases inhibition
Rhizobitoxine		<i>Bradyrhizobium</i> spp.	β -Cystathionase inhibition
Acivicin		<i>Streptomyces sviveu</i>	Glutamate-synthase
Thaxtomin A		<i>Streptomyces</i> spp.	Cellulose synthesis inhibition
Tentoxin		<i>Alternaria alternata</i>	Inhibition of chloroplast development
Cyperin		<i>Ascochyta cypericola</i>	Plant enoyl reductase
Ophiobolin A		<i>Bipolaris</i> spp, <i>Drechslera gigantea</i>	Antagonism of calmodulin
Cytochalasin B		<i>Phoma exigua</i> , <i>Zygosporium masonii</i>	Actin polymerization inhibition
Hydantocidin		<i>Streptomyces hygroscohis</i>	Adenylosuccinate synthetase inhibition
Gliotoxin		<i>Leptosphaeria maculans</i>	Protein Binding

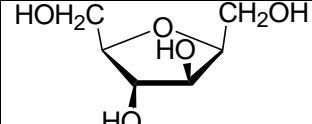
Anhydro-D-glucitol		<i>Fusarium solani</i>	Fructose-1,6-bisphosphate aldolase inhibition
--------------------	---	------------------------	---

Table 2. Species of *Botryosphaeriaceae* currently known to infect grapevines.

Botryosphaeriaceae species and authority	Culture	Anamorph-Teleomorph connectiona	Hosts No. ^b
<i>Botryosphaeria dothidea</i> (Moug. ex Fr.) Ces. & De Not.	CMW8000.	<i>Fusicoccum aesculi</i>	338
<i>Diplodia corticola</i> A.J.L. Phillips, A. Alves & J. Luque	CBS 112549	“ <i>Botryosphaeria</i> ” <i>corticola</i>	8
<i>Diplodia mutila</i> (Fr.) Mont.	CBS 112553.	“ <i>Botryosphaeria</i> ” <i>stevensii</i>	26
<i>Diplodia seriata</i> De Not.	CBS 112555.	“ <i>Botryosphaeria</i> ” <i>obtusa</i>	59
<i>Dothiorella iberica</i> A.J.L. Phillips, J. Luque & A. Alves	CBS 115035.	“ <i>Botryosphaeria</i> ” <i>iberica</i>	5
<i>Dothiorella americana</i> J.R. Úrbez-Torres, F. Peduto & W.D. Gubler	CBS128309 .	Unknown	2
<i>Guignardia bidwellii</i> (Ellis) Viala & Ravaz	IMI 207141 .	Unknown	19
<i>Lasiodiplodia crassispota</i> T.I. Burgess & Barber	CBS11874 .	Unknown	6
<i>Lasiodiplodia missouriana</i> J.R. Úrbez-Torres, F. Peduto & W.D. Gubler	CBS128311 .	Unknown	2
<i>Lasiodiplodia theobromae</i> (Pat.) Griff. & Maubl.	K(M)118158.	“ <i>Botryosphaeria</i> ” <i>rhodina</i>	442
<i>Lasiodiplodia viticola</i> J.R. Úrbez-Torres, F. Peduto & W.D. Gubler	CBS128313 .	Unknown	2
<i>Neofusicoccum australe</i> (Slippers, Crous & M.J. Wingf.) Crous, Slippers & A.J.L. Phillips	CMW6838 .	“ <i>Botryosphaeria</i> ” <i>australe</i>	30
<i>Neofusicoccum luteum</i> (Pennycook & Samuels) Crous, Slippers & A.J.L. Phillips	CBS 110299 .	“ <i>Botryosphaeria</i> ” <i>lutea</i>	16
<i>Neofusicoccum macroclavatum</i> (T.I. Burgess, Barber & Hardy) T.I. Burgess, Barber & Hardy	CBS 118223 .	Unknown	3
<i>Neofusicoccum mediterraneum</i> Crous, M.J. Wingf. & A.J.L. Phillips	CBS 121718 .	Unknown	13
<i>Neofusicoccum parvum</i> (Pennycook & Samuels) Crous, Slippers & A.J.L. Phillips	CMW9081 .	“ <i>Botryosphaeria</i> ” <i>parva</i>	34
<i>Neofusicoccum ribis</i> (Slippers, Crous & M.J. Wingf.) Crous, Slippers & A.J.L. Phillips	CMW7772 .	Unknown	242
<i>Neofusicoccum viticlavatum</i> (Van Niekerk & Crous) Crous, Slippers & A.J.L. Phillips	CBS 112878 .	Unknown	1
<i>Neofusicoccum vitifusiforme</i> (Van Niekerk & Crous) Crous, Slippers & A.J.L. Phillips	CBS 110887 .	Unknown	1
<i>Phaeobotryosphaeria porosa</i> (Van Niekerk & Crous) Crous & A.J.L. Phillips	CBS 110496 .	Unknown	1
<i>Spencermartinsia viticola</i> (A.J.L. Phillips & J. Luque) A.J.L. Phillips, A. Alves & Crous	CBS 117009 .	<i>Dothiorella viticola</i>	4

^a Robert *et al.*, 2005.

^b Number of different plant hosts, including *Vitis* spp., described for each Botryosphaeriaceae species Retrieved from Farr and Rossman, July 2011: <http://nt.ars-grin.gov/fungaldatabases/fungushost/fungushost.cfm> Acronyms of cultures collections: CMW: Culture Collection Forestry and Agricultural Biotechnology Institute, University of Pretoria, South Africa; WAC: Department of Agriculture Western Australia, Plant Pathogen Collection; CBS: Centraalbureau Schimmelcultures, Utrecht, Netherlands; IMI: CABI Filamentous Fungi Database (Formerly IMI), Egham, United Kingdom.

^{ce} Ex-epitype

^{et} Ex-type

^h Holotype

Table 3. Secondary metabolites by *Botryosphaeriaceae* involved in grapevine trunk diseases

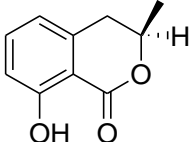
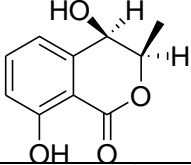
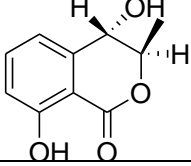
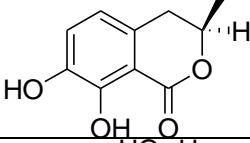
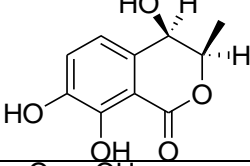
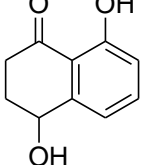
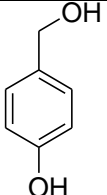
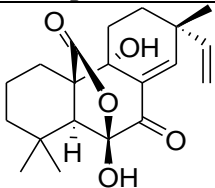
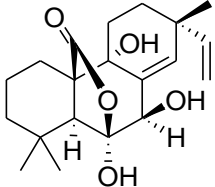
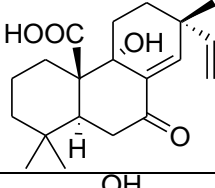
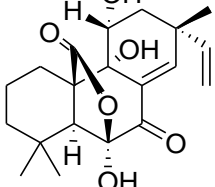
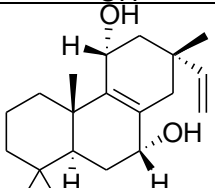
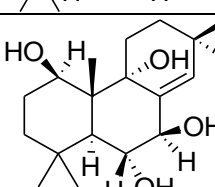
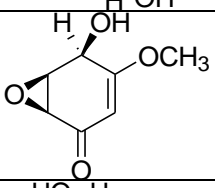
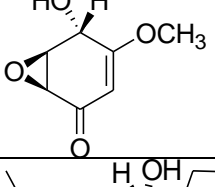
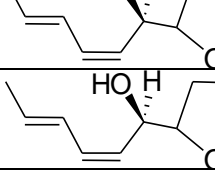
Name	Compound	Source
(R)-Mellein		<i>Botryosphaeria obtusa</i>
(3R,4R)-4-hydroxymellein		<i>B. obtusa</i> <i>Neofusicoccum parvum</i>
(3R,4S)-4-hydroxymellein		<i>N. parvum</i>
(3R)-7-Hydroxymellein		<i>B. obtusa</i>
(3R,4R)-4,7-Dihydroxy-mellein		<i>B. obtusa</i>
Isoscleron		<i>N. parvum</i>
Tyrosol		<i>N. parvum</i>

Table 4. Secondary metabolites by *Botryosphaeriaceae* involved in forest plant diseases

Name	Compound	Surce	Host
Sphaeropsidin (Sph) A		<i>Diplodia cupressi</i> <i>D. corticola</i> <i>D. africana</i>	Cupressus spp. Cork oak Phoenicean juniper
Sph B		<i>D. cupressi</i> <i>D. corticola</i>	“
Sph C		<i>D. cupressi</i> <i>D. corticola</i>	“
Sph D		<i>D. cupressi</i>	Cupressus spp.
Sph E		<i>D. cupressi</i>	“
Sph F		<i>D. cupressi</i>	“
Sphaeropsidone		<i>D. cupressi</i>	Cupressus spp.
epiSphaeropsidone		<i>D. cupressi</i> <i>D. africana</i>	Cupressus spp. Phoenicean juniper
Sapinofuranone A		<i>Sphaeropsis sapinea</i>	Cupressus spp.
Sapinofuranone B		<i>S. sapinea</i> <i>D. corticola</i>	Cupressus spp. Cork oak

Sapinopyridione		<i>S. sapinea</i>	Cupressus spp.
Diplobifuranilone A		<i>D. corticola</i>	Cork oak
Diplobifuranilone B		<i>D. corticola</i>	Cork oak
(R)-Mellein		<i>D. africana</i> <i>S. sapinea</i>	Cork oak Pine
(3R,4R)-4-hydroxymellein		<i>D. corticola</i> <i>D. africana</i> <i>S. sapinea</i>	Cork oak Cork oak Pine
(3R,4S)-4-hydroxymellein		<i>D. corticola</i> <i>D. africana</i> <i>S. sapinea</i>	Cork oak Cork oak Pine
Diplopyrone		<i>D. corticola</i> <i>D. mutila</i>	Cork oak Cork oak
Diplofuranone A		<i>D. corticola</i>	Cork oak
Diplofuranone B		<i>D. corticola</i>	Cork oak
Oxysporone		<i>D. africana</i>	Cork oak
Afritoxinone A		<i>D. africana</i>	Cork oak
Afritoxinone B		<i>D. africana</i>	Cork oak

Table 5. *Botryosphaeriaceae* involved in GTDs and canker and dieback in forest plants object of thesis.

Species	Code	Host	Isolation site	ITS Accessor number
<i>Neofusicoccum australe</i>	BOT48	<i>Vitis vinifera</i> L.	Northern Sardinia	HQ011406
<i>Neofusicoccum australe</i>	BL24	<i>Juniperus phoenicea</i> . L.	Caprera island	JX312356
<i>Lasiodiplodia mediterranea</i>	BL101	<i>Vitis vinifera</i> L.	Northern Sardinia	KJ170150 KJ170151 ^c
<i>Lasiodiplodia mediterranea</i>	B6	<i>Vitis vinifera</i> L.	Sicily	KP178596 KJ638331 ^c
<i>Diplodia quercivora</i>	BL9	<i>Quercus canariensis</i> Willd.	Tunisia	JX894206 JX894230 ^c
<i>Diplodia africana</i>	DA1	<i>Juniperus phoenicea</i> . L.	Sardinia	JF302648 JN157807 ^c

^aBOT/BL/DA1: sequence deposited in Sardinia

^bB6: sequence deposited in Sicily

^cAccess number EF1- α (elongation factor 1- α)

Table 6. ^1H and ^{13}C NMR Data and HMBC correlations for cyclobotryoxide (**1**) in CDCl_3 ^{a,b}

Position	δC^c	δH (J in Hz)	HMBC
1	52.1 <i>d</i>	3.45 (1H) <i>d</i> (3.0)	H-3, H-5, H-6
2	194.3 <i>s</i>	-	H-1, CH_3
3	165.5 <i>s</i>	-	CH_3 , OH, H-1, OCH ₃ , H-5
4	112.0 <i>s</i>	-	H-5, OH, CH_3
5	60.9 <i>d</i>	4.88 (1H) <i>m</i>	H-6, OH, CH_3
6	54.2 <i>d</i>	3.79 (1H) <i>dd</i> (3.0, 1.0)	H-5, H-1
OCH ₃	56.1 <i>q</i>	4.05 (3H) <i>s</i>	H-5
CH_3	7.9 <i>q</i>	1.26 (3H) <i>br s</i>	
OH ^d	-	3.60 (1H) <i>d</i> (11.0)	

^aThe chemical shifts are in δ values (ppm) from TMS.

^b2D ^1H , ^1H (COSY) ^{13}C , ^1H (HSQC) NMR experiments delineated the correlations of all the protons and the corresponding carbons.

^cMultiplicities were assigned by DEPT spectrum.

^dThe shift is variable; this value was observed in CDCl_3 at room temperature.

Table 7. NMR Data of lasiojasmonate A (**5**)^{a,b}

Position	5		
	δC^c	δH (<i>J</i> in Hz)	HMBC
1	37.6 <i>d</i>	2.10 (1H) <i>m</i>	H-2, H ₂ -5, H ₂ -6
2	53.9 <i>d</i>	1.90 (1H) <i>ddd</i> (10.2, 5.3)	H ₂ -4, H ₂ -8, H-9
3	218.3 <i>s</i>	-	H-1, H ₂ -5, H-8
4	38.7 <i>t</i>	2.74 (1H) <i>dd</i> , (20.0, 8.2) 2.37 <i>m</i>	H ₂ -5
5	27.2 <i>t</i>	2.33 <i>m</i> 1.50 (1H) <i>m</i>	H-1, H ₂ -4
6	37.9 <i>t</i>	2.32 <i>m</i>	
7	171.7 <i>s</i>	-	H ₂ -5, H ₂ -6, H-8'
8	25.5 <i>t</i>	2.37 <i>m</i>	H-9, H-10
9	124.9 <i>d</i>	5.26 (1H) <i>m</i>	H ₂ -8, H-11
10	134.2 <i>d</i>	5.45 (1H) <i>m</i>	H ₂ -8, H ₂ -11, Me-12
11	20.6 <i>t</i>	2.04 (2H) <i>m</i>	Me-12
12	14.1 <i>q</i>	0.95 (3H) <i>t</i> (7.4)	H ₂ -11
2'	177.6 <i>s</i>	-	H-3', Me-7', H-8'B
3'	38.6 <i>t</i>	2.49 (1H) <i>dq</i> (11.0, 7.1)	Me-7'
4'	50.5 <i>d</i>	2.04 (1H) <i>m</i>	H-3', Me-6', Me-7'
5'	77.0 <i>d</i>	4.26 (2H) <i>m</i>	Me-6', H ₂ -8'
6'	19.9 <i>q</i>	1.47 (3H) <i>d</i> (6.1)	H-3'
7'	14.1 <i>q</i>	1.28 (3H) <i>d</i> (7.1)	H-3'
8'	62.5 <i>t</i>	4.26 (2H) <i>m</i> 4.21 (1H) <i>dd</i> (11.0, 5.7)	H-3', H-5'A

^aThe chemical shifts are in δ values (ppm) from TMS.

^b 2D ¹H, ¹H (COSY) ¹³C, ¹H (HSQC) NMR experiments delineated the correlations of all the protons and the corresponding carbons.

^c Multiplicities were assigned by DEPT spectrum

Table 8. ¹H NMR Data of 16-*O*-acetylbotryosphaerilactones A and C (**6** and **7**)^a

Position	6	7
	δ H (<i>J</i> in Hz)	δ H (<i>J</i> in Hz)
2		
3	2.53 (1H) <i>dq</i> (9.2, 6.7)	2.57 (1H) <i>dq</i> (11.3, 7.1)
4	1.90 (1H) <i>m</i>	1.91 (1H) <i>m</i>
5	4.29 (1H) <i>dq</i> (8.4, 6.0)	4.32 (1H) <i>dq</i> (9.2, 6.2)
6	1.43 (3H) <i>d</i> (6.2)	1.45 (3H) <i>d</i> (6.2)
7	1.26 (3H) <i>d</i> (7.1)	1.26 (3H) <i>d</i> (7.1)
8	3.83 (1H) <i>dd</i> (10.3, 4.3)	3.84 (1H) <i>dd</i> (10.0, 5.4)
	3.41 (1H) <i>dd</i> (10.3, 4.8)	3.41 (1H) <i>dd</i> (10.2, 4.8)
10	4.67 (1H) <i>d</i> (2.3)	4.79 (1H) <i>d</i> (4.6)
12	3.91 (1H) <i>dq</i> (12.3, 6.2)	3.97 (1H) <i>dq</i> (12.3, 6.2)
13	1.51 (1H) <i>m</i>	1.51 (1H) <i>m</i>
14	2.03 (1H) <i>m</i>	2.05 (1H) <i>m</i>
15	1.13 (3H) <i>d</i> (7.0)	1.04 (3H) <i>d</i> (7.0)
16	4.15 (1H) <i>dd</i> (11.0, 5.6)	4.21 (1H) <i>dd</i> (11.3, 4.5)
	4.04 (1H) <i>dd</i> (11.0, 7.9)	4.06 (1H) <i>dd</i> (11.3, 7.6)
17	1.31 (3H) <i>d</i> (6.2)	1.30 (3H) <i>d</i> (6.2)
COCH ₃	2.06 (3H) <i>s</i>	2.07 (3H) <i>s</i>

^aThe chemical shifts are in δ values (ppm) from TMS.

Table 9. ¹H NMR Data of lasiojasmonates B and C (**8** and **9**)^a

Position	8	9
	δ H (J in Hz)	δ H (J in Hz)
1	2.13 <i>dq</i> (17.5, 9.8)	2.13 <i>dq</i> (15.5, 9.8)
2	1.91 <i>m</i>	1.91 <i>m</i>
4	2.70 <i>dd</i> (17.5, 6.1) 2.25 <i>m</i>	2.70 <i>dd</i> (17.5, 6.1) 2.25 <i>m</i>
5	2.37 <i>m</i> 1.63 <i>ddd</i> (14.3, 6.9, 4.6)	2.37 <i>m</i> 1.63 <i>ddd</i> (14.3, 6.9, 4.6)
6	2.37 <i>m</i>	2.37 <i>m</i>
8	2.37 <i>m</i>	2.37 <i>m</i>
9	5.25 <i>m</i>	5.25 <i>m</i>
10	5.46 <i>m</i>	5.46 <i>m</i>
11	2.04 <i>dq</i> (7.5, 1.0)	2.04 <i>dq</i> (7.5, 1.0)
12	0.96 <i>t</i> (7.5)	0.96 <i>t</i> (7.5)
3'	2.54 <i>m</i>	2.54 <i>m</i>
4'	2.00 <i>m</i>	2.00 <i>m</i>
5'	4.30 (<i>m</i>)	4.30 <i>m</i>
6'	1.44 <i>d</i> , (6.2)	1.45 <i>d</i> (6.2)
7'	1.26 <i>d</i> (7.1)	1.26 <i>d</i> (7.1)
8'	3.86 <i>dd</i> (10.0, 4.3) 3.41 <i>dd</i> (10.0, 5.6)	3.87 <i>dd</i> (10.0, 4.3) 3.41 <i>dd</i> (10.0, 5.3)
10'	4.68 <i>d</i> (2.0)	4.80 <i>d</i> (4.5)
12'	3.90 <i>dq</i> (12.3, 6.1, 2.8)	3.96 <i>dq</i> (12.6, 6.2, 1.6)
13'	1.50 <i>m</i>	1.50 <i>m</i>
14'	2.03 <i>m</i>	2.03 <i>m</i>
15'	1.13 <i>d</i> (7.2)	1.05 <i>d</i> (7.0)
16'	4.17 <i>dd</i> (11.0, 6.9) 4.10 <i>dd</i> (11.0, 7.2)	4.23 <i>dd</i> (11.3, 4.5) 4.07 <i>dd</i> (11.3, 5.8)
17'	1.32 <i>d</i> (6.1)	1.30 <i>d</i> (6.2)

^aThe chemical shifts are in δ values (ppm) from TMS.

Table 10. ^1H - and ^{13}C -NMR Data, and HMBC correlations of **15** and **16**^a. Atom numbering as indicated in Figure 2.

Position	15		16		HMBC
	$\delta(\text{C})^{\text{b}}$	δH (J in Hz)	$\delta(\text{C})^{\text{b}}$	δH (J in Hz)	
2	103.8 d	5.06 (1H) <i>brs</i>	99.6 <i>d</i>	5.24 (1H) <i>d</i> (4.1)	H-3, H-7
3	43.9 d	2.10 (1H) <i>ddq</i> (8.5, 7.2, 6.0)	41.5 <i>d</i>	2.04 (1H) <i>ddq</i> (6.8, 5.0, 4.1)	H-2, H-4, H-5, H-7
4	54.9 d	1.56 (1H) <i>m</i>	52.2 <i>d</i>	1.82 (1H) <i>m</i>	H-2, H-5, H-3, H-8
5	76.5 d	4.20 (1H) <i>dq</i> (7.0, 6.1)	76.5 <i>d</i>	4.02 (1H) <i>dq</i> (8.2, 6.1)	H-3, H-4, H-6,
6	21.4 q	1.33 (3H) <i>d</i> (6.1)	23.2 <i>q</i>	1.39 (3H) <i>d</i> (6.1)	H-4, H-5
7	19.2 q	1.14 (3H) <i>d</i> (7.2)	11.9 <i>q</i>	1.07 (3H) <i>d</i> (6.8)	H-2, H-3, H-4
8	62.7 t	3.75 (1H) <i>dd</i> (10.4, 4.6)	62.5 <i>t</i>	3.75 (1H) <i>dd</i> (10.4, 4.6)	H-4
		3.71 (1H) <i>dd</i> (10.4, 4.0)		3.71 (1H) <i>dd</i> (10.4, 4.0)	
OH		3.60 (1H) <i>brs</i>		2.38 (1H) <i>brs</i>	

^a ^1H , ^1H (COSY) ^{13}C , ^1H (HSQC) NMR experiments delineated the correlations of all the protons and the corresponding carbons. The chemical shifts are in δ values (ppm) from TMS.

^b Multiplicities were assigned by DEPT spectrum.

Table 11. HRESIMS Data of **15** and **16**

Ion peak m/z	Calculated	Molecular Formula	Description
313.1456	313.1417	C ₁₄ H ₂₆ KO ₅	[M+K] ⁺
297.1649	297.1668	C ₁₄ H ₂₆ NaO ₅	[M+Na] ⁺
169.0818	169.0823	C ₇ H ₁₄ NaO ₃	[M-C ₇ H ₁₃ O ₂ +H+Na] ⁺
129.0897	129.0878	C ₇ H ₁₃ O ₂	[M-C ₇ H ₁₃ O ₃] ⁺

Table 12. ¹H-NMR Data of 13-O-Methylbotryosphaeriodopodin, and its 7-O-(S)-, and 7-O-(R)-MTPA Esters (**19-21** respectively). Atom numbering as indicated in Figure 7.

^aThe chemical shifts are in δ values (ppm) from TMS

Position	19	20	21
	δH^a (J in Hz)	δH (J in Hz)	δH (J in Hz)
3	5.23 <i>dq</i> (6.4, 3.1)	5.222 (1H) <i>dq</i> (6.0, 3.2)	5.260 (1H) <i>dq</i> (6.1, 3.0)
4	1.97 (H _a) <i>m</i> ; 1.63 (H _b) <i>m</i>	2.001 (H _a) <i>m</i> ; 1.688 (H _b) <i>m</i>	2.028 (H _a) <i>m</i> ; 1.767 (H _b) <i>m</i>
5	1.69 (H _a) <i>m</i> ; 1.55 (H _b) <i>m</i>	1.736 (H _a) <i>m</i> ; 1.579 (H _b) <i>m</i>	1.792 (<i>m</i> , H _a); 1.582 (H _b) <i>m</i>
6	1.63 (H _a) <i>m</i> ; 1.53 (H _b) <i>m</i>	1.638 (H _a) <i>m</i> ; 1.601 (H _b) <i>m</i>	1.682 (H _a) <i>m</i> ; 1.607 (H _b) <i>m</i>
7	3.80 <i>m</i>	5.341 <i>m</i>	5.331 <i>m</i>
8	1.49 (H _a) <i>m</i> ; 1.33 (H _b) <i>m</i>	1.508 (H _a) <i>m</i> ; 1.389 (H _b) <i>m</i>	1.502 (H _a) <i>m</i> ; 1.374 (H _b) <i>m</i>
9	1.94 (H _a) <i>m</i> ; 1.55 (H _b) <i>m</i>	1.983 (H _a) <i>m</i> ; 1.473 (H _b) <i>m</i>	1.983 (H _a) <i>m</i> ; 1.451 (H _b) <i>m</i>
10	2.73 (H _a) <i>ddd</i> (14.0, 9.3, 6.2); 2.57 (H _b) <i>ddd</i> (14.0, 6.2)	2.813 (1H) <i>ddd</i> (13.8, 9.0, 6.0); 2.587 (1H) <i>ddd</i> (13.8, 6.0)	2.714 (1H) <i>ddd</i> (13.8, 9.0, 6.0); 2.485 (1H) <i>ddd</i> (13.8, 6.0)
12	6.32 <i>d</i> (2.0)	6.308 (1H) <i>brs</i>	6.302 (1H) <i>d</i> (1.9)
14	6.30 <i>d</i> (2.0)	6.308 (1H) <i>brs</i>	6.269 (1H) <i>d</i> (1.9)
17	1.33 <i>d</i> (6.4)	1.334 (3H) <i>d</i> (6.0)	1.356 (3H) <i>d</i> (6.1)
CH ₃ O-15	3.78 <i>s</i>	3.798 (3H) <i>s</i>	3.783 (3H) <i>s</i>
CH ₃ O-13	3.80 <i>s</i>	3.785 (3H) <i>s</i>	3.783 (3H) <i>s</i>
Ph	-	7.535-7.404 (5H) <i>m</i>	7.548-7.407 (5H) <i>m</i>
CH ₃ O	-	3.549 (3H) <i>s</i>	3.575 (3H) <i>s</i>

Table 13. ^1H and ^{13}C NMR Data and HMBC of Diplopimarane (**24**)^{a,b}

position	δC^c	δH (J in Hz)	HMBC
1	27.9 CH ₂	2.44 (2H) <i>m</i>	H ₂ -2
2	19.8 CH ₂	1.72 (2H) <i>m</i>	H ₂ -1
3	41.7 CH ₂	1.60 (2H) <i>m</i>	H ₂ -2
4	33.9 C		H ₂ -1, H ₂ -2, H ₂ -3, Me-18, Me-19
5	119.6 C		H ₂ -1, H ₂ -3, HO-6
6	142.2 C		HO-6
7	141.5 C		HO-7, H-14
8	131.2 C		H-1, HO-7, Me-17
9	124.5 C		H ₂ -1, H ₂ -2, H ₂ -11, H-14
10	127.0 C		H ₂ -1, H ₂ -11
11	23.2 CH ₂	2.54 (1H) <i>ddd</i> (17.2, 11.2, 5.6) 2.52 (1H) <i>ddd</i> (17.2, 6.1, 3.2)	H ₂ -12
12a	33.1 CH ₂	1.88 (1H) <i>ddd</i> (13.6, 5.6, 3.2)	H ₂ -11, H-15, Me-17
12b		1.75 (1H) <i>m</i>	
13	40.2 C	-	H-14, H-15, H ₂ -16
14	76.0 CH	4.70 (1H) <i>d</i> (9.9)	H ₂ -11, H ₂ -12, H-15, H ₂ -16, Me-17, OH-14
15	139.1 CH	6.04 (1H) <i>dd</i> (17.6, 11.0)	H ₂ -12, H-14, H ₂ -16, Me-17
16	118.7 CH ₂	5.34 (1H) <i>brd</i> (11.0) 5.31 (1H) <i>brd</i> (17.6)	H-14
17	23.2 CH ₃	1.25 (3H) <i>s</i>	H ₂ -12, H-14, H-15
18 ^d	27.6 CH ₃	1.42 (3H) <i>s</i>	H ₂ -3
19 ^d	28.6 CH ₃	1.45 (3H) <i>s</i>	H ₂ -3
HO-14		2.18 (1H) <i>d</i> (9.9)	
HO-7	-	5.85 (1H) <i>s</i>	
HO-6	-	8.55 (1H) <i>s</i>	

^aThe chemical shifts are in δ values (ppm) from TMS.

^b2D ^1H , ^1H (COSY), and 2D ^{13}C , ^1H (HSQC) NMR experiments delineated the correlations of all the protons and the corresponding carbons.

^cMultiplicities were assigned by DEPT spectrum.

^dThe attributions of these signals could be inverted

Table 14. ¹H NMR Data of diplopimarane derivatives^a

	25	26	27	28	29 ^c
position	δ_{H} (J in Hz)	δ_{H} (J in Hz)	δ_{H} (J in Hz)	δ_{H} (J in Hz)	δ_{H} (J in Hz)
1	2.46 (2H) <i>m</i> ^d	2.47 (2H) <i>m</i>	2.54 (3H) <i>m</i> ^d	2.48 (3H) <i>m</i> ^d	2.09 (2H) <i>m</i>
2	1.73 (3H) <i>m</i> ^d	1.74 (3H) <i>m</i> ^d	1.80 (3H) <i>m</i> ^d	1.78 (3H) <i>m</i> ^d	1.74 (2H) <i>m</i>
3	1.59 (2H) <i>m</i>	1.57 (2H) <i>m</i>	1.64 (2H) <i>m</i>	1.57 (2H) <i>m</i>	1.02 (2H) <i>m</i>
11	2.67 (1H) <i>ddd</i> (14.9, 6.3, 3.7)	2.65 (1H) <i>ddd</i> (17.8, 6.4, 2.6)	2.76 (1H) <i>ddd</i> (17.9, 5.8, 1.0)	2.62 (1H) <i>ddd</i> (17.2, 10.8, 1.2)	1.69 (2H) <i>m</i>
12	2.46 (3H) <i>m</i> ^d	2.46 (3H) <i>m</i>	2.54 (3H) <i>m</i> ^d	2.48 (3H) <i>m</i> ^d	1.29 (1H) <i>m</i>
	2.13 (1H) <i>ddd</i> (17.8, 11.2, 6.3)	2.09 (1H) <i>ddd</i> (17.3, 10.9, 6.4)	2.10 (1H) <i>m</i>	1.89 (1H) <i>ddd</i> (17.2, 10.8, 6.3)	
	1.73 (3H) <i>m</i> ^d	1.74 (3H) <i>m</i> ^d	1.80 (3H) <i>m</i> ^d	1.78 (3H) <i>m</i> ^d	1.20 (1H) <i>m</i>
14	4.56 (1H) <i>d</i> (3.0)	4.59 (1H) <i>d</i> (1.2)	5.80 (1H) <i>brs</i>	4.71 (1H) <i>d</i> (9.3)	
15	6.08 (1H) <i>dd</i> (17.5, 11.1)	6.10 (1H) <i>dd</i> (17.5, 11.1)	5.88 (1H) <i>dd</i> (17.5, 10.9)	6.05 (1H) <i>dd</i> (17.6, 11.4)	1.04 (2H) <i>q</i> (7.4)
16	5.24 (1H) <i>dd</i> (1.1, 1.2)	5.21 (1H) <i>dd</i> (11.1, 1.2)	5.08 (1H) <i>dd</i> (17.5, 1.0)	5.36 (1H) <i>dd</i> (11.4, 1.0)	0.71 (3H) <i>t</i> (7.4)
	5.20 (1H) <i>dd</i> (17.5, 1.2)	5.19 (1H) <i>dd</i> (17.5, 1.2)	5.06 (2H) <i>dd</i> (10.9, 1.0)	5.32 (1H) <i>dd</i> (17.6, 1.0)	
17	0.95 (3H) <i>s</i>	0.97 (3H) <i>s</i>	0.97 (3H) <i>s</i>	1.24 (3H) <i>s</i>	0.62 (3H) <i>s</i>
18 ^b	1.42 (3H) <i>s</i>	1.39 (3H) <i>s</i>	1.33 (3H) <i>s</i>	1.32 (6H) <i>s</i> ^d	1.34 (3H) <i>s</i>
19 ^b	1.40 (3H) <i>s</i>	1.38 (3H) <i>s</i>	1.28 (3H) <i>s</i>	1.32 (6H) <i>s</i> ^d	1.32 (3H) <i>s</i>
HO-14	2.17 (1H) <i>d</i> (3.0)	2.3 (1H) <i>d</i> (1.2)		2.24 (1H) <i>d</i> (9.3)	
HO-7	5.75 (1H) <i>s</i>				
HO-6				8.64 (1H) <i>s</i>	
MeO-6	3.88 (3H) <i>s</i>	3.88 (3H) <i>s</i>			
MeO-7		3.86 (3H) <i>s</i>			
COCH ₃			2.29 (3H) <i>s</i>		
			2.24 (3H) <i>s</i>		
			1.92 (3H) <i>s</i>		
2'-6'				8.11 (2H) <i>d</i> (8.4)	
3'-5'				7.65 (2H) <i>d</i> (8.4)	

^aThe chemical shifts are in δ values (ppm) from TMS.^bThe attributions of these signals could be inverted.^cThis spectrum was recorded in C₆D₆.^dThese signals were overlapped.

Table 15. ¹H NMR Data of 14-*O*-(*S*)-, 14-*O*-(*R*)-MTPA esters of 6,7-*O*,*O*'-Dimethyldiplopirane (**30** and **31**, respectively)^a

position	30	31
	δ H (<i>J</i> in Hz)	δ H (<i>J</i> in Hz)
1	2.472 (3H) <i>m</i> ^b	2.468 (3H) <i>m</i> ^b
2	1.735 (3H) <i>m</i> ^b	1.746 (3H) <i>m</i> ^b
3	1.603 (2H) <i>m</i>	1.567 (2H) <i>m</i>
11	2.647 (1H) <i>dd</i> (16.5, 8.3)	2.662 (1H) <i>dd</i> (19.0, 5.3)
	2.472 (3H) <i>m</i> ^b	2.468 (3H) <i>m</i> ^b
12	1.915 (1H) <i>m</i>	2.006 (1H) <i>m</i>
	1.735 (3H) <i>m</i> ^b	1.746 (3H) <i>m</i> ^b
14	6.199 (1H) <i>s</i>	6.185 (1H) <i>s</i>
15	5.934 (1H) <i>dd</i> (17.6, 11.5)	6.086 (1H) <i>dd</i> (16.7, 11.9)
16	5.024 (1H) <i>dd</i> (17.6, 1.0)	5.117 (1H) <i>dd</i> (16.7, 1.0)
	4.992 (1H) <i>dd</i> (11.5, 1.0)	5.113 (1H) <i>dd</i> (11.9, 1.0)
17	0.994 (3H) <i>s</i>	1.026 (3H) <i>s</i>
18	1.387 (6H) <i>s</i> ^b	1.346 (3H) <i>s</i> ^c
19	1.387 (6H) <i>s</i> ^b	1.339 (3H) <i>s</i> ^c
CH ₃ O-6	3.794 (3H) <i>s</i>	3.746 (3H) <i>s</i>
CH ₃ O-7	3.756 (3H) <i>s</i>	3.642 (3H) <i>s</i>
Ph	7.528-7.300 (5H) <i>m</i>	7.602-7.306 (5H) <i>m</i>

^aThe chemical shifts are in δ values (ppm) from TMS.

^bThese signals were overlapped.

^cThe attributions of these signals could be inverted.

Table 16. ¹H NMR Data of oxysporone (35) and its derivatives (38-45)^a

No.	35	38	39	40	41	42	43 ^b	44 ^c	45
	δ_H (J in Hz)	δ_H (J in Hz)	δ_H (J in Hz)	δ_H (J in Hz)	δ_H (J in Hz)	δ_H (J in Hz)	δ_H (J in Hz)	δ_H (J in Hz)	δ_H (J in Hz)
2	6.46 <i>d</i> (5.9)	6.52 <i>d</i> (6.1)	3.97 <i>dt</i> (11.8, 4.2) 3.85 <i>ddd</i> (11.8, 10.3, 2.6)	6.75 <i>dd</i> (10.0, 4.2)	6.59 <i>d</i> (6.2)	7.75 <i>dd</i> (5.7, 0.7)	3.90 <i>t</i> (5.2)	4.55 <i>t</i> (7.0)	7.74 <i>dd</i> (5.8, 1.0)
3	5.07 <i>ddd</i> (5.9, 5.4, 1.0)	5.06, <i>brdd</i> (6.1, 5.3)	1.98 <i>m</i> 1.73 <i>m</i>	6.17 <i>dd</i> (10.0, 1.5)	5.14 <i>dd</i> (6.2, 5.4)	6.30 <i>d</i> (5.7)	2.05 <i>m</i> 1.73 <i>m</i>	2.62 <i>t</i> (7.0)	6.38 <i>d</i> (5.8)
4	4.14 <i>dd</i> (5.4, 1.9)	5.13 <i>d</i> (5.3)	3.78 <i>ddd</i> (10.0, 7.9, 4.2)	-	5.35 <i>d</i> (5.4)	-	4.94 <i>m</i>		
5	2.90 <i>m</i>	2.90 <i>m</i>	2.32 <i>m</i>	3.40 <i>m</i>	3.04 <i>m</i>		2.54, <i>m</i>		
6	5.90 <i>d</i> (4.9)	5.86 <i>d</i> (4.8)	5.83 <i>d</i> (4.4)	6.30 <i>d</i> (5.2)	5.94 <i>d</i> (4.8)	7.83 <i>brs</i>	5.75 <i>d</i> (3.9)	7.52 <i>s</i>	7.8 <i>brd</i> (1.0)
7	2.59 <i>dd</i> (17.1, 8.1)	2.69 <i>dd</i> (17.1, 8.3)	2.74 <i>dd</i> (17.3, 4.1)	2.97 <i>dd</i> (17.5, 9.3)	2.72 <i>dd</i> (17.1, 8.4)	2.00 <i>s</i>	2.60 <i>m</i>	3.09 <i>s</i>	3.39 <i>d</i> (1.0)
	2.39 <i>dd</i> (17.1, 12.2)	2.41 <i>dd</i> (17.1, 12.6)	2.67 <i>dd</i> (17.3, 6.5)	2.62 <i>dd</i> (17.5, 6.4)	2.46 <i>dd</i> (17.1, 12.6)				
2' and 6'					7.87 <i>d</i> (8.5)				
3' and 5'					7.61 <i>d</i> (8.5)				
COCH ₃		2.09 <i>s</i>					2.10 <i>s</i>		3.72 <i>s</i>

^aThe chemical shifts are in δ values (ppm) from TMS^bThe spectrum is very similar to that previously recorded (Salvatore et al., 1994)^cThe spectrum is very similar to that previously recorded (Wu et al., 2010)

Table 17. Phytotoxicity of compounds **1-4** evaluated at different concentrations on three plant species. area lesions (mm²) ± SE.

Compound	Species	Concentration (mg/mL)			
		1	0.5	0.25	0.125
1	Cork oak	53.1 ± ^{1.7}	22.4 ± ^{4.2}	4.5 ± 1.3	n.a.
	Holm	27.7 ±	5.5 ± 1.9	1.9 ± 0.7	n.a.
	Grapevin	24.3 ± ^{4.0}	5.2 ± 0.3	1.2 ± 0.2	0.9 ± ^{0.06}
2	Cork oak	13.1 ±	5.2 ± 1.7	2.4 ± 0.9	n.a.
	Holm	19.4 ± ^{1.6}	3.5 ± 1.9	1.4 ± 0.4	n.a.
	Grapevin	6.9 ± 0.4 ^{2.0}	3.4 ± 0.4	1.3 ± 0.2	0.8 ± ^{0.06}
3	Cork oak	1.0 ± 0.1	n.a.	n.a.	n.a.
	Holm	1.0 ± 0.1	n.a.	n.a.	n.a.
	Grape	4.9 ± 0.9	1.9 ± 0.5	1.0 ± 0.2	n.a.
4	Cork oak	0.9 ± 0.2	n.a.	n.a.	n.a.
	Holm	0.8 ± ^{0.05}	n.a.	n.a.	n.a.
	Grape	8.3 ± ^{1.2}	n.a.	n.a.	n.a.

Table 18. Phytotoxicity of compounds **22** and **23** evaluated at different concentrations on three plant species. area lesions (mm²) \pm SE.

Compound	Species	Concentration (mg/mL)			
		1	0.5	0.25	0.125
22	Cork oak	4.8 \pm 1.6	2.3 \pm 0.5	0.8 \pm 0.3	n.a.
	Holm oak	3.3 \pm 0.6	n.a.	n.a.	n.a.
	Grape	11.9 \pm 2.2	2.5 \pm 0.3	0.6 \pm 0.1	n.a.
23	Cork oak	n.a.	n.a.	n.a.	n.a.
	Holm oak	n.a.	n.a.	n.a.	n.a.
	Grape	n.a.	n.a.	n.a.	n.a.

Table 19. Phytotoxicity and zootoxicity data for diplopimarane (**24**), its derivatives (**25-27**, **29**), sphaeropsidin A (**32**), sphaeropsidin C (**33**) and (+)-epiepoformin (**34**)

compound	leaf puncture bioassay ^a			cuttings ^b	% <i>Artemia salina</i> larval mortality ^c
	holm oak	cork oak	tomato		
1	na	na	na	stewing	70.8
2	na	na	na	stewing	100
3	na	na	na	na	94.6
4	na	na	na	na	79.5
5	nt	nt	nt	nt	nt
6	nt	nt	nt	stewing	98.6
9	10.85 ± 1.34	15.03 ± 4.40	120.92 ± 13.37	stewing	85.6
10	na	na	na	stewing	na
11	6.68 ± 0.88	9.49 ± 2.33	13.49 ± 1.98	stewing/wilting	78.8

^aThe compounds were tested at concentration of 1 mg/mL. Data are expressed as median area lesions ± error standard (mm²).

^bSymptoms developed within 3 days on tomato cuttings at 0.1 mg/mL.

^cThe compounds were tested at concentration of 200 µg/mL. The activity was evaluated after 36 h of exposure. na = inactive. nt = not tested

Table 20. Inhibitory activity of diplopimarane (**24**), sphaeropsidin A (**32**), sphaeropsidin C (**33**) and (+)-epiepoformin (**34**) against agrarian and forest phytopathogens at 100 µg/mL

Compound	Mycelial growth inhibition (%)			
	<i>Athelia rolfsii</i>	<i>Diplodia corticola</i>	<i>Phytophthora cinnamomi</i>	<i>Phytophthora plurivora</i>
1	55	54,5	53,5	51,3
9	83,2	19,8	100	100
10	na	na	na	na
11	41,9	39,7	72,3	62,1
PCNB	87,2	81,01	nt	nt
Metalaxyl-M	nt	nt	100	100

na = inactive. nt = not tested

Table 21. Biological data for oxysporone (**35**) and its derivatives (**38-45**)

Bioassay	Leaf puncture bioassay ^a			Cuttings ^b	Antifungal activity ^c				
	Target	Holm oak	Cork oak		Grapevine	Tomato	<i>Diplodia corticola</i>	<i>Phytophthora cinnamomi</i>	<i>Phytophthora plurivora</i>
Compound									
1		19.58± 1.62	15.81 ± 1.75	23.04± 0.97	Wilting	na	na	na	na
4		4.05 ± 0.53	3.50 ± 0.47	7.83± 1.85	Stewing	na	na	na	na
5		na	na	na	na	na	na	na	na
6		4.28 ± 0.37	4.42 ± 0.92	7.86± 0.66	Stewing	na	na	na	na
7		na	na	na	na	35.6	77.2	100	100
8		na	na	na	na	na	na	na	na
9		na	na	na	na	na	na	na	na
10		na	na	na	na	nt	nt	nt	nt
11		na	na	na	na	nt	nt	nt	nt

^aThe compounds were tested at concentration of 1mg/ml. Data are expressed as median area lesions ± error standard (mm²)

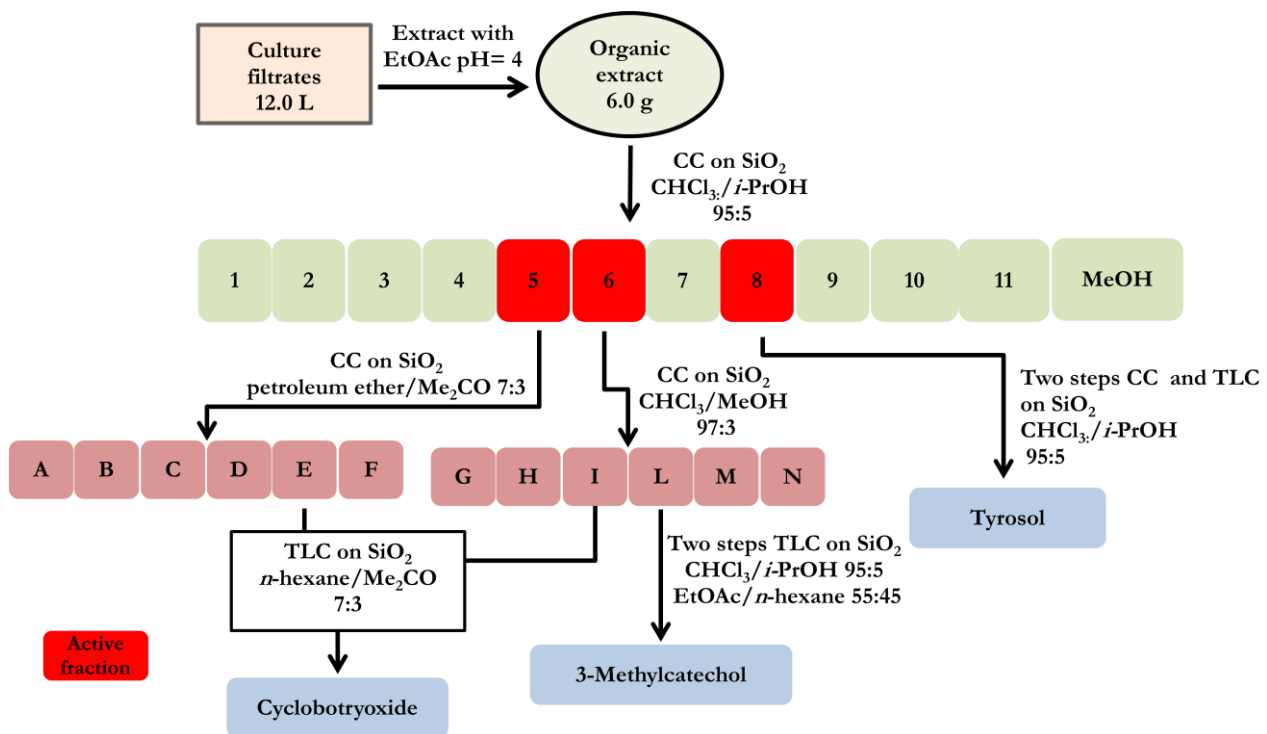
^bSymptoms developed within 2 days on tomato at 0.2 mg/ml;

^cData expressed as percentage of linear growth inhibition at 100 µg/ml
na = inactive; nt = not tested

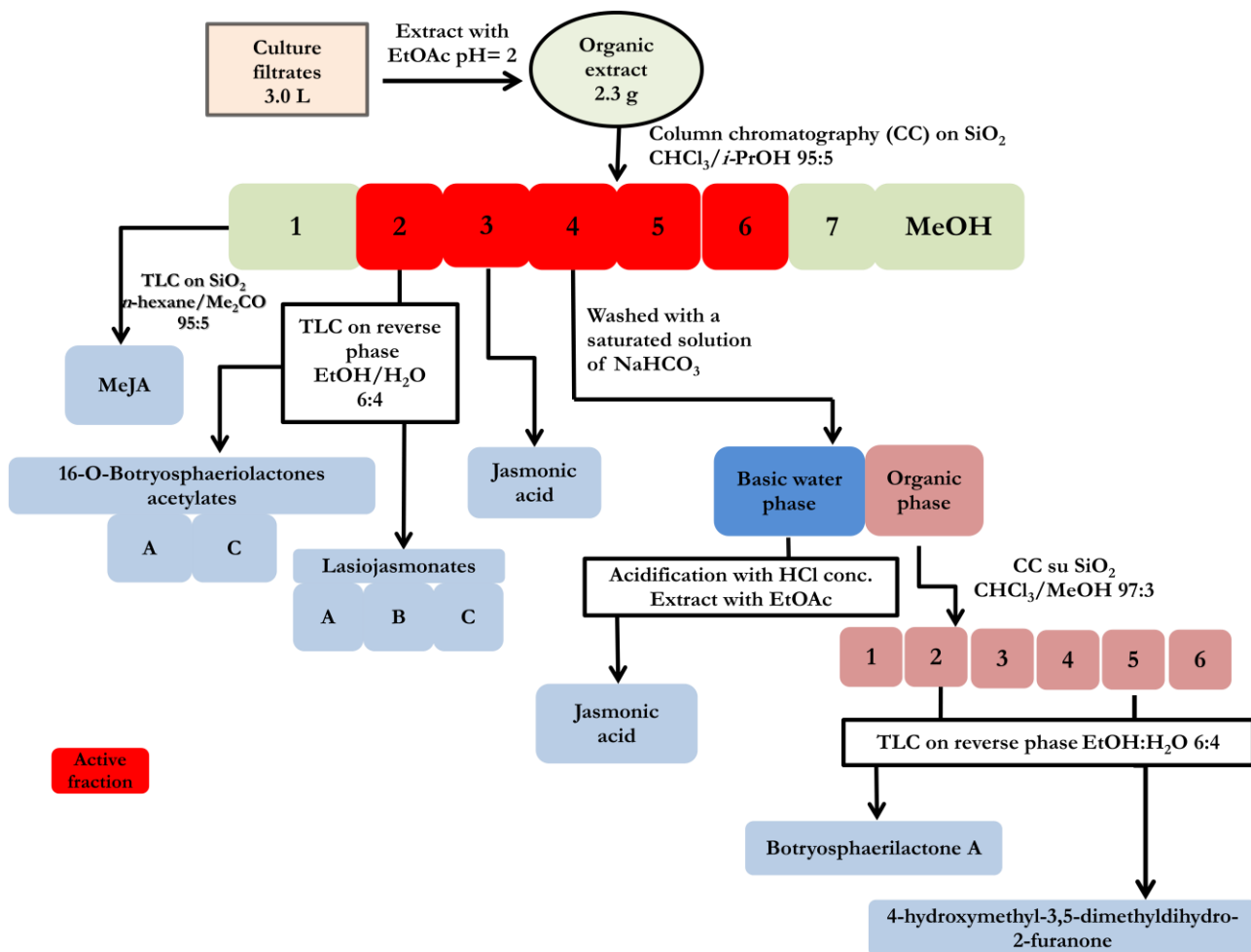
Table 22. EC₅₀ Values of derivative **41**, toclofos-methyl, PCNB and metalaxyl-M against three pathogens belonging to Oomycetes and Basidiomycetes

Target	ED ₅₀ (µg/ml)		
	<i>Phytophthora cinnamomi</i>	<i>Phytophthora plurivora</i>	<i>Athelia rolfsii</i>
Compound			
Derivative 5	43,5	29,47	37,12
Toclofos-methyl	nt	nt	1,02
PCNB	nt	nt	11,47
Metalaxyl-M	0,49	0,41	nt

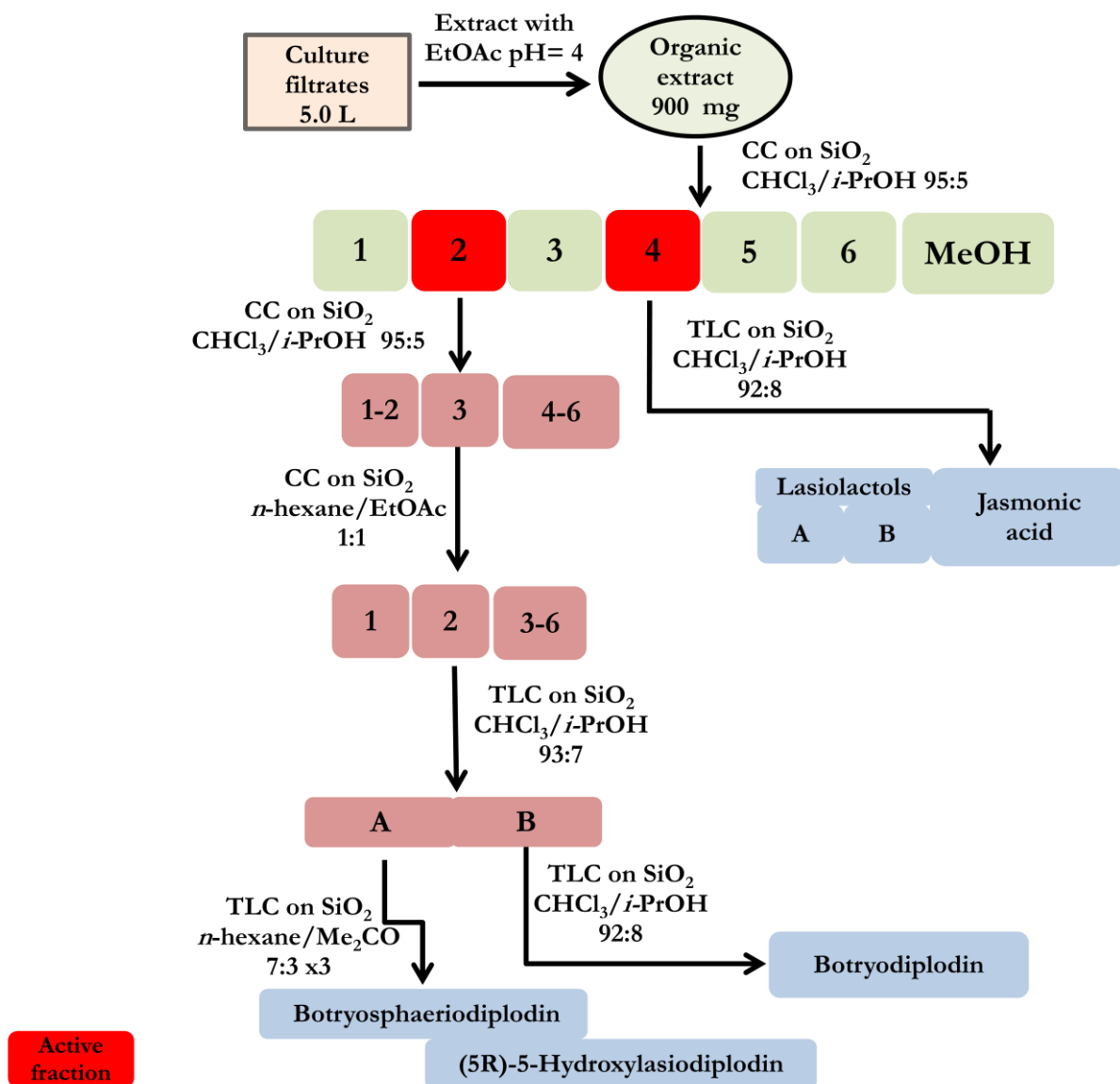
nt=not tested.



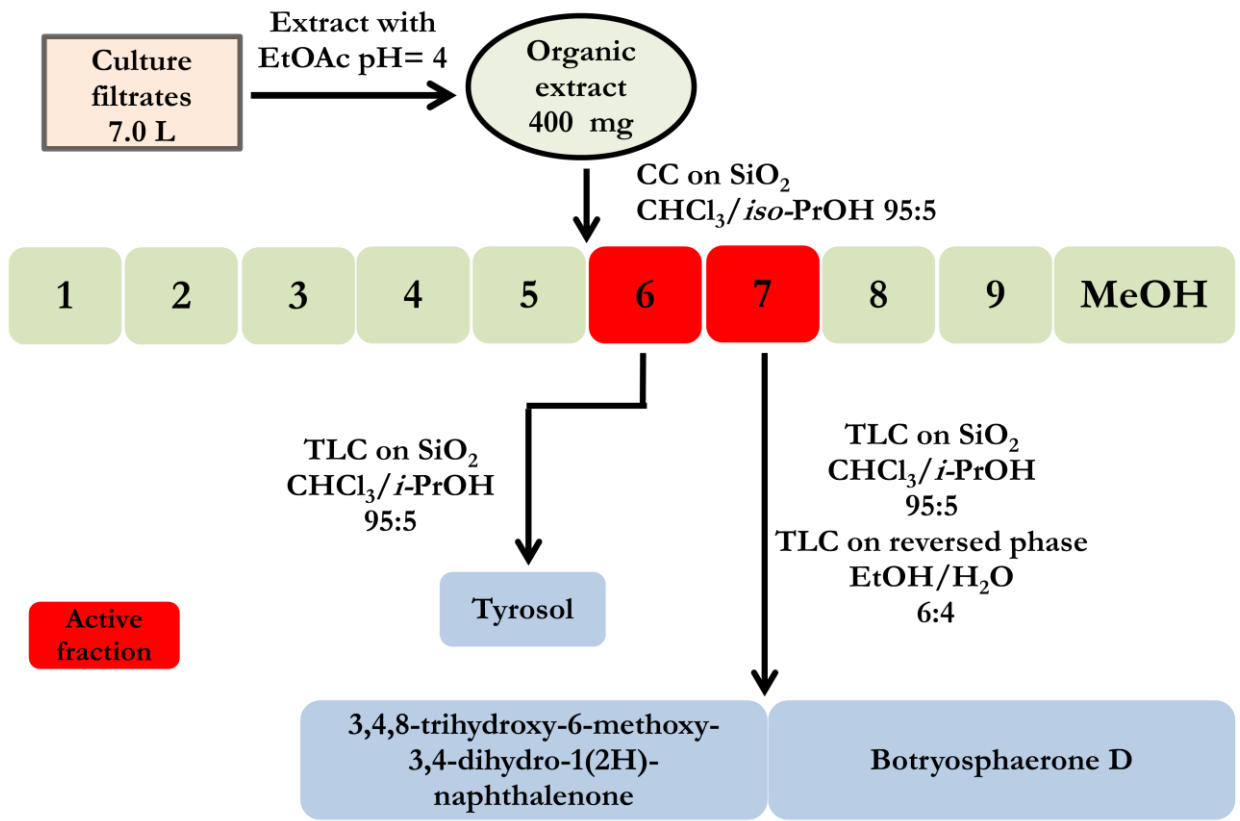
Scheme 1. Purification scheme of *Neofusicoccum australe* strain BOT48.



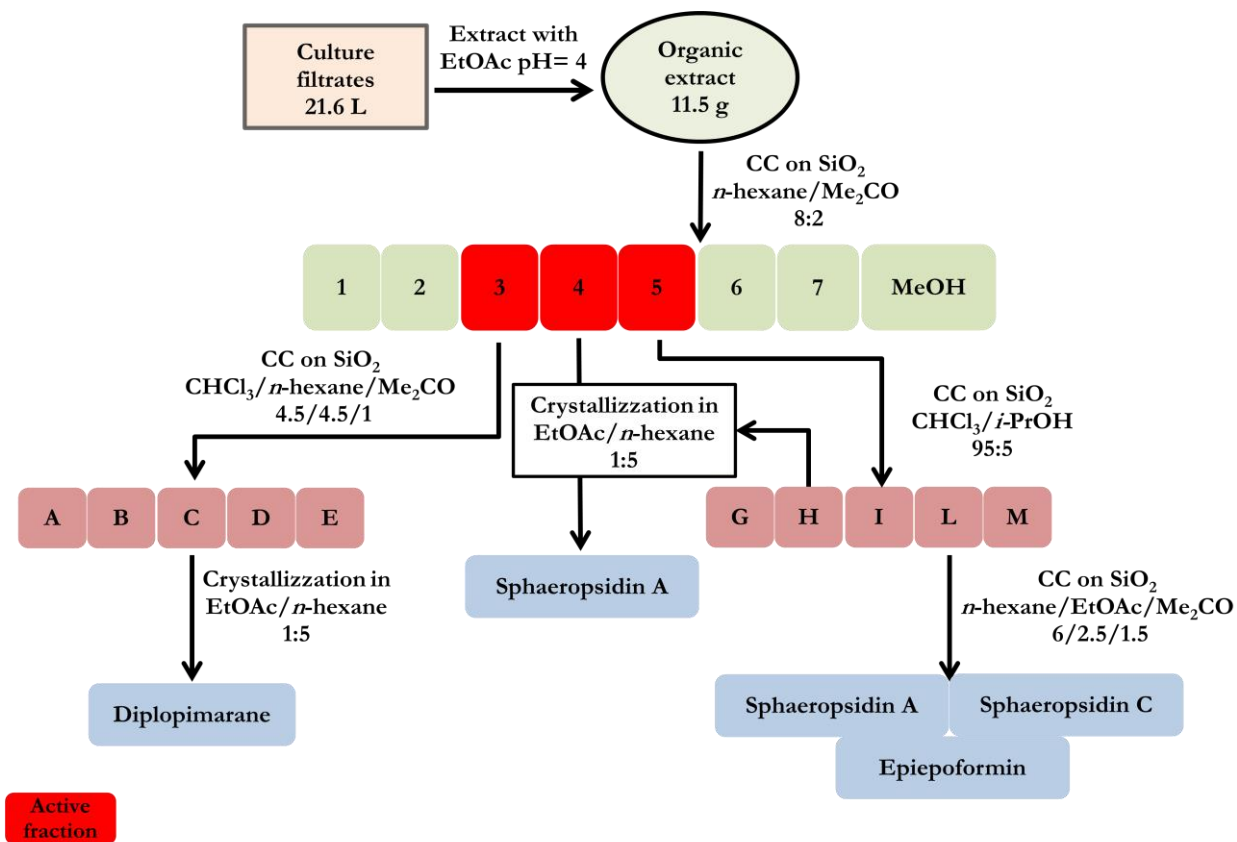
Scheme 2. Purification scheme of *Lasiodiplodia mediterranea* strain BL101.



Scheme 3. Purification scheme of *Lasiodiplodia mediterranea* strain B6.



Scheme 4. Purification scheme of *Neofusicoccum australe* strain BL24 (haplotype H1).



Scheme 5. Purification scheme of *Diplodia quercivora* strain BL9.

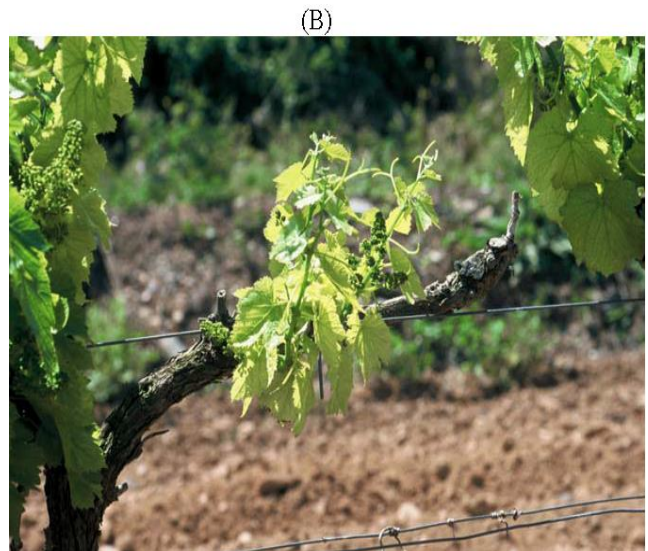


Figure 1. Symptoms of grapevine affected with various species of *Botryosphaeriaceae*. (A) Stunting early in the season; (B) Foliar chlorosis; (C) wedge-shaped necrosis in a trunk cross-section.

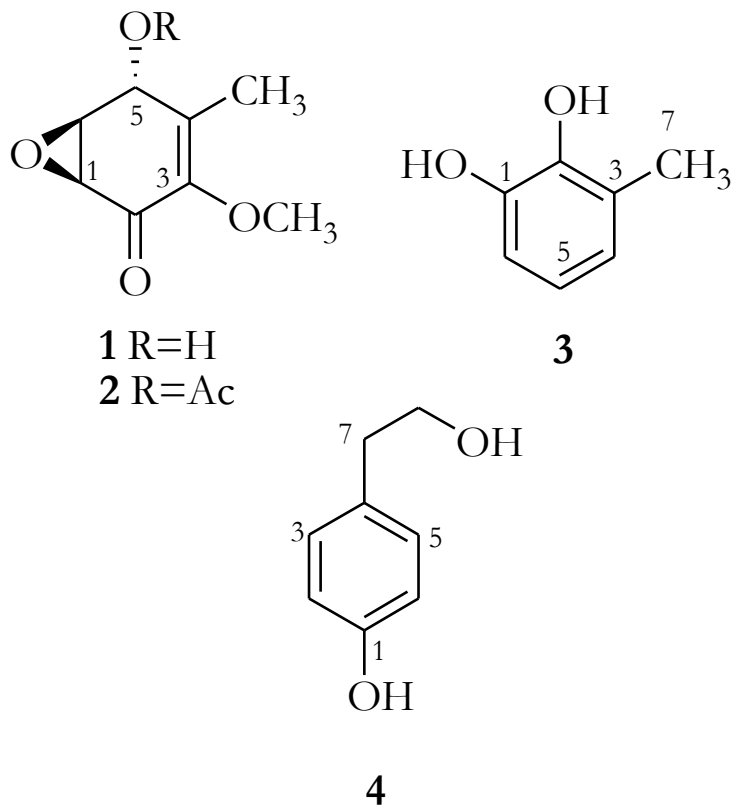


Figure 2. Structures of cyclobutryoxide and its acetyl derivative, 3-methylcatechol, tyrosol, (1-4) produced by *N. australis* from grapevine.

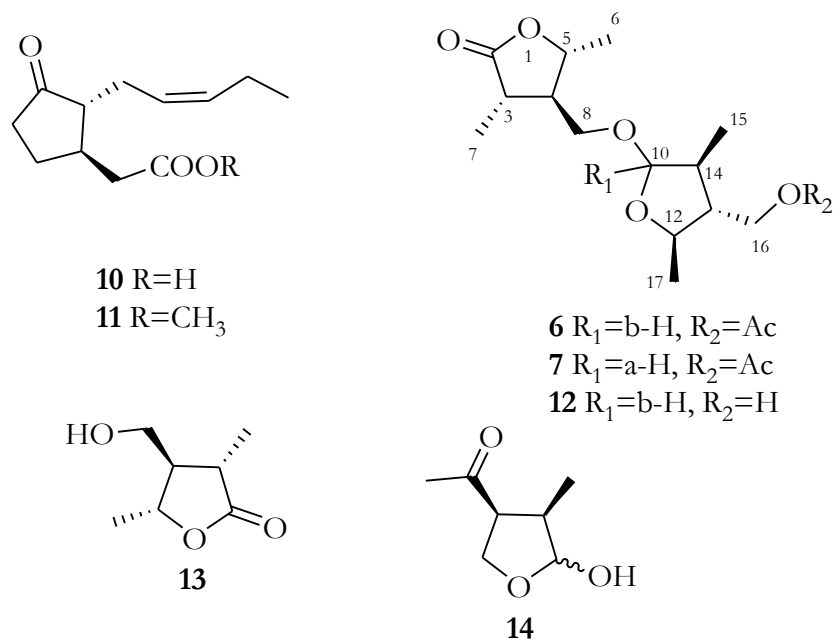


Figure 3. Structures of 16-*O*-acetylbotryosphaerilactone A and C, (-)-jasmonic acid and its methyl ester, botryosphaerilactone A, 4-hydroxymethyl-3,5-dimethyldihydro-2-furanone and (3*R*,4*S*)-botryodiplodin (**6,7, 10-14**) produced by *Lasiodiplodia mediterranea*.

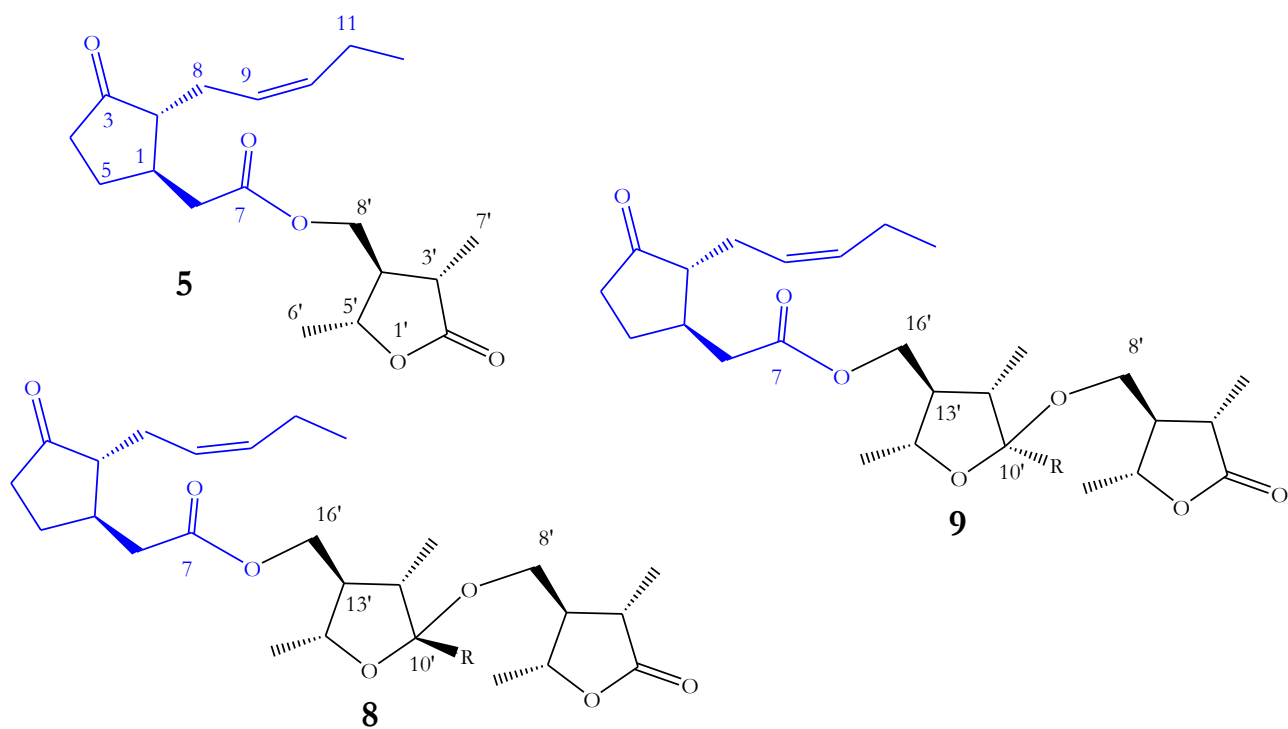


Figure 4. Structures of Lasiojasmonates A-C (5, 8 and 9), new metabolites produced by *Lasiodiplodia mediterranea*.

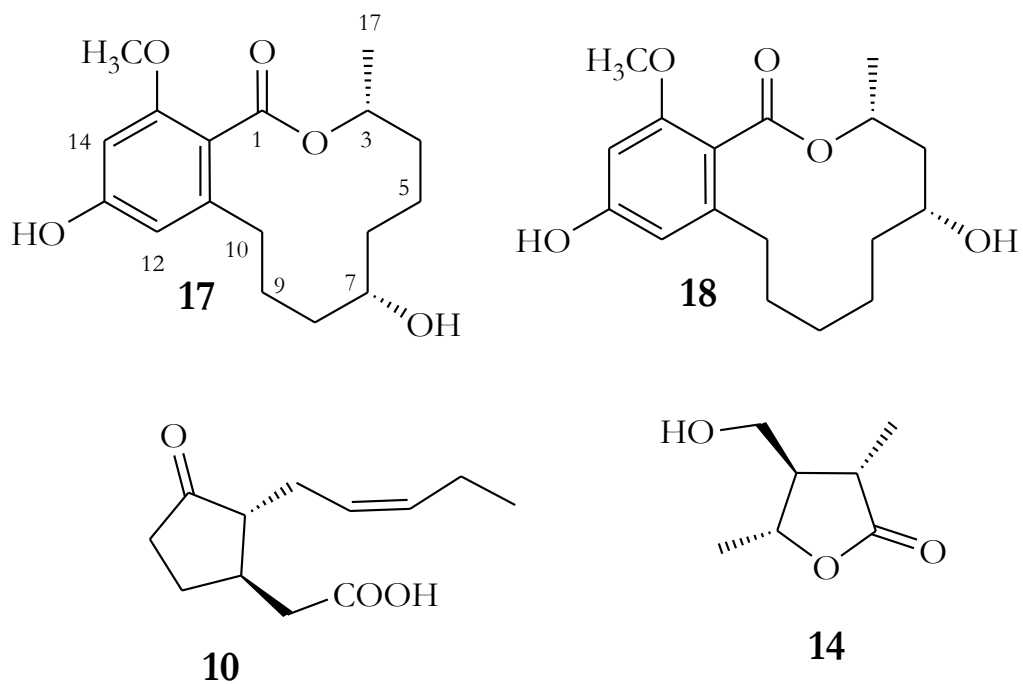


Figure 5. Structures of botryosphaeriodiplodin, (5R)-5-hydroxylasiodiplodin (**18**), (-)-jasmonic acid (**10**), 4-hydroxymethyl-3,5-dimethyldihydro-2-furanone (**14**), 13-O-methylbotryosphaeriodiplodin (**17**).

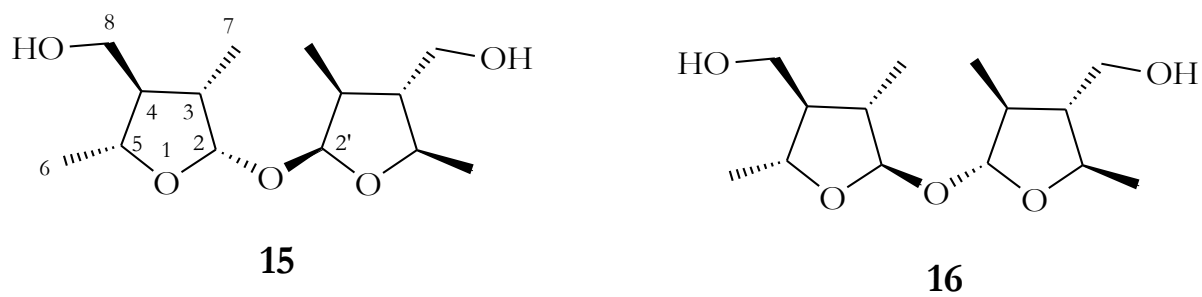


Figure 6. Structures of lasiolactols A and B (**15** and **16**), new metabolites produced by *Lasiodiplodia* sp.

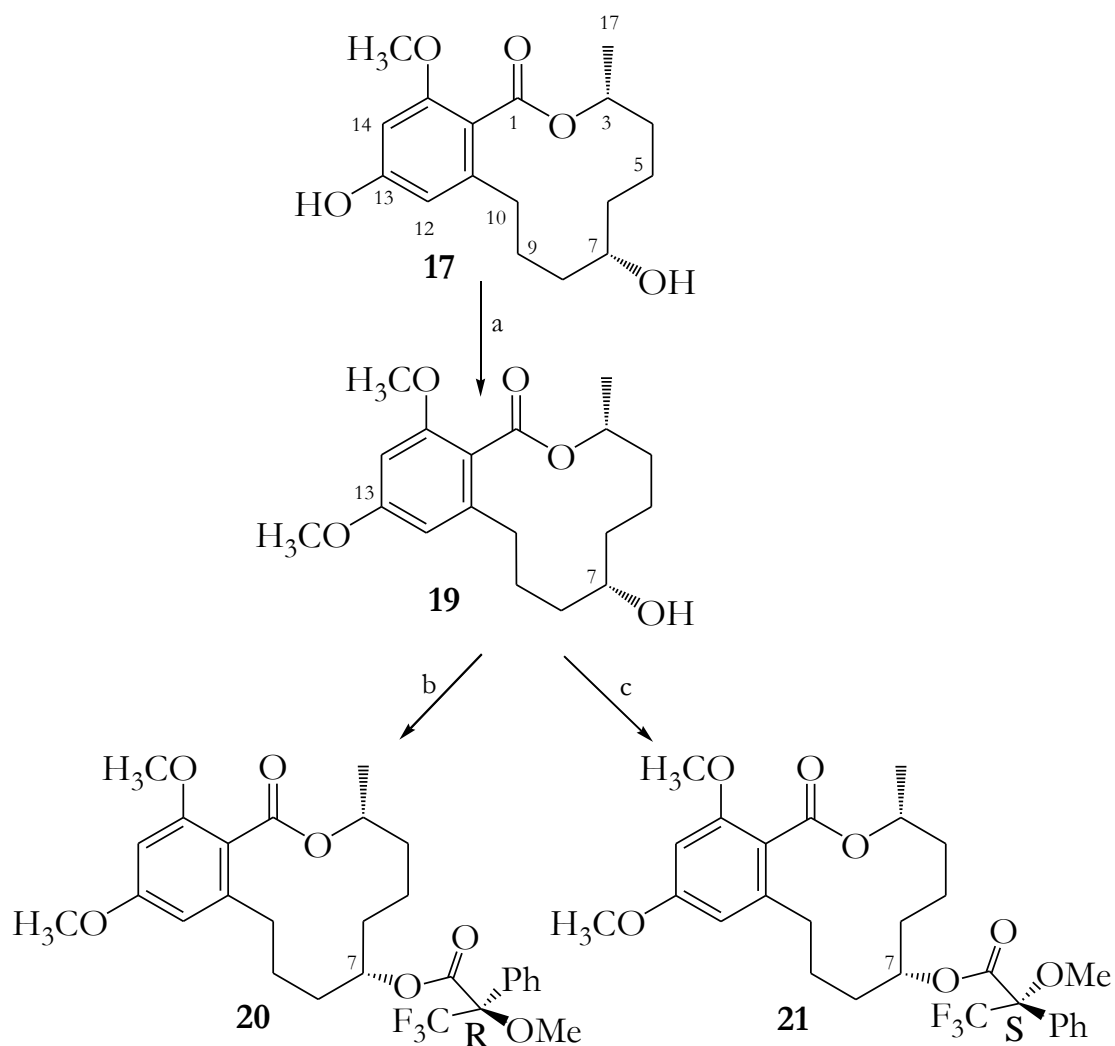


Figure 7. Reagent and condition to convert 17 into 19-21: (a) CH_2N_2 , MeOH , rt, 6 h; (b) (R) -(-)-MPTA-Cl, pyridine, rt, o.n.; (c) (S) -(+)-MPTA-Cl, pyridine, rt, o.n.

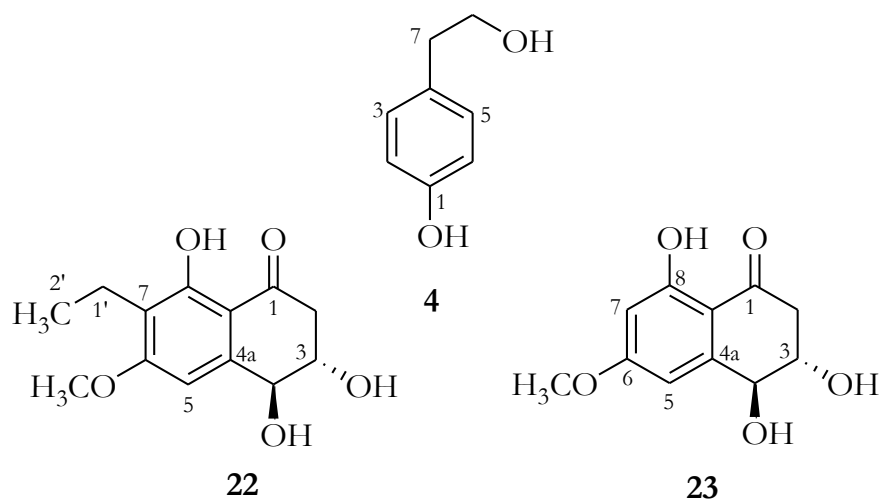


Figure 8. Structures of tyrosol, botryosphaerone D and (3*S*,4*S*)-3,4,8-trihydroxy-6-methoxy-3,4-dihydro-1(2*H*)-naphthalenone (**4**, **22** and **23**) produced by *N. australe* from juniper.

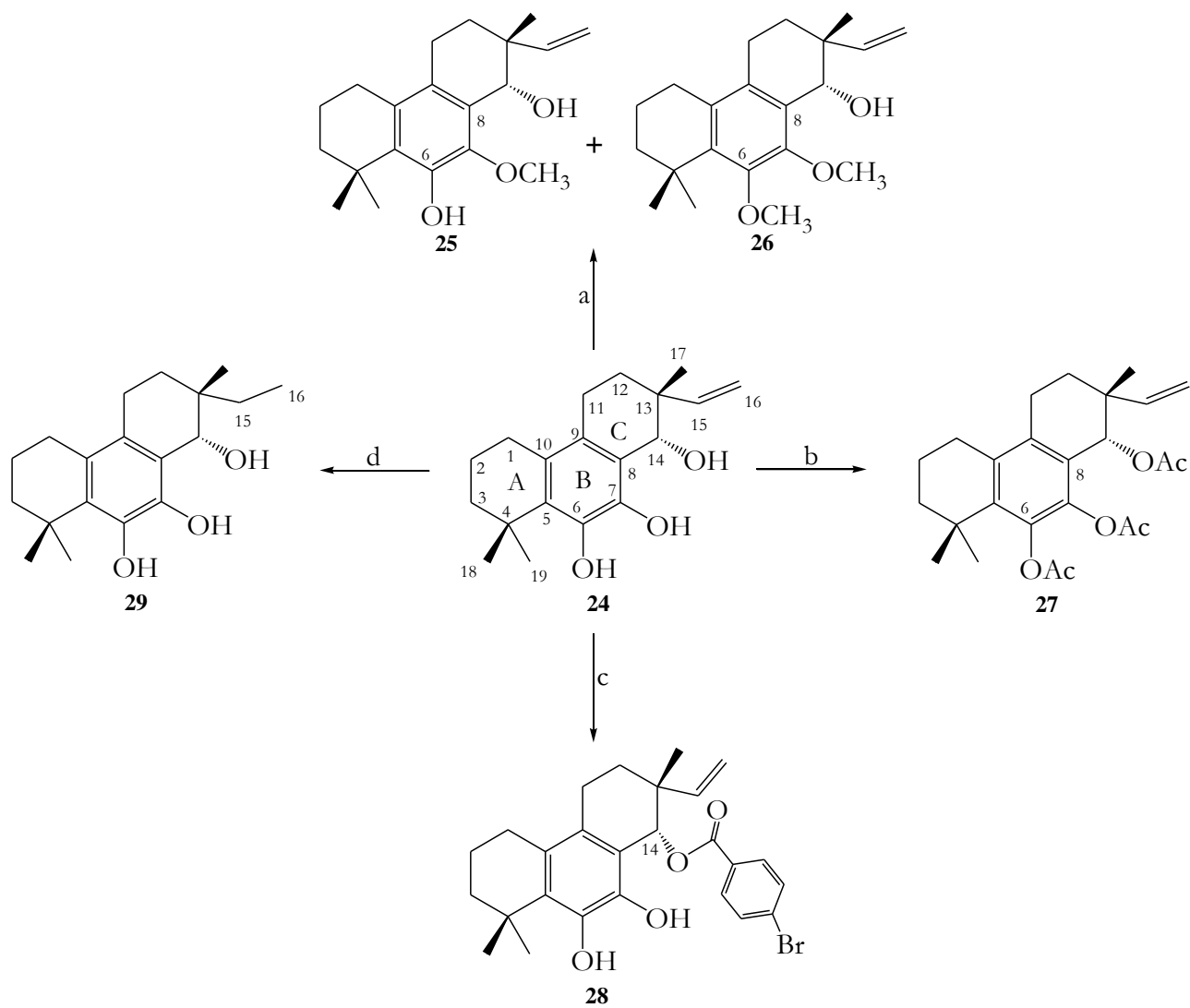


Figure 9. Reagent and condition to convert **24** into **25-29**: (a) CH_2N_2 , MeOH, rt, 78 h; (b) Ac_2O , pyridine, rt, 1 h; (c) $p\text{-Br-BzCl}$, DMAP, MeCN, rt, 2 h; (d) H_2 , Pd/C 10%, MeOH, rt, o.n.

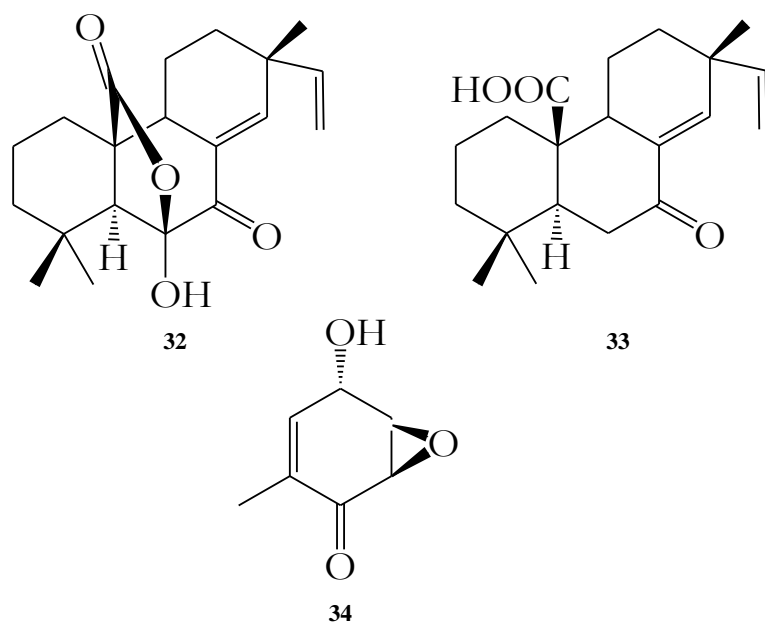


Figure 10. Structures of Sphaeropsidins A and C, and (+)-epiepoformin (32-34)

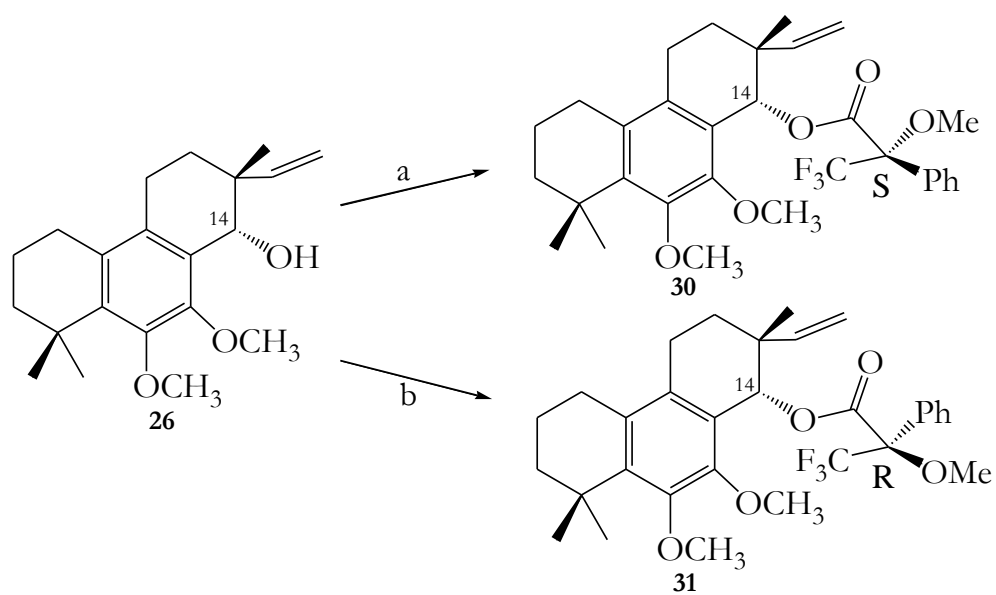


Figure 11. Reagent and condition to convert **26** into **30** and **31**: (a) *(R)*-(-)-MPTA-Cl, pyridine, rt, 2 h; (b) *(S)*-(+)-MPTA-Cl, pyridine, rt, 2 h

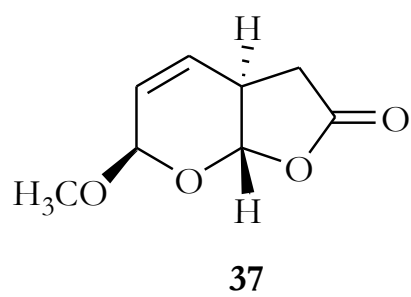
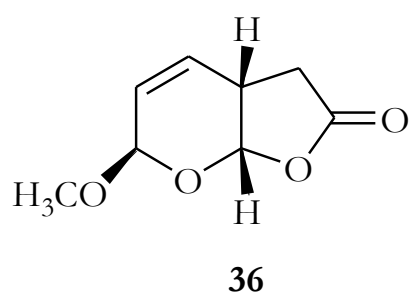
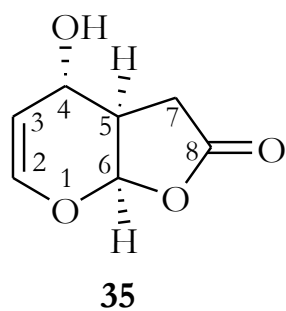


Figure 12. Structures of oxysporone, and afritoxinones A and B (**35**, **36** and **37**, respectively)

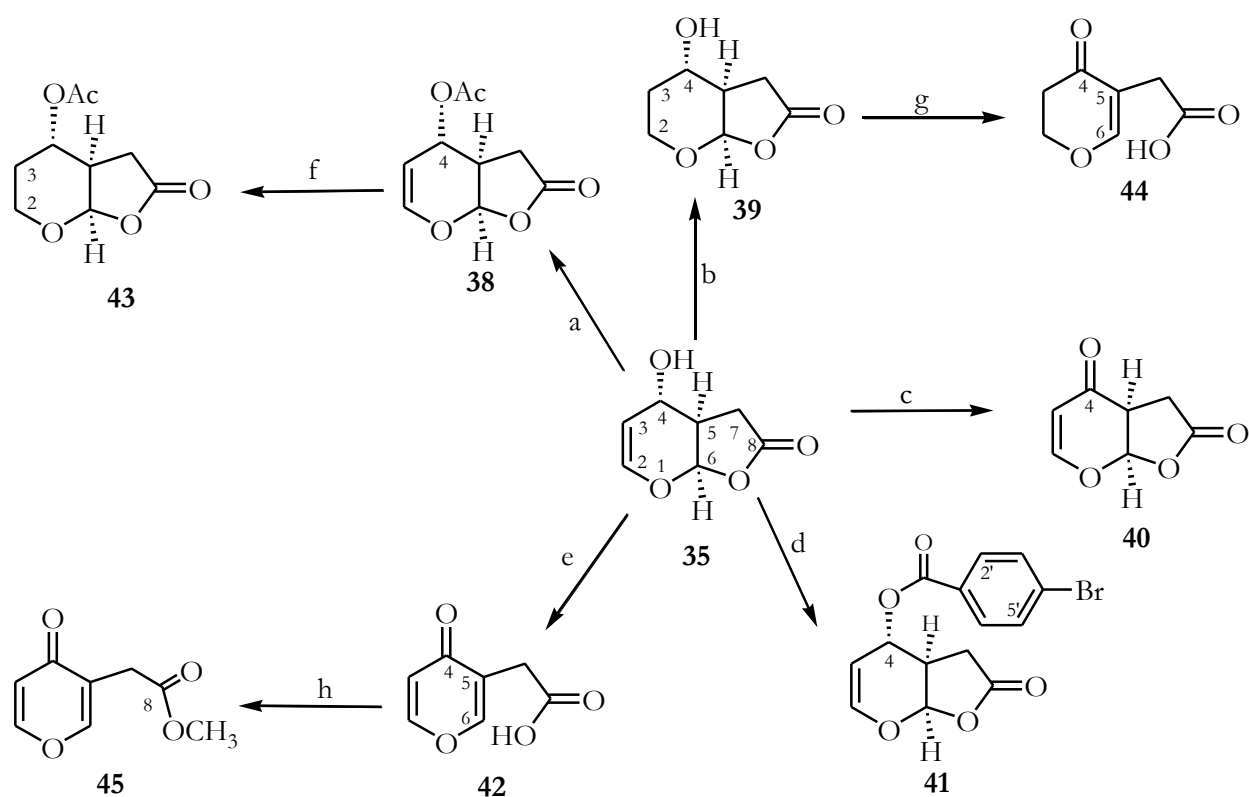


Figure 13. Reagent and condition to convert **35** into **38-45**: (a) Ac_2O , pyridine, rt, 2 h; (b) H_2 , Pt 5%, MeOH, rt, 4 h; (c) Corey's reagent, CH_2Cl_2 , rt, 1 h; (d) p-Br-BzCl, DMAP, MeCN, rt, 4 h; (e) Jones's reagent, Me_2CO , 0°C , 10 min; (f) H_2 , Pt 5%, MeOH, rt, 5 h; (g) Jones reagent, Me_2CO , 0°C , 10 min; (h) CH_2N_2 , MeOH, rt.



Figure 14. Grapevine diseases symptoms associated with *Neofusicoccum australe* strain Bot48.

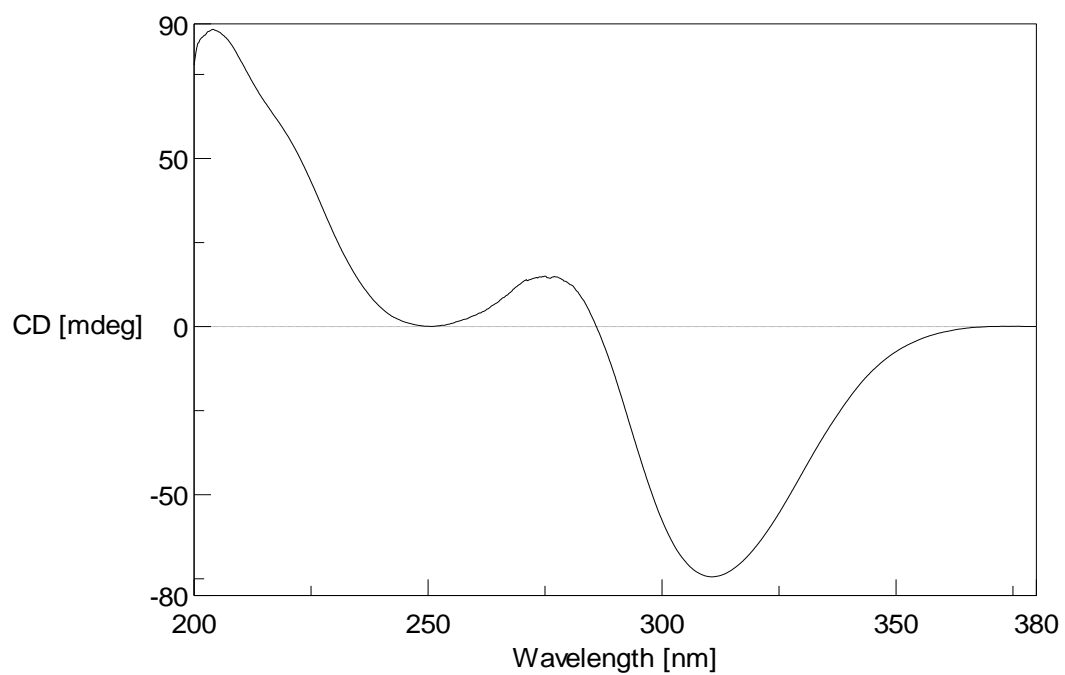


Figure 22. CD spectra of cyclobutryoxide recorded in EtOH.

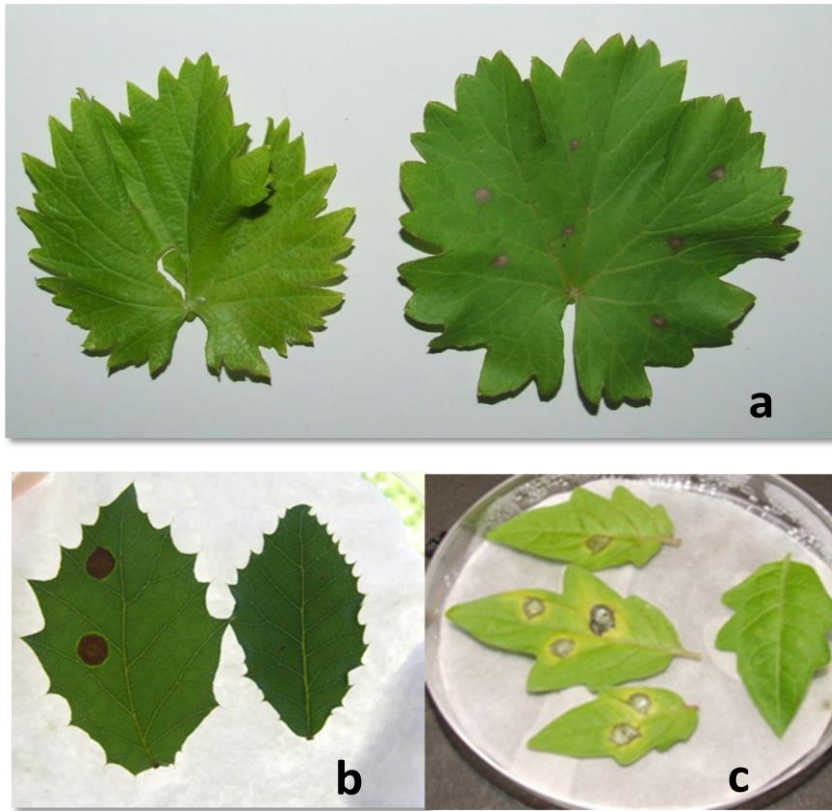


Figure 24. Phytotoxic activity of cyclobotrioxide by leaf drop assays at concentration of 0.25 mg /mL on leaves of greaevine (a), holm oak (b) and tomato (c).



Figure 25. Grapevine diseases symptoms associated with *Lasiodiplodia mediterranea*.

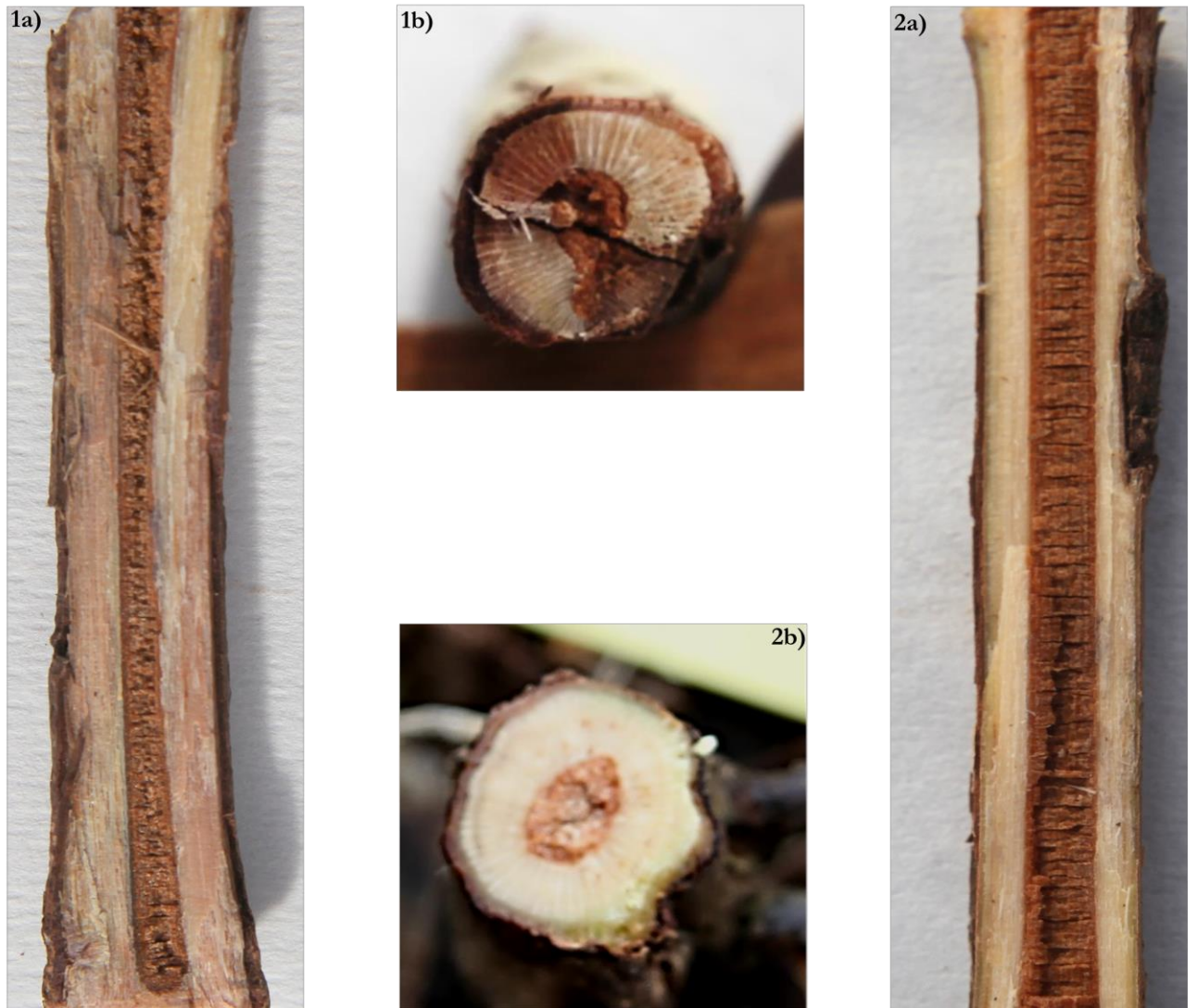


Figure 41. 1) Brown necrosis caused by *L. mediterranea* extending along a large part of the trunk in longitudinal section (a) and cross section (b). 2) Absence of xylematic symptom in the control in longitudinal section (a) and cross section (b).

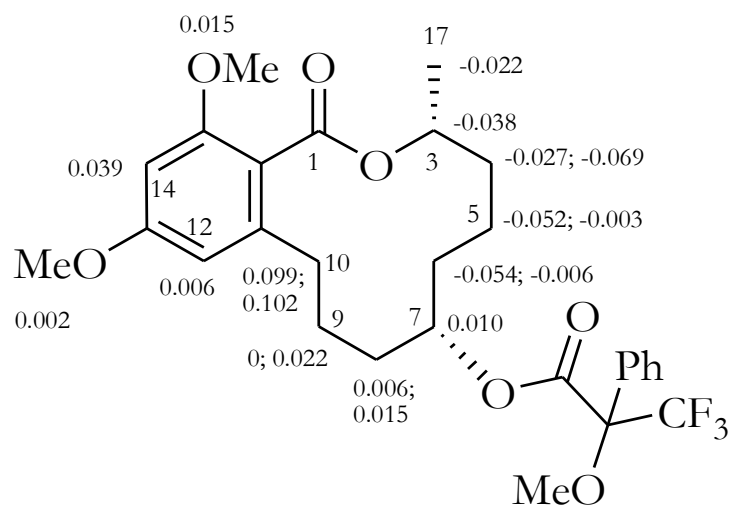


Figure 53. Structures of 7-O-S- and 7-O-R-MPTA esters of 13-O-methylbotriosphaeriodiplodin (**20** and **21**), reporting the $\Delta\delta$ value obtained by comparison(**20** and **21**) of each proton system.

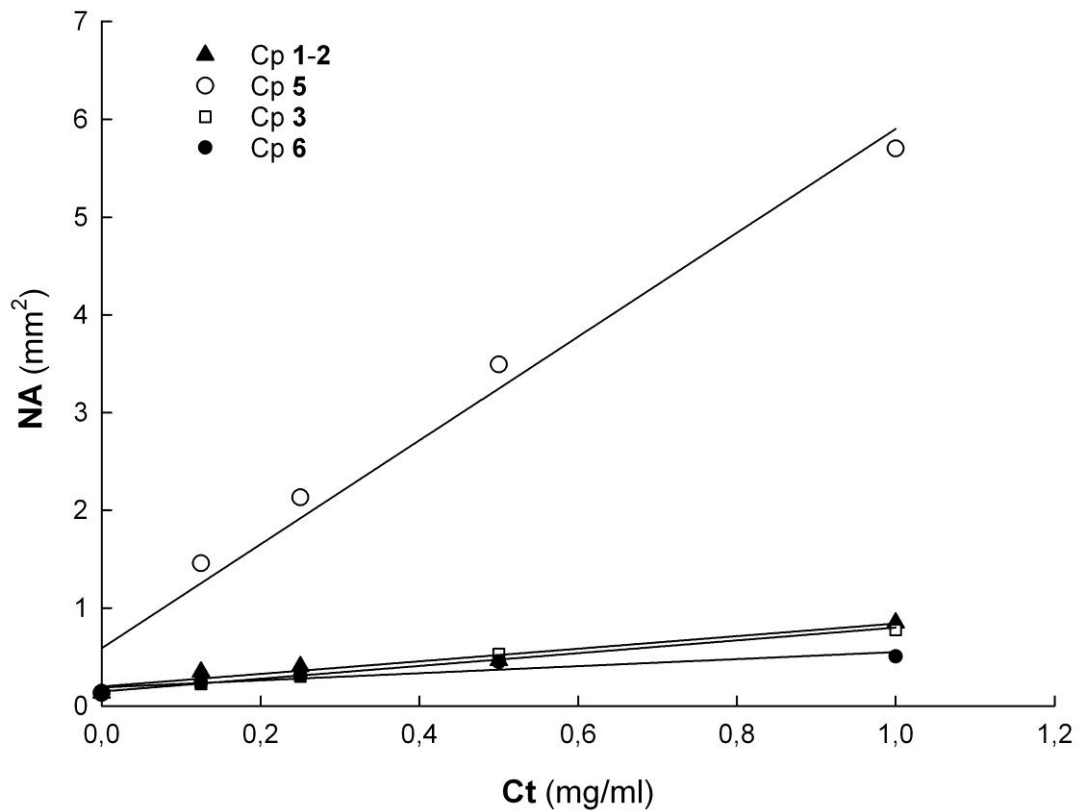


Figure 54. Linear association between necrotic area (NA) and concentration (Ct) of assayed compounds. **15-16:** $NA = 0.198 + 0.644Ct$ $R^2 = 0.947$ $P < 0.001$; **10:** $NA = 0.590 + 5.312Ct$ $R^2 = 0.978$ $P < 0.001$; **17:** $NA = 0.147 + 0.653Ct$ $R^2 = 0.985$ $P < 0.001$; **14:** $NA = 0.189 + 0.362Ct$ $R^2 = 0.8709$ $P < 0.001$.



Figure 55. Juniper diseases symptoms associated with *Neofusicoccum australe* strain BL24.

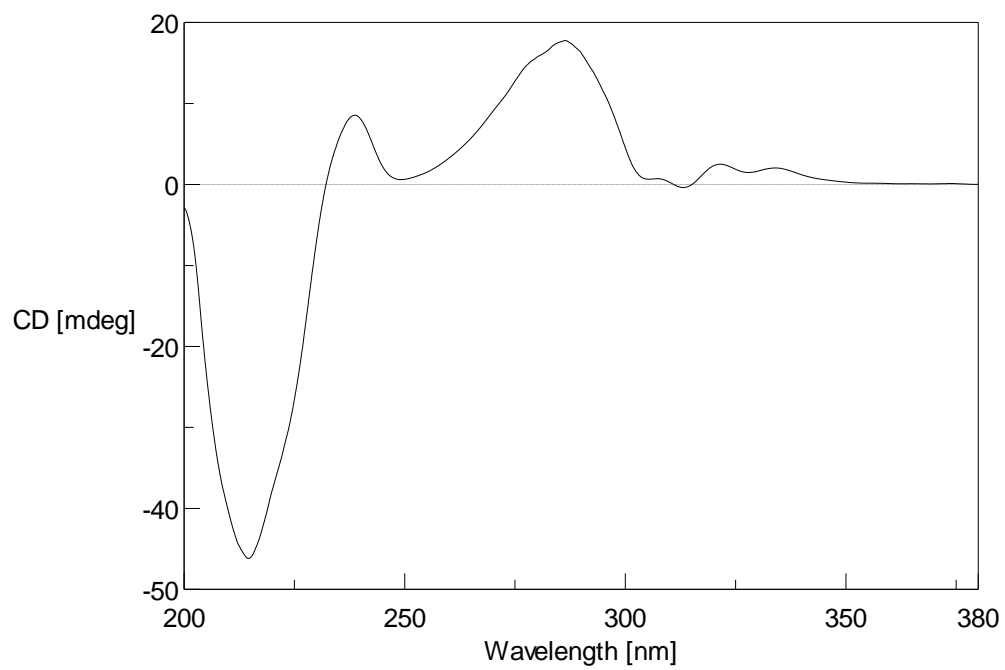


Figure 58. ECD spectra of botryosphaerone D (**22**) recorded in EtOH.



Figure 59. Quercus diseases symptoms associated with *Diplodia quercivora* strain BL9.

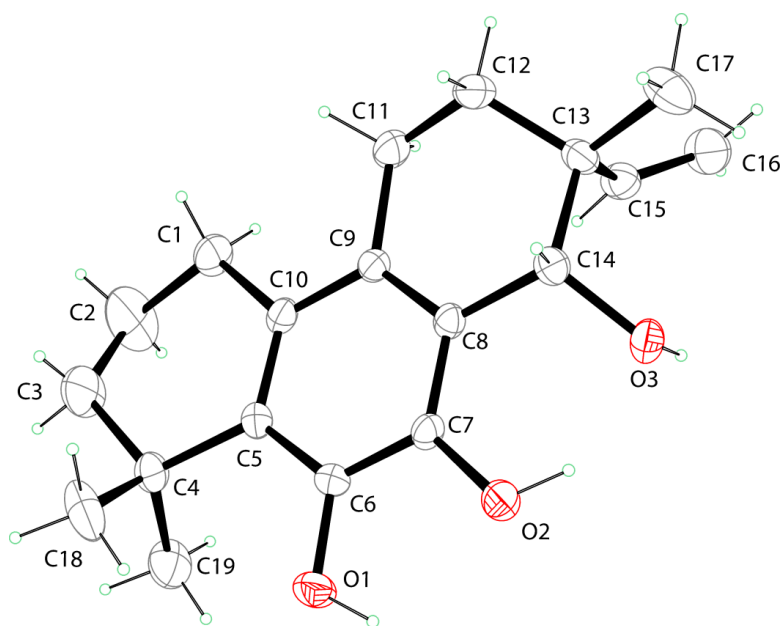


Figure 70. ORTEP view of diplopimarane (**24**) showing atomic labelling. Displacement ellipsoids are drawn at the 30% probability level.

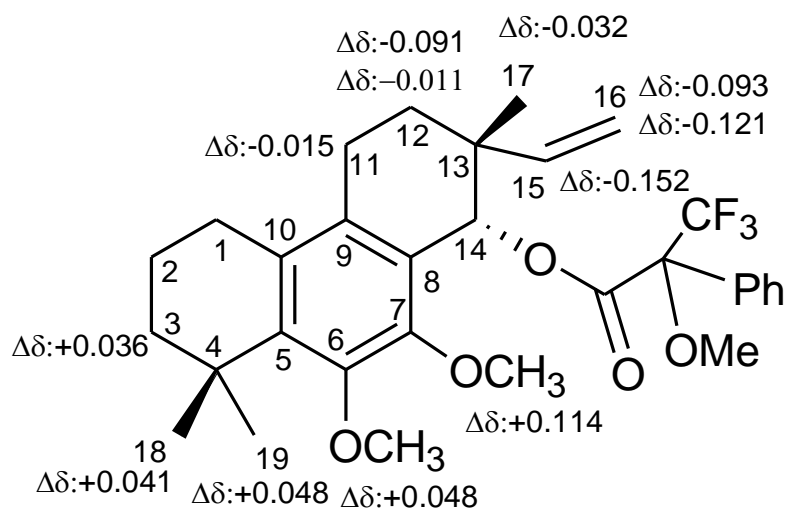


Figure 74. Structures of 14-*O*-*S*- and 14-*O*-*R*-MPTA esters of 6,7-*O*,*O*'-dimethyldiplopimarane (**30** and **31**), reporting the $\Delta\delta$ value obtained by comparison (**30** and **31**) of each proton system.

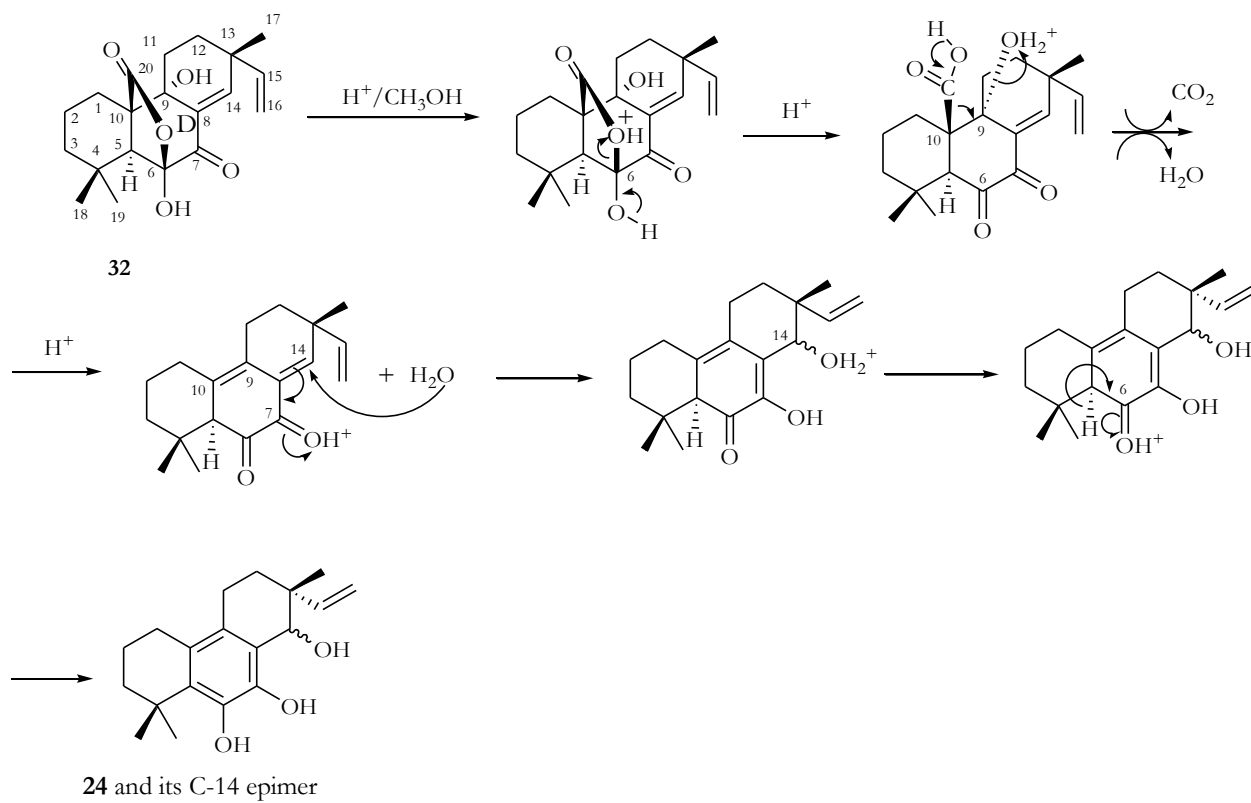


Figure 75. Probable mechanism of biosynthetic conversion of sphaeropsidin A (**32**) into diplopimarane (**24**)

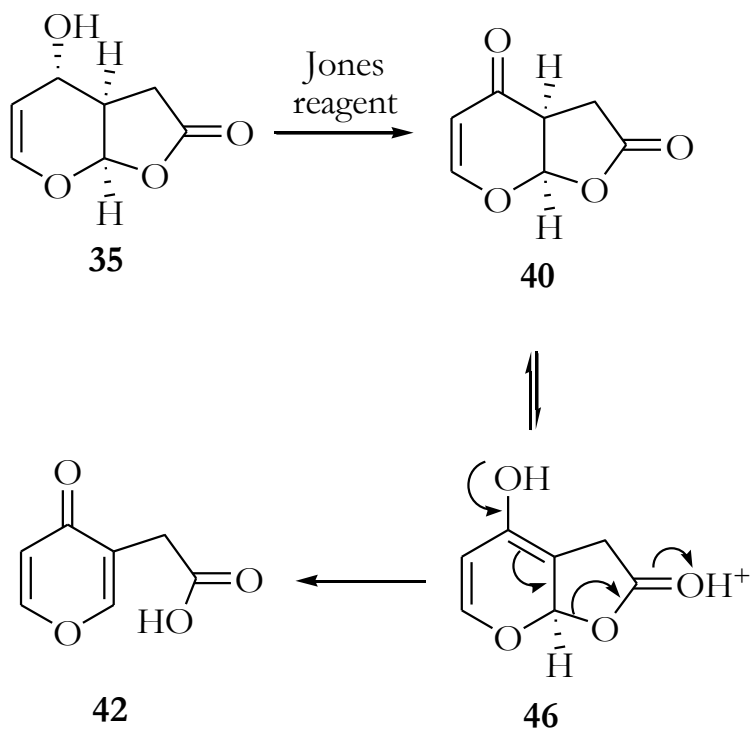


Figure 76. Reaction mechanism probably involved in the conversion of **35** into **42** in strong acid conditions

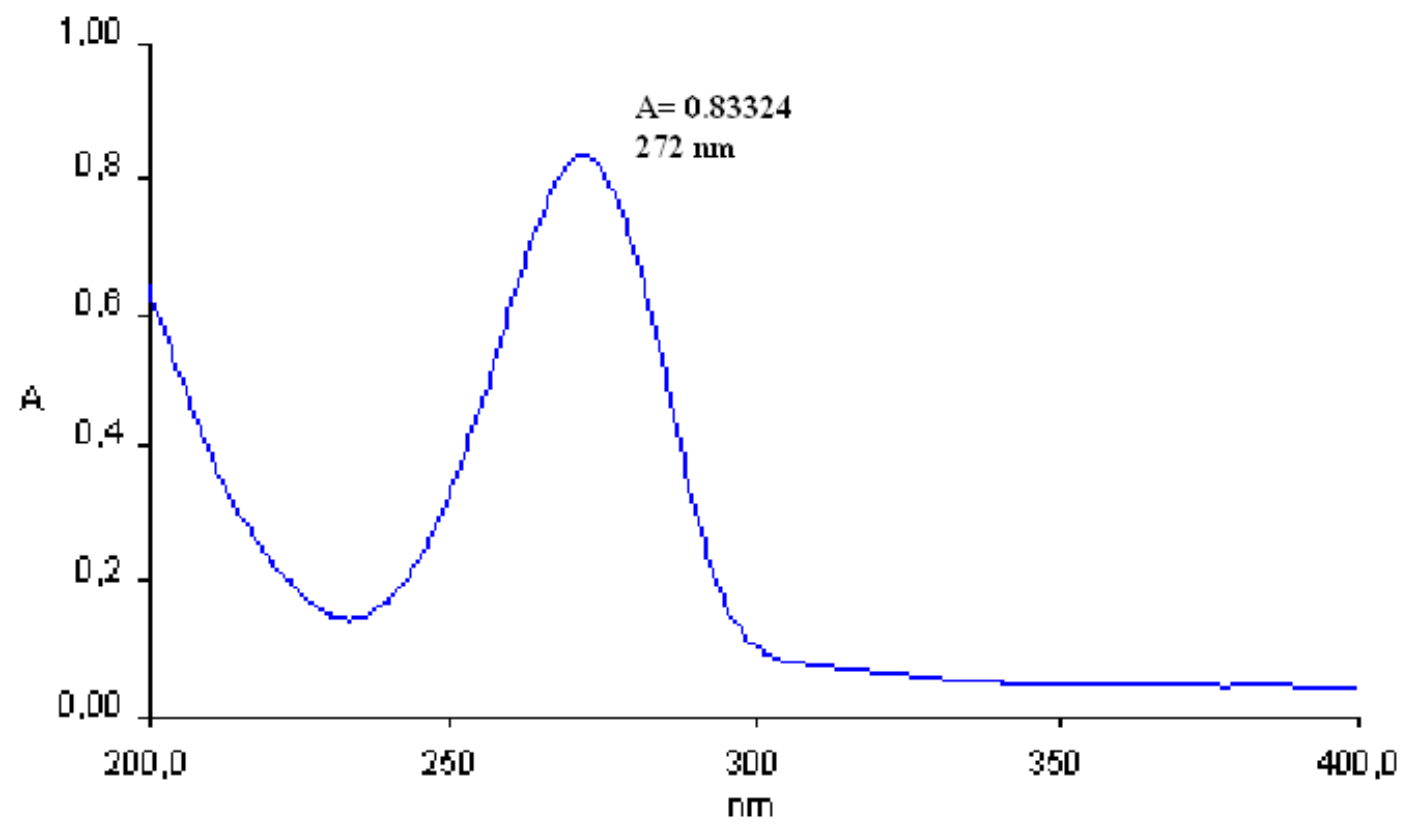


Figure 15. UV spectrum of cyclobotryoxide (1) recorded in MeCN.

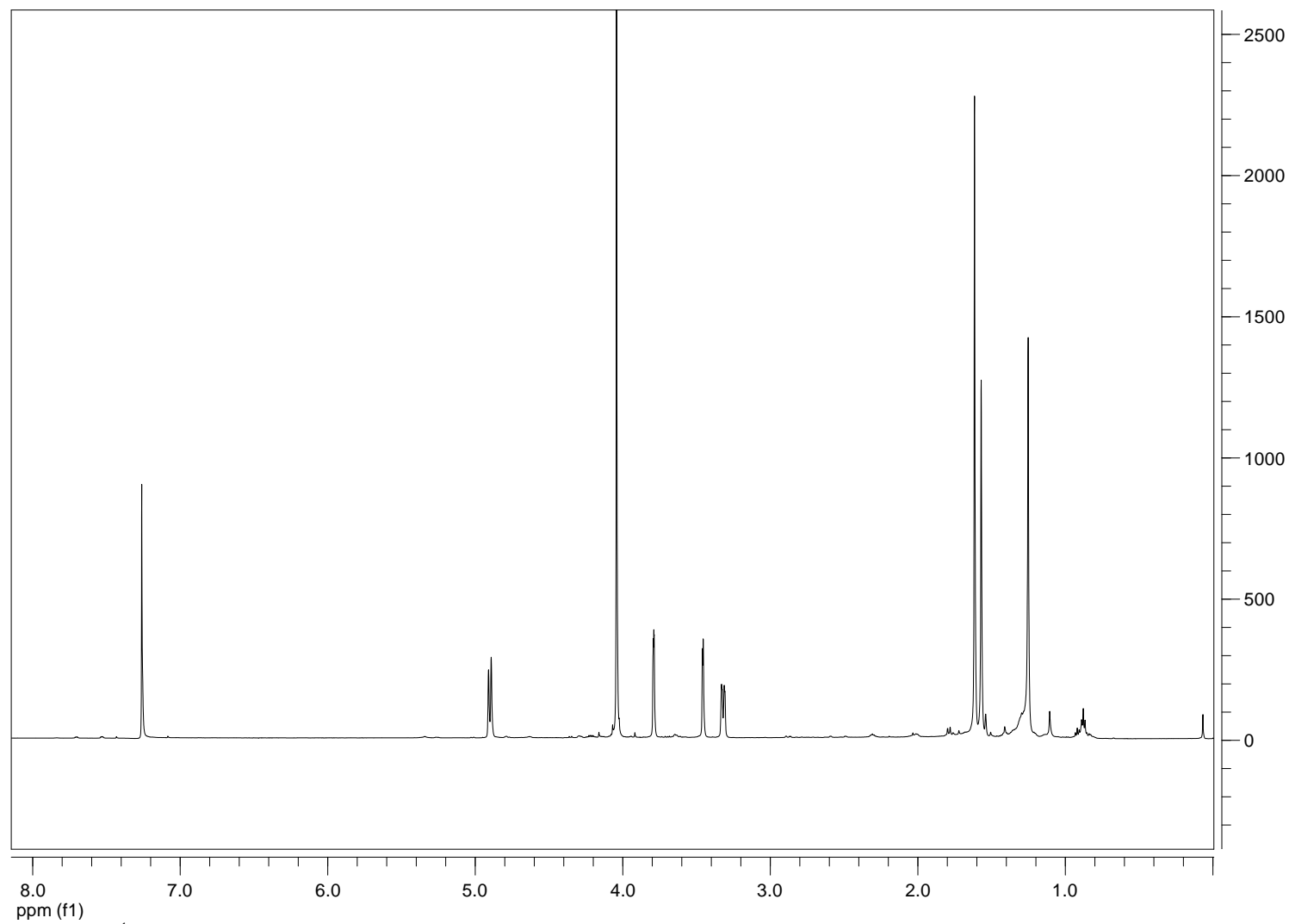


Figure 16. ^1H NMR spectrum of cyclobutryoxide (**1**) recorded in CDCl_3 at 400 MHz.

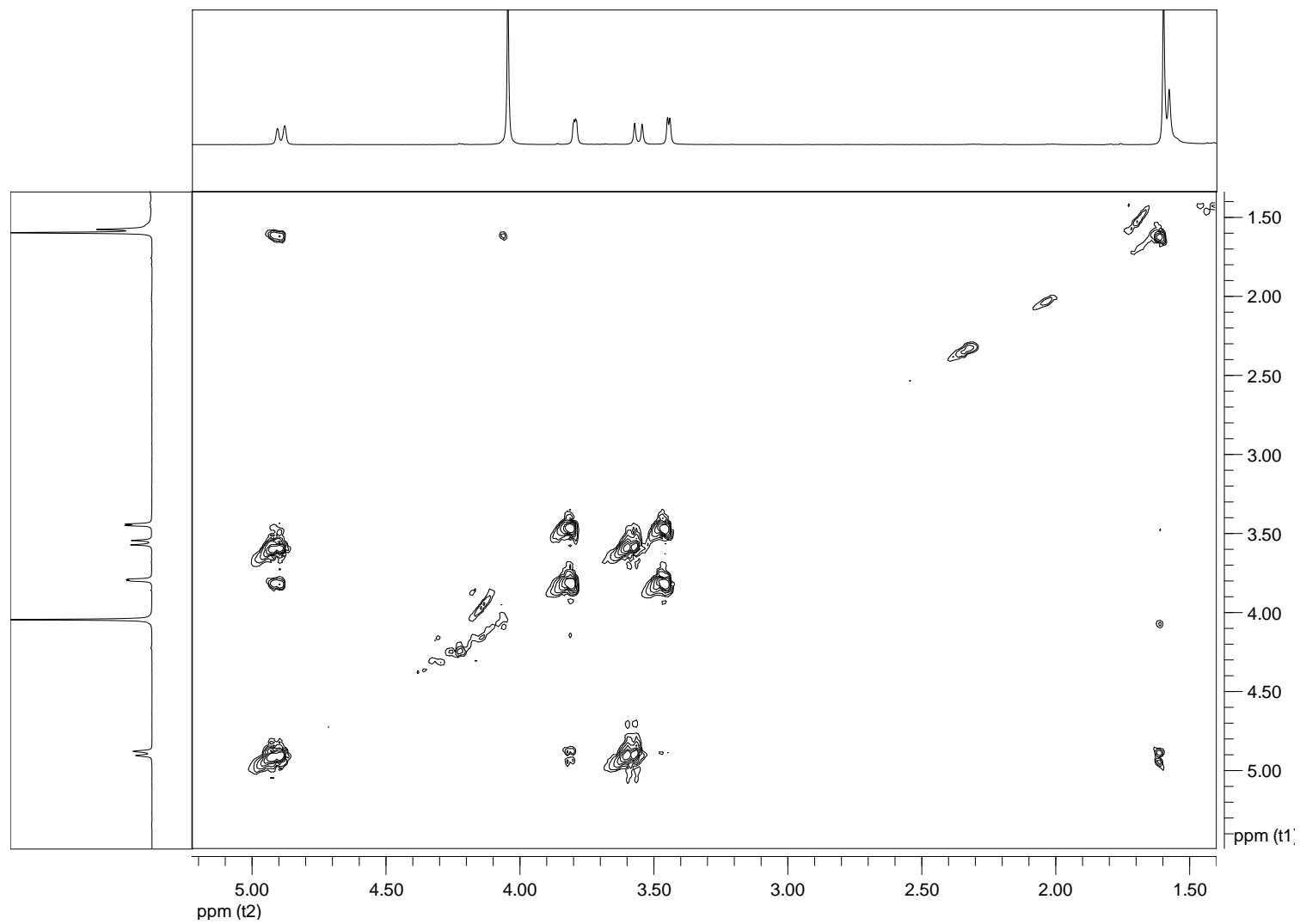
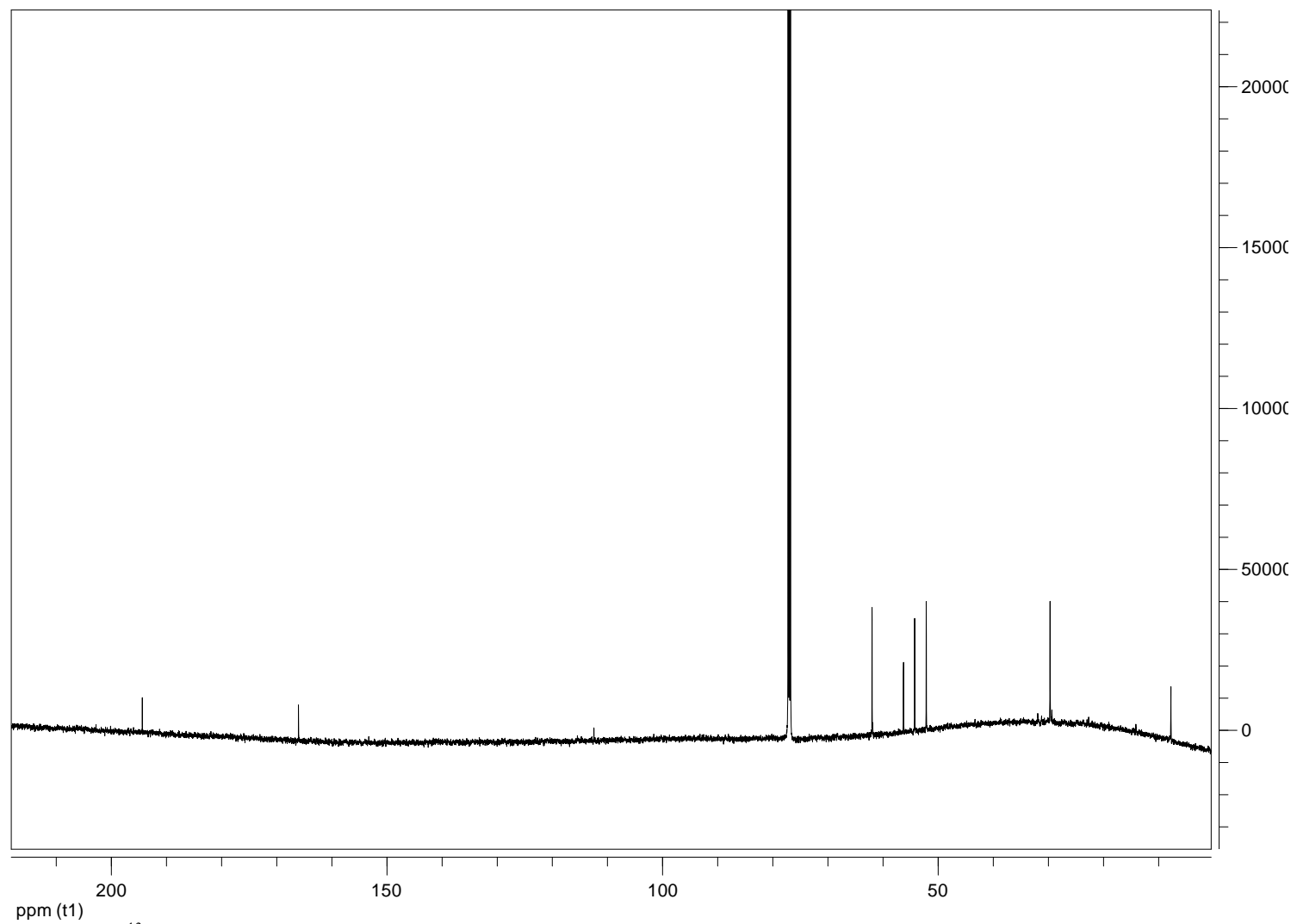


Figure 17. COSY spectrum of cyclobutryoxide (**1**) recorded in CDCl_3 at 400 MHz.



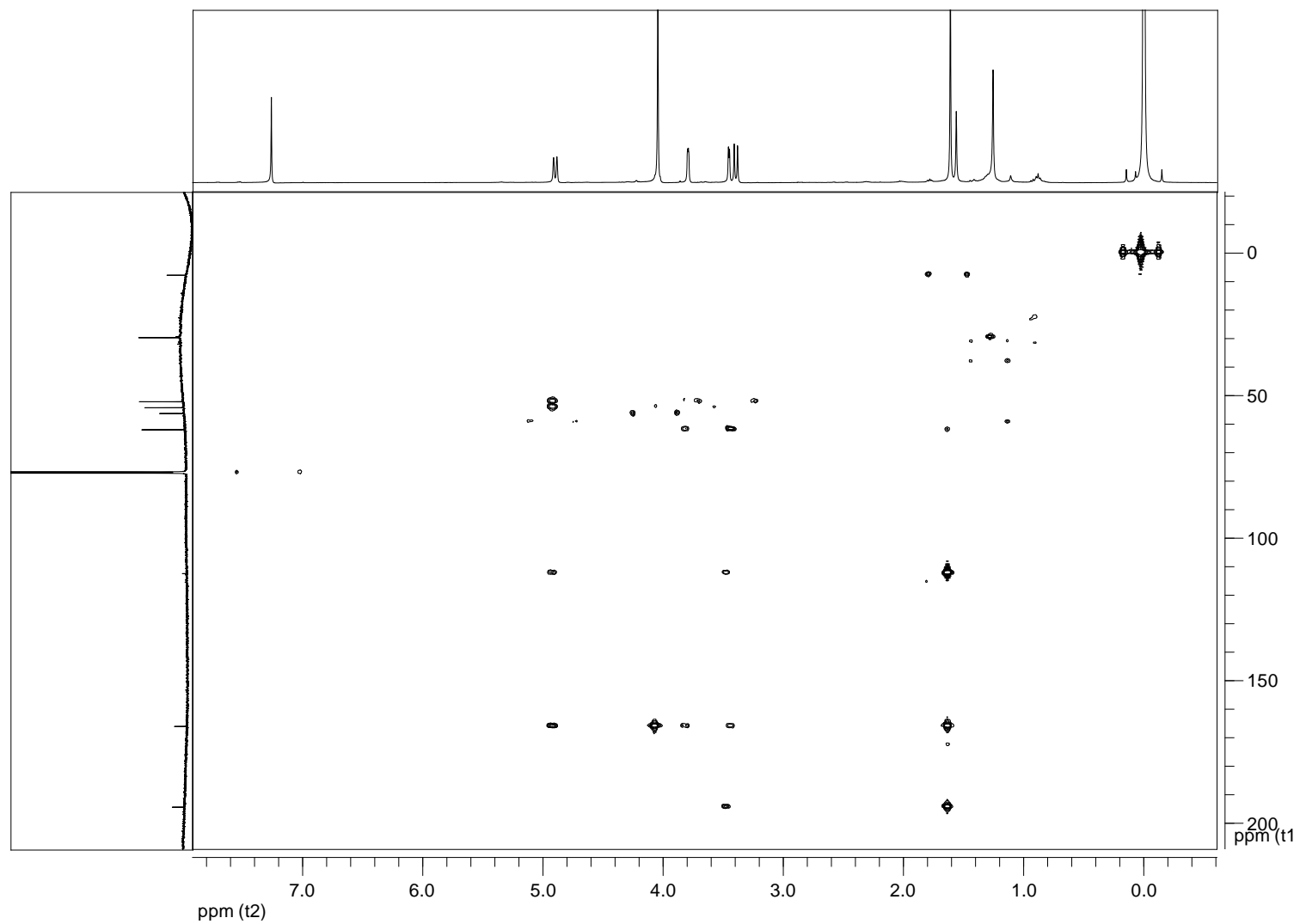


Figure 19. HMBC spectrum of cyclobutryoxide (1) recorded in CDCl₃ at 400 MHz.

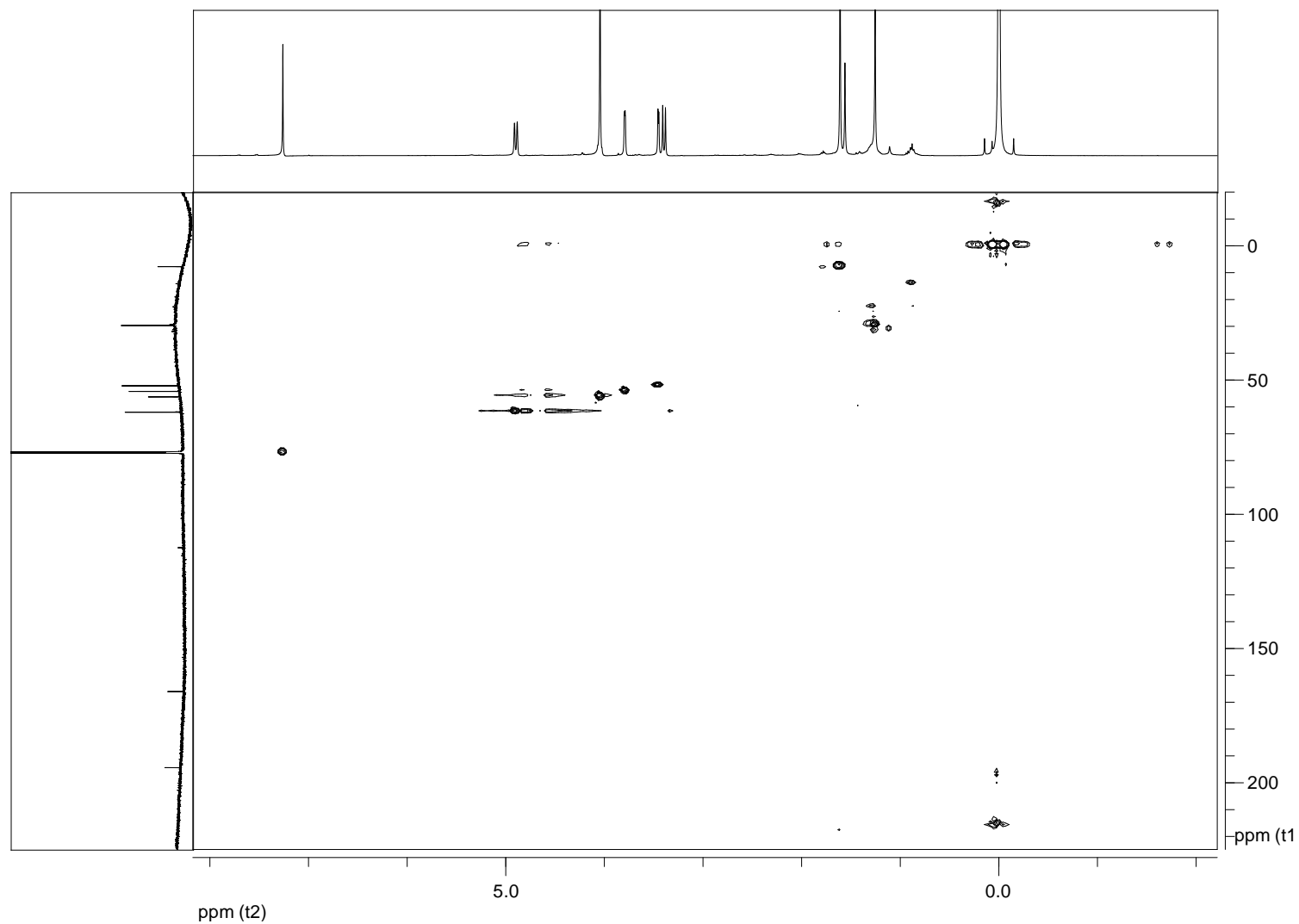


Figure 20. HSQC spectrum of cyclobutryoxide (**1**) recorded in CDCl₃ at 400 MHz.

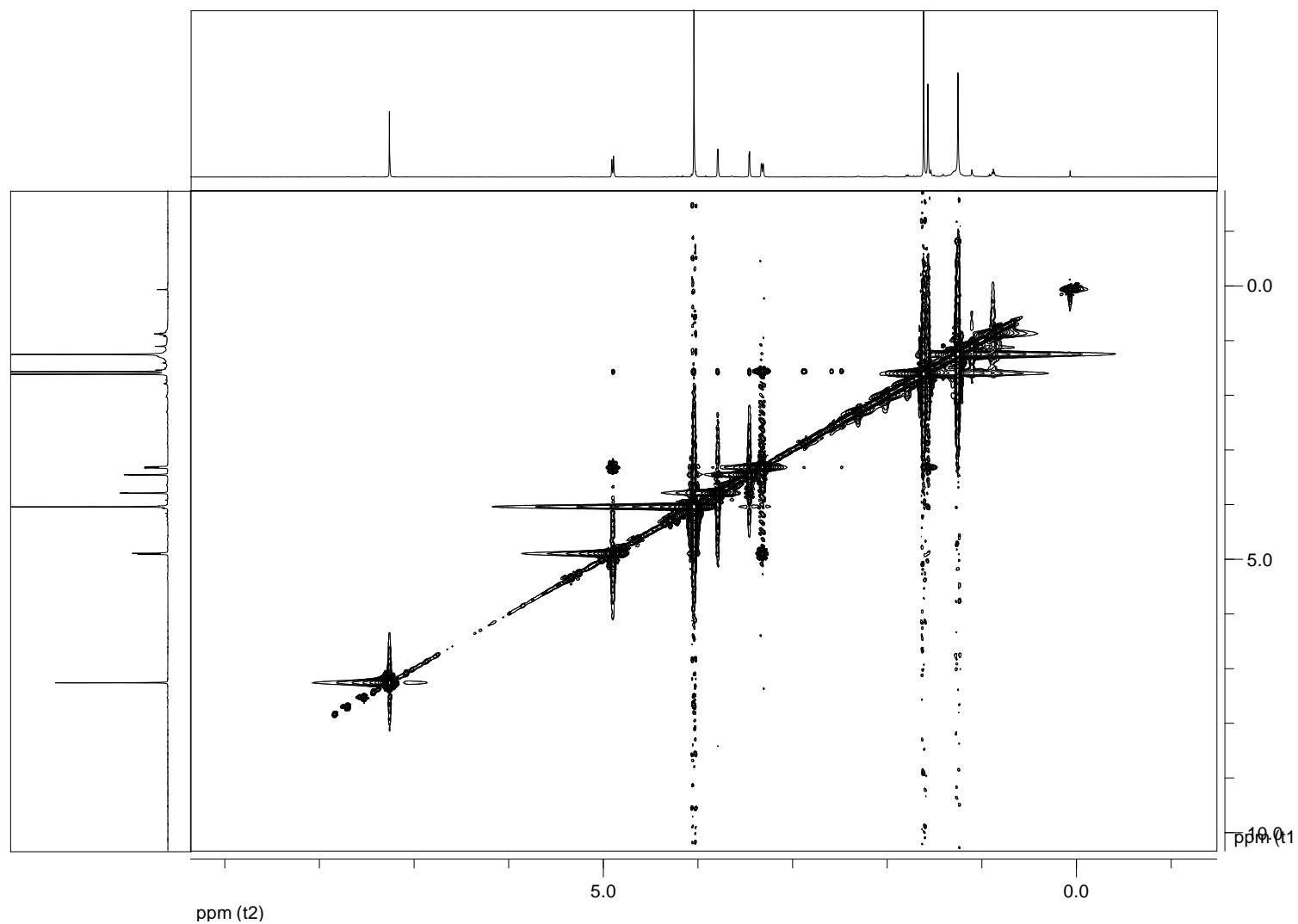
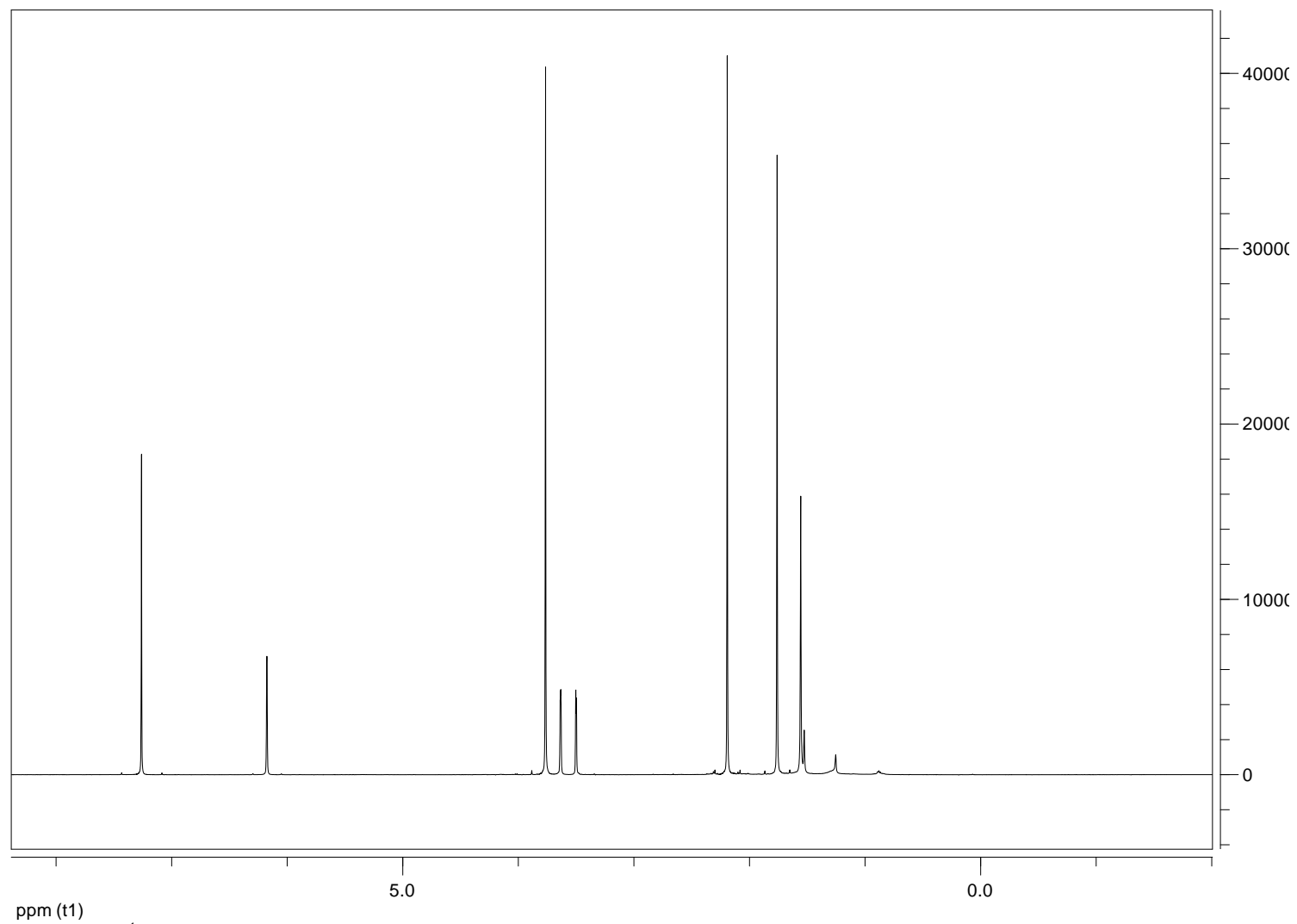


Figure 21. NOESY spectrum of cyclobutryoxide (**1**) recorded in CDCl_3 at 400 MHz.



ppm (t1)
Figure 23. ^1H NMR spectrum of 5-*O*-acetyl cyclobutryoxide (**2**) recorded in CDCl_3 at 400 MHz.

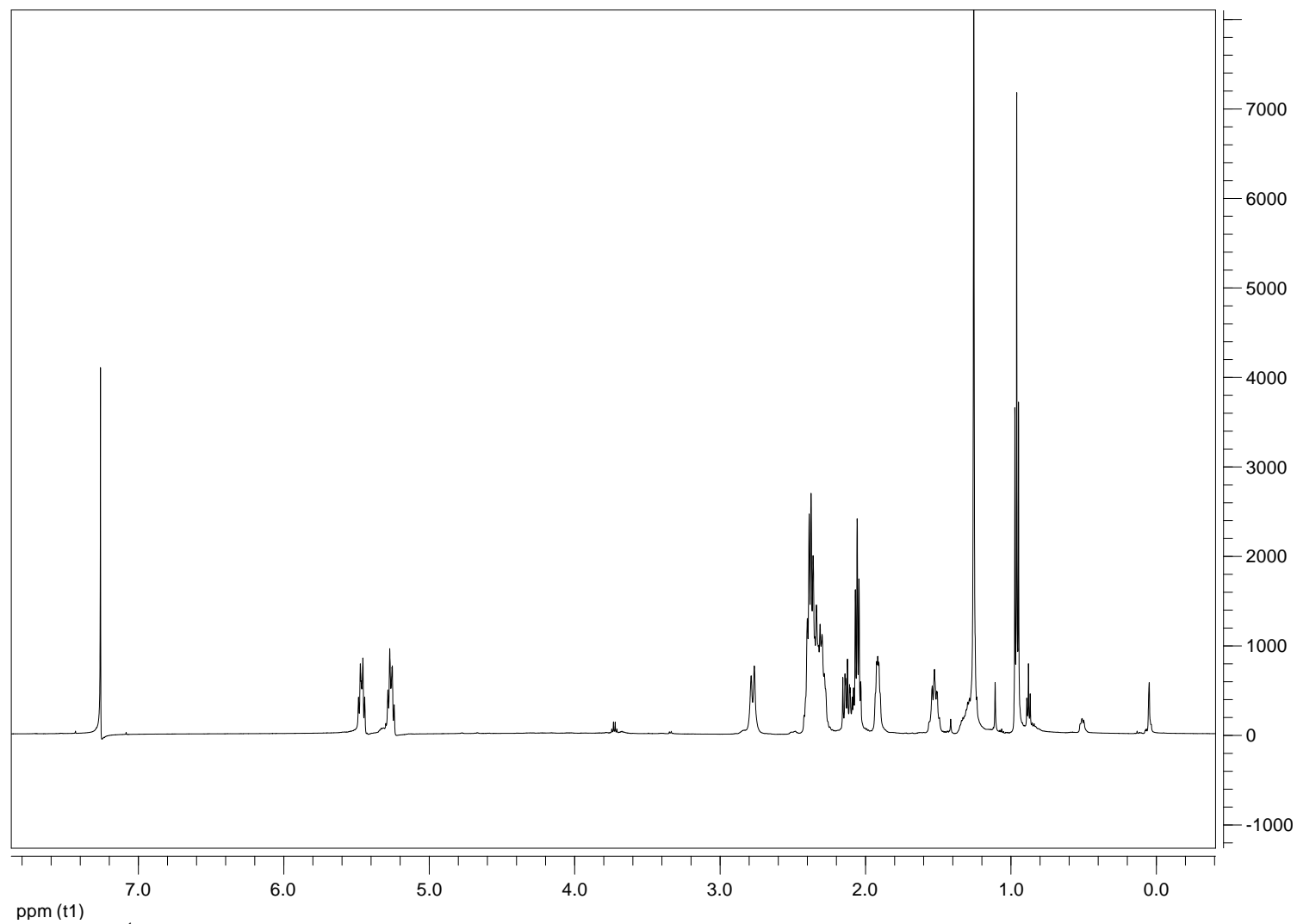


Figure 26. ^1H NMR spectrum of (1*R*,2*R*)-jasmonic acid (**10**) recorded in CDCl_3 at 400 MHz.

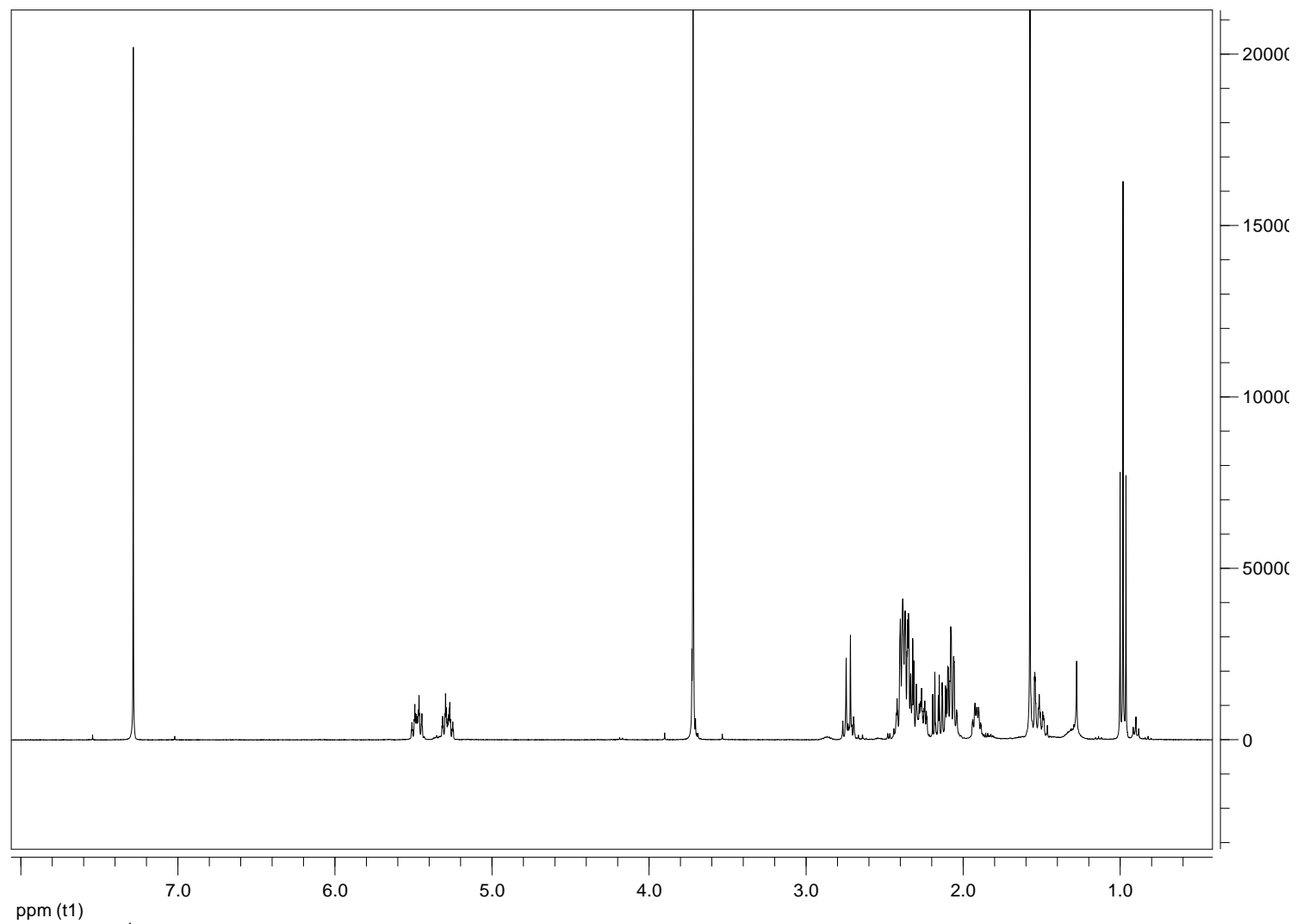


Figure 27. ^1H NMR spectrum of (1*R*,2*R*)-methyl jasmonate (**11**) recorded in CDCl_3 at 400 MHz.

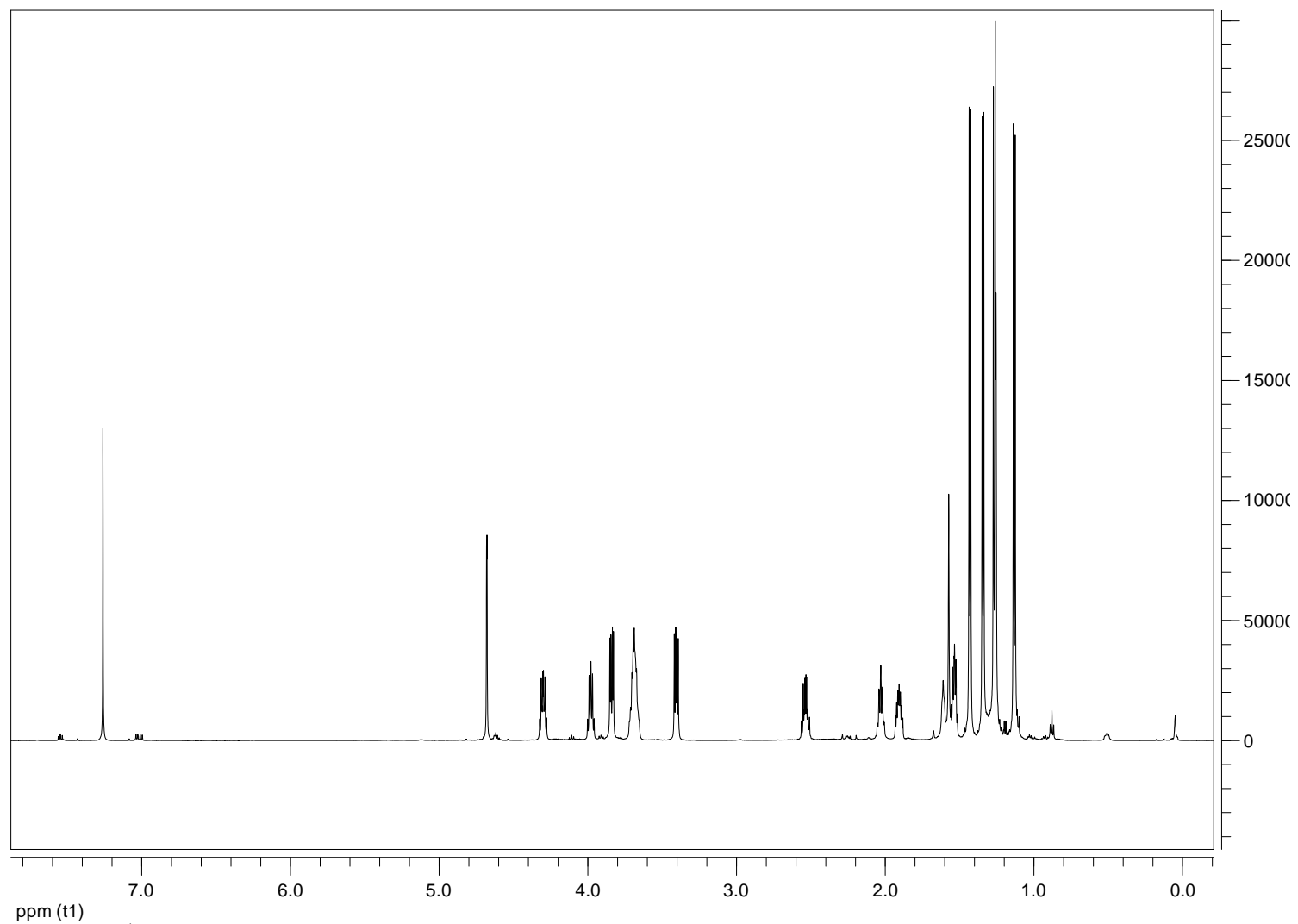


Figure 28. ¹H NMR spectrum of botryosphaerilactone A (**12**) recorded in CDCl₃ at 400 MHz.

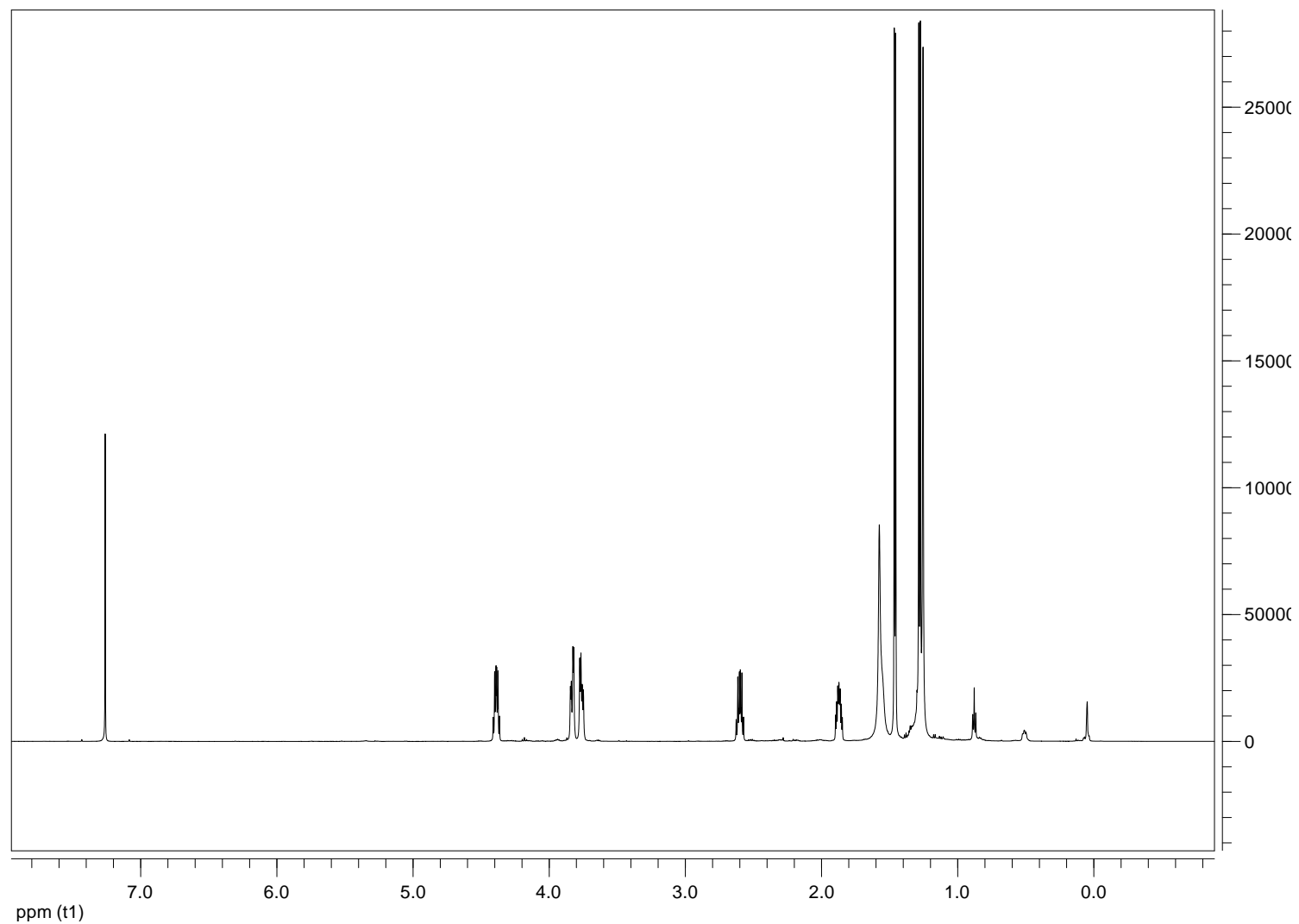


Figure 29. ¹H NMR spectrum of (3*S*,4*R*,5*R*)-4-hydroxymethyl-3,5-dimethyl-2-furanone (**13**) recorded in CDCl₃ at 400 MHz.

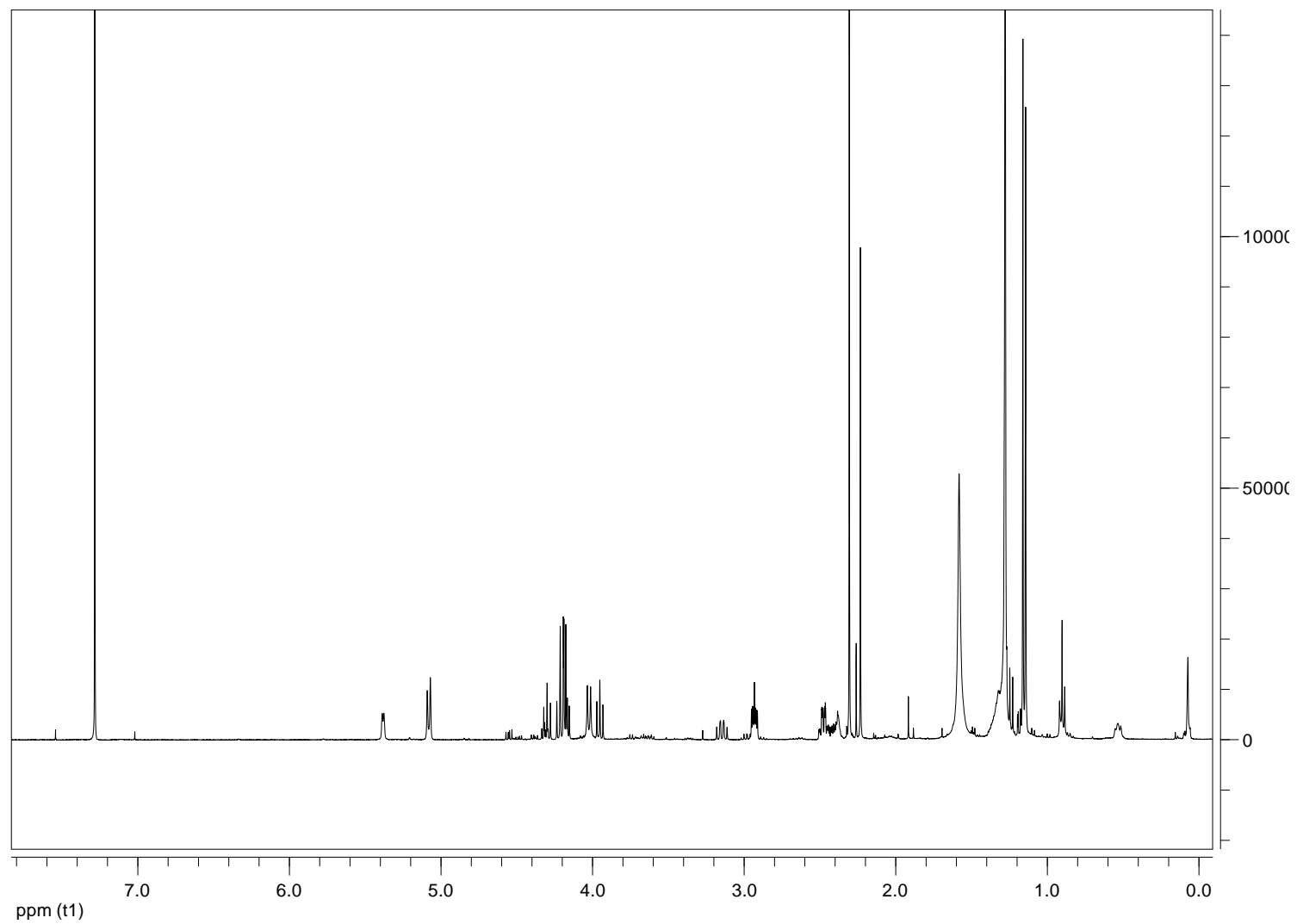


Figure 30. ¹H NMR spectrum of (3R,4S)-botryodiplodin (**14**) recorded in CDCl₃ at 400 MHz.

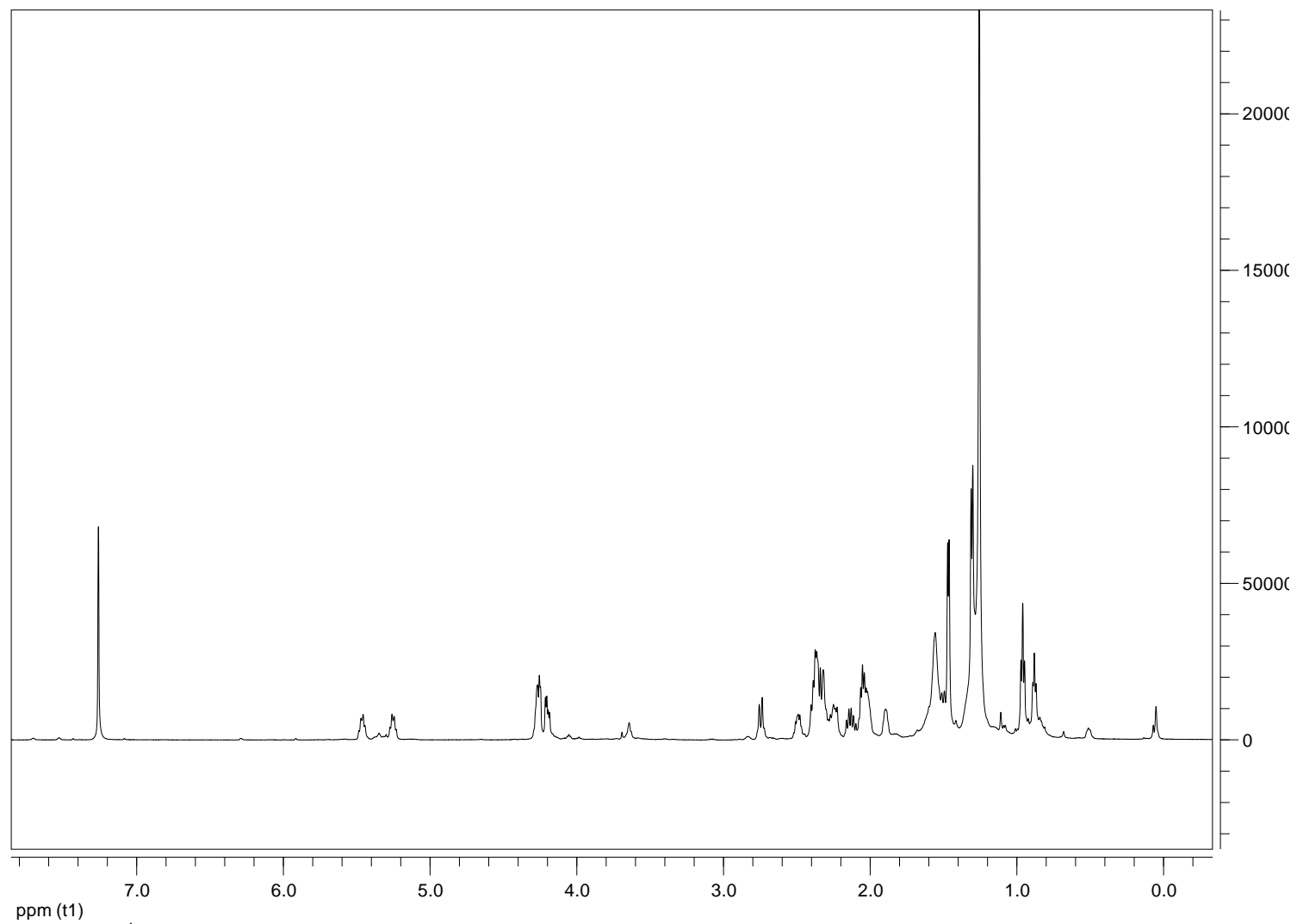


Figure 31. ¹H NMR spectrum of lasiojasmonate A (5) recorded in CDCl₃ at 400 MHz.

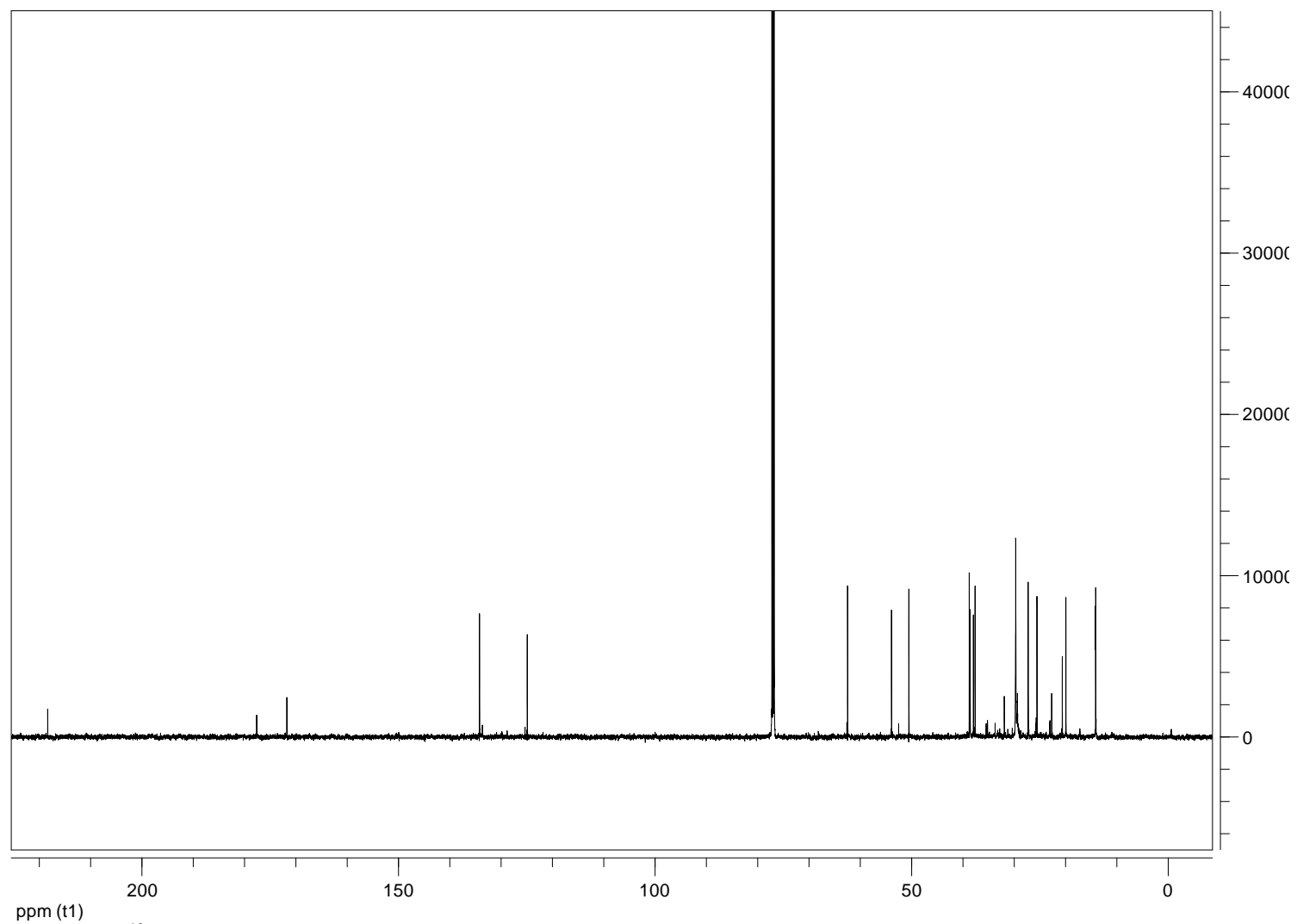


Figure 32. ^{13}C NMR spectrum of lasiojasmonate A (5) recorded in CDCl_3 at 100 MHz.

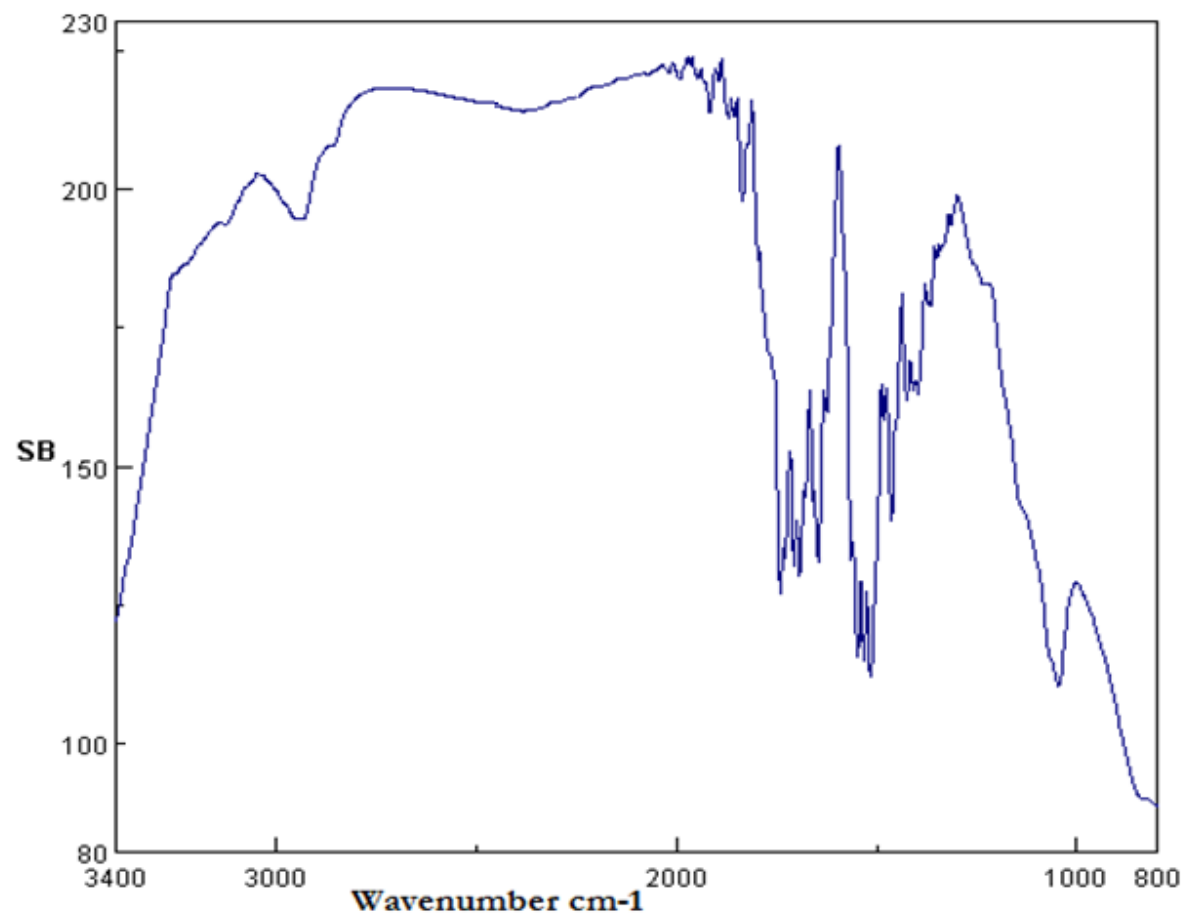


Figure 33. IR spectrum of lasiojasmonate A (5) recorded as glassy film.

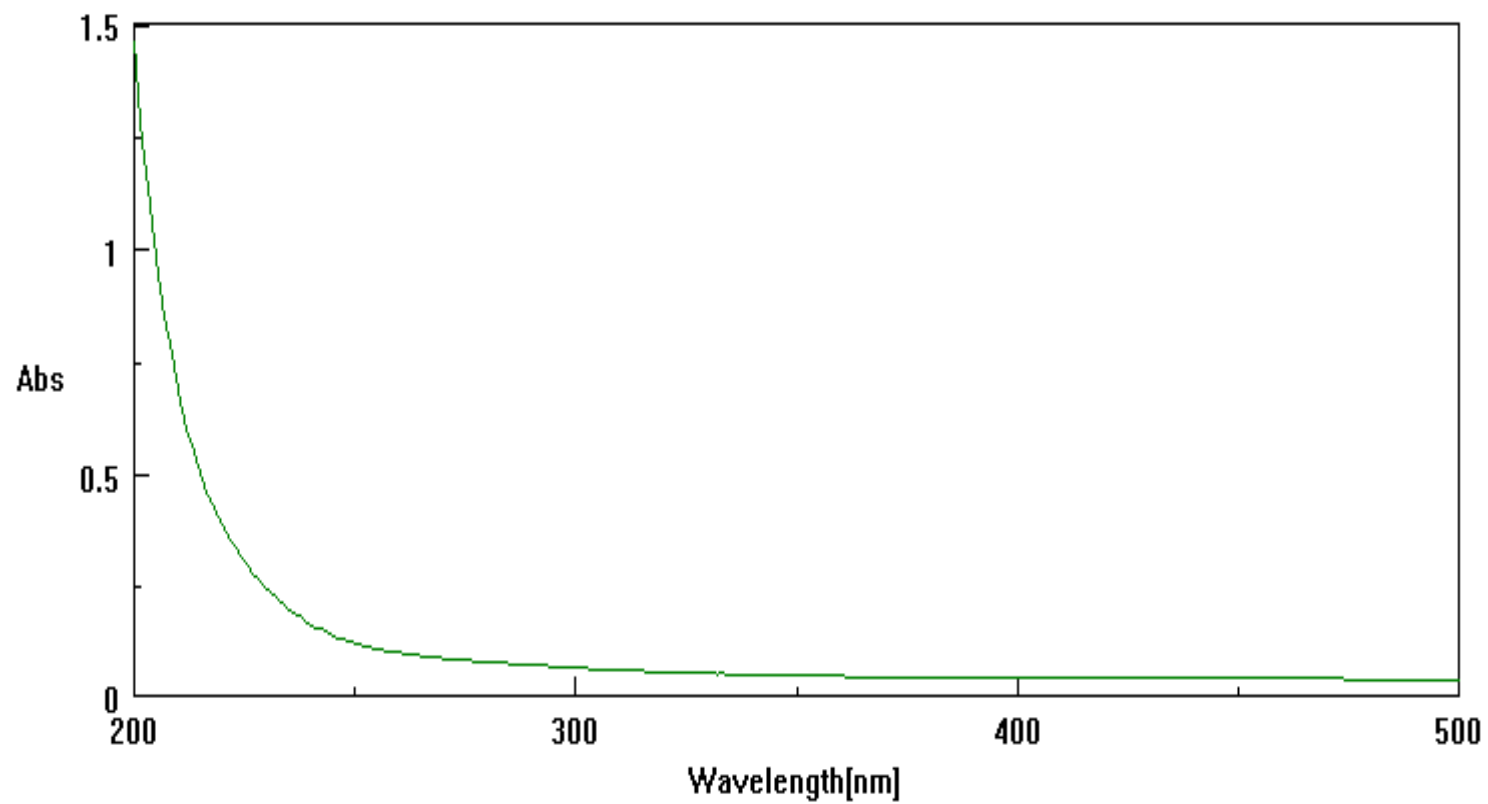


Figure 34. UV spectrum of lasiojasmonate A (5) recorded in MeCN.

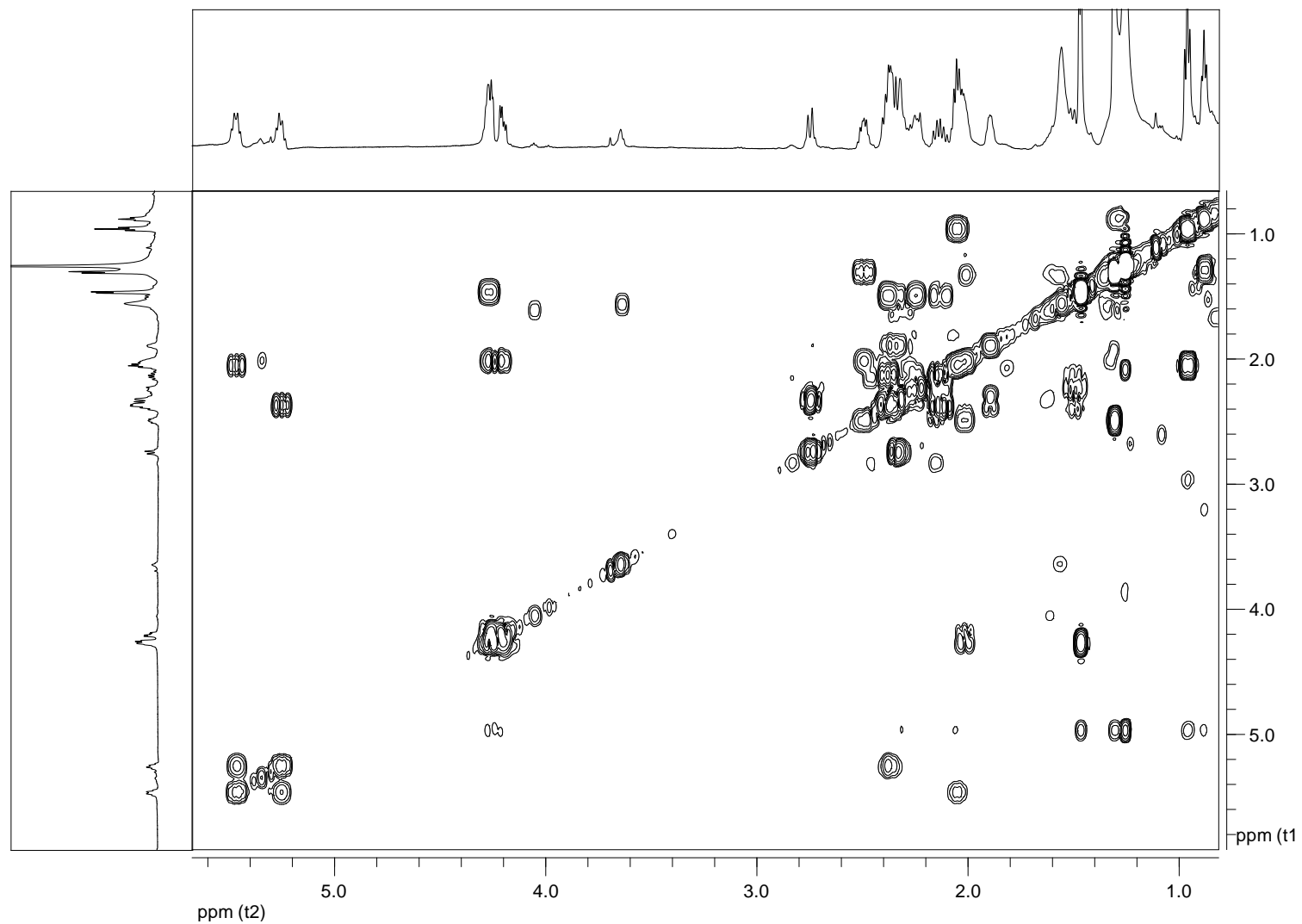
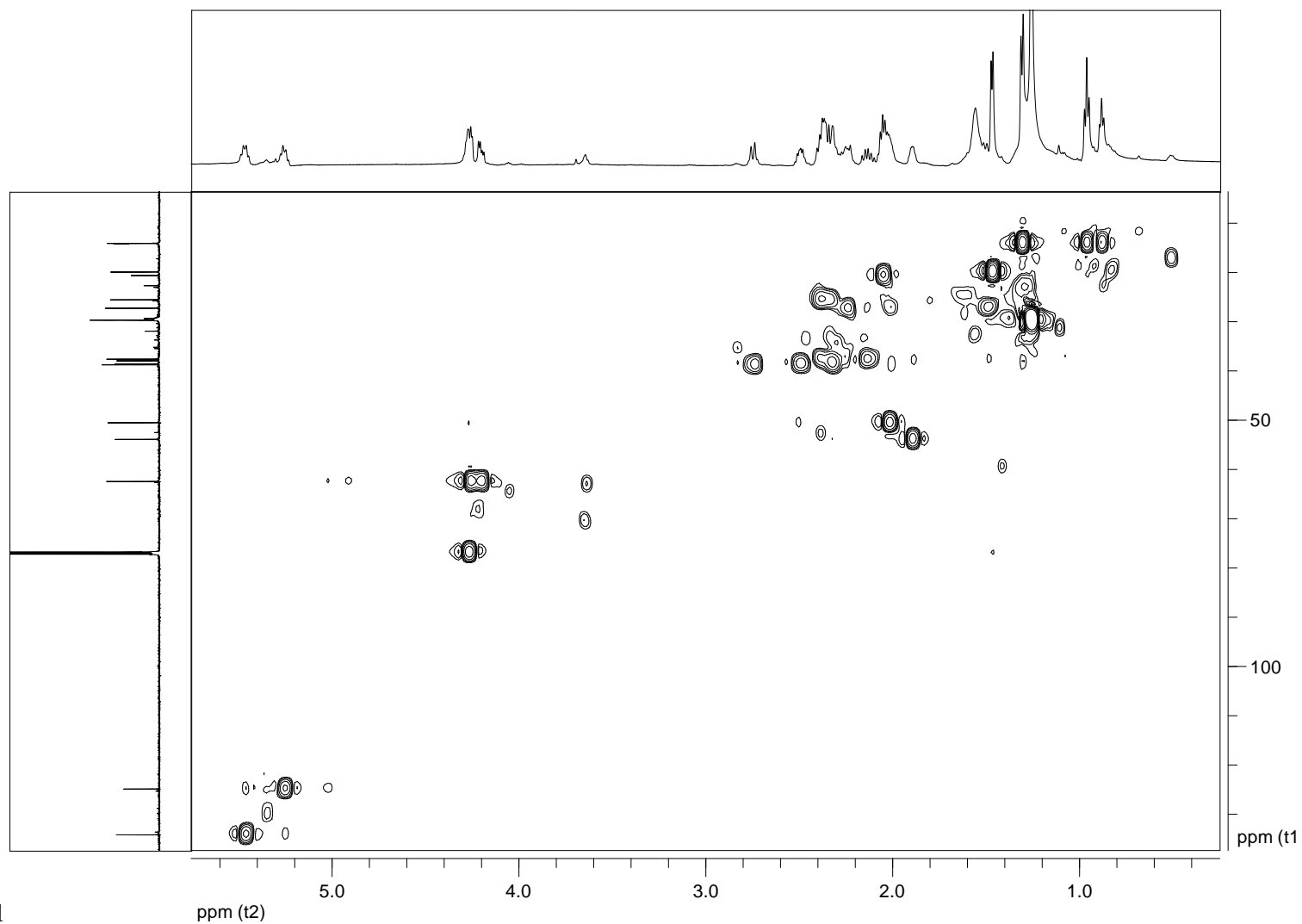


Figure 35. COSY spectrum of lasiojasmonate A (**5**) recorded in CDCl_3 at 400 MHz.



1

Figure 36. HSQC spectrum of lasiojasmonate A (**5**) recorded in CDCl₃ at 400 MHz.

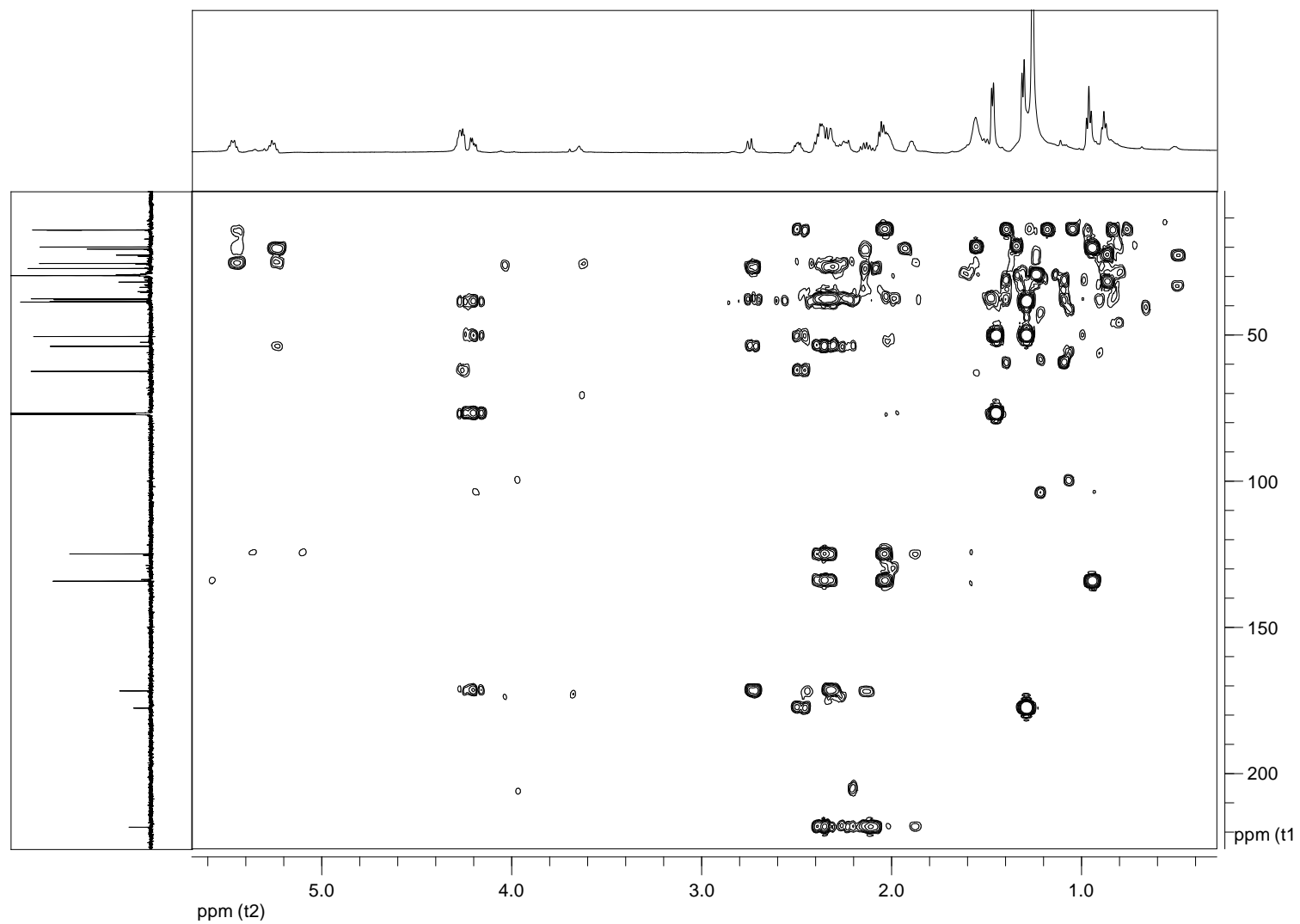


Figure 37. HMBC spectrum of lasiojasmonate A (5) recorded in CDCl₃ at 400 MHz.

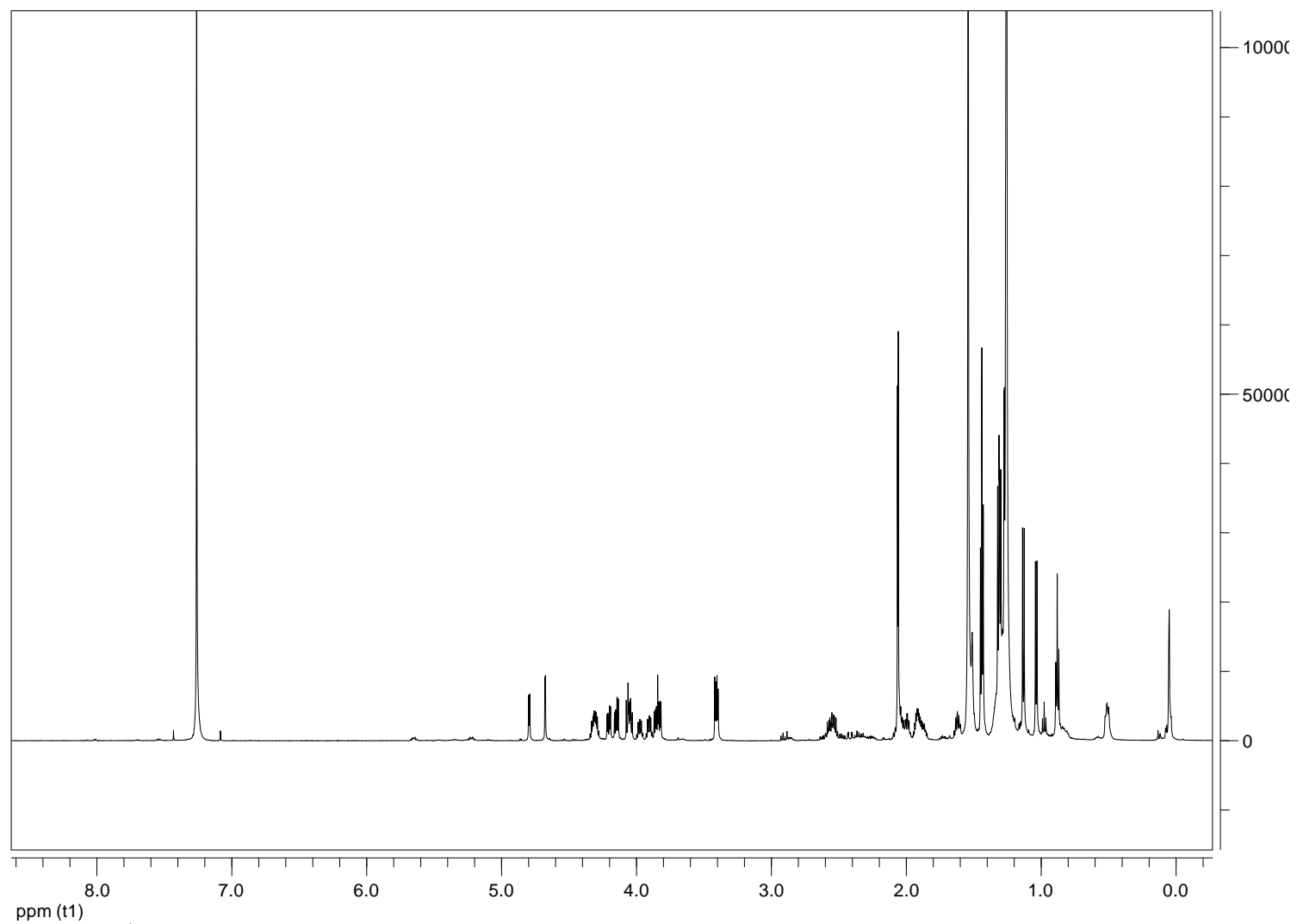


Figure 38. ¹H NMR spectrum of 16-*O*-acetylbotryosphaerilactone A and C (**6** and **7**) recorded in CDCl₃ at 400 MHz.

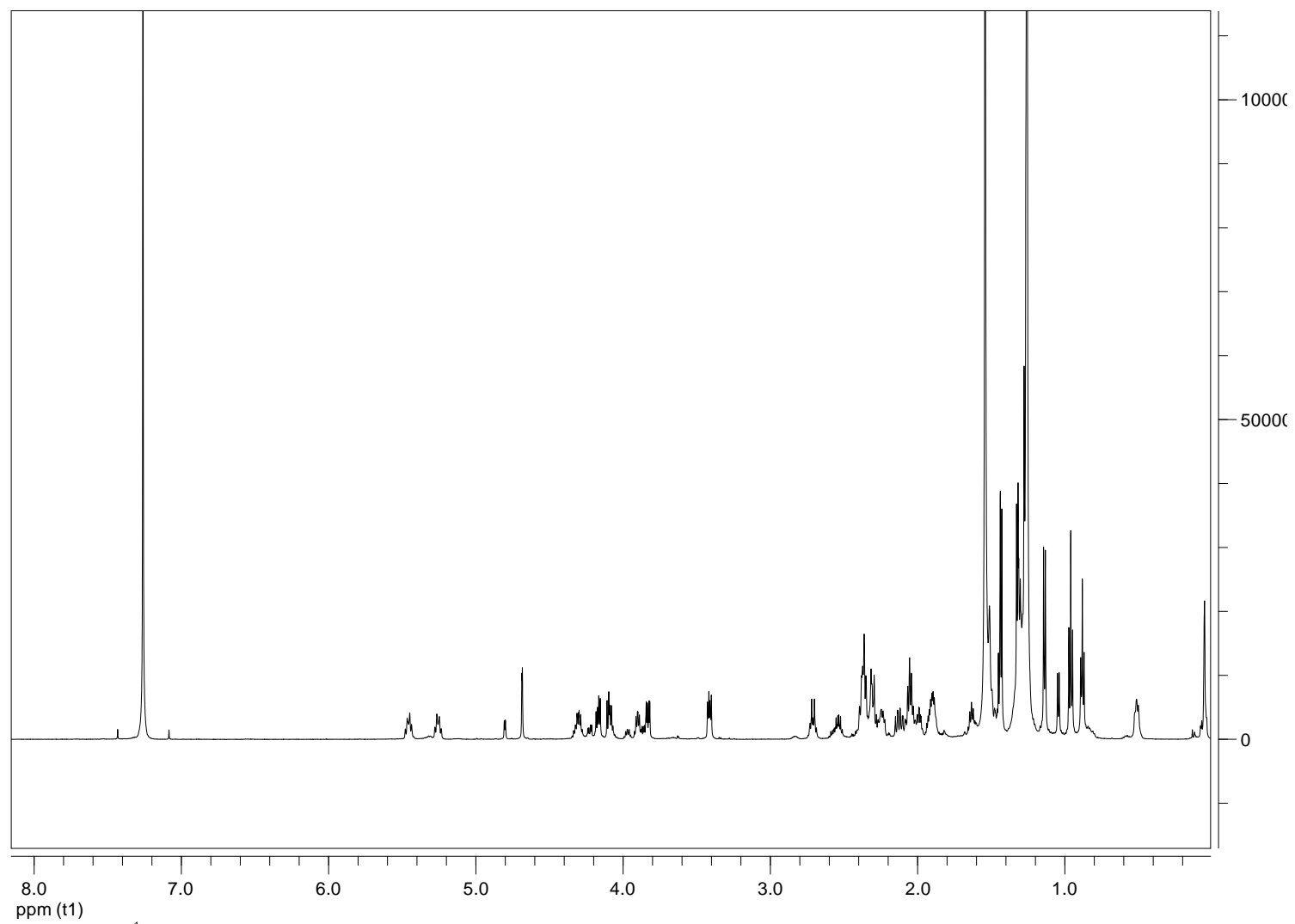


Figure 40. ^1H NMR spectrum of lasiojasmonates B and C (**8** and **9**) recorded in CDCl_3 at 400 MHz.

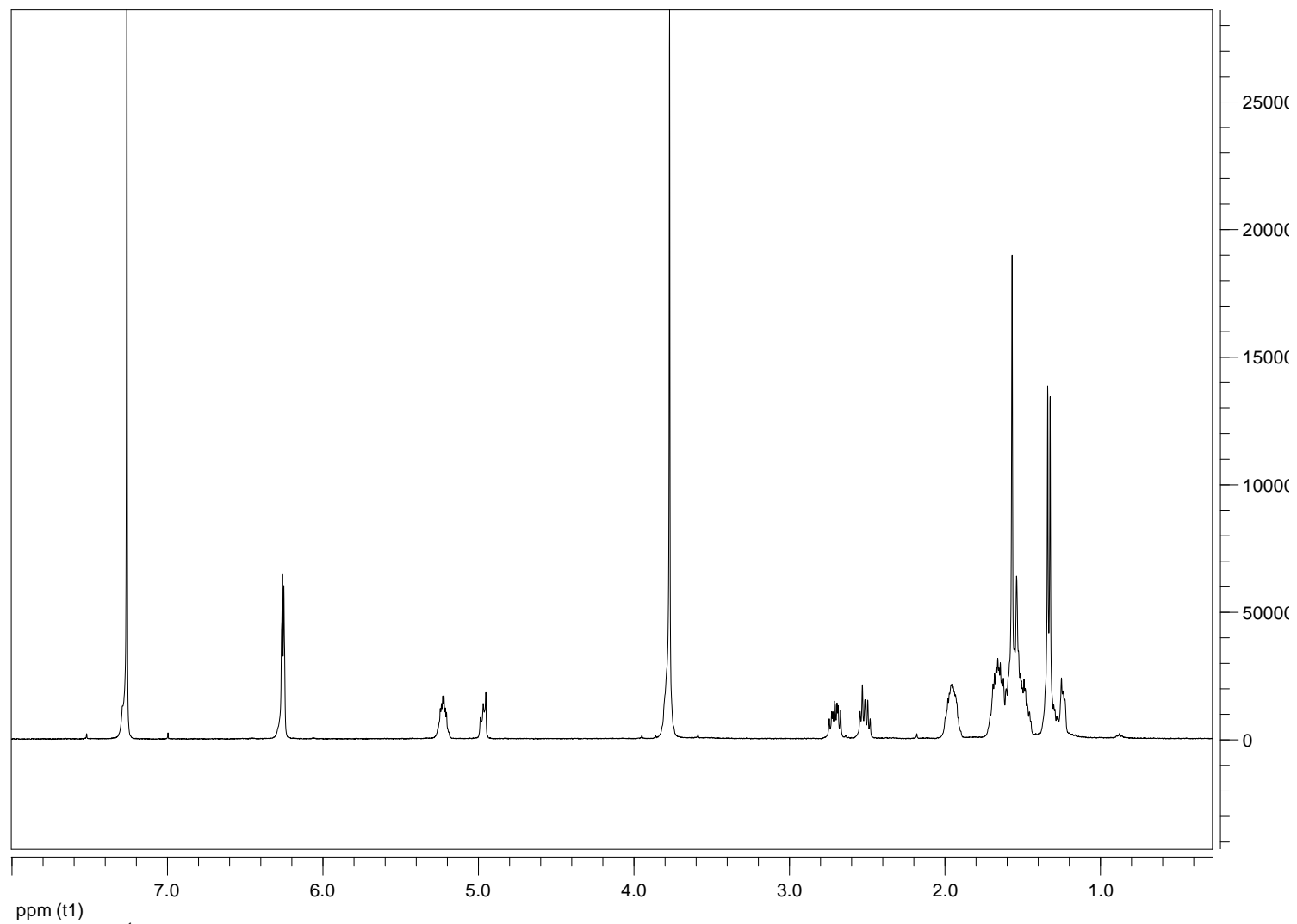


Figure 42. ^1H NMR spectrum of botryosphaeriodiplodin (17) recorded in CDCl_3 at 400 MHz.

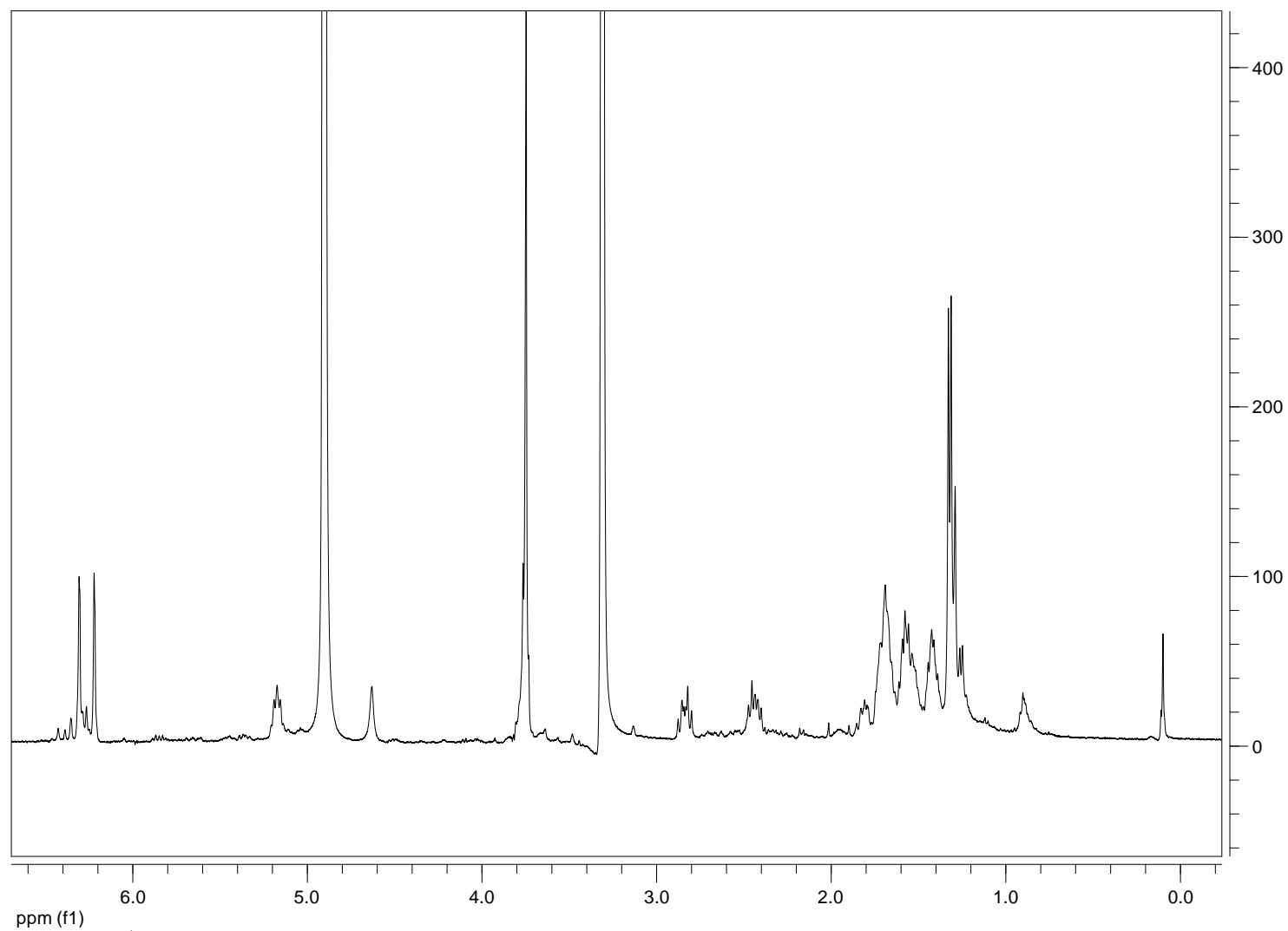


Figure 43. ¹H NMR spectrum of (5R)-5-hydroxylasiiodiplodin (**18**) recorded in MeOD at 400 MHz.

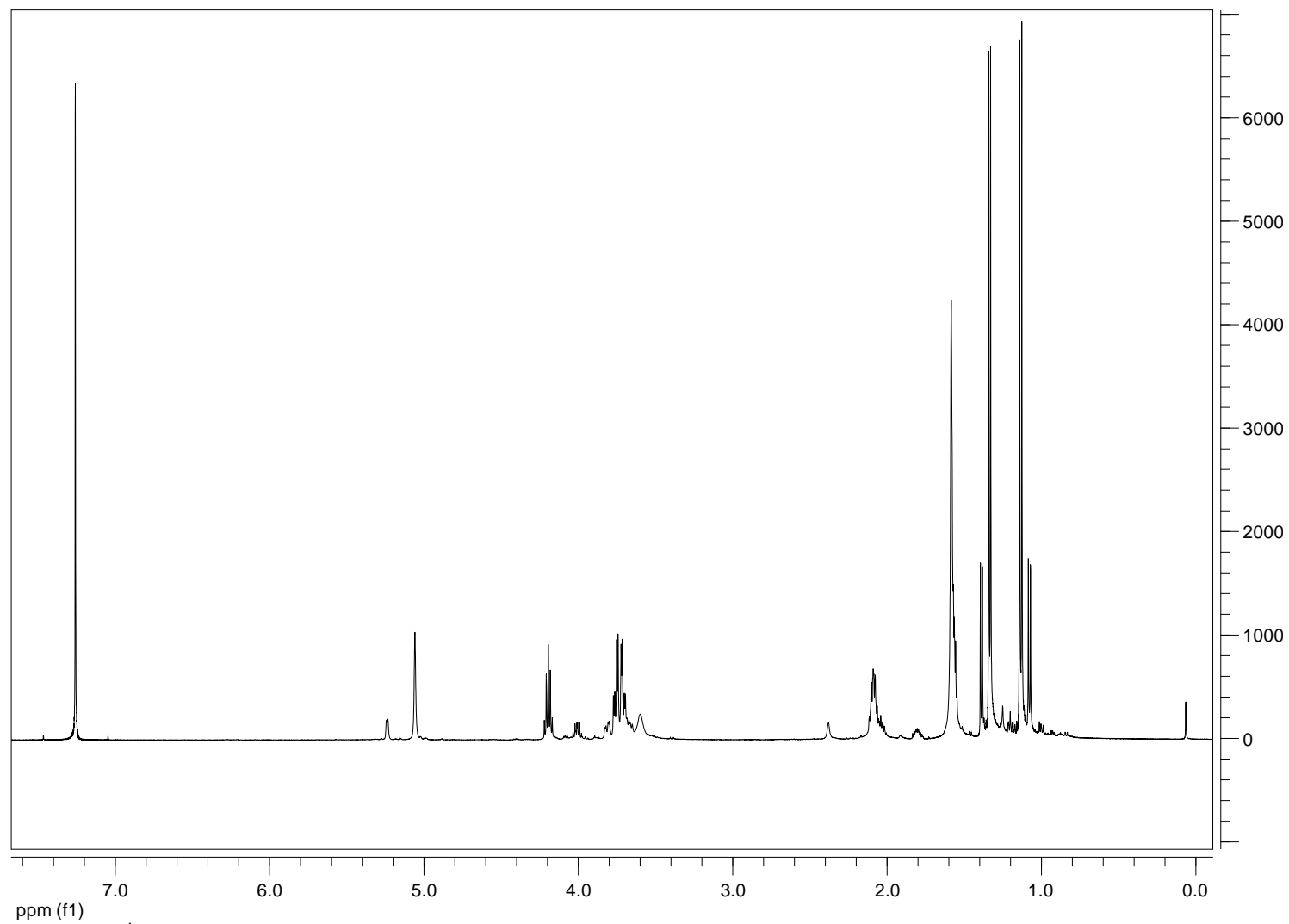
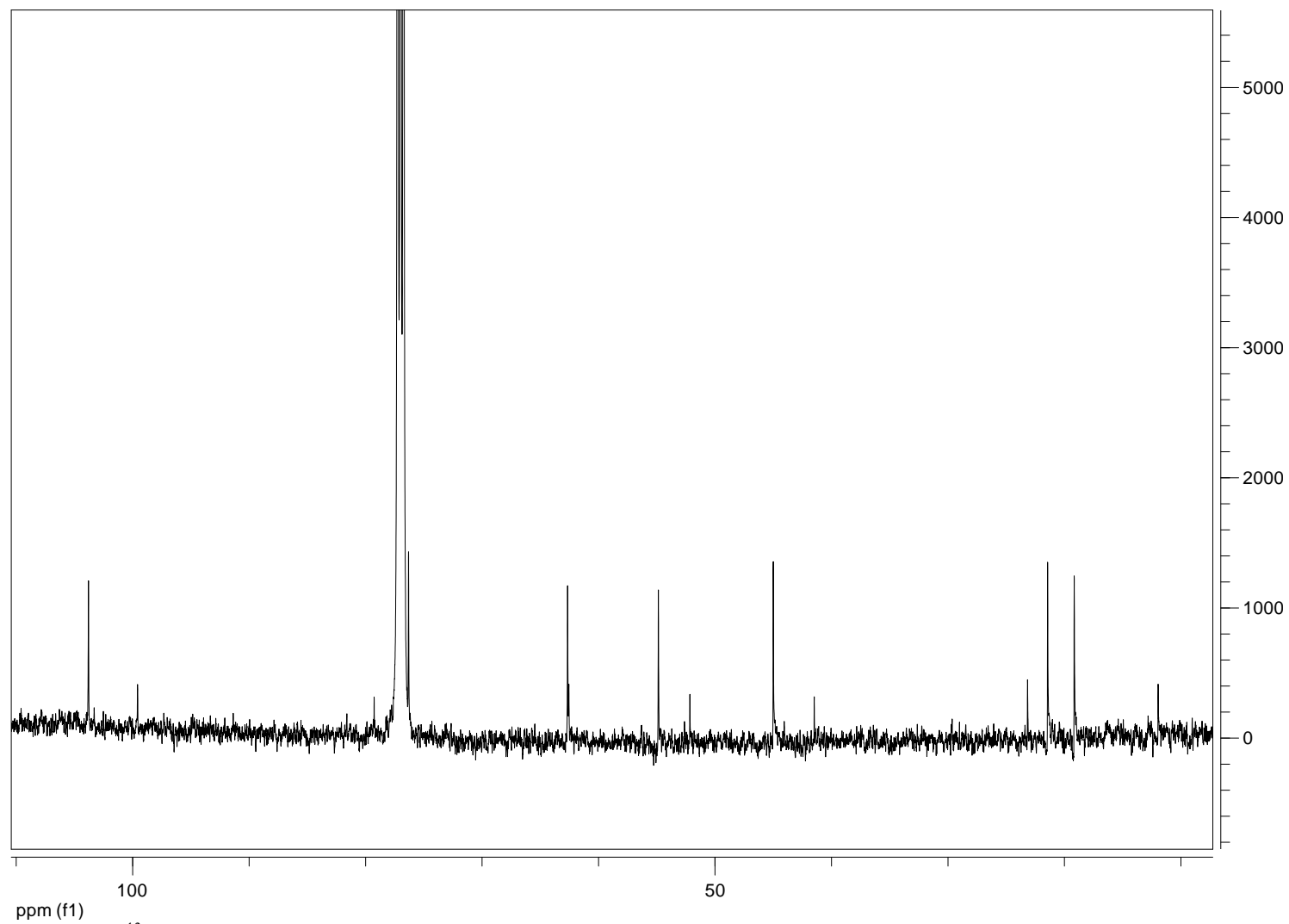


Figure 44. ¹H NMR spectrum of lasiolactols A and B (**15** and **16**) recorded in CDCl₃ at 400 MHz.



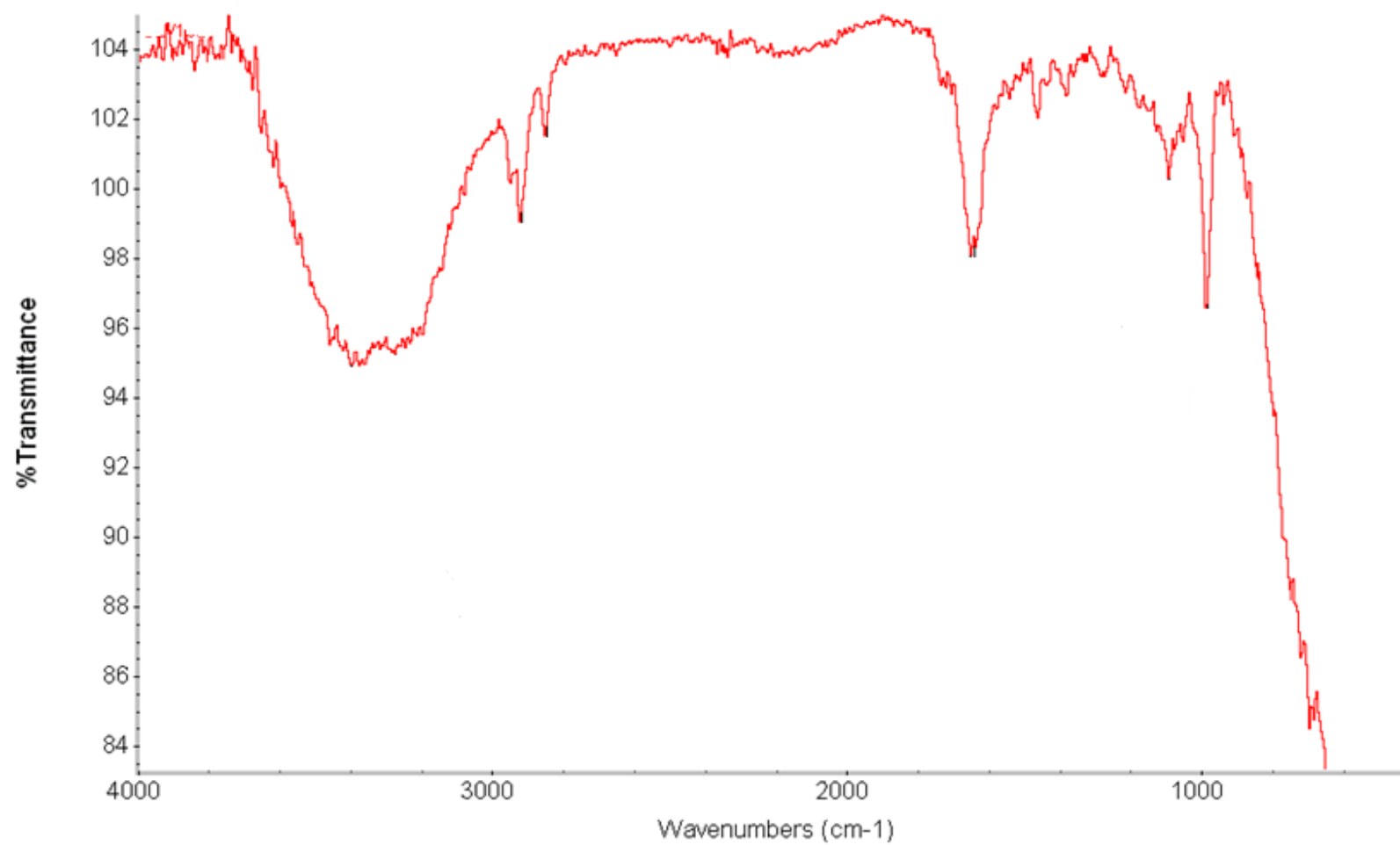


Figure 46. IR spectrum of lasiolactols A and B (**15** and **16**) recorded as glassy film.

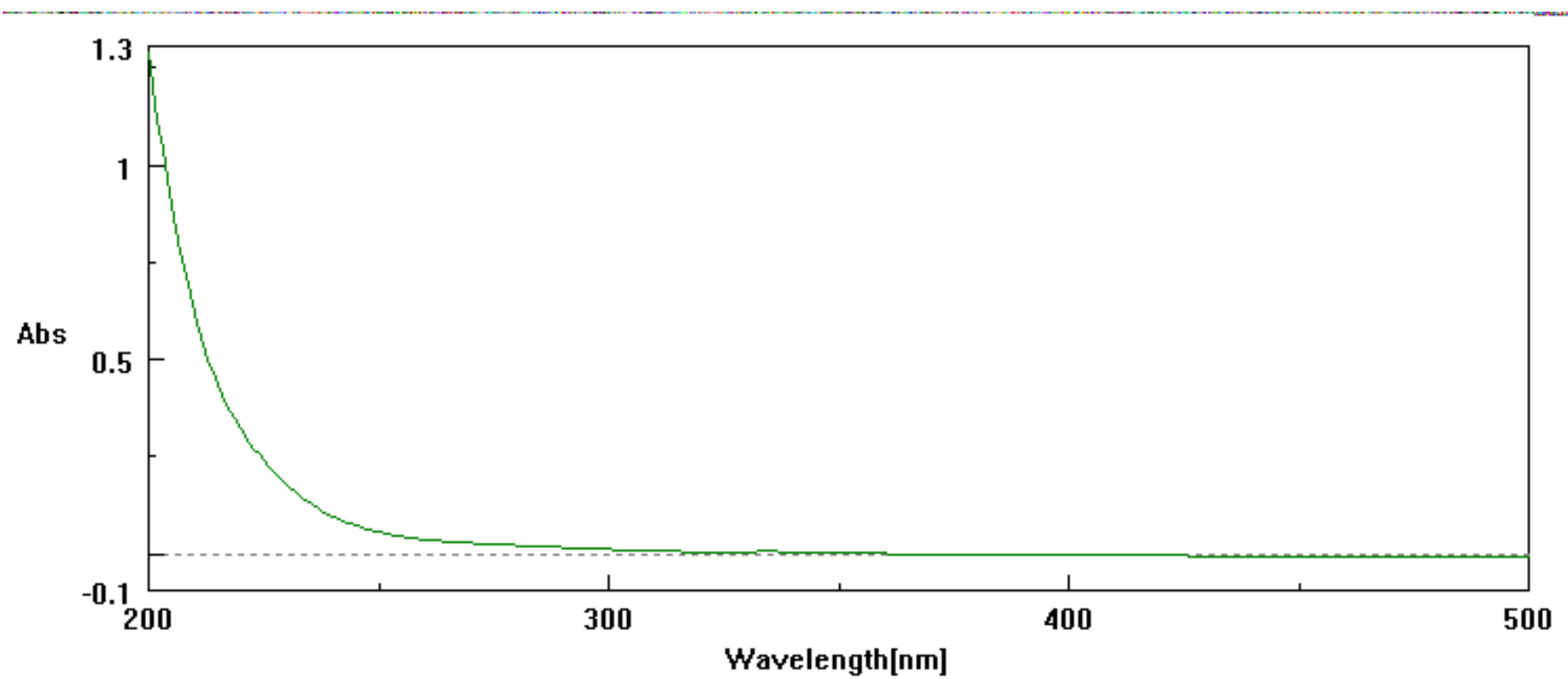


Figure 47. UV spectrum of lasiolactols A and B (15 and 16) recorded in MeCN.

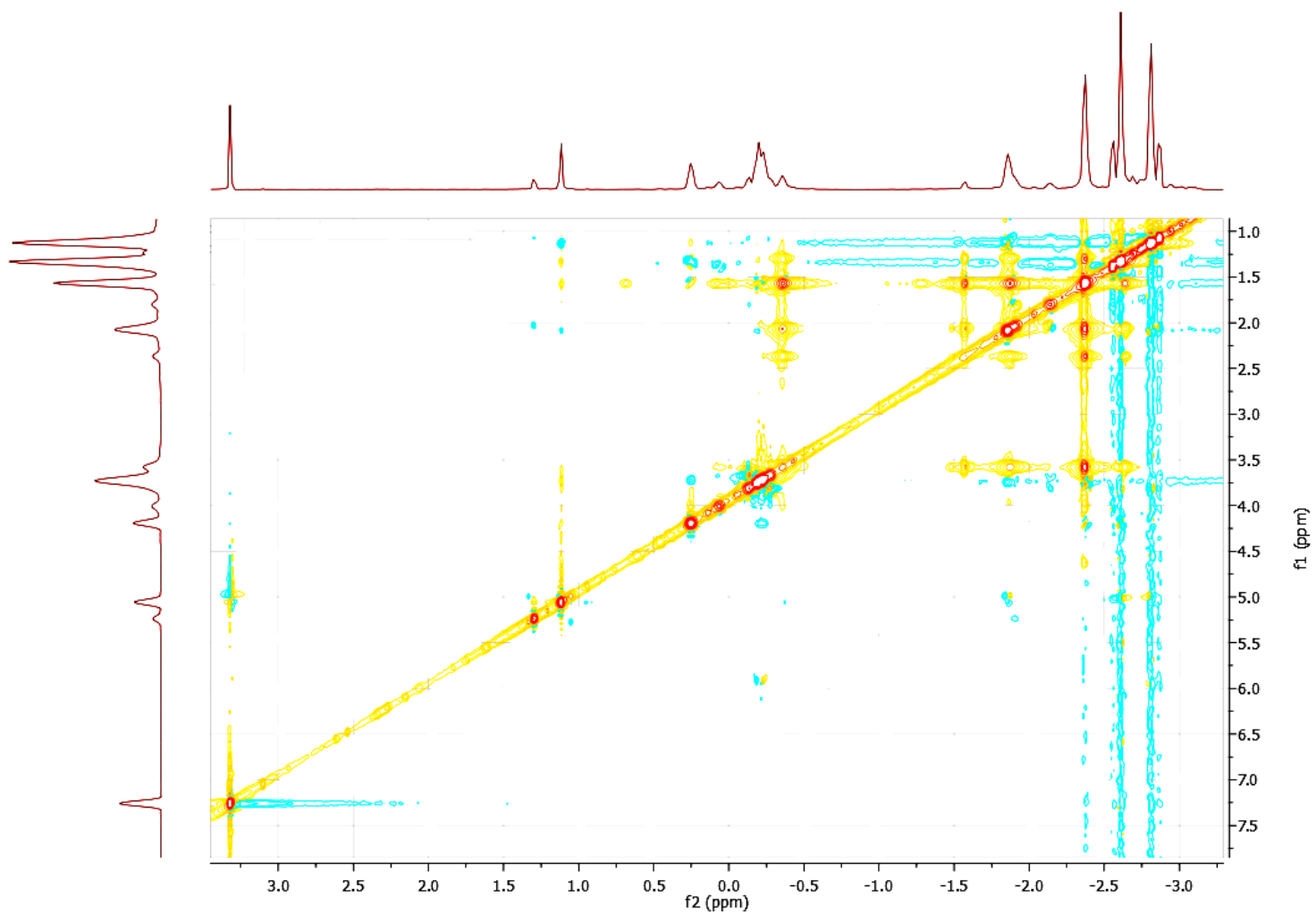


Figure 49. NOESY spectrum of lasiolactols A and B (**15** and **16**) recorded in CDCl₃ at 400 MHz.

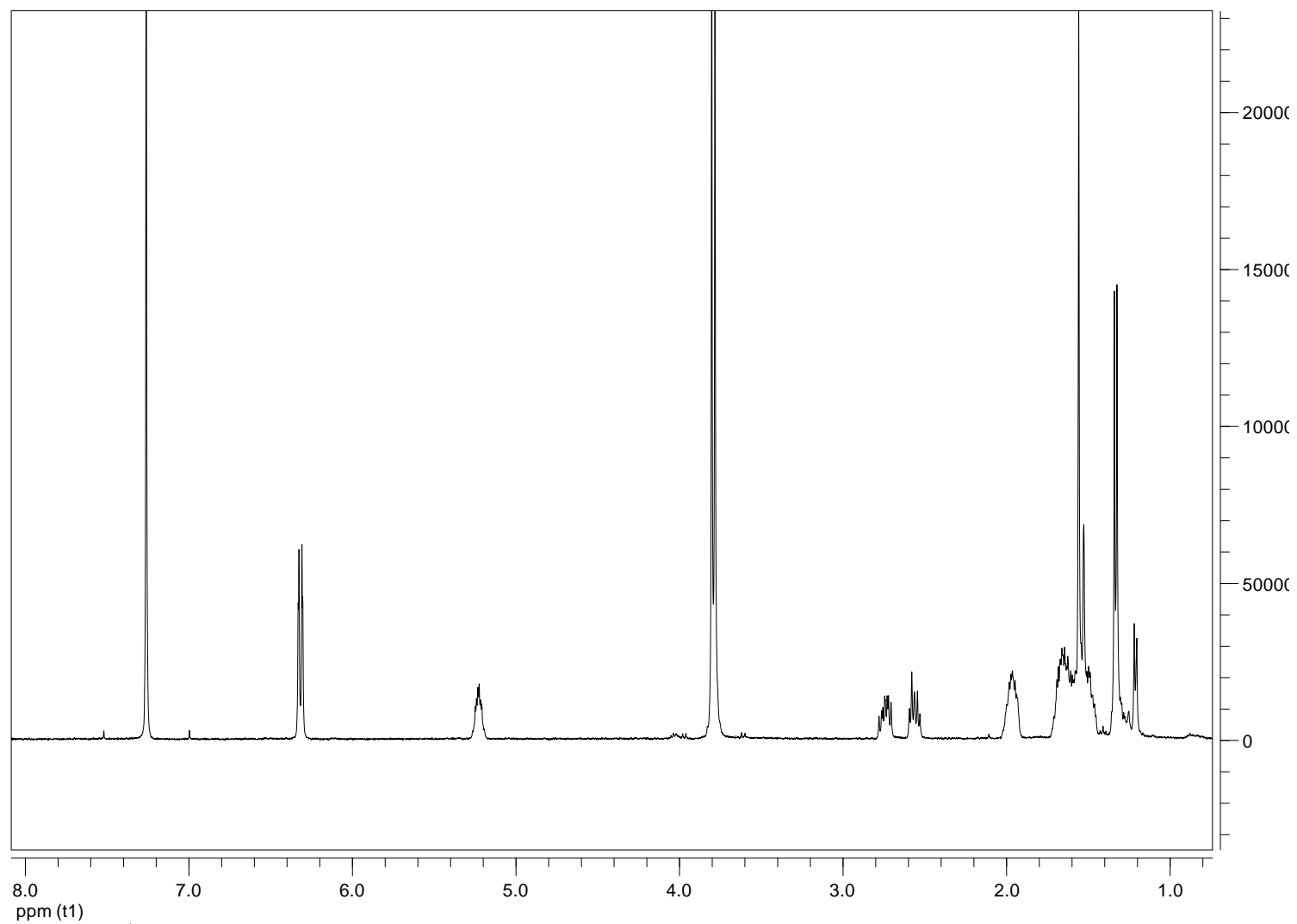


Figure 50. ¹H NMR spectrum of 13-O-methylbotryosphaerioidin (**19**) recorded in CDCl₃ at 400 MHz.

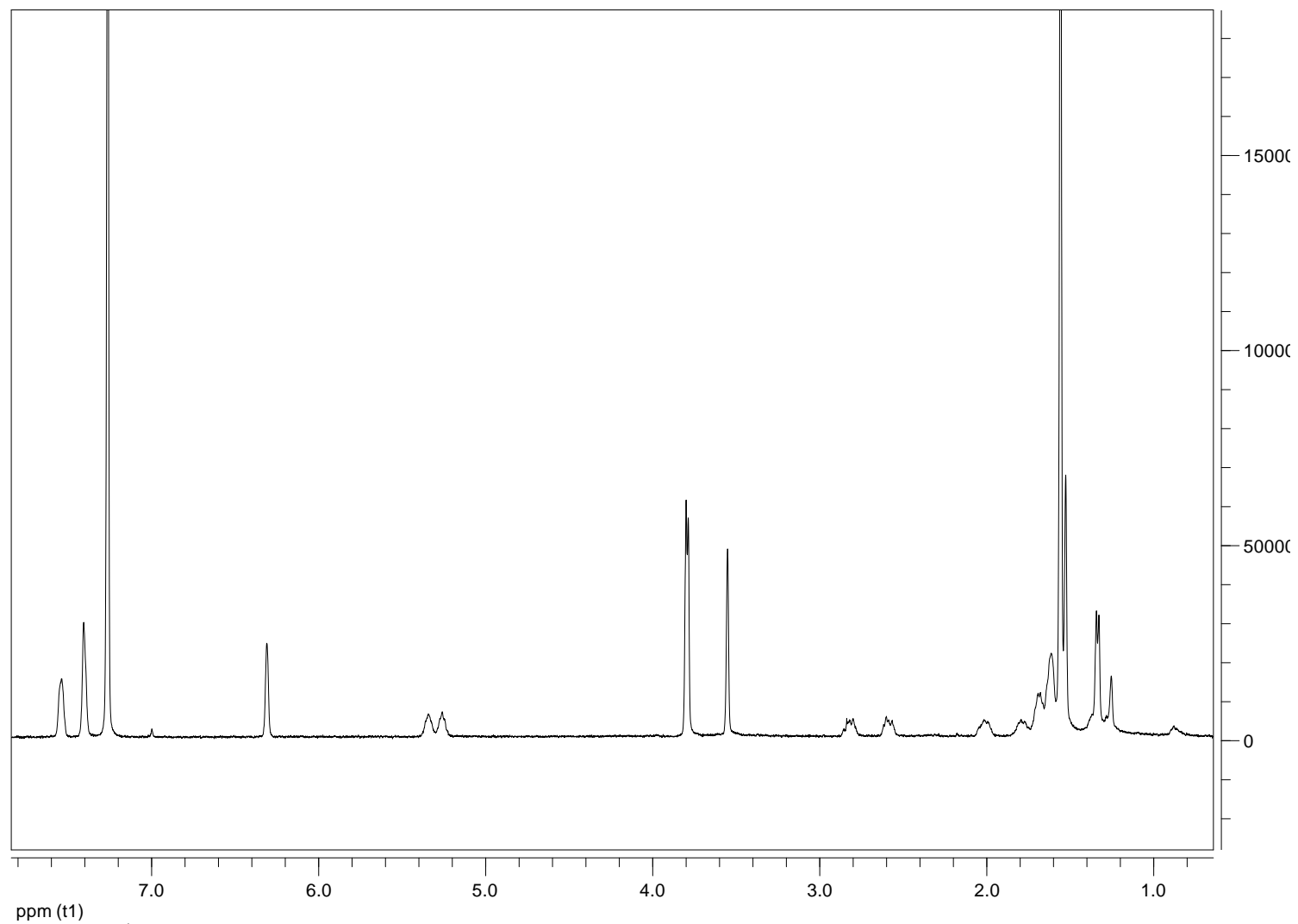


Figure 51. ¹H NMR spectrum of 7-O-(*S*)- α -methoxy- α -trifluoromethyl- α -phenylacetate (MTPA) of 17 (**20**) recorded in CDCl₃ at 400 MHz.

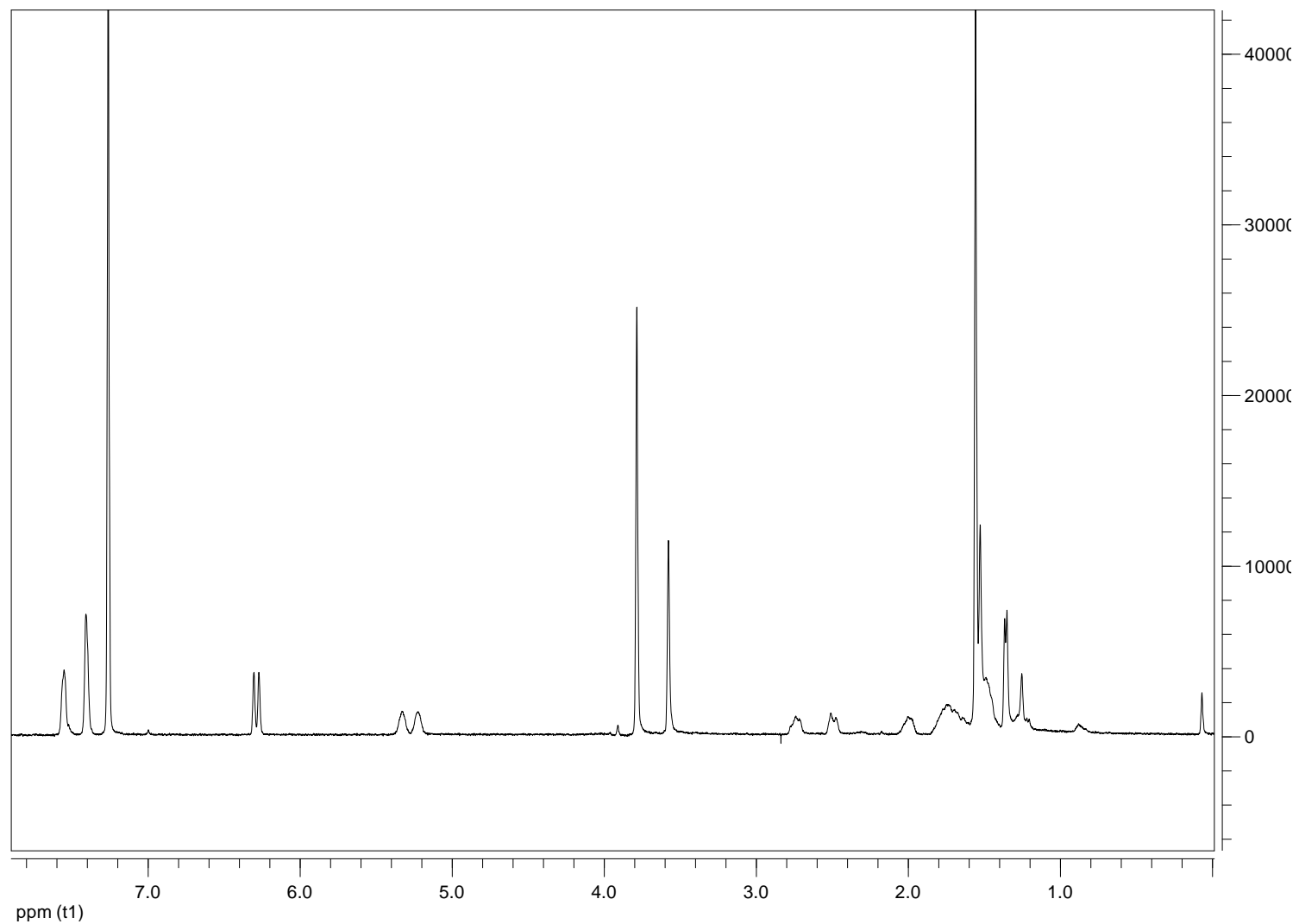


Figure 52. ¹H NMR spectrum of 7-O-(R)- α -methoxy- α -trifluoromethyl- α -phenylacetate (MTPA) of 17 (**21**) recorded in CDCl₃ at 400 MHz.

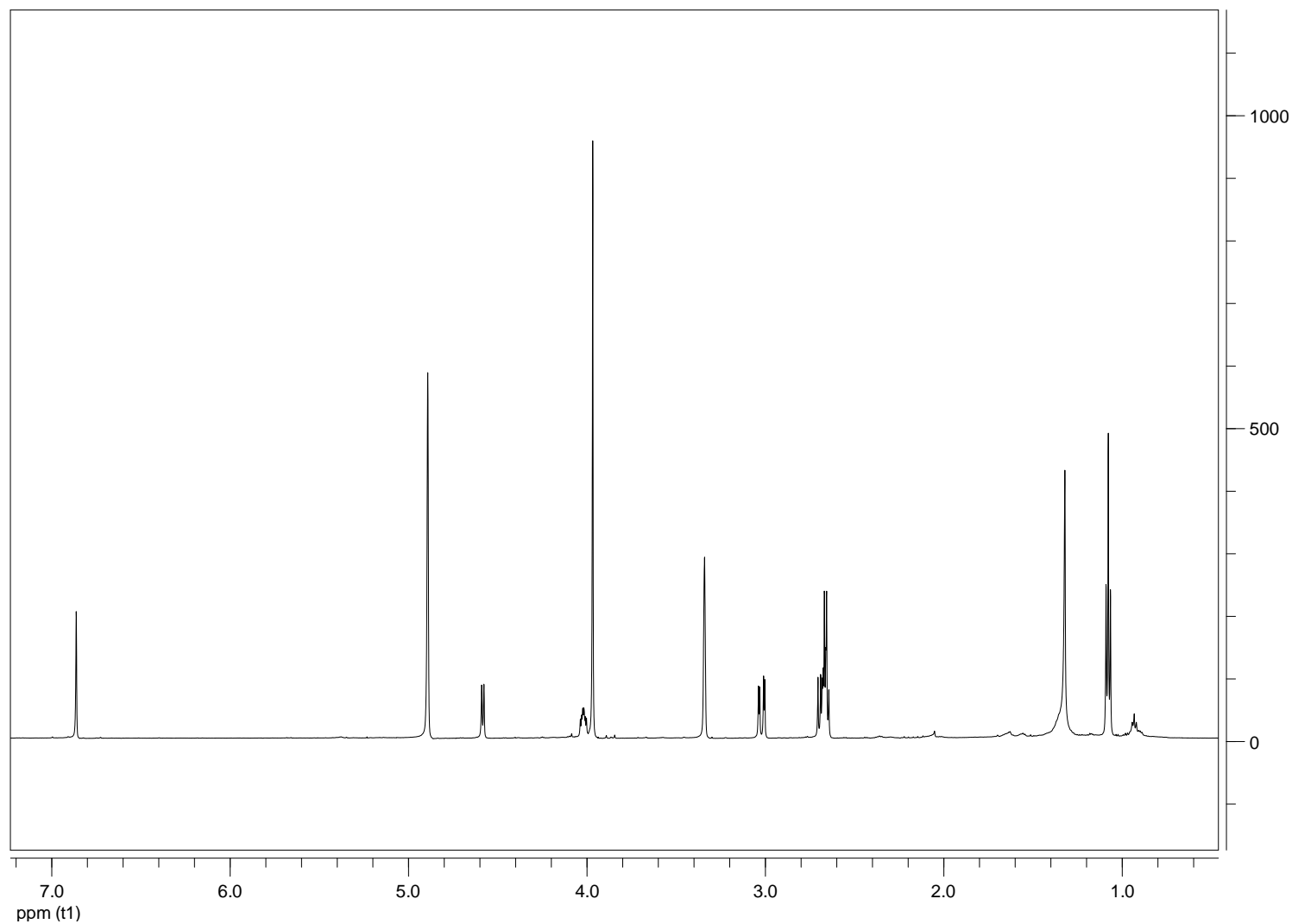


Figure 56. ^1H NMR spectrum of botryosphaerone D (**22**) recorded in CDCl_3 at 400 MHz.

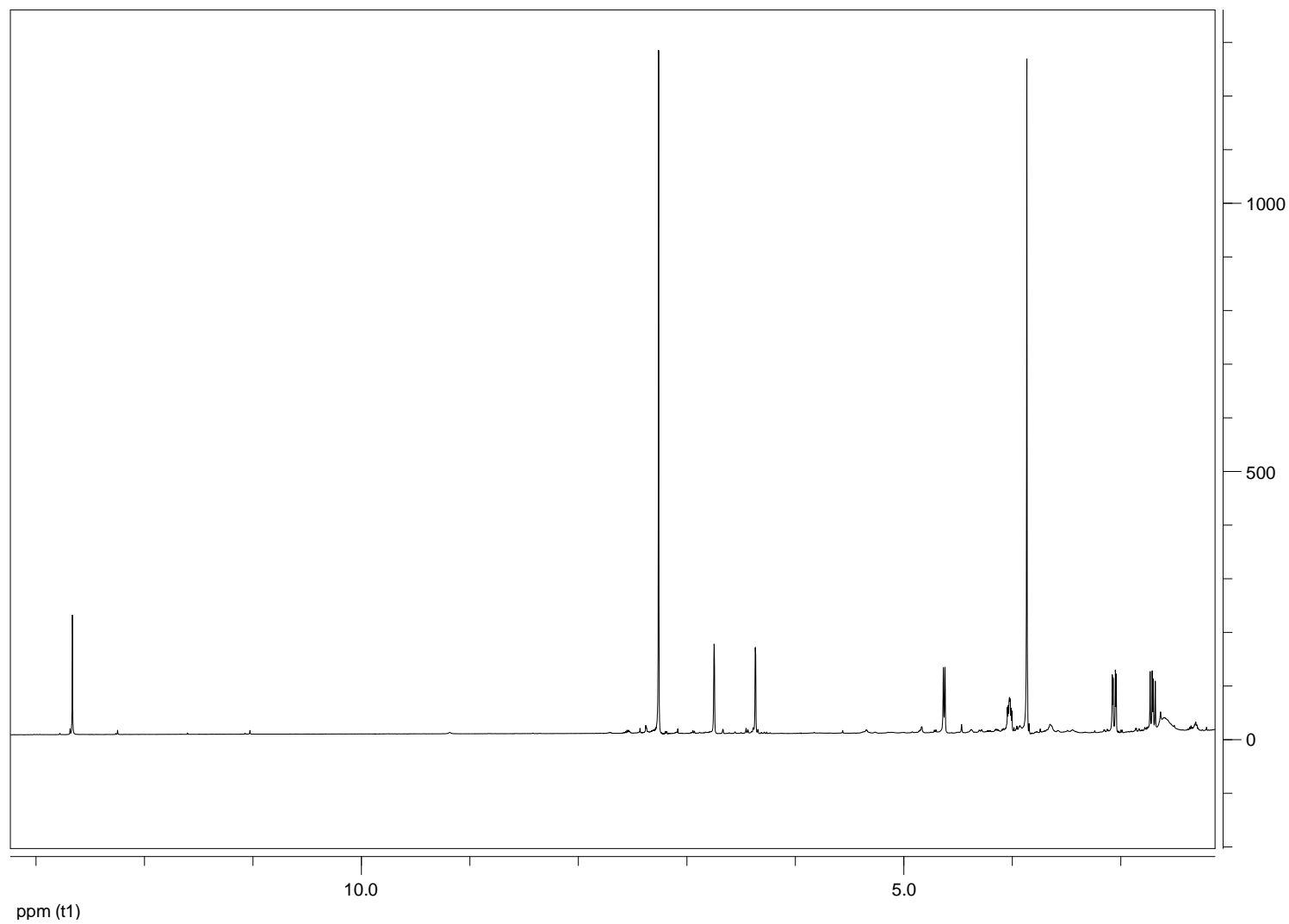


Figure 57. ¹H NMR spectrum of 3,4,8-trihydroxy-6-methoxy-3,4-dihydro-1(2H)-naphthalenone (**23**) recorded in MeOD at 400 MHz.

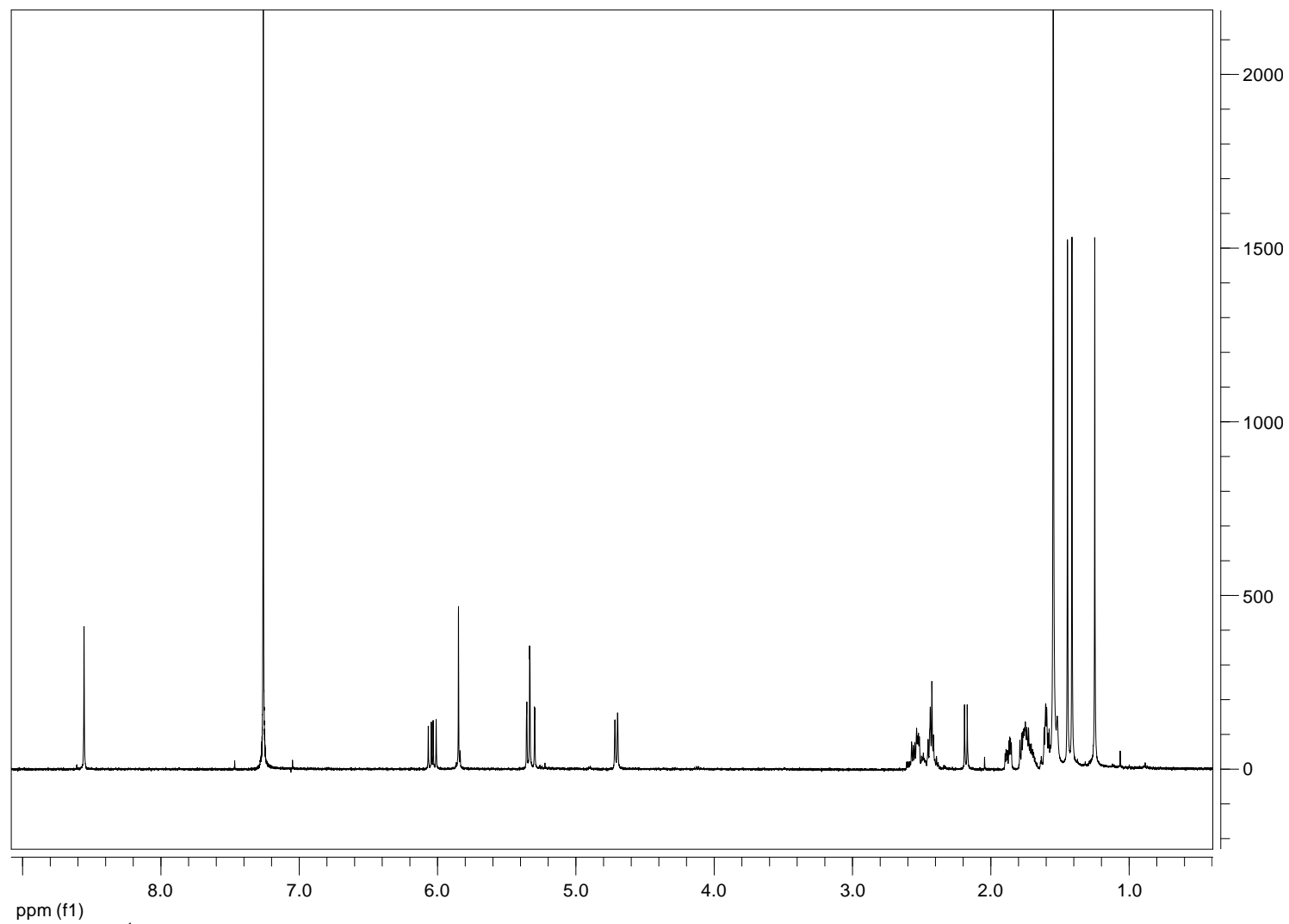
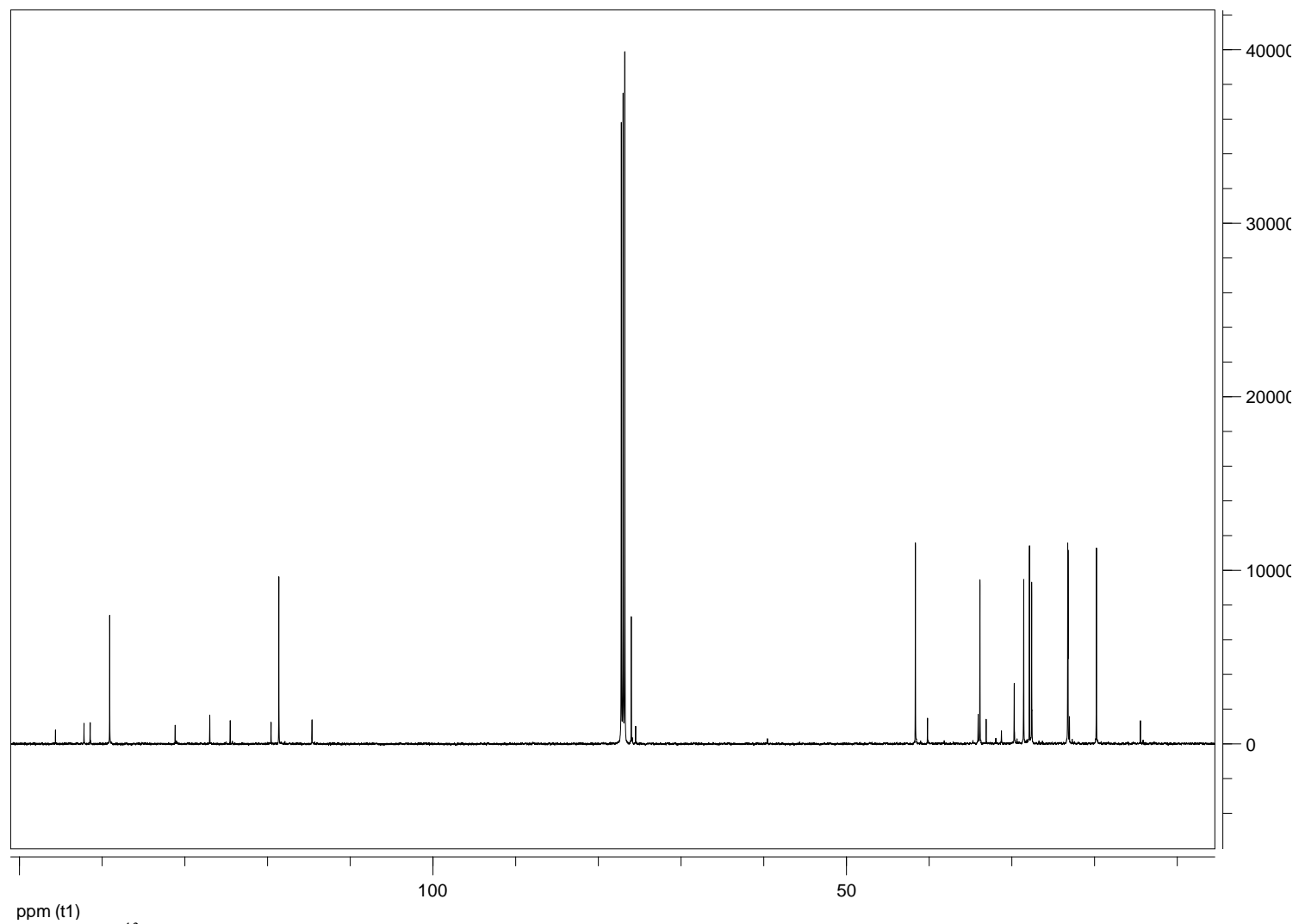


Figure 60. ^1H NMR spectrum of diplopimarane (**24**) recorded in CDCl_3 at 400 MHz.



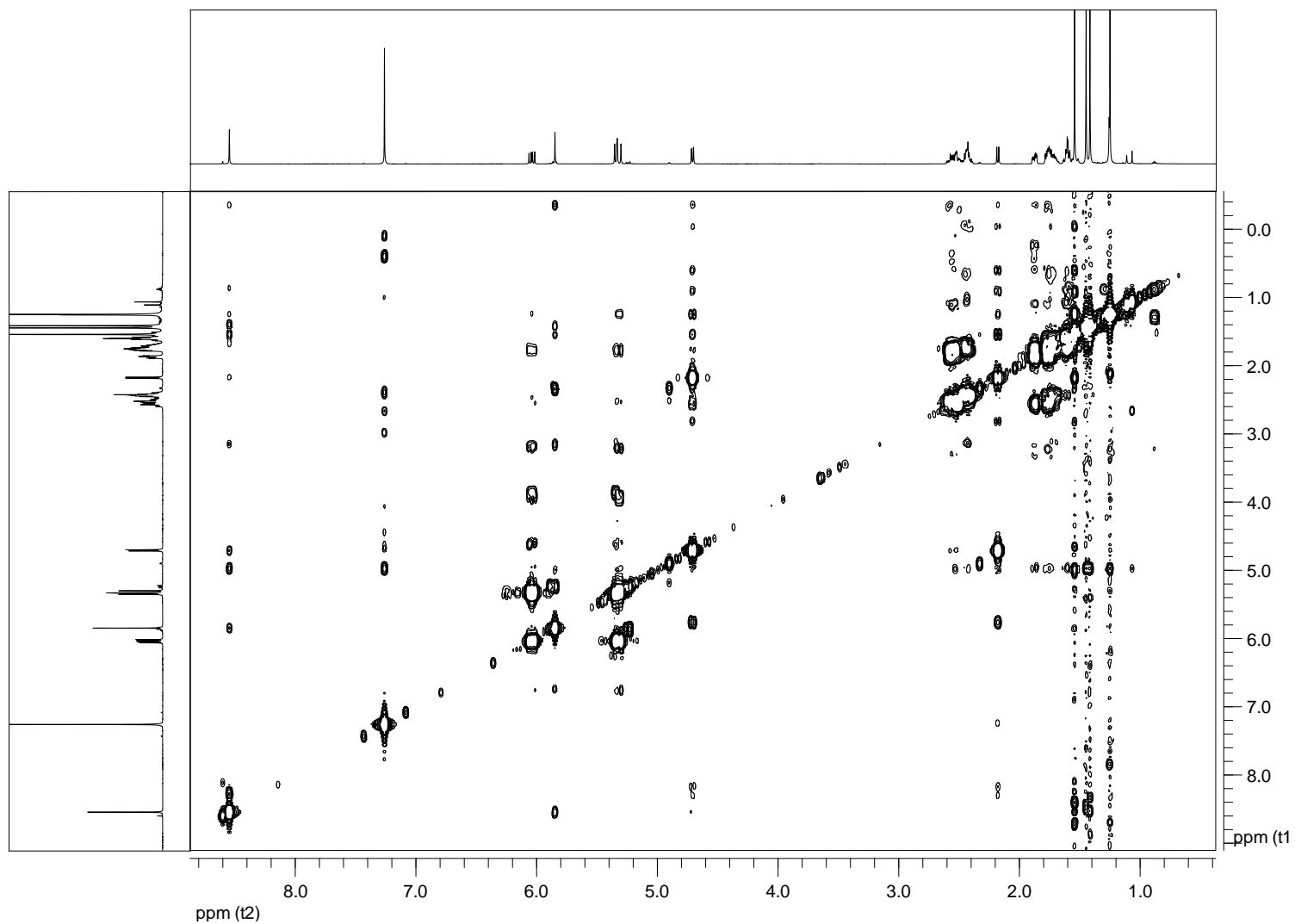
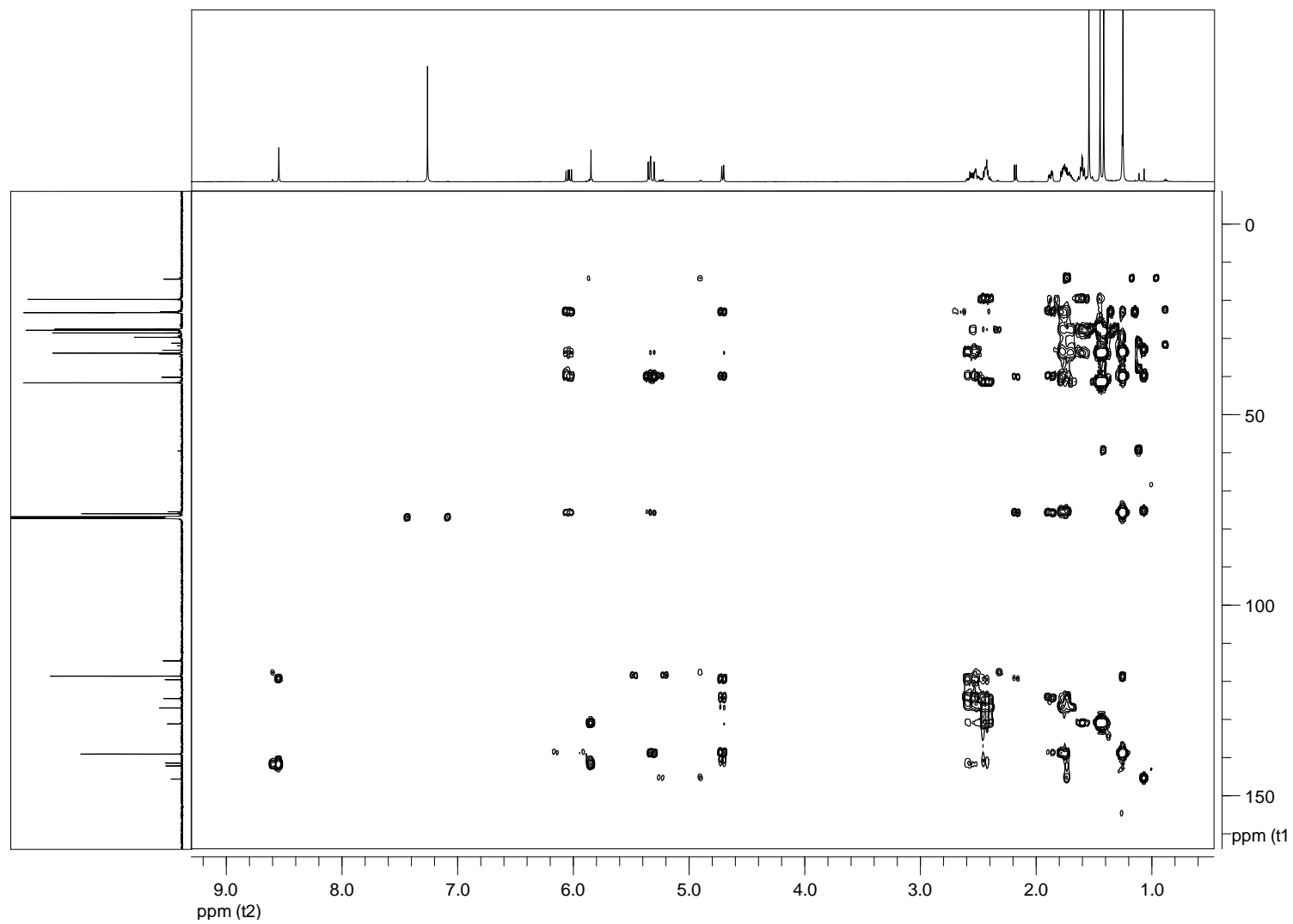


Figure 62. COSY spectrum of diplopimarane (**24**) recorded in CDCl₃ at 400 MHz.



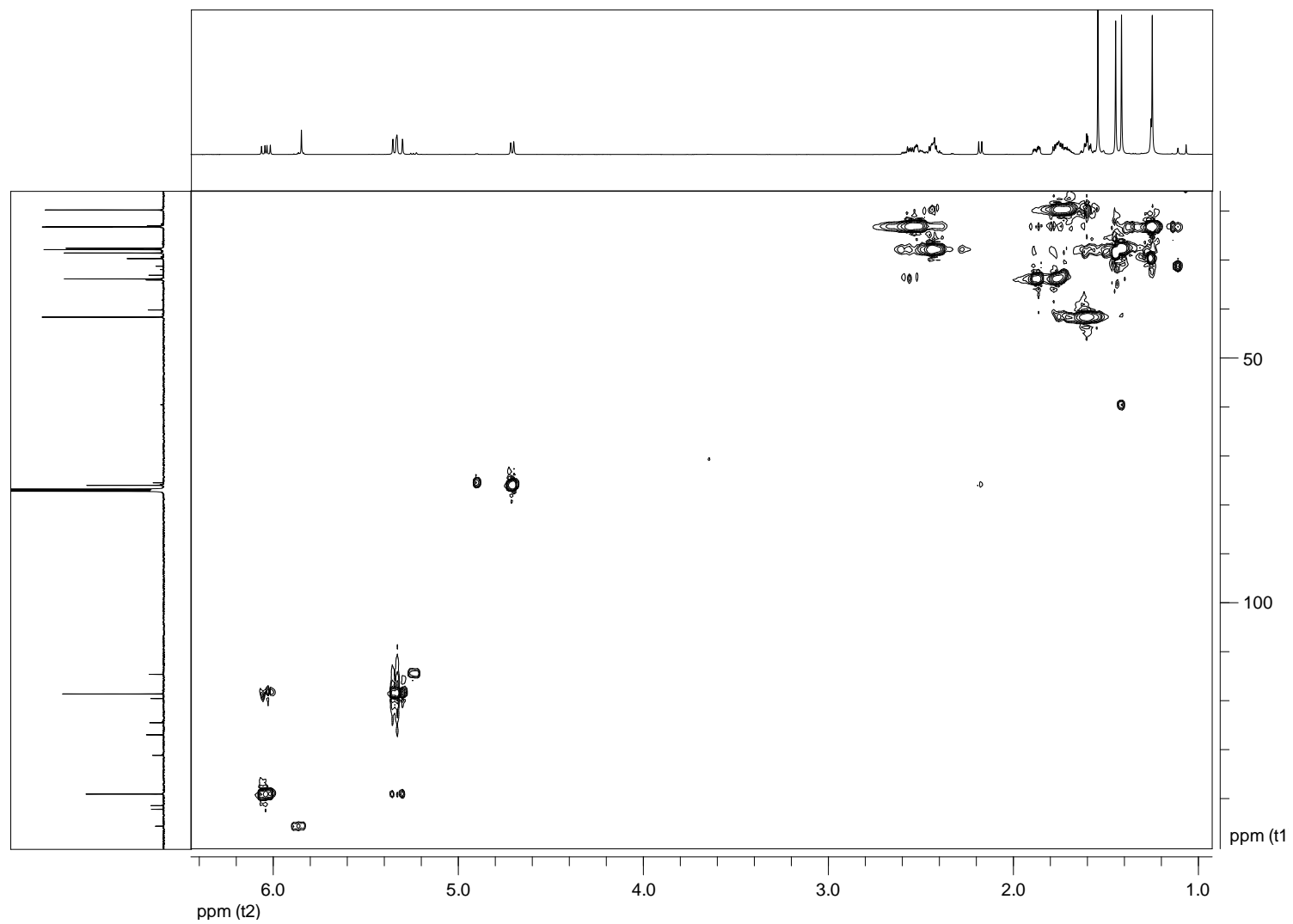


Figure 64. HSQC spectrum of diplopimarane (**24**) recorded in CDCl_3 at 400 MHz.

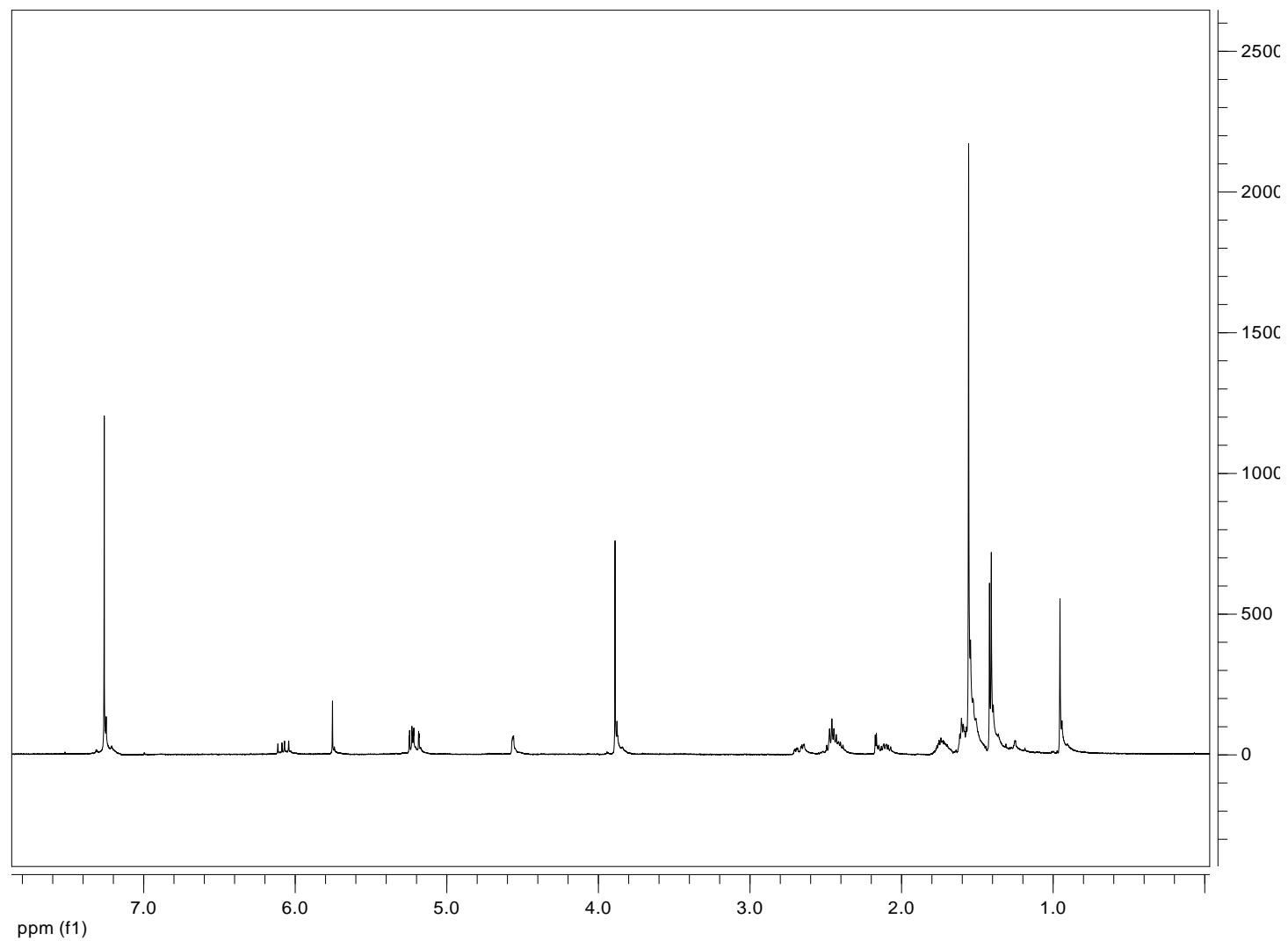


Figure 65. ¹H NMR spectrum of 6-O-methyldiplopimarane (**25**) recorded in CDCl₃ at 400 MHz.

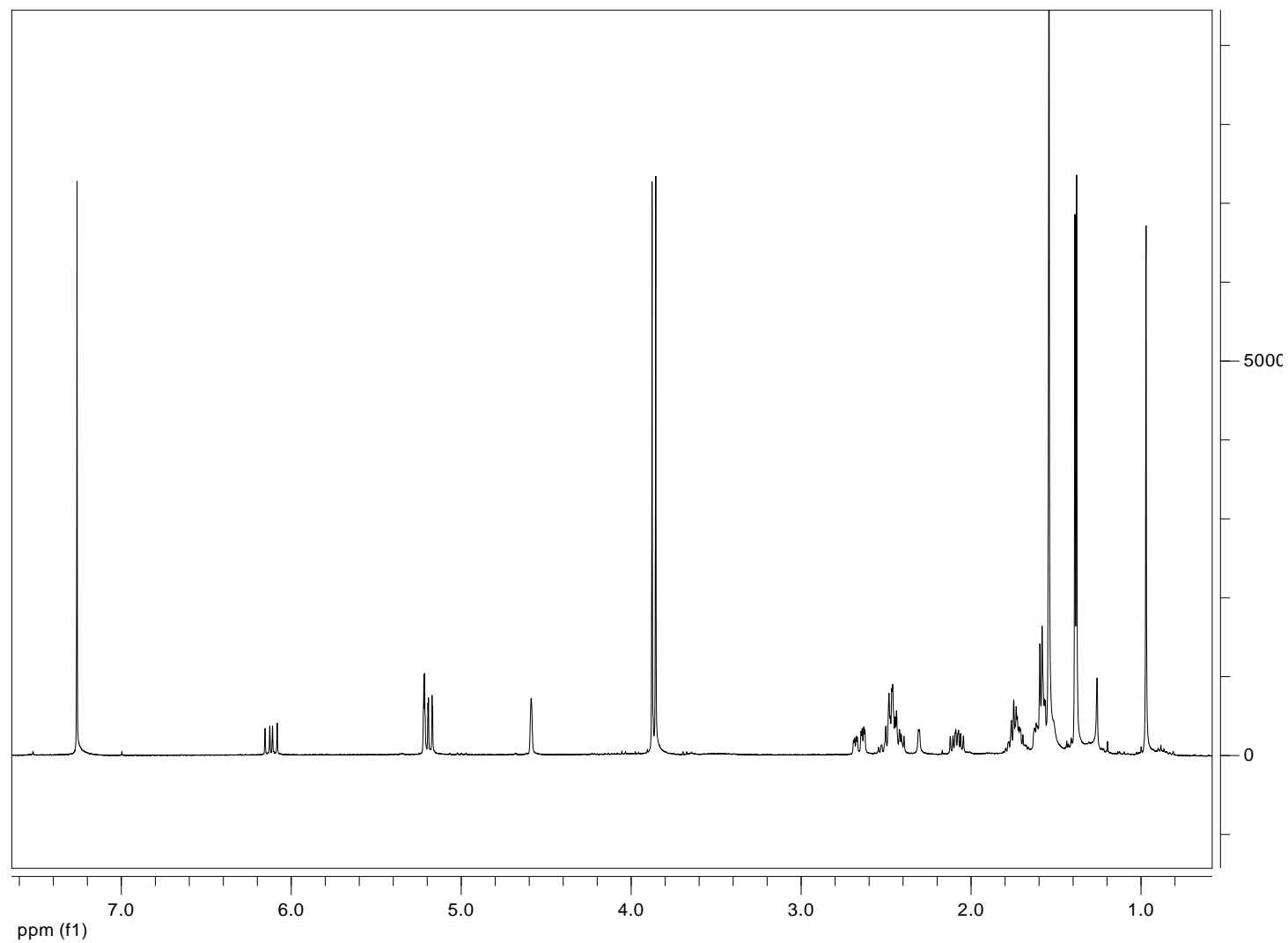


Figure 66. ¹H NMR spectrum of 6-O,7-O-dimethyldiplopimarane (**26**) recorded in CDCl₃ at 400 MHz.

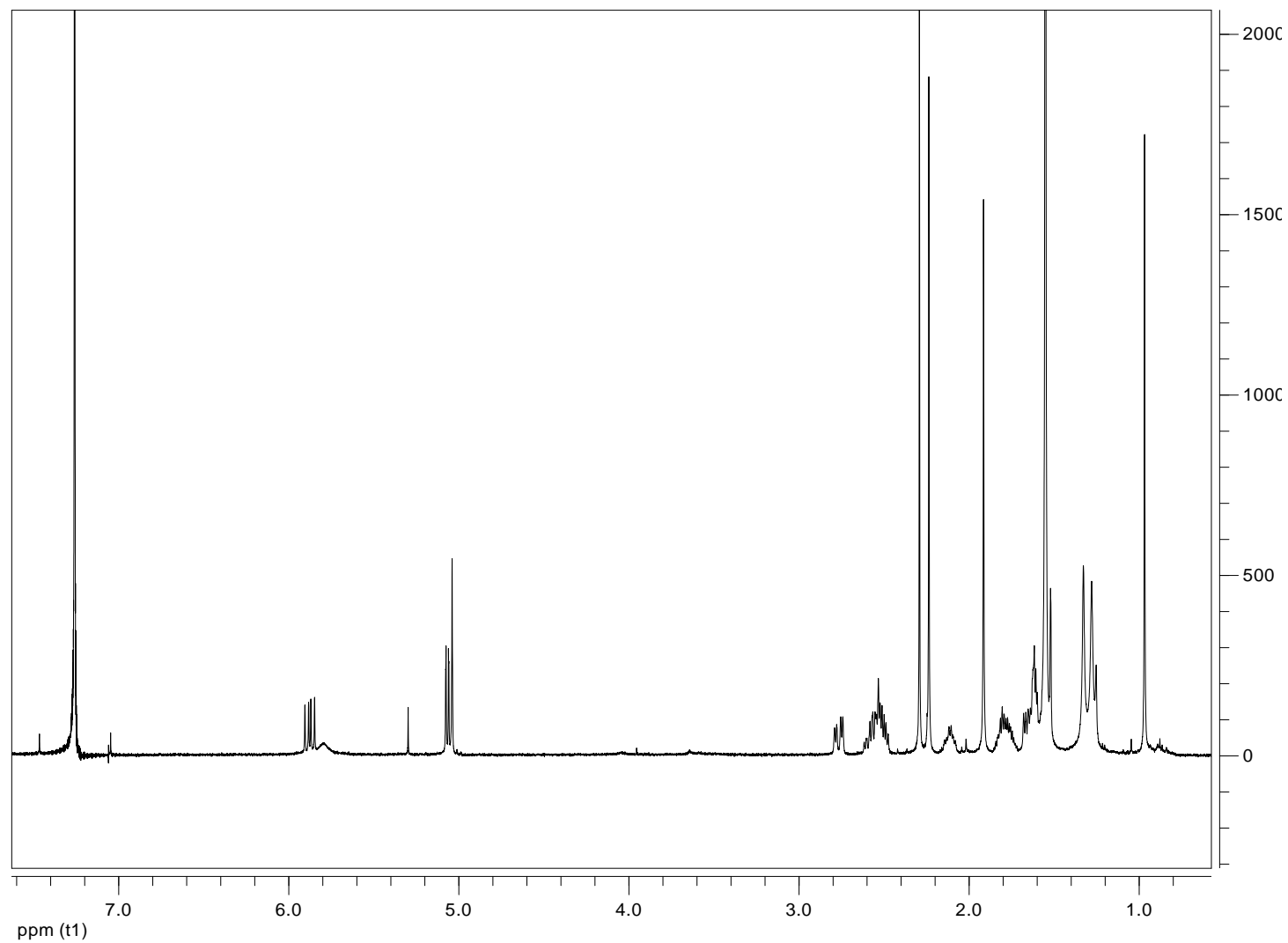


Figure 67. ¹H NMR spectrum of 6-O,7-O,14-O-triacetyldiplopimarane (**27**) recorded in CDCl₃ at 400 MHz.

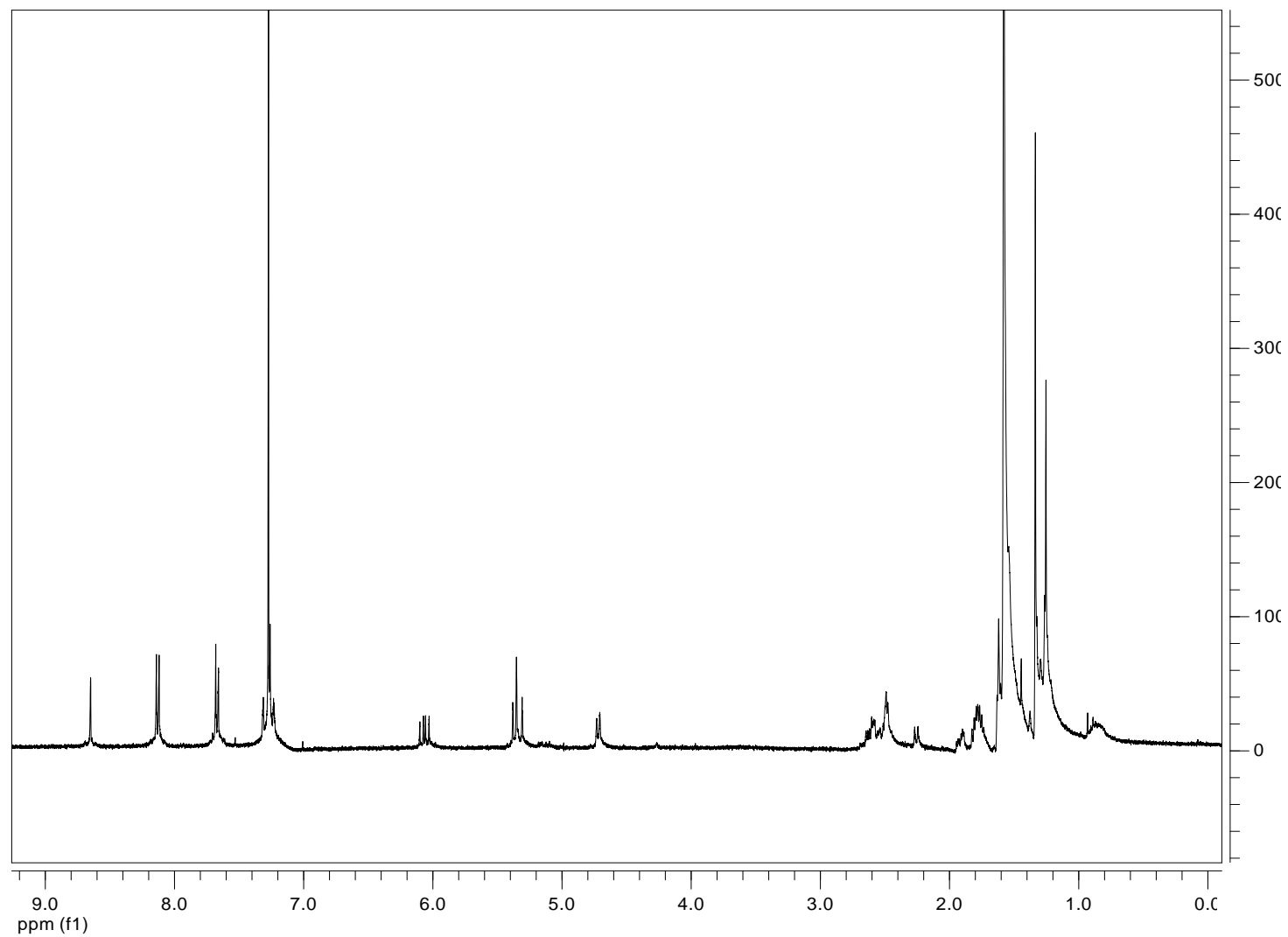


Figure 68. ^1H NMR spectrum of 6-*O*-*p*-bromobenzoyl ester of diplopimarane (**28**) recorded in CDCl_3 at 400 MHz.

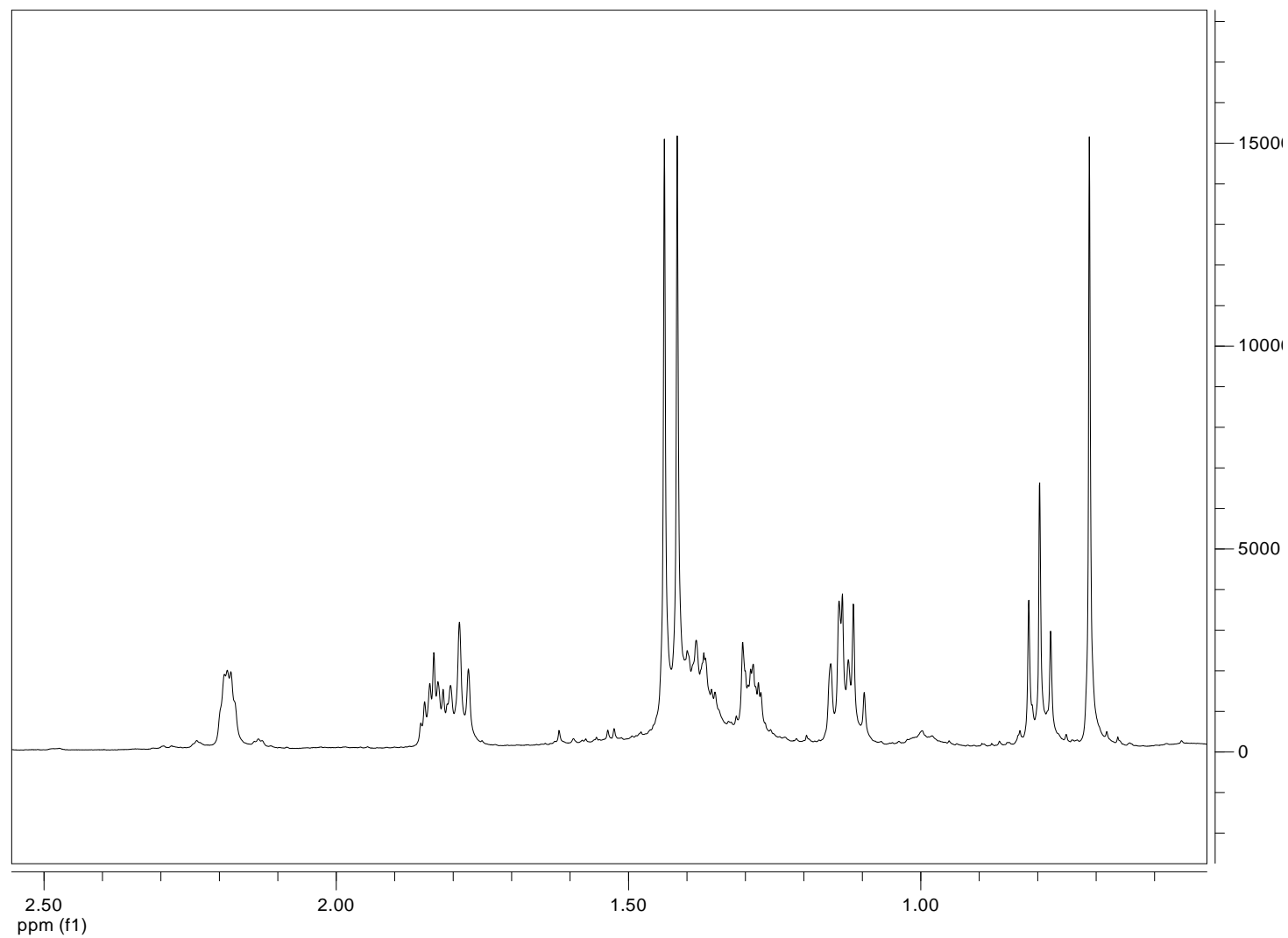


Figure 69. ¹H NMR spectrum of 15,16-dihydrodiplopimarane (**29**) recorded in CDCl₃ at 400 MHz.

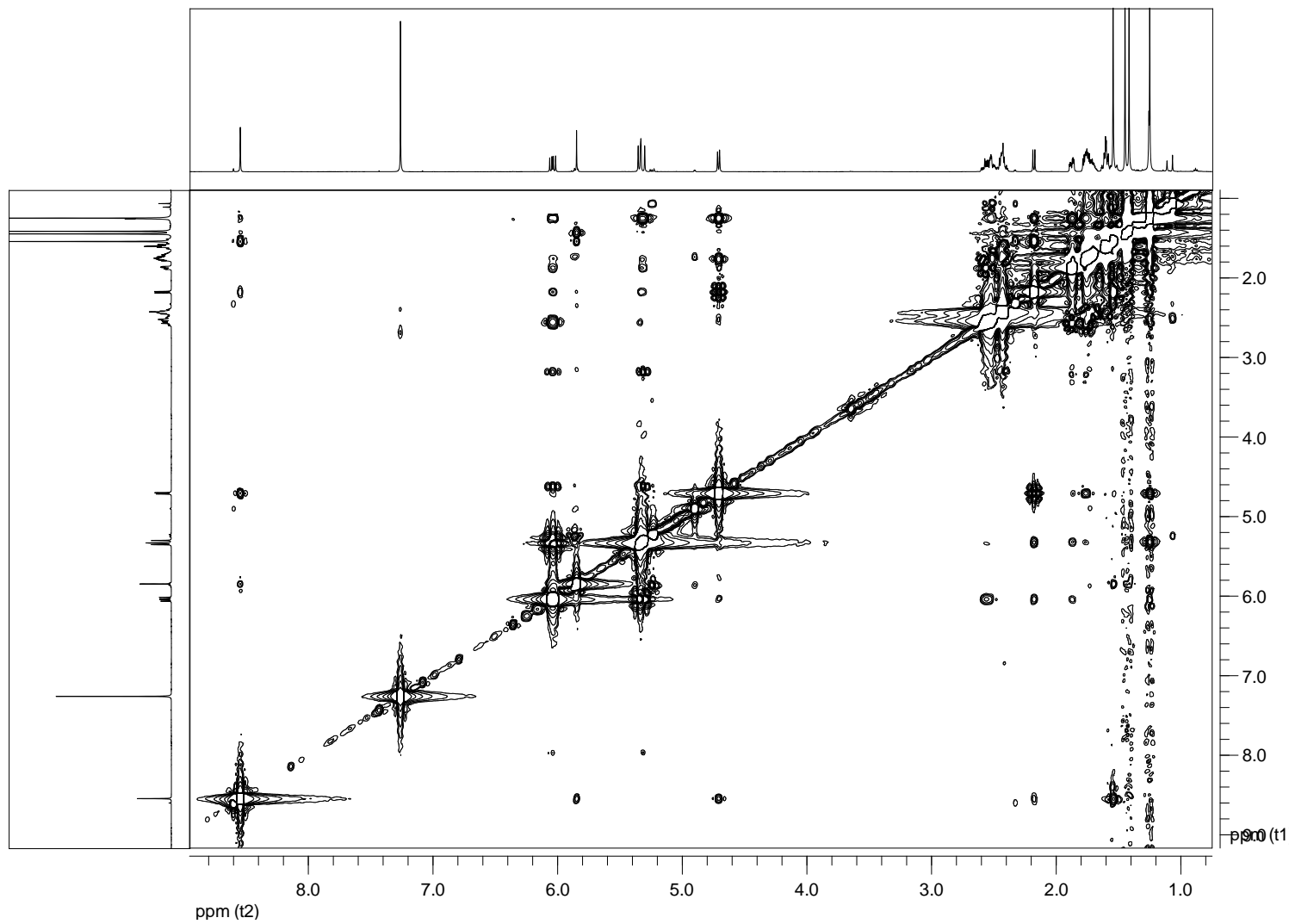


Figure 71. NOESY spectrum of diplopimarane (24) recorded in CDCl₃ at 400 MHz.

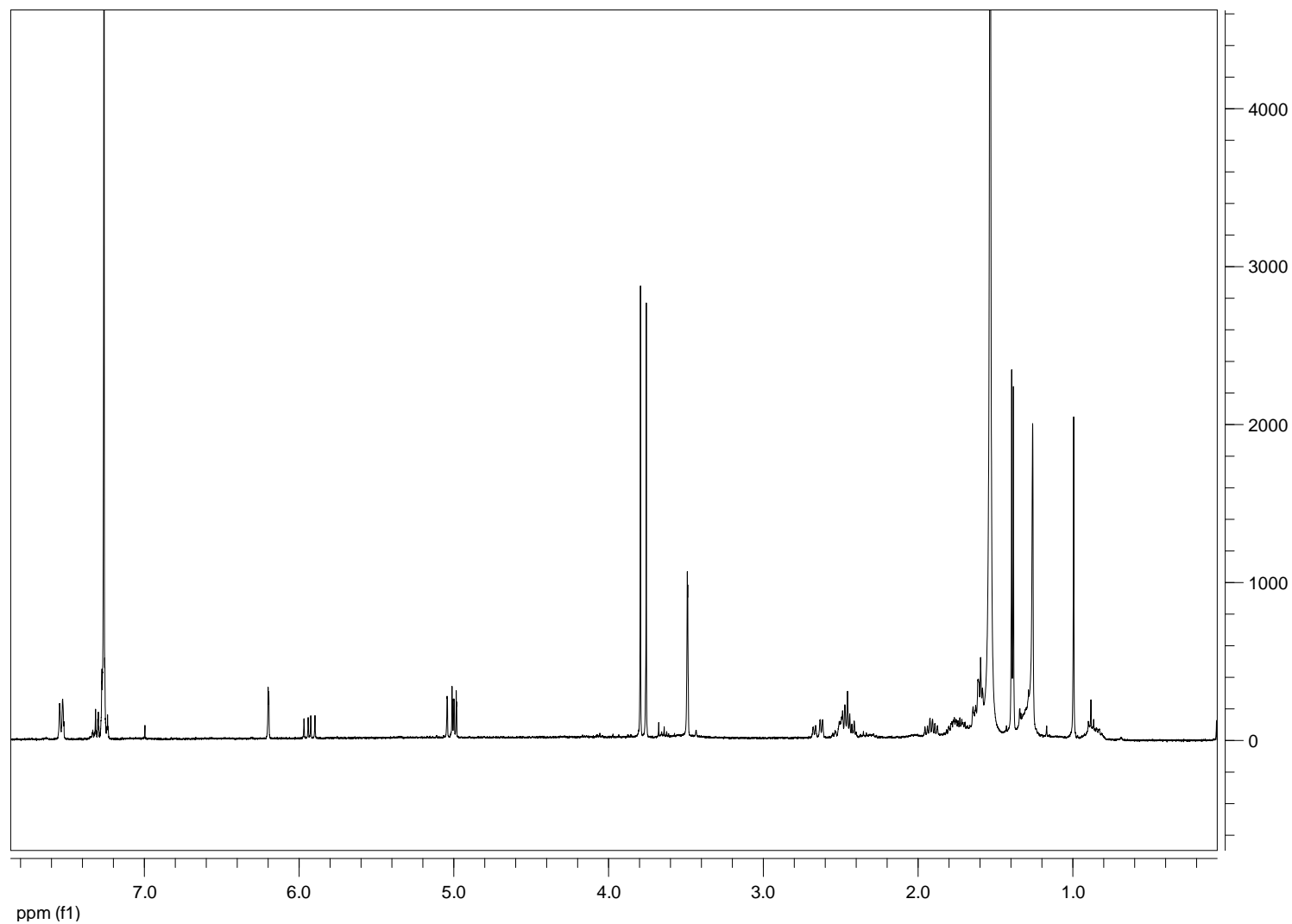


Figure 72. ^1H NMR spectrum of 14-*O*-(*S*)- α -methoxy- α -trifluoromethyl- α -phenylacetate (MTPA) ester of 6-*O*,7-*O*-dimethyldiplopimaramine (**30**) recorded in CDCl_3 at 400 MHz.

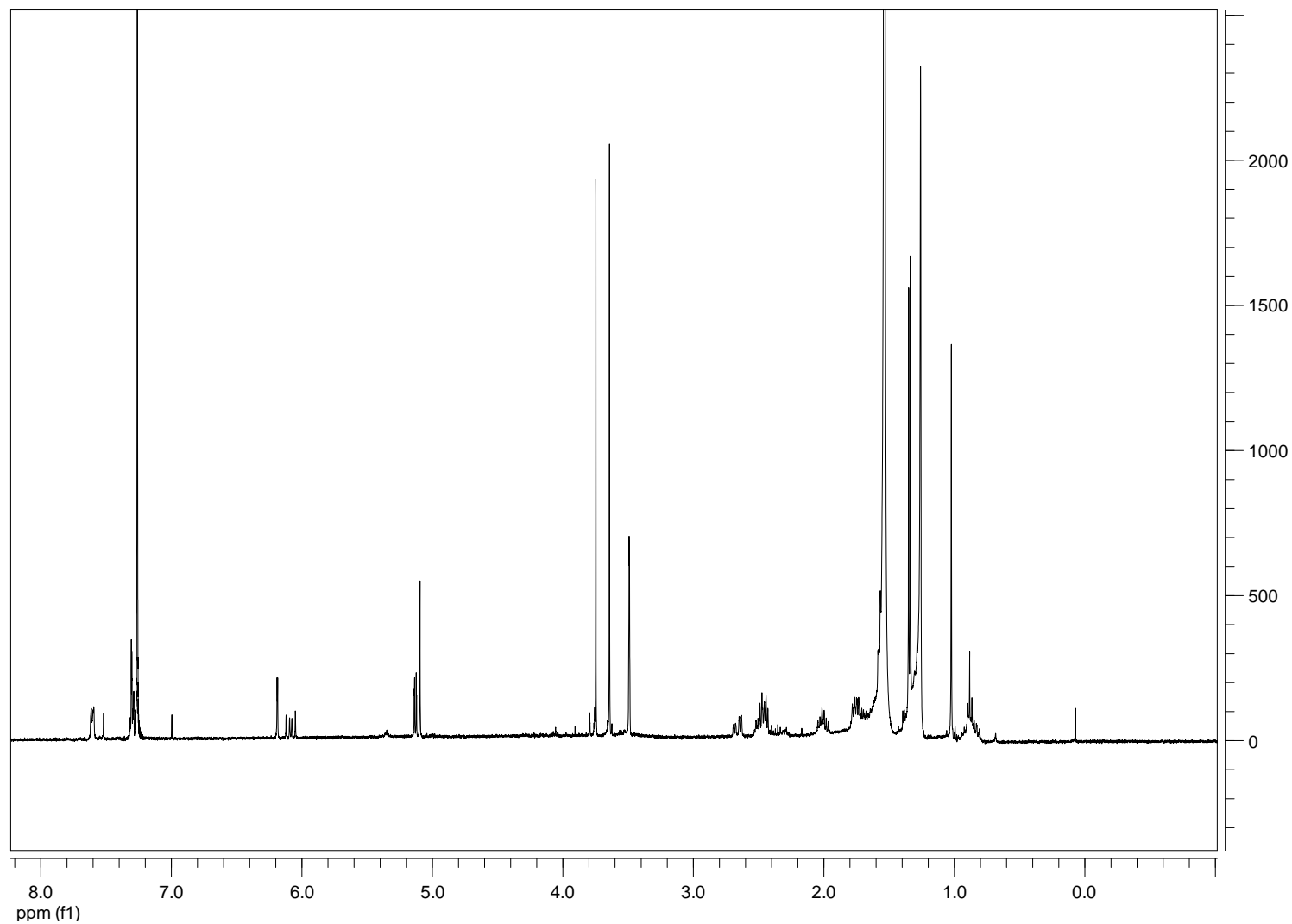


Figure 73. ^1H NMR spectrum of 14-O-(*R*)- α -methoxy- α -trifluoromethyl- α -phenylacetate (MTPA) ester of 6-O,7-O-dimethyldipirane (**31**) recorded in CDCl_3 at 400 MHz.

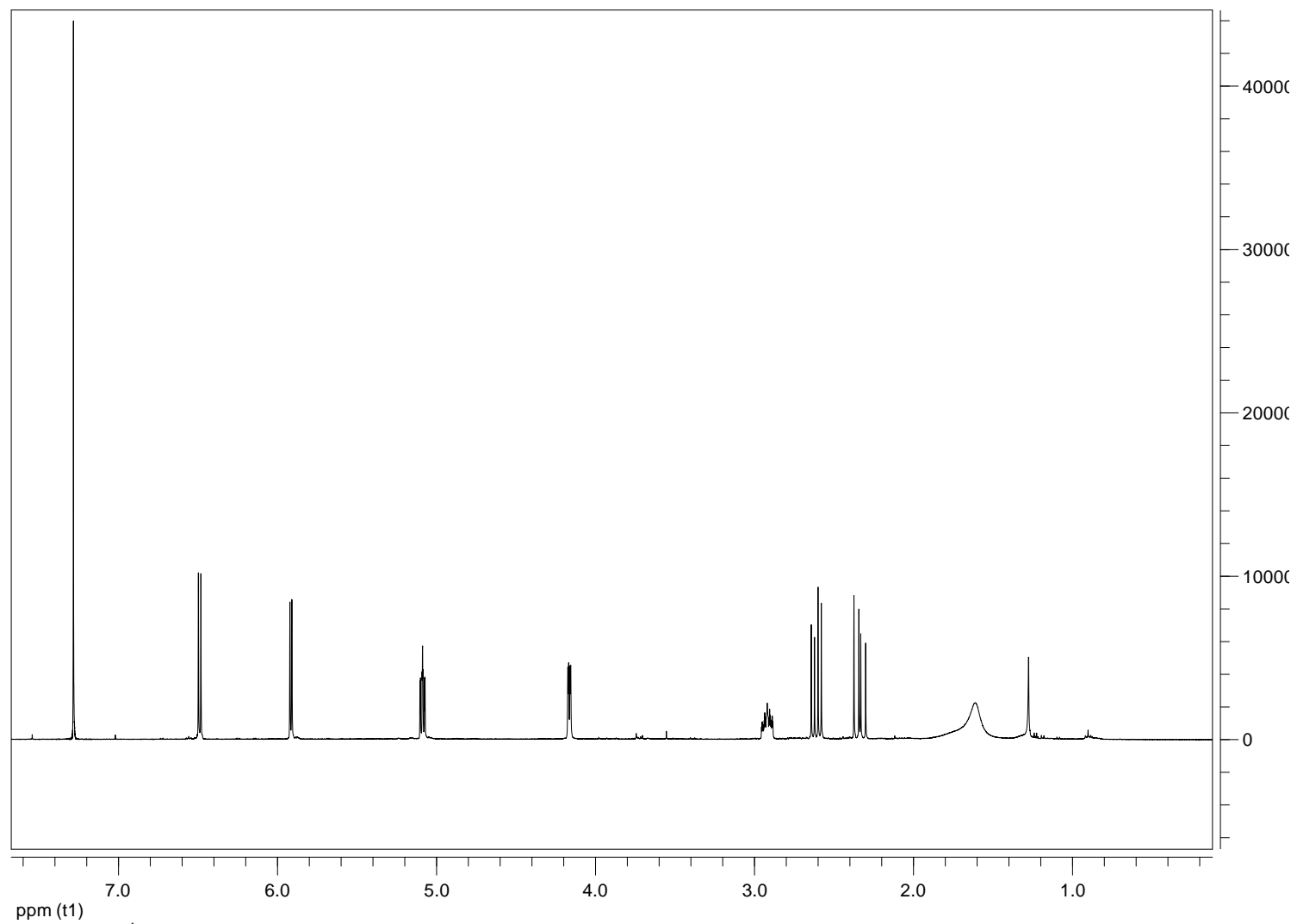


Figure 77. ^1H NMR spectrum of oxysporone (35) recorded in CDCl_3 at 400 MHz.

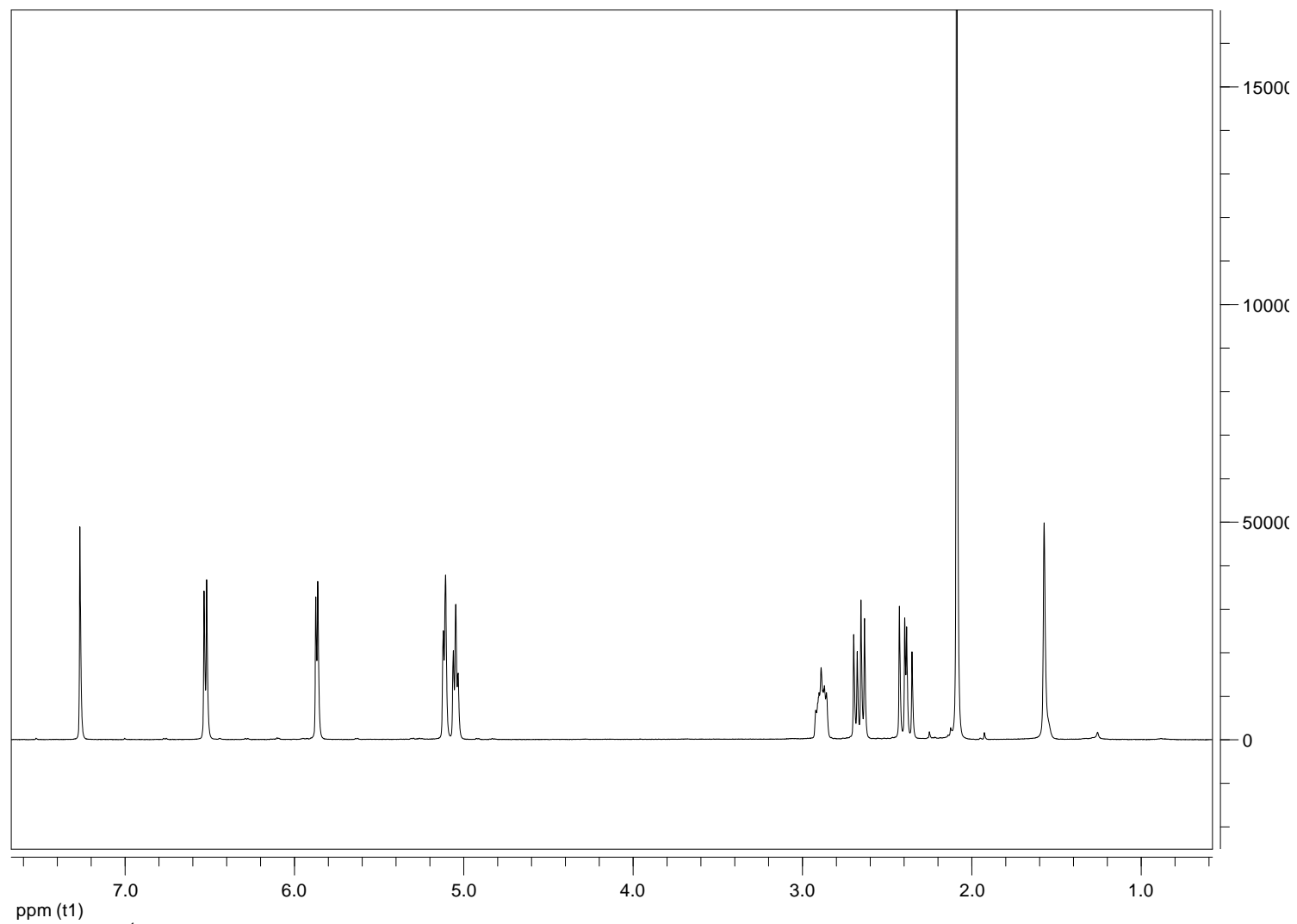


Figure 78. ^1H NMR spectrum of 4-O-acetyloxysporone (**38**) recorded in CDCl_3 at 400 MHz.

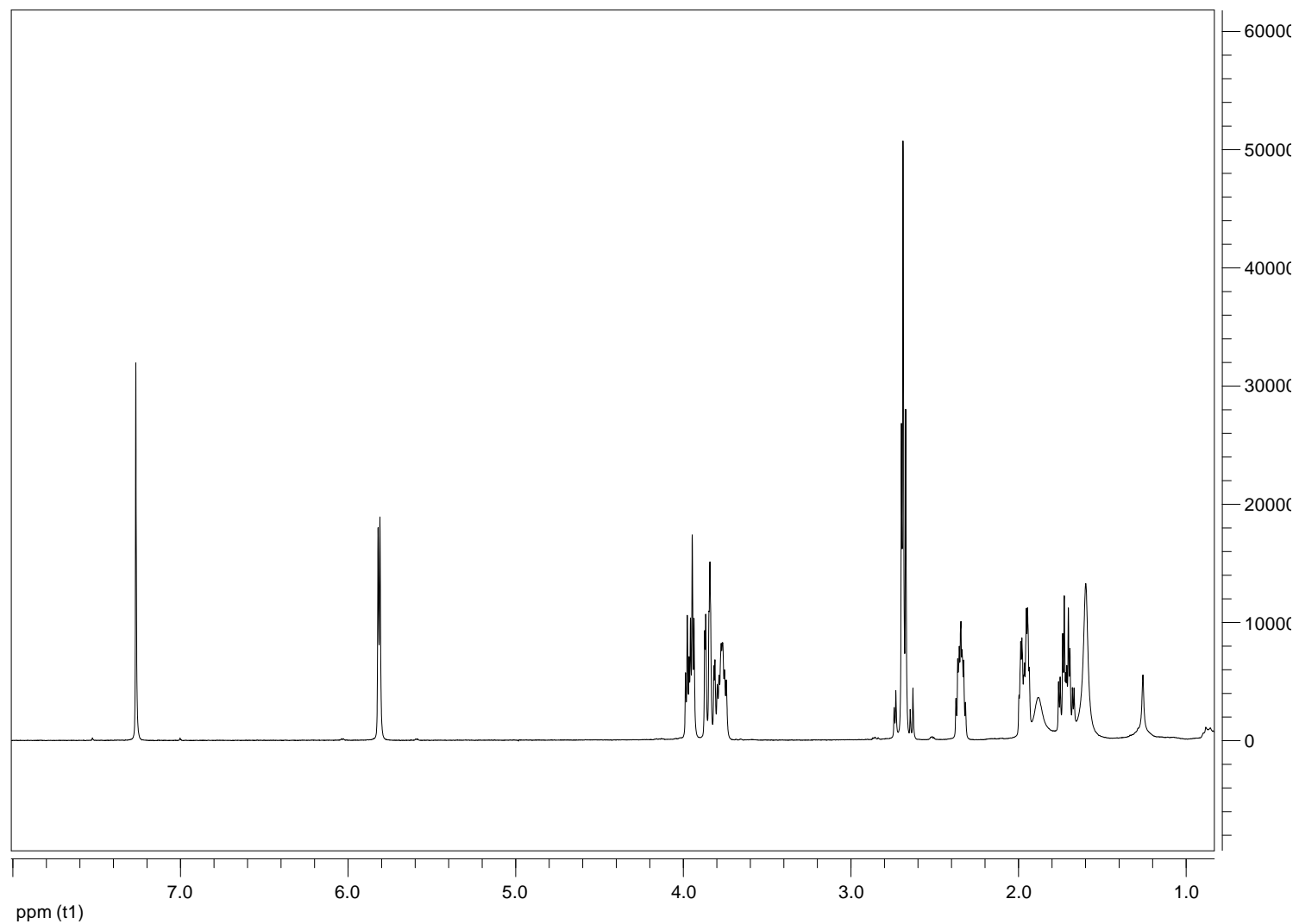


Figure 79. ^1H NMR spectrum of 2,3-dihydrooxysporone (**39**) recorded in CDCl_3 at 400 MHz.

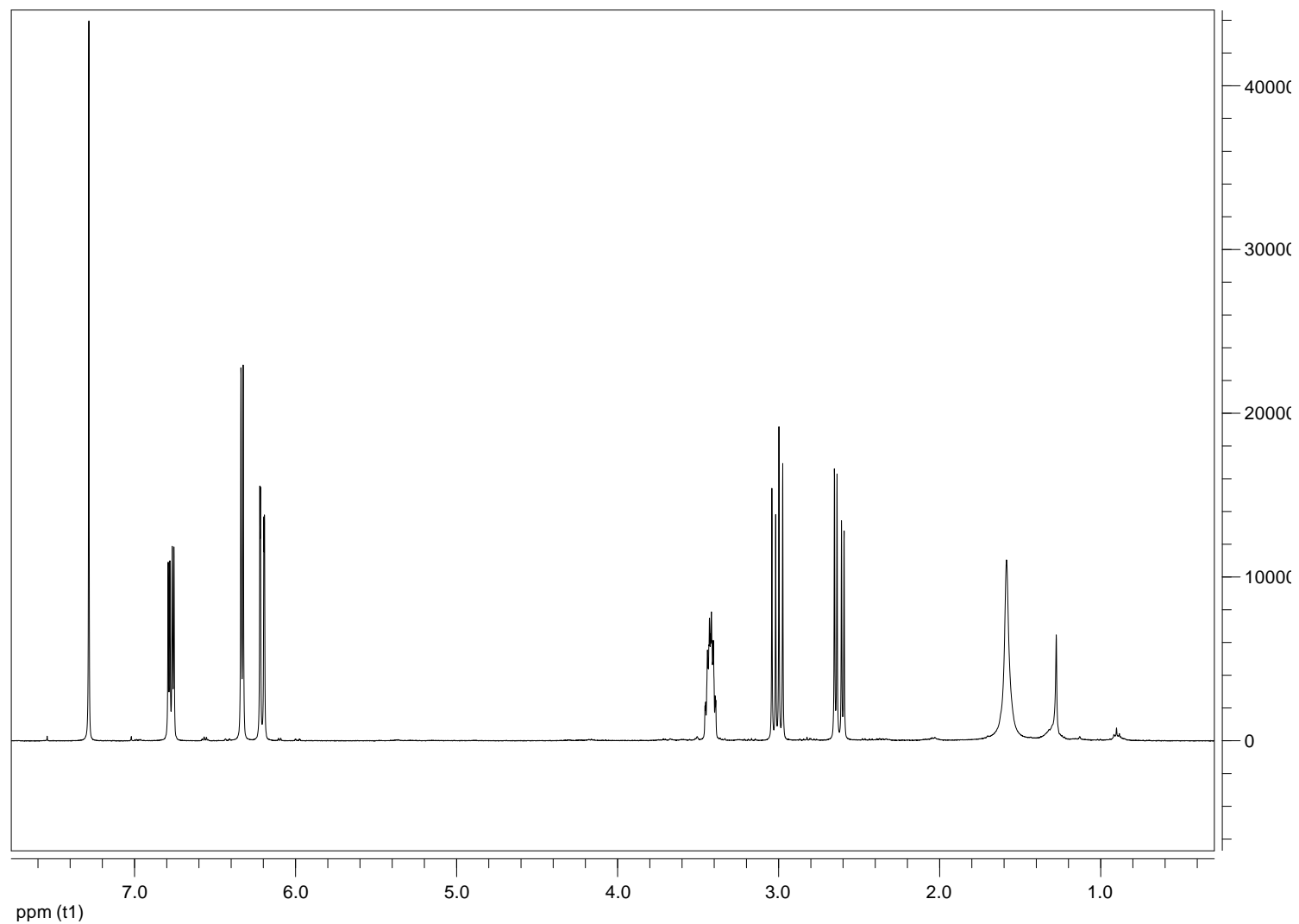


Figure 80. ¹H NMR spectrum of 4,*O*-dehydroxysporone (**40**) recorded in CDCl₃ at 400 MHz.

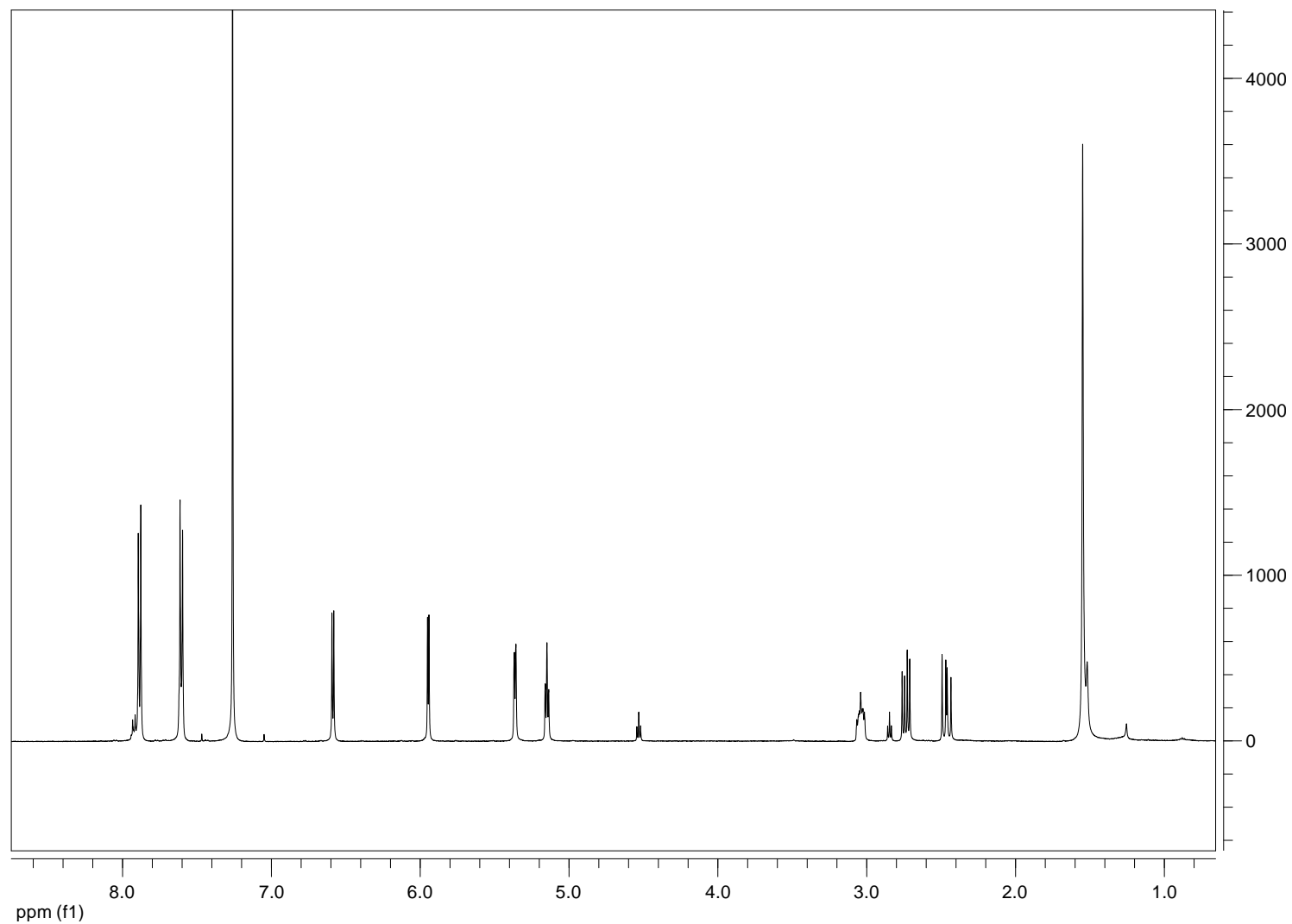


Figure 81. ¹H NMR spectrum of 4-O-*p*-bromobenzoyloxysporone (**41**) recorded in CDCl₃ at 400 MHz.

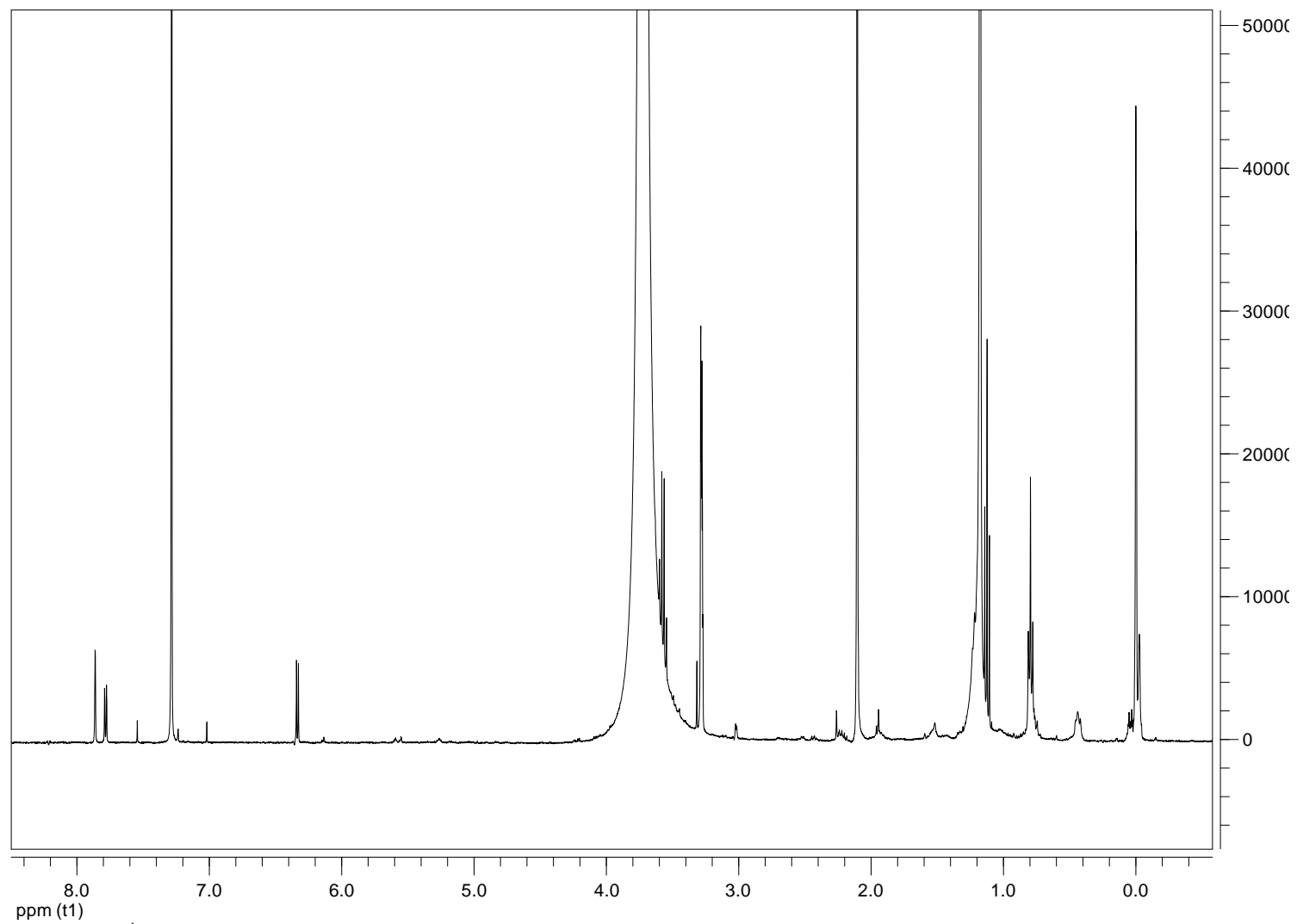


Figure 82. ¹H NMR spectrum of 2-(4-pyronyl)acetic acid (**42**) recorded in CDCl₃ with 10 μL of MeOD at 400 MHz.

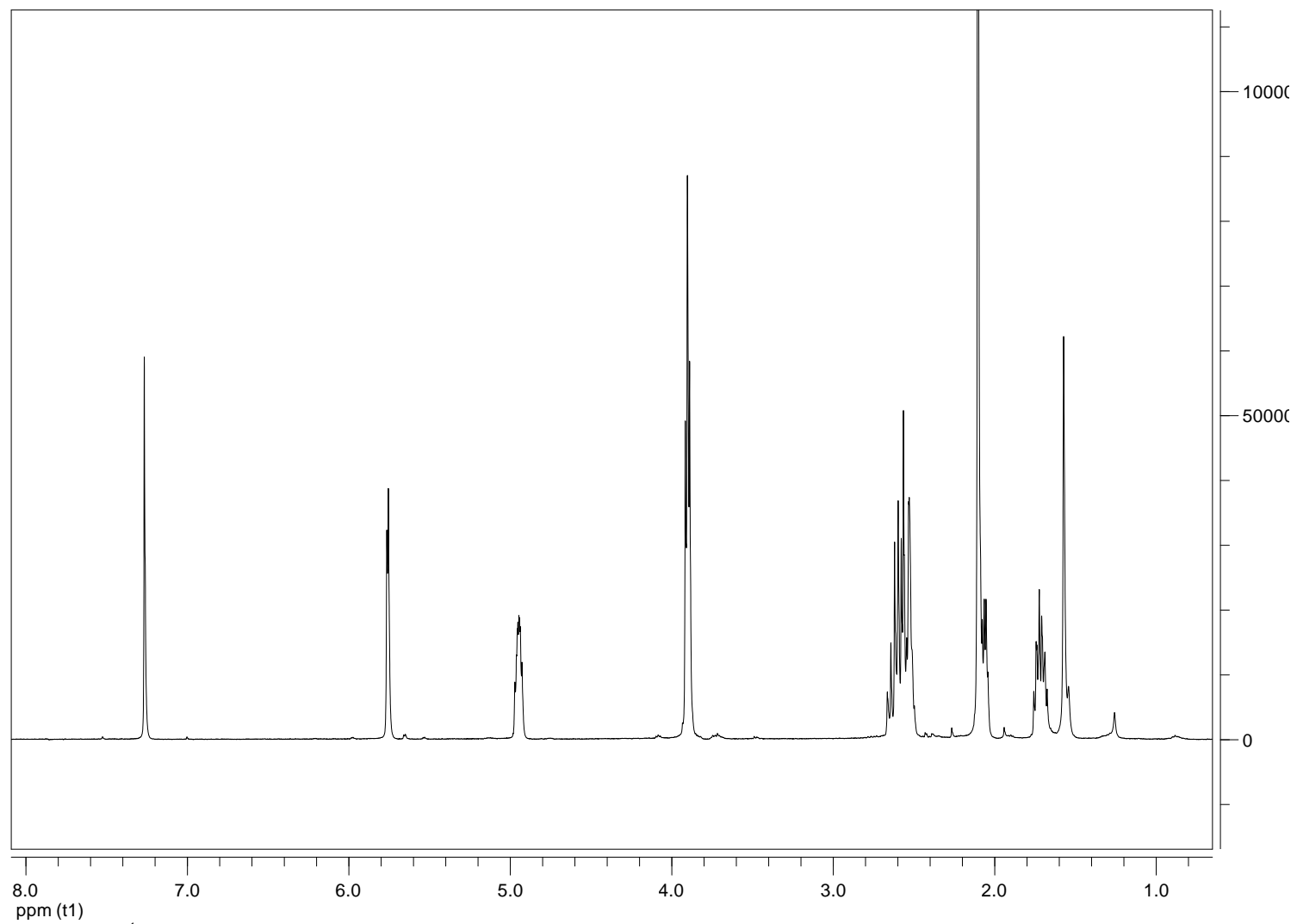


Figure 83. ¹H NMR spectrum of 4-O-acetyl-2,3-dihydrooxysporone (**43**) recorded in CDCl₃ at 400 MHz.

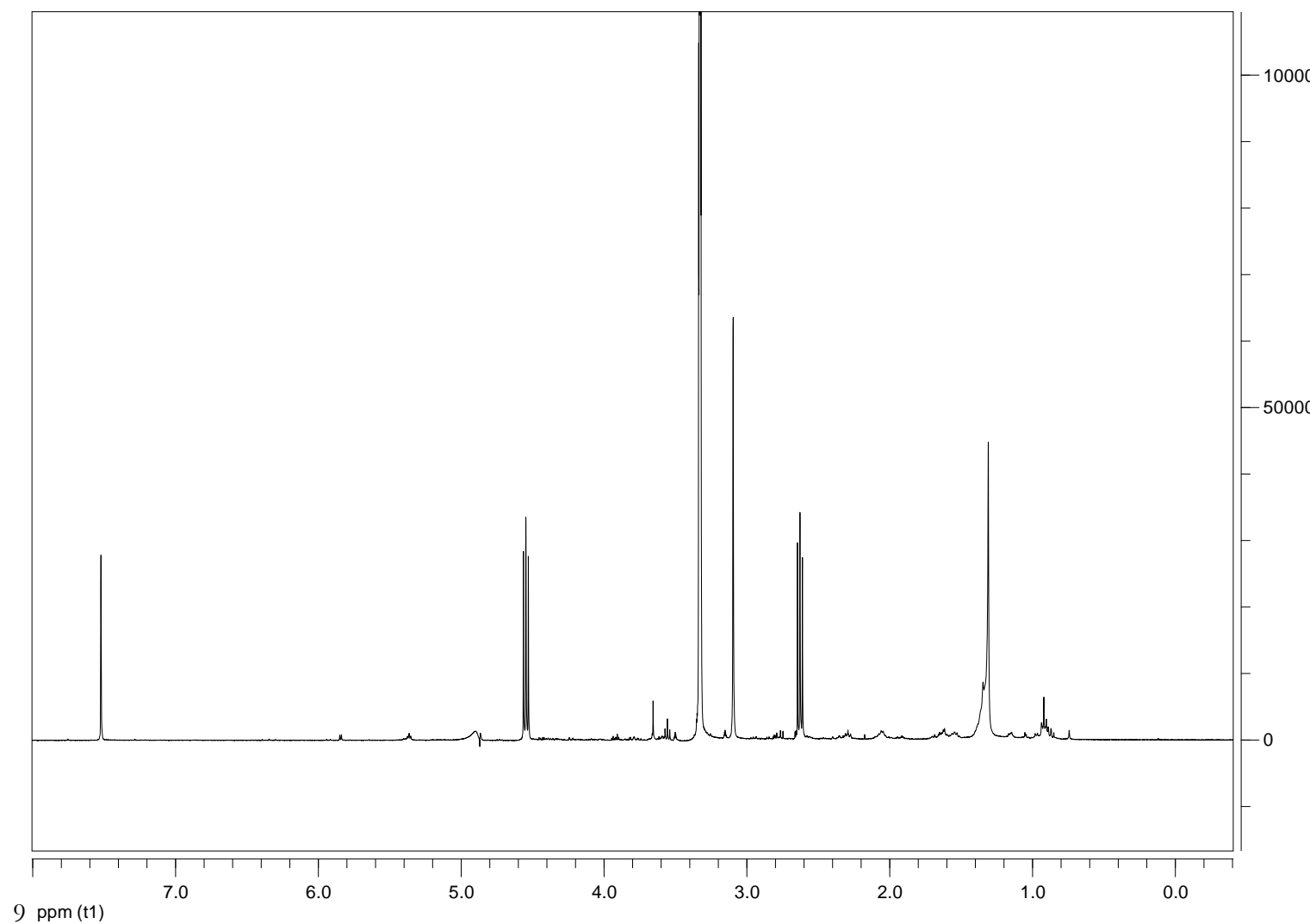


Figure 84. ^1H NMR spectrum of 2-(2,3-dihydro-4-pyronyl)acetic acid (44) recorded in CDCl_3 at 400 MHz.

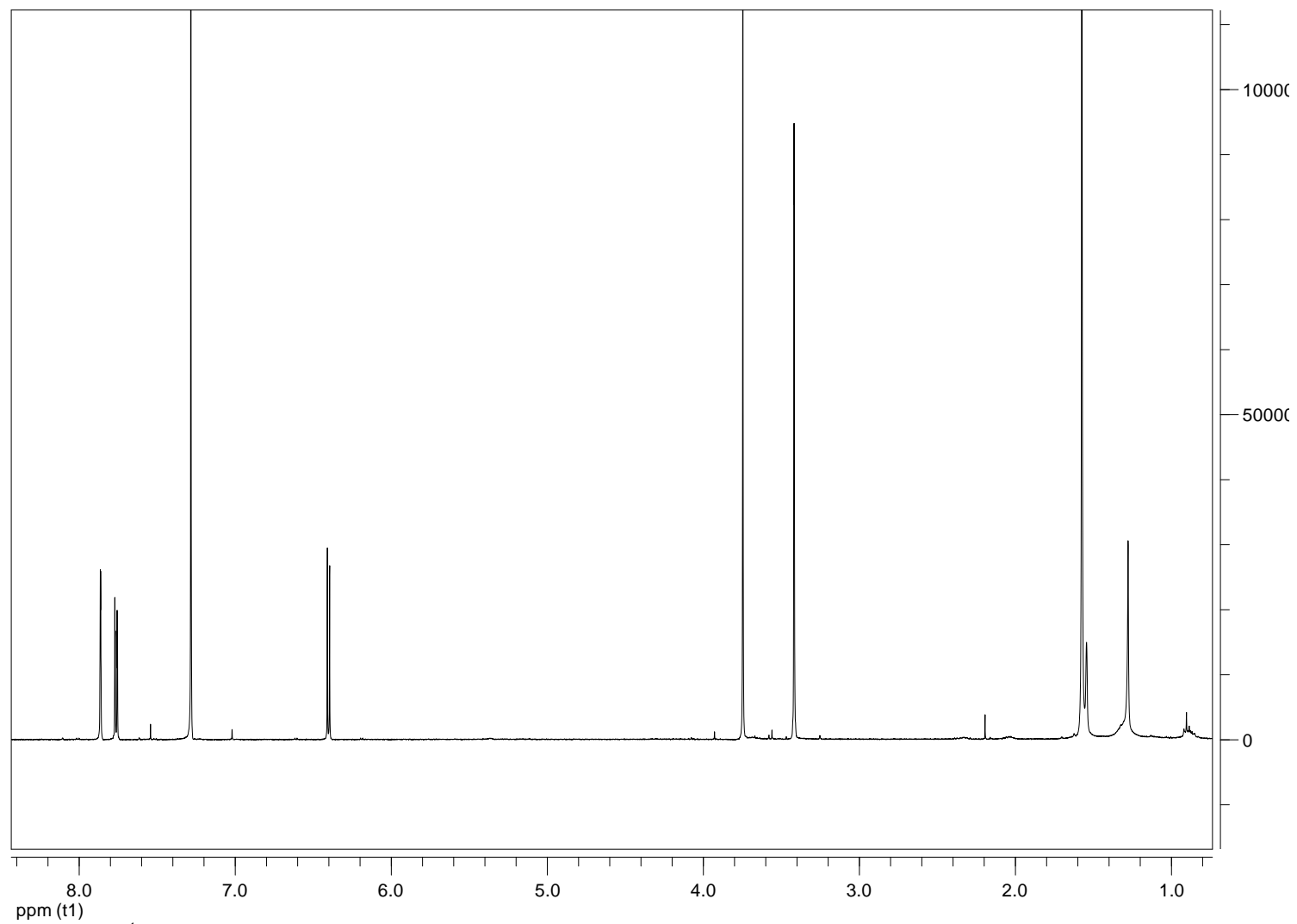


Figure 85. ^1H NMR spectrum of methyl ester of 2-(4-pyronyl)acetic acid (**45**) recorded in CDCl_3 at 400 MHz.

